Amine-modified SBA-15
(prepared by co-condensation)
for adsorption of copper from aqueous solutions

by Enshirah Da'na

Thesis submitted to the
Faculty of Graduate and Postdoctoral Studies
In a partial fulfillment of the requirements for the degree of

Doctorate in Philosophy

In the

Department of Chemical and Biological Engineering
Faculty of Engineering
University of Ottawa

Abstract

During the last few decades, concerns about water shortages and pollution have increased. Consequently, environmental legislations and regulations for wastewater discharge have been issued. The objective of this work was to contribute in developing an efficient adsorbent for removing heavy metal ions from wastewater. The thesis focused on evaluating amine-modified SBA-15 as copper and other heavy metal ions adsorbent, by determining a variety of adsorptive properties with the aim of gaining a deep understanding of its behavior and to outline its advantages and limitations.

The influence of synthesis conditions on the mesostructural stability of the resultant materials after different water treatments was systematically investigated. N_2 adsorption results indicated that the material prepared via co-condensation and aged at 100 ºC was not stable and lost its ordered mesoporous structure after contacting water even at room temperature. Aging at 130 ºC and addition of inorganic salts resulted in materials that maintained their mesporous structure under different water treatments. The material synthesized in the presence of KCl was used as adsorbent for the rest of the thesis work. It was shown that the structural collapse observed in amine-modified SBA-15 prepared by conventional method when contacted with aqueous solutions is associated with the drying process, and not the treatment itself. This structural collapse was avoided by replacing water with more volatile liquids such as acetone, before drying.

Amino-functionalized SBA-15 was tested for the removal of copper ions from aqueous solutions under different temperatures, pH, initial concentrations and agitation speeds. The obtained results indicated that the amino-functionalized SBA-15 was very efficient and equilibrium was achieved in less than 30 min at room temperature. The adsorption capacity increased dramatically with increasing temperature, initial copper concentration and pH. Under suitable conditions, the material exhibited high adsorption capacity even at very low copper concentration.

To further investigate the effect of adsorption parameters, a 2^4 factorial design experiments were used to screen the factors affecting the copper removal efficiency. All the parameters main effects were significant within a 95 % confidence level. Surface composite design was used to develop a reliable model representing the adsorption process. The statistical tests used proved the adequacy of the second order model. Optimization of the factors levels was carried out and the recommended optimum conditions are: copper concentration of 20 mg/L, adsorbent/solution ratio of 1.57 g/L, pH of 6.5, and T = 294 K with 95% copper removal.

The effect of regeneration conditions was investigated after three adsorption–desorption cycles, under different batchwise regeneration conditions. Using a composite surface design methodology, the effect of the regeneration conditions on the performance of the adsorbent was

investigated. It was found that all the studied parameters have a statistically significant influence on the working adsorption capacity. With respect to structural properties and amine content, none of the factors was found to be significant. Regeneration using EDTA was found to be more efficient than acid treatment.

Amino-functionalized SBA-15 was studied as potential absorbent for Cd^{2+}, Co^{2+}, Cu^{2+}, Zn^{2+}, Pb^{2+}, Ni^{2+}, Al^{3+} and Cr^{3+}. The adsorption capacity and selectivity of the material were investigated in single and multi-metal solutions. Using very dilute solutions, i.e., 10 ppm, more than 95% of cations were removed, except for Co^{2+} and Cr^{3+}, indicating the high sensitivity of the current adsorbent. The adsorption capacities in multi-metal solutions were lower than in single-metal ones because of competition between metallic elements for the amine groups. The adsorbent was not affected in the presence of sodium, potassium, and calcium, indicating that the ionic strength does not affect the adsorption properties. Application of this material to remove copper in tap water, river water, and electroplating wastewater was shown to be successful.

Dynamic experiments were carried out on the adsorption of copper ions in a laboratory packed-bed of amine-modified SBA-15. Breakthrough curves were analyzed at different flowrates and after two adsorption-desorption cycles. Furthermore, a model based on mass balance was developed and tested for predicting the breakthrough curves under different experimental conditions used. The results suggested that the developed model was in good agreement with the experimental data. Bed regeneration was performed by circulating 0.2 M EDTA solution through the column for 30 min.

Résumé

Durant les quelques dernières décennies, les préoccupations concernant les pénuries d'eau et la pollution en général ont augmenté. Par conséquent, des législations et des réglementations environnementales pour les rejets d'eaux usées ont été introduites. L'objectif de ce travail était de contribuer au développement d'un adsorbant efficace pour éliminer les ions de métaux lourds des eaux usées. Cette thèse porte sur l'évaluation de SBA-15 modifiée avec des amines comme adsorbant pour le cuivre et d'autres ions de métaux lourds par la détermination d'une multitude de propriétés d'adsorption dans le but d'acquérir une profonde compréhension de son comportement et d'identifier ses avantages et ses limites.

L'influence des conditions de synthèse sur la stabilité des matériaux mésoporeux obtenus après différents traitements a été étudié de façon systématique. Les résultats d'adsorption de N_2 ont indiqué que le matériel préparé par co-condensation et vieilli à 100 °C n'était pas stable et a perdu sa structure mésoporeuse ordonnée après avoir été en contact avec l'eau même à température ambiante. Le vieillissement à 130 °C, avec ajout de sels inorganiques, a abouti à des matériaux qui ont maintenu leur structure mésoporeuse sous différents traitements en présence d'eau. Le matériau synthétisé en présence de KCl a été utilisé comme adsorbant pour le reste du travail de cette thèse. Il a été démontré que l'effondrement de la structure observé dans la SBA-15 modifiée aux amines, préparée par la méthode conventionnelle en contact avec des solutions aqueuses est associé avec le processus de séchage, et non le traitement lui-même. Cet effondrement de structure a été évité en remplaçant l'eau avec des liquides plus volatils tels que l'acétone, avant le séchage.

La SBA-15 amino-fonctionnalisée a été testée pour l'élimination des ions de cuivre des solutions aqueuses à différentes températures, pH, concentrations initiales et vitesses d'agitation. Les résultats obtenus ont indiqué que la SBA-15 amino-fonctionnalisée était très efficace et l'équilibre a été atteint en moins de 30 min à température ambiante. La capacité d'adsorption a considérablement augmenté avec la température, la concentration initiale de cuivre et le pH. Sous des conditions appropriées, le matériau a manifesté une grande capacité d'adsorption, même à des concentrations très faibles en cuivre.

Afin d'étudier l'effet des paramètres d'adsorption, un plan factoriel de 2^4 expériences a été utilisé pour dépister les facteurs affectant l'efficacité d'élimination du cuivre. Tous les effets principaux des paramètres étaient importants à 95% de niveau de confiance. La méthodologie de la surface composite a été utilisée pour développer un modèle fiable qui représente le processus d'adsorption. Les tests statistiques utilisés ont prouvé la pertinence du modèle de second ordre. L'optimisation des niveaux des facteurs a été effectuée et les conditions optimales recommandées sont: la concentration en

cuivre de 20 mg/L, le rapport adsorbant/solution de 1.57 g/L, pH de 6.5 et T = 294 K pour l'élimination de 95% de cuivre.

L'effet des conditions de régénération a été étudié après trois cycles d'adsorption-désorption, sous différentes conditions de régénération. En utilisant la méthodologie de la surface composite, l'effet des conditions de régénération sur la performance de l'adsorbant a été étudié. Il a été constaté que tous les paramètres étudiés ont une influence statistiquement significative sur la capacité de travail d'adsorption. En ce qui concerne les propriétés structurelles et la teneur en amine, aucun des facteurs n'a été jugé significatif. La régénération à l'aide d'EDTA a été jugée plus efficace que le traitement acide.

La SBA-15 amino-fonctionnalisée a été étudiée comme absorbant potentiel de Cd^{2+}, Co^{2+}, Cu^{2+}, Zn^{2+}, Pb^{2+}, Ni^{2+}, Al^{3+} and Cr^{3+}. La capacité d'adsorption et la sélectivité du matériau ont été étudiées dans des solutions mono- et multi-métalliques. En utilisant des solutions très diluées, soit 10 ppm, plus de 95% de cations ont été enlevés, sauf pour le Co^{2+} et Cr^{3+}, indiquant la forte sensibilité de l'adsorbant. Les capacités d'adsorption dans les solutions multi-métalliques étaient inférieures à celles des solutions mono-métalliques en raison de la concurrence entre les éléments métalliques pour les groupes amine. L'adsorbant n'a pas été affecté par la présence de sodium, de potassium et de calcium, ce qui indique que la force ionique n'affecte pas les propriétés d'adsorption. L'usage avec succès de ce matériau pour éliminer le cuivre dans l'eau de robinet, l'eau de rivière et les eaux usées de galvanoplastie a été démontré.

Des expériences dynamiques ont été réalisées sur l'adsorption des ions de cuivre par la SBA-15 amine-modifiée sur une colonne à lit fixe de laboratoire. Les courbes de perçage ont été analysées à des débits différents et après deux cycles d'adsorption-désorption. De plus, un modèle basé sur le bilan de matière a été développé et testé pour prédire les courbes de perçage sous les différentes conditions expérimentales utilisées. Les résultats suggèrent que le modèle développé est en bon accord avec les données expérimentales. La régénération du lit a été réalisée en faisant circuler une solution EDTA à 0.2 M à travers la colonne pendant 30 min.

Acknowledgements

I would like to express my appreciation and acknowledgements to my thesis supervisor, Prof. Abdelhamid Sayari. This thesis would not have been possible without his guidance, advices, and the unique research environment he created.

Special thanks and appreciation to Dr. Jules Thibault and Dr. Handan Tezel who have been so helpful and willing to take some time to provide me with lots of their experiences regarding the modeling of the packed-column. Their advices and suggestions about my thesis proposal were really valuable and appreciated.

Thanks to Dr. Nimal D. Silva from the department of earth science who helped in running the online ICP experiments.

I am thankful to the people in the workshop of the Faculty of Engineering for their help in the development of my experimental setup.

Particular thanks and gratitude go to the Civil Engineering Department for supplying the electroplating wastewater samples.

Great of thanks and love to my husband and my wonderful kids Majid, Mohammad, and Hashim, whose patient love enabled me to complete this work. You are the candles lighting my life. Also my parents and brothers, who provided the item of greatest worth-opportunity. Thank you for standing by me through the many trials and decisions of my educational career.

I would also like to thank my friends and colleagues at the University of Ottawa who made my research very pleasant, and gave me everlasting, wonderful memories.

Statement of Contributions of Collaborators

I hereby declare that I am the sole author of this thesis. I performed the experimental design, all experiments and the associated data analysis.

My supervisor, Prof. Abdelhamid Sayari provided continual guidance throughout this work and made editorial comments and corrections to my written work.

Dr. Nimal De Silva helped in running the online kinetic experiments directly connected to the ICP instrument. He is the co-author of the manuscript presented in chapter 5.

Table of Contents

List of Figures

List of Schemes

List of Tables

List of Symbols

a	Interfacial area per unit volume of packed-bed	(m^2/m^3)
a_p	Interfacial area per unit volume of a particle	(m^2/m^3)
B	The slope of the linear segment in the Boyd plot	
B_t	Mathematical function of F	(mg/L)
C	Concentration of copper	
C_0	Concentration of copper at time 0	(mg/L)
C_L	Liquid phase copper concentration	(mg/L)
C_{L0}	Liquid phase copper concentration at time 0	(mg/L)
C_L^*	Liquid phase copper concentration at the solid-liquid interface	(mg/L)
C_P	Concentration of copper in the mobile phase	(mg/L)
C_P^*	Concentration of copper in the mobile phase at equilibrium	(mg/L)
D	Permeability (m)	(cm^2/s)
D_b	Bulk diffusivity of copper in water	(cm^2/s)
D_e	Effective diffusivity of copper in pores	(cm^2/s)
E	Axial dispersion coefficient	
F	Fractional attainment of equilibrium at time *t*	
J	Liquid flux	$(gm^{-2}s^{-1})$
k_{ads}	External mass transfer coefficient	(cm/s)
k_L	External mass transfer coefficient	(cm/s)
K_s	Sips model constant	
L	Column length	(cm)
M	Mass flow rate for copper	(mg/min)
n	An integer that defines the infinite series solution	
N_S	Sips isotherm constant	
P	Liquid tension	(Nm^{-2})
q_e	Equilibrium adsorption capacity	(mg/g)
q_s	Monolayer adsorption capacity obtained by Sips model	(mg/g)
q_t	Adsorption capacity at time t	(mg/g)
R_e	Reynolds number	
r	Radial distance measured from particle center or radius of curvature	(cm)
r_p	Particle radius	(cm)
Sc	Schmidt number	
Sh	Sherwood dimensionless number	
S_P	Specific surface area	(m^2g^{-1})
t	Time	(min)
u_L	Interstitial velocity	(cm/s)
W	Mass of the adsorbent	(g)
z	Vertical distance measured from bottom of the bed	(cm)
ε_c	Column voidage	
ε_p	Particle voidage	
ν	Kinematic viscosity	(cm^2/s)
V_E	Rate of evaporation	$(gm^{-2}s^{-1})$
V_P	Pore volume	(cm^3g^{-1})
γ_{LV}	Surface tension	(Nm^{-1})
θ	Solid-liquid contact angle	
ρ	Density	(gcm^{-3})
η_L	Liquid viscosity	$(kg.s.m^{-2})$

List of Abbreviations

-A	Sample treated with acidic solution
–AB	Sample treated with acidic solution followed by basic solution
AAPTS	Bis(triethoxysilyl)ethane and *N*-(2-aminoethyl)-3-aminopropyl-trimethoxy silane
AEDTC	*N*-(2-aminoethyl)dithiocarbamate
AlMCM-41	Aluminum-containing MCM-41
APH	Acetamide phosphonate silane
APH-MCM-41	Acetamide phosphonate silane modified MCM-41
APTES	Aminopropyltriethoxysilane
APTES–MCM-41	MCM-41 modified with aminopropyltriethoxysilane
APTES–SBA-15	SBA-15 modified with aminopropyltriethoxysilane
APTS-SBA-15-100	SBA-15 modified with aminopropyltriethoxysilane aged at 100 °C
APTS-SBA-15-130	SBA-15 modified with aminopropyltriethoxysilane aged at 130 °C
APTS-SBA-15-AB	SBA-15 modified with aminopropyltriethoxysilane-acid/base treated
APTS-SBA-15-KCl	SBA-15 modified with aminopropyltriethoxysilane prepared with KCl
APTS-SBA-15-SO_4^{2-}	SBA-15 modified with aminopropyltriethoxysilane prepared with$(NH_4)_2SO_4$
C	Calcination or co-condensation
CRP	Constant rate period
C-H	Calcination-hydration
C-SBA-15-N	Monoamine-modified SBA-15 prepared by co-condensation
C-SBA-15-NN	Diamine-modified SBA-15 prepared by co-condensation
C-SBA-15-NNN	Triamine-modified SBA-15 prepared by co-condensation
CTAB	Cetyltrimethylammonium bromide
CTES	Carboxylate- -triacetic acid-functionalized organosilanes
DDA	Dodecylamine
DMDDA	N-N dimethyldodecylamine
DMDA	*N*,*N*-dimethyldecylamine
DTPA	Diethylenetriaminepentaacetic acid
E	Extraction
EDATAS	Ethylenediamine-triacetic acid-functionalized organosilanes
EDTA	Sodium ethylene-diaminetetraacetic acid
–EDTA	Sample treated with EDTA solution
ETES	Ethyl- -triacetic acid-functionalized organosilanes
FSM-16	Folded sheet material type 16
G	Grafting
GPTMS	3-glycidoxypropyltrimethoxy–silane
G-SBA-15-N-E	SBA-15 extracted then grafted with monoamine
G-SBA-15-N-C-H	SBA-15 calcined then haydrated then grafted with monoamine
G-SBA-15-N-C	SBA-15 calcined then grafted with monoamine
HMS	Hexagonal mesoporous silica
LDAPY	Pyrimidine
LDAPY-MCM-41	Pyrimidine-Functionalized MCM-41
MCFs	Mesocellular siliceous foams
MCM-41	Mesoporous catalytic material type 41
MCM-48	Mesoporous catalytic material type 48
MPTMS	Mercaptopropyltrimethoxysilane
MPTMS-MCM-41	Mercaptopropyltrimethoxysilane modified MCM-41
M41S	Molecular sieves
OSU-6-W	Type of mesoporous silica

OSU-6-W-GPTMS	Mesoporous silica modified with3-glycidoxypropyltrimethoxy–silane
PE-MCM-41	Pore-expanded MCM-41
PMSs	Periodic mesoporous silicas
PPH	Propionamide phosphonate silane
PPH-MCM-41	Propionamide phosphonate silane modified MCM-41
PZC	Point of zero charge
N	Monoamine
NN	Diamine
NNN	Triamine
NH2−MCM-41	Aminopropyl-functionalized MCM-41
NH2-SBA-15	Aminopropyl-functionalized SBA-15
NH2-SBA-15-G1	Aminopropyl-functionalized SBA-15 via 1 grafting step
NH2-SBA-15-Gn	Aminopropyl-functionalized SBA-15 via n grafting step
NH2-SBA-15-Gn-EDTA	Aminopropyl-functionalized SBA-15 via n grafting step followed by EDTA loading
SBA-15	Santa Barbara silica type 15
SH−MCM-41	Mercaptopropyl-functionalized MCM-41
TCPP	tetrakis (4-carboxyphenyl)porphyrin
TEOS	Tetraethylorthosilicate
TiMCM-41	Titanium- containing MCM-41
TMAOH	Tetramethylammonium hydroxide
TMB	1,3,5-trimethylbenzene
TMOS	Tetramethylorthosilicate
v-MCM-41	Vinyl-functionalized MCM-41
-W	Sample treated with water

You can teach a student a lesson for a day; but if you can teach him to learn by creating curiosity, he will continue the learning process as long as he lives.

Clay P. Bedford

Chapter 1

1.1 Introduction

Heavy metals are introduced into water streams by means of various industrial activities such as mining, refining ores, fertilizer industries, tanning, batteries, pesticides etc. and pose a serious threat to the environment. Copper is one of the major metal ions hazardous to humans as well as other forms of life due to its toxicity. The presence of these cationic species in aquatic ecosystems results in their accumulation in living organisms, which causes several adverse effects. Therefore, the removal of heavy-metal ions from water has become a major concern for many processing industries. Several techniques, including chemical coagulation, membrane separation, ion exchange, and adsorption have been developed for water treatment. Many of these methods may be less effective than required and generate secondary pollution with intermediates such as sludge. Adsorption has attracted much interest among researchers due to its low energy requirements and effectiveness even at low concentrations.

The use of various adsorbents such as activated carbon, coal, natural zeolites, agriculture wastes and natural minerals has been intensively reported due to their low cost, availability, and simple preparation. Unfortunately, several drawbacks with respect to the use of these adsorbents have been identified including heterogeneous pore structure, low adsorption capacity, slow kinetics and poor stability. An ideal adsorbent should have features such as strong affinity to target ions, high selectivity and stability, and large surface area with uniform and open pore structure with uniform distribution of adsorption sites. Therefore, numerous researches have focused on mesoporous materials such as SBA-15 because of their high surface area, controlled pore sizes and narrow pore-size distributions.

Beside the aforementioned requirements for an ideal adsorbent, environmental applications of mesoporous materials for adsorption of copper as well as other heavy metals require the material to exhibit specific binding sites for the metal ions. This can be achieved via immobilization of suitable functional groups in the mesopores [1, 2]. Modification with ligands, such as amines, on the surface of mesoporous materials is necessary to obtain selective adsorption and large capacity. Amine groups are excellent ligands because of their strong affinity to various heavy metal ions. Co-condensing of amine and silica precursor is a facile approach to synthesizing amine-functionalized silica, since it allows high loading of organic functional groups and homogeneous surface coverage. However, despite the advantages of SBA-15 as support and for co-condensation as a preparation route, amine-modified SBA-15 prepared by this method was found to have poor copper adsorption performance [3]. Consequently, this thesis was devoted to exploring in depth the reasons of the reported poor performance of this material as copper adsorbent, understand the effect of different parameters on its

performance and setting the conditions to achieve the best adsorption and regeneration performance. In preliminary studies, this material exhibited an adsorption performance that made it promising in this area of research.

1.2 Thesis Structure

This work is focused on gaining a better understanding of the characteristics of amine-functionalized SBA-15 in order to establish the potential and limitations of this material as copper and other heavy metals adsorbent. It is thus a contribution toward the development of amine-functionalized adsorbents for heavy metals removal. The present thesis is organized as follows:

Chapter 2, Adsorption of copper on functionalized-mesoporous silica: A review. This is a summary of the main contributions regarding the development of new copper adsorbents. This chapter aims at providing the reader with background information about the factors affecting the performance of functionalized-mesoporous silica adsorbents such as support structural properties, functional groups chemical properties, and properties of the combined inorganic-organic structure. Furthermore, it answers the question why to use SBA-15 as support and co-condensation as functionalization route.

Chapter 3, Stability of amine-modified SBA-15 prepared by co-condensation in applications involving water. This section presents a detailed explanation on the synthesis of the chosen adsorbent and the determination of the effect of synthesis conditions on its structural stability. The method to successfully produce amine-functionalized SBA-15 by co-condensation that can withstand different harsh aqueous environments. Furthermore, it deals with the effect of drying process on the stability of the developed adsorbents.

Chapter 4, Adsorption of copper on amine-functionalized SBA-15 prepared by co-condensation: Equilibrium properties. One of the most important characteristics of an adsorbent is its capacity at equilibrium. Thus, in this chapter a series of batch experiments were performed under different conditions to investigate the effect of these parameters on the surface properties of the adsorbent and on the overall adsorbent performance and to gain a clear understanding on the phenomena occurring between supported amine and copper ions.

Chapter 5, Adsorption of copper on amine-functionalized SBA-15 prepared by co-condensation: Kinetics properties. The development of efficient adsorbents for the removal of heavy

metals that exhibit fast kinetics would be of great significance. Furthermore, it is important to be able to predict the rate of copper adsorption as a key step to design appropriate treatment units. Hence, the goal of this chapter was to carry out an in-depth study on the effect of adsorption process parameters on the performance of the adsorbent. Furthermore, this chapter dealt with the development of general predictive models to describe the relationship between the initial concentration and the adsorption temperature with the rate of copper removal.

Chapter 6, Optimization of copper removal efficiency by adsorption on amine-modified SBA-15: Experimental design methodology. To gain a clear understanding of the process parameters and to optimize the adsorption process, a 2^4 factorial design experiments followed by surface composite design methodologies were used to develop a reliable model describing the adsorption system and to find the optimum conditions for utilizing the adsorbent with best removal efficiency and lowest possible cost.

Chapter 7, Effect of regeneration conditions on the cyclic performance of amine-modified SBA-15 for removal of copper from aqueous solutions: Composite surface design methodology. To be economically viable, the adsorbent has to be recycled repeatedly. It is thus essential to ensure that the adsorbent has an adequate structural stability and steady metal uptake in a series of adsorption–desorption cycles. Thus, the objective of this chapter was to shed light on the behavior of amine-functionalized SBA-15 as copper adsorbent over three cycles as a function of regeneration conditions using the composite surface design methodology.

Chapter 8, Adsorption of heavy metals on amine-functionalized SBA-15 prepared by co-condensation. To have a good adsorbent, the material has to have a good selectivity in the presence of sodium and calcium, good affinity to other metal ions, and be applicable in real situations. Hence, in this chapter, the ability of the adsorbent to remove copper and other heavy metal ions was tested using different real wastewater samples.

Chapter 9, Modeling adsorption of copper on amine-functionalized SBA-15: Predicting breakthrough curves. The practical application of heavy metals adsorption is most effectively carried out in a packed bed column, as it efficiently utilizes the sorbent capacity and results in an improved quality of the effluent. Hence, in the present chapter, the ability of amine-modified SBA-15 to remove copper in a packed up-flow column was evaluated. Furthermore, a model predicting the breakthrough curves has been developed and tested.

Chapter 10, General discussion and recommendations, This chapter summarizes the main findings of the thesis and gives some recommendations for future work.

References

[1] H. Yoshitake, Highly-controlled synthesis of organic layers on mesoporous silica: their structure and application to toxic ion adsorptions, *New J. Chem.* 29 (2005) 1107-1117.

[2] A. Sayari, S. Hamoudi, Periodic mesoporous silica-based organic-inorganic nano-composite materials, *Chem. Mater.* 13 (2001) 3151-3168.

[3] J. Aguado, J.M. Arsuaga, A. Arencibia, M. Lindo, V. Gascón, Aqueous heavy metals removal by adsorption on amine-functionalized mesoporous silica, *J. Hazard. Mater.* 163 (2009) 213-221.

Chapter 2

Adsorption of copper on functionalized-mesoporous silica: A review

Abstract.

This review is a summary of the main contributions regarding the development of copper adsorbents. Emphasis has been placed on the factors affecting the performance of the adsorbents such as support structural properties, functional groups chemical properties, and properties of the combined inorganic-organic structure. The review includes adsorbents synthesized by modification of mesoporous silica by two major synthesis routes namely (i) grafting and (ii) co-condensation. A review of the literature is provided with the aim of tracing the main achievements toward the development of an efficient copper adsorbent.

2.1 Introduction

Heavy metal ions are introduced into the aquatic streams by means of numerous industrial processes such as mining, refining ores, fertilizer industries, tanning, batteries, pesticides, etc. and pose a serious threat to the environment [1]. Similar to other metals, beyond a threshold concentration in water, copper is hazardous to humans as well as other forms of life due to its toxicity and bio-accumulation. Nonetheless, it is one of the trace elements that are essential nutrients required by the human body. However, ingestion at high dosages can lead to health problems such as irritation of the central nervous system, and liver and kidney damage [2]. It is therefore important to remove excess copper in industrial effluents before discharging it, for the protection of human health and the environment.

Conventional methods for removing metal ions from aqueous solutions include chemical precipitation, coagulation–flocculation, flotation, ion exchange, reverse osmosis, and ultra filtration. However these techniques have their own limitations such as low efficiency, sensitive operating conditions, and production of secondary sludge as shown in Table 2.1 [3]. Hence, there is a constant need for more viable and environmentally friendly technologies. Adsorption is now considered among the most effective, economic and selective methods for water treatment and analysis purposes [4]. Activated carbon has been widely used in water treatment [5] because of its high specific surface area, chemical stability and durability. However, their irregular pore structures limit metal ions access to the adsorption sites, which in turn, lowers the metal removal capacities. Furthermore, depleted source of

commercial coal-based activated carbon resulted in increasing price [4], which encouraged many researchers to concentrate their efforts in developing cheaper and more effective adsorbents based on naturally occurring materials such as agricultural waste materials. In addition to being economic and environment friendly due to their unique chemical composition, agricultural waste is abundant, renewable, and low in cost. These agricultural waste materials are used in the removal of metal ions either in their natural form or after some physical or chemical modification as reported in many recent reviews [3, 6-8]. Bacteria, fungi, yeast and algae can also remove heavy metals from aqueous solutions in substantial quantities [9].

Another approach was to utilize natural materials for the development of new adsorbents. Among these adsorbents, clays and soil constituents [10], red mud [11], chitosan [12], natural zeolites [13] and fly ashes [14] have many advantages such as availability in large quantities and low cost. In addition, they can be chemically modified to increase their binding capacity. However, these adsorbents show many disadvantages because of their wide pore size distribution, heterogeneous pore structure, low selectivity and low capacity due to their weak interactions with metallic ions. Whether dealing with adsorption of copper or any other heavy metal ions, there is a need to develop novel adsorbents that meet specific requirements, including:

(i) Well-designed pore size and geometry with open pore structure to achieve fast kinetics,

(ii) Accessible adsorption sites and suitable surface properties to achieve high adsorption capacity,

(iii) High Cu selectivity in the presence of other ions such as Na^{+} and Ca^{2+},

(iv) Simple synthesis,

(v) Low cost, taking into consideration not only the material synthesis cost, but also equipment cost, which depends on adsorbent performance,

(vi) Regeneration ability under mild conditions,

(vii) Long term stability upon adsorption-desorption cycling.

Mesoporous materials such as SBA-15, MCM-41, MCM-48, and HMS are considered to be superior in this type of applications because of their high surface area, controlled pore sizes and narrow pore-size distributions [15]. Furthermore, it is possible to introduce a wide variety of functional groups onto the surface to increase its affinity towards the target metal ions to be removed [16, 17]. This review focus on recent progress in the synthesis and evaluation of mesoporous copper adsorbent. These materials will be divided into two main categories based on the functionalization route, the advantages and disadvantages of each route in addition to the factors affecting the adsorbent efficiency and selectivity will be discussed qualitatively in details.

Table 2-1. Advantages and disadvantages of some methods used to remove metal ions from wastewaters [3].

Method	Advantages	Disadvantages
Chemical Precipitation	• Simple • Inexpensive • Most of metals can be removed	• Large amounts of sludge produced • Disposal problems
Chemical coagulation	• Sludge settling • Dewatering	• High cost • Large consumption of chemicals
Ion-exchange	• High regeneration of materials • Metal selective	• High cost • Less number of metal ions removed
Electrochemical methods	• Metal selective • No consumption of chemicals • Pure metals can be achieved	• High capital cost • High running cost • Initial solution pH and Current density
Adsorption on activated carbon	• Most of metals can be removed • High efficiency (>99%)	• Cost of activated carbon • No regeneration • Performance depends upon adsorbent
Adsorption on natural zeolite	• Most of metals can be removed • Relatively less costly materials	• Low efficiency
Membrane process	• Less solid waste produced • Less chemical consumption • High efficiency (>95% for single metal)	• High initial and running cost • Low flow rates • Removal (%) decreases with the presence of other metals

2.2 General properties of mesoporous materials

Mesoporous materials with ordered pore structures have attracted much attention due to their significant practical applications such as catalysis [18-22], environmental protection such as adsorption of CO_2 [23-27], adsorption of heavy metals from aqueous solutions [28-30], adsorption of organic pollutants [31-34], and adsorption of volatile organic compounds [35], separation [36-41], medical [42-47], and sensing applications [48, 49]. The importance of mesoporous materials stemmed from their pore sizes which allow not only accessibility for large molecules, but also possible controllability, depending on pore geometry. Furthermore, the ordered mesoporous materials have open pore structure, which allows better accessibility and transfer of molecular species compared to bottleneck pores of amorphous materials, which hinder molecular diffusion and accessibility to the functional groups [50].

In 1990, Kuroda and coworkers [51] first reported the preparation of mesoporous silica with uniform pore size distribution. These novel materials were named Folded Sheet Materials (FSM-16). In 1992, scientists at Mobil described the synthesis, characterization, and proposed mechanism of formation of a new family of silica and aluminosilica mesoporous molecular sieves designated as M41S and reported that MCM-41 and MCM-48 members of this family [52, 53]. In 1995, Tanev and

Pinnavaia [54] reported the synthesis of Hexagonal Mesoporous Silica (HMS) using neutral templates. In 1998, Stucky and coworkers [55, 56] reported the synthesis of one of the most promising mesoporous materials. This highly ordered material known as Santa Barbara Amorphous (SBA-15) has thick pore walls and two dimensional hexagonal structure. As this material possesses tunable pore diameter, it seems to be a good candidate for adsorption and separation applications.

Environmental applications of mesoporous materials for adsorption of copper as well as other heavy metals require the material to exhibit specific binding sites for the metal ions, but mesoporous silicas do not have such surface properties. Accordingly, immobilization of suitable functional groups in the mesopores has attracted much attention [16, 17]. In general terms, the preparation of mesoporous silica is carried out by condensing a silica source in the presence of a structure directing agent (template) followed by template removal and eventually introduction of functional groups onto the silica surface. Addition of functional groups can be achieved by different routes including: (i) using a functionalized silane, (ii) co-condensing a proper silane with the silica source, and (iii) post modification of the mesoporous silica.

The earliest reports on adsorption applications of functionalized mesoporous materials were devoted to heavy metals in wastewater using propylthiol-modified MCM-41 [57] and HMS [58] silicas. Since then, there have been a large number of literature reports dealing with adsorption of metallic species, primarily cations, in wastewater over mostly amine-modified mesoporous silicas. Among the many silica mesophases, SBA-15 has attracted much attention as a promising material not only for the removal of heavy metals [28-30, 59-64], but also for catalysis [65] and adsorption of biomolecules [66] and CO_2 [67]. The strong interest in this material was mainly due to its large surface area (600-1000 m^2/g), narrow pore size distribution, and large and tunable pore diameter (5-30 nm), which allow easy accessibility of target molecules to the inner surface of material, leading to fast kinetics of chemical or physical processes [59]. In addition, its thicker silica pore walls, around 4 nm compared to 1 nm for MCM-41 is believed to improve its hydrothermal stability [68]. In addition, enhancement of the mechanical stability due to increased pore wall thickness is important for some applications using compressed pellets [69]. All of these factors make SBA-15 an ideal support to introduce different functionalities (-NH_2, -SH, -S-, etc.) toward the development of adsorbents suitable for the target application.

2.3 Functionalization of mesoporous silica

Two main routes, grafting (post-synthesis) and co-condensation (one pot-synthesis) have been extensively studied for modifying the mesoporous materials through covalent linkage between the

functional groups and the silica framework. In addition, mesoporous materials having functional groups within the framework, called periodic mesoporous organosilicates, have also been used for the removal of copper and other heavy metals [70, 71].

The post-synthesis grafting methodology was used to incorporate a wide variety of functional groups onto the surface of pre-synthesized mesoporous silicas. The characteristics of the functionalized materials prepared by grafting are influenced by their structural properties and chemical composition.

Another main route for introducing functionality is co-condensation where the organosilane is condensed together with the silica precursor such as tetramethylorthosilicate. Co-condensation provides several advantages such as uniform distribution of the functional groups and short preparation time. Furthermore, it is much more efficient in immobilizing large amounts of functional groups onto the mesoporous material surface, while keeping them highly dispersed since post-synthesis functionalization is limited by the density of Si-OH groups on the surface.

2.3.1 Adsorption of copper on mesoporous silica prepared by grafting

The growing development of copper adsorbents depends on combining the open pore structure of mesoporous silica with suitable organic compounds that exhibit high reactivity toward copper ions. The grafting route was used for the modification of mesoporous silica by a wide variety of organic functionalities. One major factor affecting the performance of grafted adsorbents is the appropriate choice of the organic function. As an example, Liu et al. [72] synthesized thiol- and amino-functionalized SBA-15 materials and investigated their affinity for heavy metal ions, including copper. They found that the thiolated SBA-15 exhibited a negligible affinity for copper, while the aminated ones showed exceptional binding ability. Lee and Yi [73] grafted 3-(2-aminoethyl-amino)propyltrimethoxysilane onto HMS mesoporous silica surface. Their functionalized silica had copper removal capacity 10 times larger than that of commercial silica.

One main concern about post-synthesis grafting is that it reduces the pore size of the modified-materials, especially when large size or large amount of functional groups are introduced [30, 74-83], resulting in hindered diffusion to the adsorption sites as reported by Mureseanu et al. [74]. They showed that the surface area and the mesopore volume strongly decreased after grafting (Table 2.2). For example, for aminopropyl functionalized SBA-15 (NH_2-SBA-15) with an average of 3.1 aminopropyl molecules per nm^2, the BET surface area and the pore volume decreased by 53% and 52%, respectively, compared to the SBA-15 support [74]. Shiraishi et al. [84] studied adsorption of copper using several inorganic adsorbents (silica gel, MCM-41, and aluminum oxide), modified with ethylenediaminetetraacetic acid (EDTA) and diethylenetriaminepentaacetic acid (DTPA) as chelating

ligands. The loading of EDTA ligand on the surface of the adsorbents were found to be lower than the loading of DTPA ligand. However, it was found that the Cu^{2+} adsorption capacity of DTPA-modified adsorbents was significantly lower than that for EDTA-modified material. This suggests that the chelating ability of the DTPA ligand anchored on the adsorbents is lower than that of EDTA ligand, despite the fact that the stability constant of the copper–DTPA complex is reported to be higher than that of copper–EDTA complex in aqueous solution [84]. This is mainly due to the fact that the DTPA ligand is larger than EDTA ligand, and since these ligands are anchored on the surface of the inorganic adsorbents, complexation of the metals with DTPA is likely to be hindered. Furthermore, as more DTPA ligand was anchored, this caused more reduction of the pore size and may give rise to some pore blockage.

Since the dispersion of organic groups grafted on mesoporous silica is often not uniform, the apparent density of functional groups over the solid does not reflect the average distance between such groups. This inability to predict the real distributions resulted in a problem in adsorption of metal ions, which required the cooperation of two or more functional groups on the surface. Manu et al. [85] studied the effect of amine loading on the surface of mesoporous silica gel. They prepared propylamine-functionalized mesoporous silica gel with three different loadings, namely GN_1, GN_2, and GN_3. They found a nonlinear relation between the capacity and amine groups loading on the surface of silica gels, which is due to irregular distribution of functional groups obtained by grafting since large silane molecules suffer diffusion limitations to penetrate deep into the pores, and, consequently, they may tend to react with the hydroxyl groups near the pore mouth, leading to some pore blockage, thus to decreasing surface area, pore volume, and accessibility of functional groups (Table 2.2). Walcarius et al. [86] reported that a pore volume of at least 0.5 cm^3g^{-1} remaining upon grafting was necessary to keep good accessibility of adsorption sites. Accessibility to organic groups grafted within mesoporous silicas was studied by Pinnavaia and Mercier [87] in connection with Hg binding to thiol-functionalized solids. Their work demonstrated the highly improved access of target ions to the binding sites of adsorbents with well-defined mesoporous channels, compared to materials with disordered pore networks, such as amorphous silica.

To further illustrates the importance of accessibility of amine groups to improve the adsorption performance, Zhang et al. [30] prepared mono-, di- and triamine-grafted SBA-15 and showed that these multi-amine grafted silicas have almost equal affinity to Hg^{2+}, Pb^{2+}, Zn^{2+}, Cu^{2+}, Cd^{2+} in wastewater samples and can effectively remove them completely. The introduction of multi-amine silane resulted in high density N groups and high adsorption capacity indicating that the amine groups in the larger pore channels of SBA-15 have high accessibility [88], thus the adsorption capacity was

improved. Using smaller pore MCM-41 silica, Yokoi et al. [88] demonstrated that the aminosilanes react with surface silanol groups located at the openings of the pore channels and/or on the external surface. Thus, the amine-organic moieties concentrated near the entrance of the pores would restrict the diffusion of additional aminosilanes into the pore, resulting in a heterogeneous distribution of amino groups in the pores. Furthermore, the accumulation of the amine-organic moieties at the entrance of the pore would reduce the effective pore size (Table 2.2), leading to the decrease in opportunities for target molecules to interact with amine groups located inside the pores.

In addition to accessibility, the speed at which metal ions are allowed to reach adsorption sites in the mesoporous material is also an important parameter affecting its performance. Walcarius et al. [86, 89] evaluated the speed at which copper ions reached active sites of aminopropyl-grafted silica. They found that the size and the charge of the target species to be adsorbed influence the kinetic of the process. Walcarius et al. [89] compared between Cu^{2+} complexation with the amine-grafted silica gel with the protonation process of the adsorbent using HCl. The apparent Cu^{2+} diffusion coefficient calculated in the early stage of the reaction was 3−4 times lower than that corresponding to the protonation process. This difference is due to the larger size of Cu^{2+} relative to H^{+}. Furthermore, adsorption of Cu^{2+} involves diffusion of two positive charges, thus suffering more repulsive forces. The same group [86] studied the ability for a target reactant to reach the adsorption sites of APTES−MCM-41 and APTES−SBA-15 by protonation with HCl. They indicated that the quantities of protons that have been consumed to reach the equivalent point for APTES−MCM-41and APTES−SBA-15 correspond respectively to 79 and 85% of the total amounts of amine groups in each solid. The incomplete protonation is due to some pore blocking in materials with narrow apertures. Furthermore, they evaluated the speed at which copper ions reached the active sites of aminopropyl-grafted silica with pore diameter ranging between 4 and 15 nm and organic group contents of 1.4-1.9 $mmolg^{-1}$. They found that the diffusion process was dramatically restricted as compared to those observed in homogeneous solution, depending on several factors such as the adsorbent pore size and the size of the reactant, the density of grafted organic sites, and the nature of the starting silica gel. The same group [86] grafted aminopropyl on five different ordered mesoporous silica samples displaying various pore sizes and structures (two small-pore MCM-41, two large-pore MCM-41, and one small-pore MCM-48) and one amorphous silica gel. They studied adsorption of copper and characterized the accessibility to the adsorption sites and the rate at which the copper ions reach the adsorption sites. They demonstrated that both accessibility and rate of access to the adsorption sites were higher with ordered mesoporous solids than with amorphous materials of an average pore size 6-7 nm, while the ordered mesoporous structures of smaller pore size (3.5 nm) had the same performance as that of large-pore amorphous

silica. Furthermore, they demonstrated that the benefit of ordered materials can be achieved only if pore blocking is avoided during the grafting process, otherwise there would be no advantage of uniform pore structure over the corresponding amorphous material.

The ordered structure of the adsorbent is expected to improve its performance by enhancing accessibility to the adsorption sites and/or speeding up transport processes within the pores. However, this is not applicable under all conditions; Goubert-Renaudin [75] found that accessibility to the binding sites in cyclam-functionalized silica is not the determining factor influencing the maximum binding capacity and that structural order of the adsorbent does not provide any benefit to the kinetics of the copper uptake process. This is mainly because the rate-limiting step was not diffusion but the complex formation itself. The rate of Cu^{2+} complexation by cyclam ligands in aqueous solution is faster at higher pH due to protonation of the functional group at low pH. It is also the case for Cu^{2+} binding to cyclam-grafted silica gels, which shows dramatically higher adsorption rate at increasing pH. At pH 3.2, Goubert-Renaudin [75] reported no significant differences between ordered and non ordered materials since the rate-limiting step is the slow complexation reaction that governs the whole adsorption process. The situation was found to be very different at pH 5.7, where adsorption ordered SBA-15-mono was much faster in comparison to amorphous silica. In this case, the limiting step was the mass transport to the cyclam sites instead of complex formation. Thus, the benefit of ordered materials over the amorphous ones from the kinetic point of view is only achieved when the chemical reaction is not too slow in order to benefit from fast mass transport in uniform mesopore channels.

The functional groups do not always have to be directly grafted on mesoporous silica surfaces via a single step. Yantasee et al. [90] first grafted MCM-41 with acetamide phosphonate silane (APH-MCM-41) and propionamide phosphonate silane (PPH-MCM-41). Then, they converted the ester forms of functionalized materials to acid forms using trimethylsilyl iodide and water. They studied the two functionalized adsorbent as potential copper and other heavy metals adsorbent. Another two steps grafting procedure was reported by Mureseanu et al. [74]. They first grafted 3-aminopropyl-triethoxysilane (APTS) followed by salicylaldehyde (SA) as shown in Scheme 2.1. They investigated the behavior of the grafted solids for the adsorption of heavy metals ions from aqueous solutions and got high adsorption capacity and high selectivity for copper ions. They found also that modified SBA-15 is more efficient than modified amorphous silica gel, due to higher surface area and ordered structure. Furthermore, they found that at maximum loading of Cu^{2+} (0.92 $mmolg^{-1}$), the Cu/N molar ratio was 0.42, which is in agreement with the expected value of 0.5.

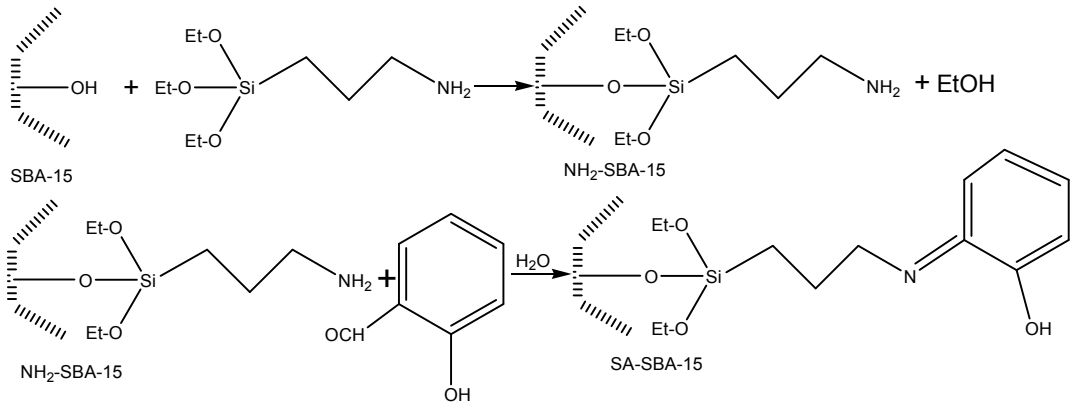

Scheme 2-1. Schematic illustration of SBA-15 functionalization [74].

Alothman and Apblett [77] prepared mesoporous silicas carrying di-, tri-, or penta-amine functional groups by prior functionalization of a mesoporous silica (OSU-6-W) with bromopropyl-functional groups (Scheme 2.2) followed by nucleophilic displacement of the bromine atoms by ethylenediamine, diethylenetriamine, or tetraethylenepentamine, respectively. They tested the capabilities of the adsorbents for the removal of copper, zinc, and cadmium from aqueous solutions and determined the metal adsorption capacities for these metals as a function of total nitrogen content. They found that the ethylenediamine derivative exhibited the highest capacities.

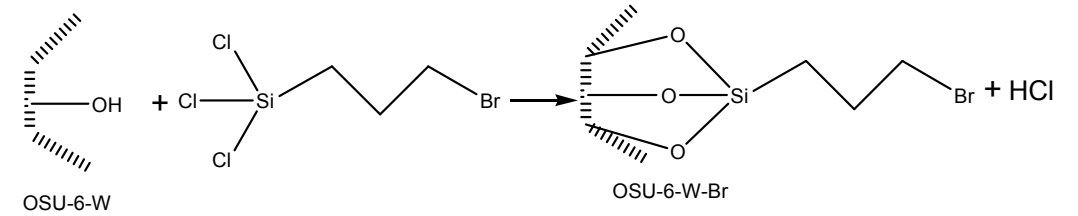

Scheme 2-2. Schematic illustration of OSU-6-W functionalization with bromopropyl-functional groups [77].

Jiang et al. [91] used a multistep process starting by grafting propyl amine onto SBA-15 following by reaction with methylacrylate in the presence of methanol as shown in step 2 in Scheme 2.3, then reaction with ethylenediamine as shown in step 3 in Scheme 2.3, resulting in the first generation NH_2-SBA-15-G1. The second, third and fourth generation were prepared in a similar process by repeating steps 2 and 3. Finally they introduced EDTA functionality via step 4 (Scheme 2.3). The NH_2-SBA-15-Gn-EDTA samples had high removal efficiency (> 94%) for Cu^{2+}. Furthermore, they found that samples with EDTA were more efficient than the other samples. For

example, the copper removal efficiency using NH_2-SBA-15-Gn did not exceed 75% compared to more than 94% using NH_2-SBA-15-Gn-EDTA.

Alothman and Apblett [78, 79] modified hexagonal mesoporous silicas (OSU-6-W) with 3-glycidoxypropyltrimethoxy–silane (GPTMS) functional groups through one and two step post-synthesis procedures. First the material was activated in the presence of triethylamine then refluxed with GPTMS as illustrated in Scheme 2.4, leading to (OSU-6-W-GPTMS). The final glycidoxypropyl functionalized mesoporous silica (OSU-6-W-GPTMS-2) was prepared by repeating the silylation step shown in Scheme 2.4. They found that the functional group loading on OSU-6-W-GPTMS-2 was higher than that of OSU-6-W-GPTMS with a maximum copper uptake of 5.3 $mmolg^{-1}$, forming a 1.7 Cu^{2+}: 1 ligand complex.

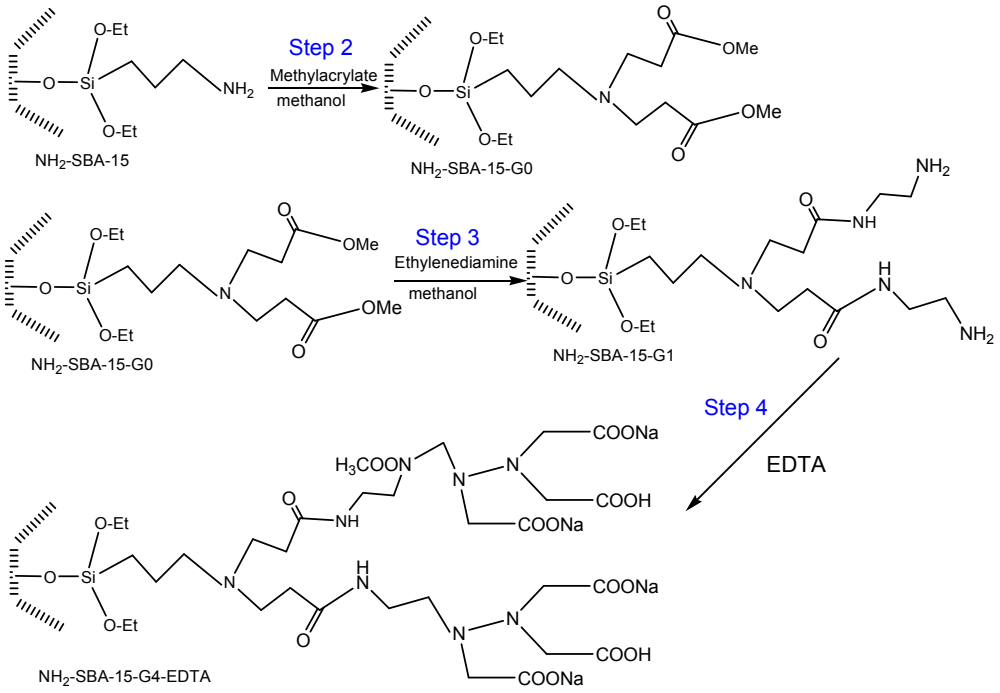

Scheme 2-3. Schematic illustration of SBA-15 functionalization [91].

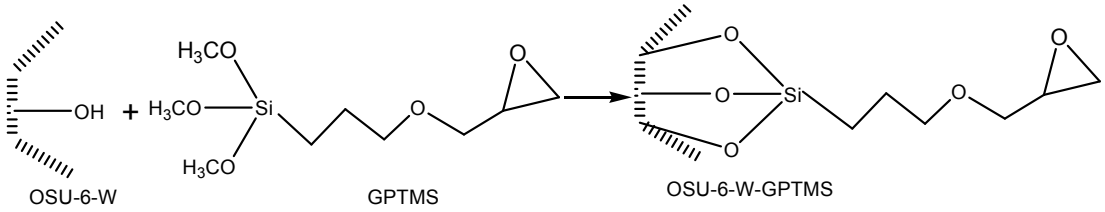

Scheme 2-4. Schematic illustration of OSU-6-W functionalization [78].

Separation of ions mixtures depends on choosing the proper functionality with higher affinity towards one ion than others. As reported by Liu et al. [72], thiolated SBA-15 exhibited a negligible complexation affinity for copper, while the aminated ones showed exceptional binding ability. Lam et al. [80, 81] applied this strategy for the separation of silver and copper [80], and separation of $Cr_2O_7^{-2}$ and copper [81] using MCM-41 grafted with suitable functional groups. For copper-silver separation [80], they compared thiolated (SH−MCM-41) and aminated (NH_2−MCM-41) mesoporous silica. They found that SH−MCM-41 has excellent affinity and capacity for silver adsorption and copper ions remain in the solution. Under similar experimental conditions, NH_2−MCM-41 selectively adsorbed copper from the binary solution (Scheme 2.5). However, the selectivity of NH_2−MCM-41 towards copper cations was found to be strongly dependent on solution pH. Adsorbents with amine groups have the ability to adsorb cationic and anionic target compounds with different pH values in aqueous solutions. Neutral amine groups with lone pair electrons are efficient for removal of heavy metal ions, while protonated amine groups can adsorb anionic pollutants by means of electrostatic attraction [81, 92]. Once the solution pH is lower than the pK_b of the grafted amine (The pK_b value corresponding to the RNH_3^+/RNH_2 couple is about 4) [93], the protonated form of amine (NH_3^+−MCM-41) loses its complexation ability for copper ions. Lam et al [81] utilized this property to separate copper ions from $Cr_2O_7^{-2}$ as shown in Scheme 2.6. They found that NH_3^+−MCM-41 has a 100% selectivity for $Cr_2O_7^{-2}$ adsorption at low pH (<3.5) with high adsorption capacity approaching the theoretical values of two amines for one $Cr_2O_7^{-2}$.

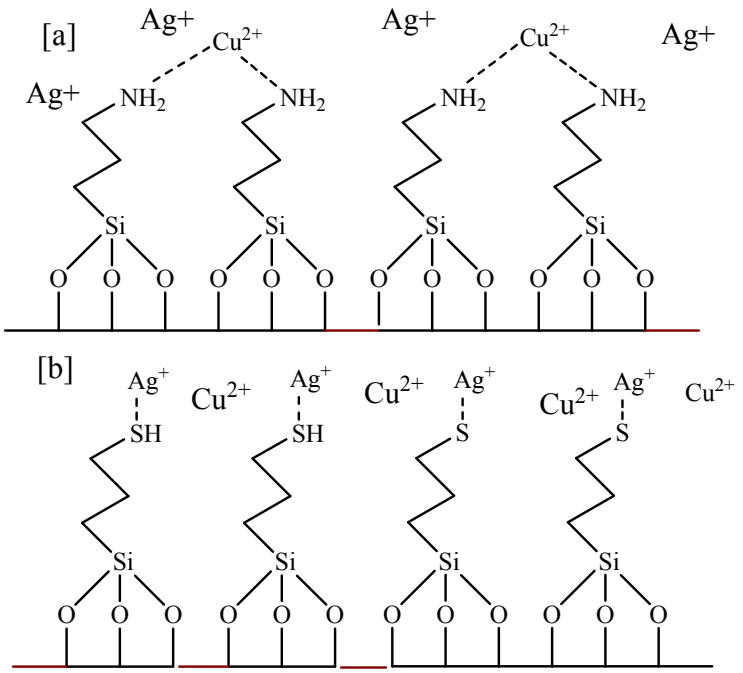

Scheme 2-5. Schematic drawings of Ag^{+} and Cu^{2+} adsorption on (a) NH_2–MCM-41 and (b) SH–MCM-41 [80].

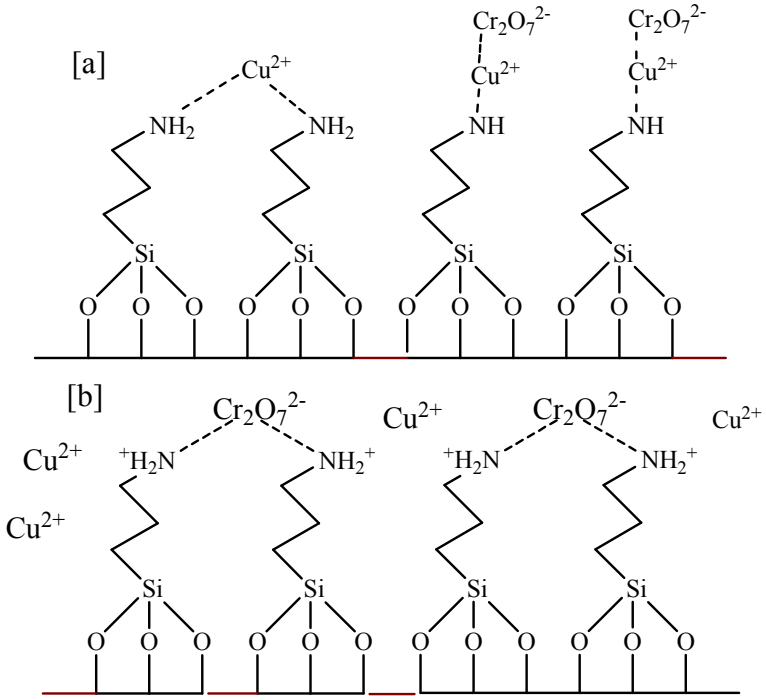

Scheme 2-6. Schematic drawings of Cu^{2+} and $Cr_2O_7^{2-}$ adsorption on NH_2–MCM-41 at pH of 5 (a), and pH of 2 (b) [81].

Solution pH does not only affect the RNH_3^+/RNH_2 ratio, but it also affects the surface charge distribution of the adsorbent. Since the surface charge of functionalized-silica is a result of the protonation or deprotonation of surface hydroxyl as well as functional groups, one of the expected consequences of the point of zero charge (PZC), which is the pH value of the solution corresponding to a net surface charge of zero, is the dependence of adsorption of copper on the solution pH. It is preferred to have low PZC since it leads to an effective copper adsorbent in a wide range of pH as the surface bears negative charge at pH > PZC, considering that for copper adsorption, the pH value must be kept below precipitation of copper hydroxide. Dimos et al. [94] reported the synthesis of MCM-41 grafted with *N*-(2-aminoethyl)dithiocarbamate (AEDTC) with a PZC of 3.2, which is among the lowest PZC reported for oxides bearing protonable surface groups. This implies that in aqueous solution at any pH value above 3.2, the $\equiv XO^-$ species will dominate and the MCM-41 surface will bear a progressively increasing negative charge. Chen et al. [95] reported a PZC of 3.5 for MCM-41 grafted with aminopropyl and obtained a maximum copper adsorption capacity of 1.3 $mmolg^{-1}$ at pH of 5, Jung et al. [71] reported PZC of 5.44 for FSM-16, whereas Da'na and Sayari [62] obtained a PZC of 8.62 for amine-functionalized SBA-15 with a maximum capacity of 0.6 $mmolg^{-1}$ at pH of 6.5. Lam et al. [80] reported a PZC of 2.95 for NH_2−MCM-41 with maximum copper adsorption capacity of 0.3 $mmolg^{-1}$ at pH of 5. The effect of solution pH on copper adsorption was studied by many other researchers [29, 62, 75, 77, 80, 97-101], and their results are shown in Figure 2.1. While generally an increase in copper adsorption capacity with increasing pH was reported, Shiraishi et al. [84] reported that EDTA ligands attached to silica surface act effectively to form a complex with copper ions at lower pH and this complexation ability decreases with increasing pH and vanishes at pH > 4, despite the fact that the chelating ability between copper and free EDTA increases with increasing pH. This is mainly because increasing the solution pH results in increasing the negative charge of the silica surface. Subsequently, the H^+ of the carboxylic group of the grafted EDTA attaches to the negatively charged surface of the adsorbent suppressing the complexation between copper and EDTA.

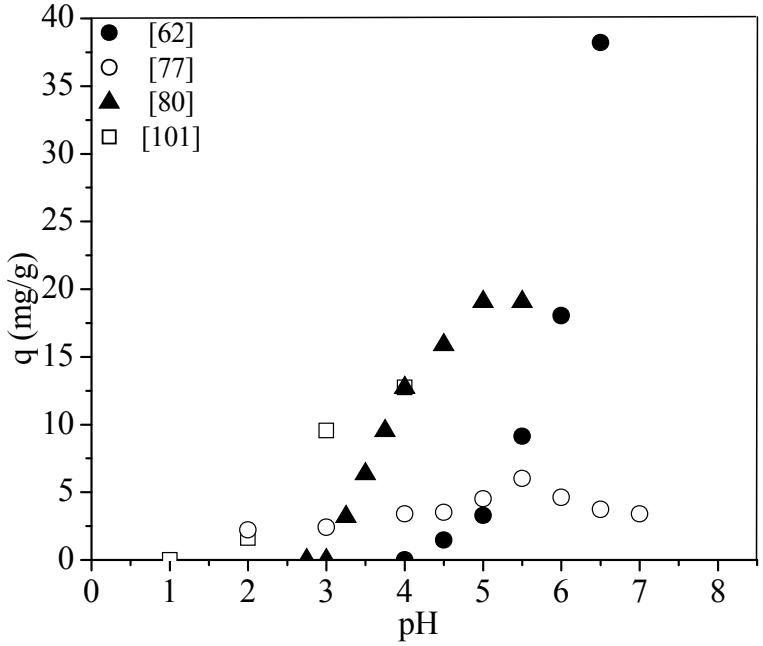

Figure 2-1. Effect of pH on the adsorption capacity.

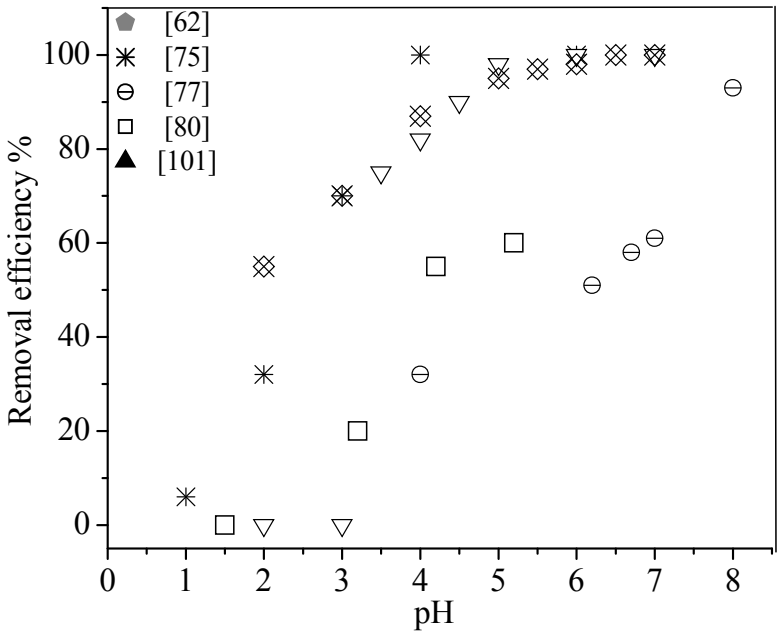

Figure 2-2. Effect of pH on the removal efficiency.

Another important application of adsorption of copper on functionalized mesoporous silica is the pre-concentration of copper for detection purposes. Ballesteros et al. [97] used a pyrimidine-

containing hybrid material (LDAPY-MCM-41) prepared by reacting aminopropyl-grafted MCM-41 with 4-chloro-2,6-diaminepyrimidine as shown in Scheme 2.7. The pyrimidine-derivated material had high selectivity toward copper, and the pre-concentration of copper from water was 100 fold. Similarly, Ganjali et al [98] grafted MCM-41 with salophen and used it for pre-concentration of Cu^{2+} ions. They obtained a pre-concentration factor of 500 with a detection limit of 34 ngL^{-1}, and a maximum capacity of 29 mgg^{-1}.

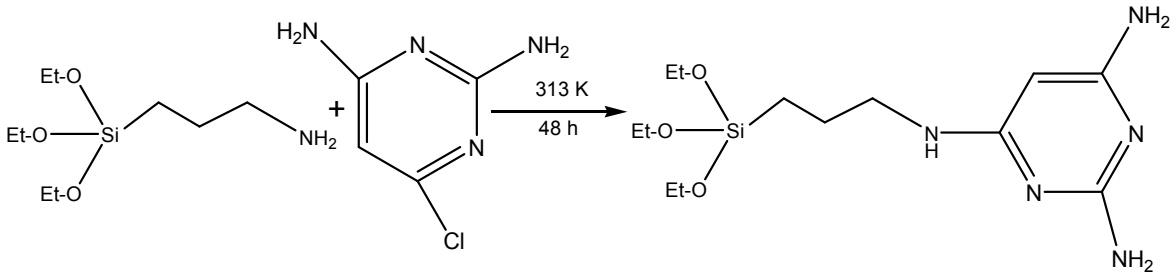

Scheme 2-7. Synthesis reaction of the organic ligand LDAPY [97].

Functionalized mesoporous silica is a fine powder, which makes it difficult to recover in batch applications. This can be overcome by employing adsorbent with magnetic properties. Basically, this method involves incorporation of magnetic materials into the nonmagnetic materials to allow these agglomerates to be separated by magnetic separation. Chen et al. [95] prepared NH_2−MCM-41 adsorbent by grafting propylamine on MCM-41 prepared in the presence of 10 wt% iron oxide to introduce magnetic properties to the adsorbent. Similarly, Lin et al. [99] synthesized amine-functionalized silica magnetite ($NH_2/SiO_2/Fe_3O_4$) by grafting amine functionality on the surface of magnetic silica to behave as an anionic or cationic adsorbent by adjusting the pH value of the aqueous solution. Kim et al. [83] grafted 3-(2-aminoethylamino)-propyltrimethoxysilane on the surface of HMS shell containing magnetite-core structure. They showed that Cu adsorption on the developed adsorbent followed the Langmuir isotherm with q_m value of 0.5 $mmolg^{-1}$ and Cu: NH_2 molar ratio of 0.049 (Table 2.3).

Not only the choice of the support and the functional groups affect the performance and the selectivity of the adsorbent prepared by grafting, the type of the counter anions in the solution affected copper adsorption on NH_2−MCM-41, with increased uptake in the presence of sulfate ions [78, 79]. Lam et al. [82] investigated the anion effect on copper adsorption on NH_2-MCM-41 using $Cu(NO_3)_2$ and $CuSO_4$ solutions. They found that the copper adsorption was higher and faster in the presence of SO_4^{2-} anions compared to NO_3^-, with the majority of the adsorption sites (70%) were readily accessible to Cu^{2+} adsorption, while the remaining sites were only accessible in the presence of SO_4^{2-}. These sites

are either inaccessible or energetically unfavorable, such as isolated amine sites and amines H-bonded with the unreacted surface hydroxyls. Fifty percent more copper (i.e., 1.33 $mmolg^{-1}$) was adsorbed from the $CuSO_4$ solution since SO_4^{2-} may stabilize 1:1 amine: copper complexes. They found that the Freundlich isotherm fits the Cu^{2+} adsorption from $Cu(NO_3)_2$ and $CuSO_4$ better than the Langmuir (Table 2.3) since on the surface of the MCM-41 both islands and isolated amine groups coexist, resulting in a heterogeneous surface. Jeong et al. [102] grafted tetrakis (4-carboxyphenyl)porphyrin (TCPP) on SBA-15 silica, and found it to have higher adsorption capacity than NH_2-SBA-15 silica with maximum adsorption capacity around 13 $mmolg^{-1}$.

Another limitation of introducing functional groups by grafting is that the loading is usually limited by the density of Si-OH groups on the pore wall surface [103]. To illustrate these limitations, Aguado et al. [76] followed different template removal procedures prior to the functionalization of SBA-15 with APTES: calcination (C), extraction (E) and calcination-hydration (C-H), the last was intended to increase the number of silanol groups available for grafting, leading to higher loadings of functional groups. They found that the amine content decreases in the following order G-SBA-15-N-E > G-SBA-15-N-C-H > G-SBA-15-N-C, because calcination produces surface dehydration, leading to a lower amine loading capacity. They also showed that the hydration step should be performed carefully to prevent water accumulation on the surface which can promote heterogeneous dispersion of organic groups, and thus pore blockage. Table 2.3 provides evidence that the copper maximum adsorption capacity of SBA-15 functionalized with propylamine is significantly smaller than the nitrogen content, due to the multiple coordination needed to form stable Cu-amine complexes. Furthermore, Table 2.3 shows that the copper loading for calcined G-SBA-15-N-C is lower than G-SBA-15-N-E and G-SBA-15-N-C-H because materials prepared after extraction and calcination-hydration exhibit higher amine loadings (around 3 against 1.9 $mmolg^{-1}$). However, these adsorption capacities of monoamine-grafted SBA-15 materials are generally lower than values reported for other mesoporous silicas [62, 82, 85, 96, 103]. They also showed that the copper adsorption on sample functionalized with diamine (G-SBA-15-NN-E) is significantly enhanced with respect to materials functionalized with monoamine, since the presence of two amine groups in the same organic chain enhances the copper adsorption capacity due to the proximity of nitrogen. Similarly, Manu et al. [103] controlled the concentration of surface hydroxyl groups on the surface of mesoporous silica gel by calcination at different temperatures (150, 300, 450, and 600 °C). Then they functionalized these materials with APTES and used them for the adsorption of Cu^{2+} ions, and indicated that the thermal treatment of the silica gel determines the density of surface hydroxyl groups and hence the NH_2 density after functionalization, which decreased from 2.34 to 1.65 $mmolg^{-1}$ when the temperature increased

from 150 to 600 °C as shown in Table 2.2. They found that the Cu^{2+} adsorption capacity calculated from Sips model decreased from 1.56 to 0.95 $mmolg^{-1}$, with the decrease in surface concentration of the amine groups from 2.34 to 1.65 $mmolg^{-1}$. Kim et al. [83] removed the surfactant from hexagonal mesoporous silica by solvent extraction and by calcination. They demonstrated that, template removal by calcination was more efficient than by solvent extraction, with surface area and pore volume of the calcined samples (1003 m^2g^{-1} and 1.05 cm^3g^{-1}) larger than that of the extracted ones (672 m^2g^{-1} and 0.75 cm^3g^{-1}). However, upon the removal of the surfactant at high calcination temperatures, significant dehydration of surface hydroxyl groups on the pore walls was observed, which limits the amount of functional groups that could be grafted and consequently, copper uptake capacity.

Immobilization of cyclic polyamines (cyclam family), which form stable complexes with a large number of metal ions [104]**,** has also been used to modify silica surfaces. Goubert-Renaudin et al. [75] prepared a series of hybrid materials by grafting silylated cyclam molecules bearing one, two, or four silyl groups onto both amorphous silica gel and ordered mesoporous silica (SBA-15) via one, two, or four arms and explored their stability and reactivity towards copper ions. They always observed less than complete copper uptake even in excess of cyclam groups with respect to solution-phase Cu, suggesting lower stability of immobilized complexes relative to those in solution. Furthermore, the number of arms attaching cyclam moieties to the silica walls was found to affect the copper binding properties of these adsorbents, with significantly larger capacities when reducing the number of arms. In parallel, multiarm binding resulted in better chemical resistance toward degradation [93].

Some applications of mesoporous silica required large pore sizes, which could be achieved by postsynthesis hydrothermal treatment of as-synthesized silica in an aqueous emulsion of suitable organic expander. In addition to increasing the pore size, this treatment introduces organic functionality to the inorganic framework. Sayari et al. [105] investigated the adsorption properties of the pore-expanded and amine-containing mesoporous silica MCM-41 toward selected metal cations such as Cu^{2+}. This material exhibited high-capacity (1.67 mmol Cu^{2+}/g) and fast adsorption, because of its open pore structure and suitable surface properties. Similarly, Benhamou et al. [106] investigated the adsorption properties of the pore-expanded mesoporous silica MCM-41 and MCM-48 toward Cu^{2+}. They materials were expanded by post-synthesis treatment with N-N dimethyldodecylamine (DMDDA) and dodecylamine (DDA) and found the expanded materials to be fast adsorbents. As shown in Table 2.3, they also found that the pore-expanded MCM-41 had higher adsorption capacity than the pore-expanded MCM-48 and that MCM-41 and MCM-48 pore-expanded

with DMDDA were more efficient than those pore-expanded with DDA indicating that the adsorption capacity depends on both, support and kind of amine used for pore expansion.

Although the grafting method has been considerably developed, it is known that a uniform dispersion of organic groups is not often achieved by this route [88,107]. Ordered mesoporous silica provides three different areas for this reaction: the internal pore surface, the surface near the pore mouth and the external particle surface. Grafting leads to the condensation of organic groups near the pore windows causing some pore blocking, which occurs more readily in silica with small pores than in those with large pores. In addition to pores blockage, grafting has the following drawbacks: (i) reducing the pore size leading to enhanced diffusion resistance within the pores, (ii) control over the concentration and distribution of organic moieties is constrained by the number of surface hydroxyl groups and by their accessibility and the grafting rates depend on the reactivity of precursors, and diffusion limitations, (iii) and most importantly, the complexity of the procedure as it often requires several steps to achieve the final material [91].

2.3.2 Adsorption of copper on mesoporous silica prepared by co-condensation

In the co-condensation route, organic functionalities are condensed together with silica source such as tetramethylorthosilicate (TMOS) and tetraethylorthosilicate (TEOS). Therefore, mesoporous silica functionalized with organic groups can be obtained directly in one step, thus reducing the number of preparation processes and time. It is generally believed that organic functional groups are uniformly dispersed in mesoporous silica prepared by direct synthesis. However, grafting method tends to form more thermally stable silica networks and higher order than co-condensation [107].

Uniform surface modification of functional groups is desired so that the coverage of functional groups on the surface may increase without adversely affecting the diffusion of molecules in the mesopores. To investigate the differences in distribution obtained by the two routes, Lim and Stein [107] prepared vinyl-functionalized MCM-41 samples by a post synthesis grafting and by a direct co-condensation. In direct syntheses of v-MCM-41 samples, hexagonally ordered products with higher loadings of vinyl groups were obtained, while vinyl-grafted MCM-41 samples exhibited higher hydrothermal stability. Furthermore, they found that most vinyl groups in a grafted sample were located on external surfaces and internal surfaces close to the pore openings. It was inferred that vinyl groups are not uniformly distributed throughout the MCM-41 surfaces. On the other hand, v-MCM-41 produced by co-condensation contained uniformly distributed vinyl groups within mesopore channels. Similar observations were recorded by Yokoi et al [88] for mono- (N), di- (NN), and tri-amine (NNN) functionalized mesoporous MCM-41 prepared by co-condensation and grafting. They reported some

differences in the activity of amine groups derived from NNN silanes via the two methods and demonstrated that, the adsorption capacities of amine-functionalized samples via the co-condensation method increased with an increase in the surface density of amine groups. However, when NNN silane was grafted on the surface, the adsorption capacity was decreased with an increase in the surface density of the amine groups implying that the locations of the amine groups introduced to the silica via the two methods are clearly different.

It is expected that the increase in the density of functional groups with retention of the open pore structure would result in a higher performance. However, organic groups, which may interfere with the silica condensation and disturb the micellar structure, have to be avoided in the co-condensation process [108]. Furthermore, deterioration of the periodic order may occur if the loading of functional groups exceeds a certain limit. Chong et al. [109] studied the effect of the type and the amount of organosilanes present in the initial synthesis mixtures of TEOS with different organosilanes in the presence of nonionic triblock co-polymer P123 under acidic conditions. They systematically studied the effect of the organosilanes on the mesostructural properties of the resultant materials by varying the molar ratios of organosilane to TEOS. They showed different levels of disorder of the mesostructures upon functionalization, depending on the type and amount of the organosilanes in the initial synthesis mixtures. The destructive effect of the organosilanes depends on their behaviors under acidic synthetic conditions and molecular sizes and shapes, which have direct impact on the interactions of P123 with silicate species and on micellation of P123 template. Walcarius and Delacôte [110] prepared a wide range of mercaptopropyl-functionalized MCM-41 (MPTMS-MCM-41) adsorbents by varying the MPTMS/TEOS ratio. They distinguished between three categories of adsorbents: (i) A well-ordered MCM-41 structure obtained when MPTMS contents < 10% used, with complete accessibility to all binding sites; but with some restrictions to mass transfer for reaching the active sites located deep in the one-dimensional mesopore channels; (ii) Less-ordered structures made of cylindrical mesopores organized in a wormhole-like three-dimensional arrangement with faster diffusion rates and a 100% access to the binding sites for up to 30% MPTMS contents . Higher loading resulted in less accessibility due to steric hindrance and/or high hydrophobicity (iii) Amorphous materials containing the highest functional group contents were subject to high restriction of mass transfer rates and limited accessibility to the binding sites.

Aguado et al. [59] synthesized thiol-functionalized mesoporous silicas by co-condensation of MPTMS and TEOS with P123 as structure directing agent. They studied the influence the molar ratio x = MPTMS/(MPTMS + TEOS) from 5 to 50%, on both the textural properties and metal ions adsorption capacity. They found that it is necessary to employ a minimum amount of TEOS in order to

preserve the mesoporous structure in the resulting material when a high quantity of propylthiol groups is incorporated. Samples prepared with MPTMS molar ratios up to 10%, exhibited a good order, while materials obtained with larger MPTMS amounts showed less order. Similarly, Xue and Li [100] synthesized thiol-functionalized SBA-16 mesoporous silica using one-pot method by changing the TEOS/ MPTMS ratio. Their results (Table 2.2) showed that by controlling an optimum molar ratio of TEOS and MPTMS between 3 and 4, the synthesized material possessed high order and higher Cu^{2+} adsorption capacity with a maximum of 36.38 mgg^{-1} in the pH range of 5–6.

Markowitz et al. [111] synthesized functionalized-SBA-15 mesoporous silicates by co-condensation of TEOS and ethyl-, carboxylate-, and ethylenediamine-triacetic acid-functionalized organosilanes (ETES, CTES, EDATAS, respectively). They showed that, silicates synthesized with up to 5 wt% of functionalized silane yielded ordered mesoporous materials, and further increasing the amount of silanes to 20% resulted in a significant decrease in the structural ordering of the resulting silicate. A high adsorption capacity of Cu^{2+} from solution was observed only for the EDATAS-functionalized silicates with Cu/N ratio of 0.15, smaller than the 1:1 stoichiometry expected for copper ions and EDTA, indicating that not all of the EDTA groups were able to bind Cu^{2+}. Burleigh et al. [112] synthesized ordered mesoporous organosilicas by co-condensation of bis(triethoxysilyl)ethane and *N*-(2-aminoethyl)-3-aminopropyl-trimethoxy silane (AAPTS). They found that as the amount of AAPTS increased, a gradual decrease in both surface area and the total pore volumes occurs, without significant change in the pore diameter (Table 2.2). More than 70% of the functional ligands were accessible for copper adsorption. Furthermore, as the amount of functional silane increases from 0.17 to 0.87 $mmolg^{-1}$, the percentage of accessible sites decreases from 80 to 70%. Algarra et al. [101] evaluated the potential of removing copper from industrial electroplating wastewaters using aminopropyl-functionalized MCM-41 prepared by co-condensation of TEOS with APTES with different TEOS/APTES molar ratios of 5, 25 and 50. They showed that the copper adsorption capacity increases when the ratio TEOS: APTES decreases, because of increased of amine loading, reaching the saturation of copper at 1.28, 0.75 and 0.54 $mmolg^{-1}$ of adsorbent, respectively. Dey et al. [113] synthesized adsorbent by co-condensation of TEOS and the organosilane *N*-[3-(trimethoxysilyl)propyl]diethylenetriamine and evaluated its adsorption performance. They obtained a maximum copper adsorption capacity of 2.2 $mmolg^{-1}$ with copper/ligand molar ratio of 1:2, considering 1.2 mmol of functional groups per gram adsorbent.

Yang et al. [114] developed a new approach for preparing mesoporous adsorbents using TMAOH as the subsidiary structure-directing agent and ethanol as the organic solvent. Table 2.2 shows that adsorbent synthesized with CTAB and TMAOH (C) as hybrid surfactant templates,

exhibited highly enlarged pore, higher surface area and pore volume since TMAOH helped to accelerate the condensation of silicates and strengthen the physical structure. Adsorbent synthesized using CTAB (B) had smaller pore size, surface area and pore volume than adsorbent prepared using P123 (A) since CTAB has a shorter molecular chain. They also tested the adsorption of copper, zinc, lead, iron, silver and manganese ions on the three adsorbents and showed that adsorbent C possessed better adsorption properties than the counterparts, with copper adsorption capacity of 0.39 $mmolg^{-1}$.

Bois et al. [115] synthesized functionalized mesoporous silicas with aminopropyl (N-S), amino-ethylamino]propyl (NN-S), (2-aminoethylamino)-ethylamino]propyl (NNN-S), and mercapto-propyl (S-S) groups using dodecylamine as structure directing agent. Table 2.2 shows a drastic decrease of the specific surface area for the monoamine-loaded sample (N-S), while for NN-S and NNN-S materials, a lower decrease was noted. On the contrary, an increase of the specific surface area was observed for the thiol-loaded material (S-S). They also indicated that the amine-loaded silicas were disordered and less porous than the thiol-loaded samples. They related that to the formation of hydrogen bonding between amine and silanol. Aminopropyl groups may be involved in a strong interaction $SiO^{-}\ldots{}^{+}NH_3$-, forming a cyclic structure, taking more space in the porous structure. In the case of longer amine chains (NN- and NNN-S), cyclic structures may be less favored. As for thiol-loaded material, there is no hydrogen bonding between thiol and silanol and so silica organization is preserved. The maximum copper ion adsorption capacities of NN-S and NNN-S materials were 0.5 $mmolg^{-1}$ with Cu/N ratios of 0.3 and of 0.4 respectively, indicating that a portion of amine groups were not accessible to copper.

Fakhfakh et al. [116] prepared mesoporous silicas functionalized with ethylenediamine groups via co-condensation under different conditions, and studied the effect of (i) the presence or absence of surfactant, (ii) the synthesis temperature, and (iii) the acid used (HCl, CH_3COOH, or C_2H_5COOH). The best textural properties were obtained using carboxylic acids in propanol as solvent without the need for any surfactant. The copper adsorption capacity was 0.53–0.90 $mmolg^{-1}$ for silica prepared with HCl or acetic acid as catalysts, while the silica prepared with propionic acid showed a lower uptake of 0.41 and 0.13 $mmolg^{-1}$ for the solid prepared at 35 and 60 ºC, respectively.

Sales et al. [117] synthesized hexagonal mesoporous silicas chemically modified with ethylenediamine moieties through the co-condensation of TEOS with *N*-[3-(trimethoxysilyl)-propyl]-ethylenediamine and new agent prepared from the incorporation of the ethylenediamine molecule into the epoxide group of the precursor 3-glycidoxypropyltrimethoxysilane to produce MNN and MGNN with structural properties shown in Table 2.2. They found that MGNN and MNN had similar maximum copper adsorption capacity of 1.4 $mmolg^{-1}$.

Aguado et al. [76] synthesized mesoporous materials SBA-15 functionalized with organic chains containing one (C-SBA-15-N), two (C-SBA-15-NN) and three (C-SBA-15-NNN) amine functional groups by co-condensation. Their materials showed negligible metal adsorption capacity despite their suitable nitrogen content and textural properties as shown in Table 2.2. Later on, Da'na and Sayari [62] suggested several reasons for the negligible adsorption capacity of this material including: (i) incomplete removal of P123 template from the pores by ethanol extraction, (ii) since SBA-15 is prepared under acidic conditions, this leads to the protonation of the amine groups [118], thus diminishing their availability for adsorption, and therefore, basic treatment is needed to recover neutral amine groups, (iii) amine-functionalized SBA-15 prepared by co-condensation was found to have very high zero point charge (ZPC) around 8.62 implying that in aqueous solution, as the pH decreases below 8.62, the $\equiv SiOH_2^+$ species will dominate and the APTS-SBA-15-AB surface will bear a progressively increasing positive charge. This means that the material will not be an effective copper adsorbent in a wide range of pH as it bears positive charge at pH < 8.62. They found that the Cu^{2+} adsorption capacity increases gradually as the solution pH increased from 4 to 6.5 with Cu/N ratio of zero at pH of 4.0. Alkylamines generally have a pK_b value around 4 [119]. Thus, at such a pH, the amine groups are mostly in the protonated state with no Cu^{2+} complexation ability. Furthermore, as the pH is lowered, the surface becomes more positive, leading to decreased interaction between copper and the binding sites due to stronger repulsive forces which inhibit the approach of positively charged copper cations to the adsorbent surface, (iv) another possible reason of low adsorption capacity is that some of the amine groups might be hydrogen-bonded to the silica surface hydroxyl groups, diminishing their availability for adsorption [82].

2.4 Adsorbents regeneration

Cost reduction for applications of an adsorption system requires that the adsorbent has an adequate structural stability and metal uptake in a series of adsorption–desorption cycles. Besides reutilization of the adsorbents, desorption studies provide useful insights into the reversibility of the adsorption process. Many researchers reported recycling of the adsorbents they used mainly by washing with HCl solution [62, 72, 74, 77-79, 81, 83, 84, 90, 97, 100, 102, 114], HNO_3 solution [75, 99] or treatment with complexing agent such as EDTA [62, 91] to elute the metal ions with their results are summarized in Table 2.4. After metal desorption with acids, the neutral amine should be recovered using $NaHCO_3$ solution [62, 74, 81]. Da'na and Sayari [62] showed that EDTA was more efficient than HCl/ $NaHCO_3$ for regeneration of amine loaded silica since it reacts with Cu(II) ion forming an octahedral complex with very high stability [120]. Acid treatment results in the protonation of the

adsorbent surface which increased positive surface charge density [62, 71, 95]. This might result in re-adsorption of negative-ligand enclosed Cu species as reported by Wambu et al. [121]. They showed that such re-adsorption may be followed by surface precipitation that would immobilize re-adsorbed copper on the adsorbent.

Another possible reason for loss of adsorption capacity is structural instability of the adsorbent, which upon regeneration treatment may lose its structural order and adsorption sites accessibility within the pores. Nitrogen adsorption data obtained by Liu et al. [72] are in good agreement with this argument. They indicated that the surface area and pore volume for SBA-15(SH) and SBA-15(NH_2) adsorbents decreased only slightly (5%), while the pore size remained unchanged. While a significant decrease in surface area and pore volume for MCM-41(SH) and MCM-41(NH_2) adsorbents were observed: the surface area and pore volume of the regenerated MCM-41(SH) are 465 (665) m^2g^{-1} and 0.41 (0.61) cm^3g^{-1}; for MCM-41(NH_2), 282 (460) m^2g^{-1} and 0.26 (0.41) cm^3g^{-1}. This result is in good agreement with the report that SBA-15 is much more stable than MCM-41 [68] and may explain the lower regeneration performance of MCM-41 based adsorbent compared to SBA-15 as shown in Table 2.4.

In some cases, the adsorption capacity increases after the first regeneration cycle especially for samples with high loadings of functional groups. This is mainly because of high steric hindrance effect and the lower accessibility of adsorption sites [74, 84]. After regeneration, the functional groups content may decrease. Therefore, the adsorption sites become better-exposed and more accessible to metal ions than the original samples. Thus the adsorption capacity increases as reported by Zhang et al. [30].

2.5 Conclusions

Organically-modified mesoporous silica materials are considered promising adsorbents for the removal of heavy metal ions. This is mainly due to the attractive properties including highly ordered structures with large surface areas and open porous structure for easy and fast access to functional groups. This has led to numerous investigations using such materials for the removal of heavy metal ions. Depending on the target species, special attention was given to the synthesis of an organic-inorganic hybrid material to ensure strong binding and, if possible, selective removal of the pollutant.

Despite the numerous investigations and interesting results presented earlier, the area of functionalized mesoporous silica materials is still far from real environmental applications. In fact, after more than a decade of vigorous activity one could not find even one commercial application of these materials. Of course it is not easy to predict what the future will be, but one can say that two major challenges are the

design of mesoporous materials suitable for the treatment of large volumes of effluents (e.g., high capacity columns) and the preparation of functionalized adsorbents exhibiting high selectivity, long-term stability, and effective reusability after regeneration. The first challenge requires efforts to increase the particle size of mesoporous adsorbents as these powdered materials are neither suited to efficient column packing nor to easy recovery by filtration after batch process. Given the restricted number of commercially-available organosilane reagents, the second challenge requires efforts in the design of such reagents bearing appropriate functional groups in order to improve the adsorption selectivity, which would be important when operating in real process. Another critical point that appears challenging is the need for increasing the long term stability of hybrid materials to avoid their degradation in either adsorption or regeneration steps. If all these factors would improve the performance of mesoporous adsorbents, one should ask if these mesoporous adsorbents could compete with commercial adsorbents in cost and stability.

Table 2-2. Structural properties and functional group content.

Adsorbent	Surface area (m^2g^{-1})	Pore size (nm)	Pore volume (cm^3g^{-1})	Functional group loading ($mmolg^{-1}$)	Ref.
SBA-15	775	6.8	1.20	-	30
N-SBA-15	373	6.0	0.76	1.41	30
NN-SBA-15	336	6.1	0.76	2.59	30
NNN-SBA-15	256	6.1	0.74	4.00	30
APTS-SBA-15-AB	673	7.6	0.75	1.77	62
FSM-16	1000	2.9	1.26	-	71
SBA-15	814	7.6		-	72
SBA-15(SH)	416	-	0.66	-	72
SBA-15(NH_2)	279	-	0.45	-	72
Commercial silica	294	14.7	1.16	-	73
HMS (Soxhelt extracted-36h)	1062	2.46	1.15	0.22[a]	73
HMS (microwave extracted)	995	2.47	1.12	0.21[a]	73
SBA-15	697	8.3	1.49	-	74
NH_2-SBA-15	368	7.8	0.77	3.1[b]	74
SA-SBA-15	317	6.9	0.53	3.2[b]	74
K60	457	-	0.81	-	75
K60-mono	316	-	0.40	0.52	75
K60-di	380	-	0.46	0.37	75
K60-tetra	399	-	0.47	0.25	75
SBA-15	836	-	1.13	-	75
SBA-15-mono	368	-	0.6	0.63	75
SBA-15-di	400	-	0.6	0.46	75
SBA-15-tetra	441	-	0.59	0.31	75
SBA-15	790	9.1	1.44	-	76
SBA-15-N-C	345	7.2	0.58	1.9	76
SBA-15-N-C-H	178	6.4	0.28	2.8	76
SBA-15-N-E	565	9.0	1.02	3.1	76
C-SBA-15-N	572	8.2	0.87	0.9	76
C-SBA-15-NN	508	8.3	0.78	1.9	76
C-SBA-15-NNN	477	8.1	0.74	1.8	76
OSU-6-W	1283	5.11	1.24	-	77-79
OSU-6-W-TCSPBr-1	1048	4.30	0.94	2.55[b]	77-79
OSU-6-W-TCSPBr-2	719	3.65	0.76	4.53[b]	77-79
MCM-41	1070	3.09	-	-	80-82
NH_2-MCM-41	772	2.82	-	1.01	80
NH_2-MCM-41	774	2.92	-	2.26	80
SH-MCM-41	990	3.02	-	1.00	80
COONa-MCM-41	679	2.85	-	1.46	81
NH_2-MCM-41	750	2.92	-	2.53	81, 82
MSM-e	672	2.9	1.05	-	83
2N-MSM-e	513	2.0	0.35	5.66[c]	83
GN1	575	4.72	0.61	-	85
GN1	444	4.03	0.58	0.51	85
GN2	363	3.95	0.49	1.01	85
GN3	360	3.58	0.40	1.45	85
APS-MCM-41-A	87	-	0.16	3.3	86
APS-MCM-41-B	428	-	0.24	2.8	86
APS-MCM-41-C	411	-	0.76	2.6	86

Table 2.2. (Continued)

Adsorbent	Surface area (m^2g^{-1})	Pore size (nm)	Pore volume (cm^3g^{-1})	Functional group loading ($mmolg^{-1}$)	Ref.
APS-SBA-15	357	-	0.73	2.2	86
APS-MCM-48	662	-	0.31	3.0	86
MPS-MCM-41-A	162	-	0.19	2.8	86
MPS-MCM-41-B	818	-	0.52	1.55	86
MPS-MCM-41-C	706	-	1.24	1.0	86
MPS-SBA-15	467	-	0.79	1.0	86
MPS-MCM-48	390	-	0.23	2.7	86
MCM-41-AEDTC	632	4.16	0.54	32[a]	94
MCM-41	1000	3.17	-	-	95
magMCM-41	800	3.2	-	-	95
NH_2-magMCM-41	670	2.92	-	2.8	95
LDAPY-MCM-41	246	1.2	0.26	0.30	97
$NH_2/SiO_2/Fe_3O_4$	73	-		-	99
SH-SBA-16-A	427	4.7	0.47	6.37	100
SH-SBA-16-B	320	4.1	0.38	6.99	100
SH-SBA-16-C	198	3.9	0.37	7.69	100
SH-SBA-16-D	188	3.7	0.29	8.23	100
SH-SBA-16-E	186	3.6	0.14	9.03	100
Na50	869	4.3	-	0.76[c]	101
Na25	881	4.8	-	0.94[c]	101
Na5	649	4.8	-	1.94[c]	101
NH_2-SBA-15	908	8	1.41	-	102
TCPP/ NH_2-SBA-15	453	7.73	0.70	-	102
GC1.5N	314	4.5	0.46	2.34	103
GC3N	360	4.7	0.50	2.10	103
GC4.5N	339	5.0	0.49	1.85	103
GC6N	347	4.2	0.49	1.65	103
DMDDA-41A	63	-	0.28	-	106
DDA-41A	89	-	0.31	-	106
DMDDA-48A	124	-	0.16	-	106
DDA-48A	59	-	0.17	-	106
NNN/SiO_2	889	3.8	-	3.5	113
$NH2/SiO_2/A$	336.3	4.6	0.488	-	114
$NH2/SiO_2/B$	128.4	2.4	0.279	-	114
$NH2/SiO_2/C$	421.9	6.1	0.556	-	114
S	687-712	5.1	-	0	115
N-S	62-65	-	-	1.8	115
NN-S	120-220	-	-	1.6	115
NNN-S	245-314	-	-	1.1	115
S-S	875-888	4.1	-	2.1	115
MNN	663	1.81	-	1.69	117
MGNN	614	1.53	-	1.62	117

a: value given as wt %, b: value given as group/nm^2, c: value given as N wt %

Table 2-3. Freundlich and Langmuir constants for copper adsorption on different adsorbents.

Adsorbent	Note	Freundlich			Langmuir			Ref.
		K_F ($Lmmol^{-1}$)	n	R^2	q_m ($mmolg^{-1}$)	K_L (Lg^{-1})	R^2	
APTS-SBA-15-AB	293 K	0.43	4.7	0.98	0.54	10.62	0.96	62
APTS-SBA-15-AB	313 K	0.73	5.14	0.97	0.88	17.10	0.96	62
APTS-SBA-15-AB	333 K	1.15	3.98	0.96	1.34	20.34	0.97	62
G-SBA-15-NN-E	-	-	-	-	0.83	-	0.99	76
G-SBA-15-N-C-E	-	-	-	-	0.39	-	0.99	76
G-SBA-15-N-E	-	-	-	-	0.35	-	0.99	76
G-SBA-15-N-C	-	-	-	-	0.24	-	0.99	76
SH-MCM-41	Cu^{2+}	0.0259	0.01	-	-	-	-	80
SH-MCM-41	Ag^{+}	0.9694	0.12	-	-	-	-	80
NH_2-MCM-41	Cu^{2+}	0.2453	0.05	-	-	-	-	80
NH_2-MCM-41	Ag^{+}	0.1077	0.06	-	-	-	-	80
NH_2-MCM-41	Cu^{2+} /pH = 2	0.00	0.00	-	-	-	-	81
NH_2-MCM-41	$Cr_2O_7^{2-}$ /pH = 2	0.84	0.30	-	-	-	-	81
COONa-MCM-41	Cu^{2+} /pH = 5	0.22	0.08	-	-	-	-	81
NH_2-MCM-41	$Cu(NO_3)_2$	0.73	0.09	-	0.76	290	-	82
NH_2-MCM-41	$CuSO_4$	1.27	0.16	-	1.33	120	-	82
2N-MSM-e	-	-	-	-	0.50	1.1	-	83
GN1	-	1.416	1.87	0.97	0.485	0.074	0.99	85
GN2	-	5.77	3.82	0.93	0.50	0.020	0.99	85
GN3	-	17.132	4.67	0.94	0.85	0.002	0.99	85
EDA-SAMMS	-	-	-	-	26.9[a]	26.6[b]	-	96
$NH_2/SiO_2/Fe_3O_4$	-	1.53	2.63	0.89	10.41[a]	0.037[b]	0.99	99
SH-SBA-16-C	-	0.5237	6.24	0.86	36.42[a]	49.27	0.98	100
GC1.5N	-	-	-	-	1.53	0.0012	0.99	103
GC3N	-	-	-	-	1.43	0.0018	0.99	103
GC4.5N	-	-	-	-	1.14	0.0202	0.99	103
GC6N	-	-	-	-	0.9	0.041	0.99	103
DDA-41A	-	1.06	1.90	0.97	3.93	0.38	0.99	106
DMDDA-48A	-	0.95	1.81	0.96	4.08	0.35	0.99	106
DDA-48A	-	0.99	1.88	0.96	3.51	0.39	0.99	106
DMDDA-41A	-	1.08	1.85	0.98	4.39	0.31	0.99	106

a: value given as mgg^{-1}, b: value given as Lmg^{-1}

Table 2-4. Copper adsorbents regeneration conditions

Adsorbent	Stripping agent	Cycles	Functionality loss %	Capacity loss %	Ref.
APTS-SBA-15-AB	0.1 M EDTA	10	< 10	10	62
APTS-SBA-15-AB	0.1 M HCl / 0.1 M $NaHCO_3$	10	< 10	40	62
SBA-15(SH)	HCl	3	-	40	72
SBA-15(NH_2)	HCl	3	-	40	72
MCM-41(SH)	HCl	3	-	65	72
MCM-41 (NH_2)	HCl	3	-	65	72
SA-SBA-15	0.3 M HCl/ 0.3 M $NaHCO_3$	4	-	3.3	74
OSU-6-W-TCSPBr-1	2.0 M HCl	4	-	30	77-79
NH_2-MCM-41	5.2 M HCl	1	-	0	81
COONa-MCM-41	5.2 M HCl/ $NaHCO_3$	1	-	0	81
2N-MSM-e	0.1 M HCl	1	5.4	-	83
SilicaED	1 M HCl	1	0	0	84
OSU-6-W-TCSPBr-1	2.0 M HCl	3	-	24	78, 79
APH-MCM-41	20 wt% HCl	10	-	0	90
EDTA-G4-PAMAM-SBA-15	0.1 M EDTA	1	-	5 - 7	91
LDAPY-MCM-41	1 M HCl	3	-	0	97
$NH_2/SiO_2/Fe_3O_4$	0.1 M HNO_3	-	-	-	99
SH-SBA-16-C	1 M HCl	7	11.6	9.9	100
TCPP -SBA-15	0.2 M HCl	3	-	2.3	102
$NH_2/SiO_2/C$	1M HCl	8	-	9.1	114

References

[1] H.B. Bradl, Heavy metals in the environment: origin, interaction and remediation, Amsterdam, Elsevier Academic Press, 2005.

[2] C.M. Futalan , C.C. Kan, M.L. Dalida, C. Pascua, M.W. Wan, , Fixed-bed column studies on the removal of copper using chitosan immobilized on bentonite**,** *Carbohydrate Polymers* 83 (2011) 697-704.

[3] D.W. O'Connell, C. Birkinshaw, T.F. O'Dwyer, Heavy metal adsorbents prepared from the modification of cellulose: a review, *Bioresour. Technol.* 99 (2008) 6709-6724.

[4] F. Fu, Q. Wang, Removal of heavy metal ions from wastewaters: a review**,** *J. Environ. Manage.* 92 (2011) 407-418.

[5] M.A.A. Zaini, Y. Amano, M. Machida, Adsorption of heavy metals onto activated carbons derived from polyacrylonitrile fiber**,** *J. Hazard. Mater.* 180 (2010) 552-560.

[6] D. Sud, G. Mahajan, M.P. Kaur, Agricultural waste material as potential adsorbent for sequestering heavy metal ions from aqueous solutions - a review**,** *Bioresour. Technol.* 99 (2008) 6017-6027.

[7] U. Farooq, J.A. Kozinski, M.A. Khan, M. Athar, Biosorption of heavy metal ions using wheat based biosorbents - a review of the recent literature**,** *Bioresour. Technol.* 101 (2010) 5043-5053.

[8] W.S. Wan Ngah, M.A. Hanafiah, Removal of heavy metal ions from wastewater by chemically modified plant wastes as adsorbents: a review**,** *Bioresour. Technol.* 99 (2008) 3935-3948.

[9] N.R. Bishnoi, A. Garima, Fungus - An alternative for bioremediation of heavy metal containing wastewater: a review**,** *J. Sci. Ind. Res.* 64 (2005) 93-100.

[10] B.I. Olu-Owolabi, D.B. Popoola, E.I. Unuabonah, Removal of Cu^{2+} and Cd^{2+} from aqueous solution by bentonite clay modified with binary mixture of goethite and humic acid**,** *Water Air Soil Pollut.* 211 (2010) 459-474.

[11] H. Nadaroglu, E. Kalkan, N. Demir, Removal of copper from aqueous solution using red mud**,** *Desalination* 251 (2010) 90-95.

[12] B. Kannamba, K.L. Reddy, B.V. AppaRao, Removal of Cu(II) from aqueous solutions using chemically modified chitosan, *J. Hazard. Mater.* 175 (2010) 939-948.

[13] H.S. Ibrahim, T.S. Jamil, E.Z. Hegazy, Application of zeolite prepared from Egyptian kaolin for the removal of heavy metals: II. Isotherm models**,** *J. Hazard. Mater.* 182 (2010) 842-847.

[14] S. Wang, H. Wu, Environmental-benign utilization of fly ash as low-cost adsorbents**,** *J. Hazard. Mater.* 136 (2006) 482-501.

[15] M. Kruk, M. Jaroniec, A. Sayari, New insights into pore-size expansion of mesoporous silicates using long-chain amines, *Microporous Mesoporous Mater.* 35 (2000) 545-553.

[16] H. Yoshitake, Highly-controlled synthesis of organic layers on mesoporous silica: their structure and application to toxic ion adsorptions, *New J. Chem.* 29 (2005) 1107-1117.

[17] A. Sayari, S. Hamoudi, Periodic mesoporous silica-based organic-inorganic nano-composite materials, *Chem. Mater.* 13 (2001) 3151-3168.

[18] Y. Yang, A. Sayari, Synthesis and catalytic properties of organically modified Ti-HMS, *Stud. Surf. Sci. Catal.* 141 (2002) 189-196.

[19] J. Panpranot, , J.G. Goodwin Jr., A. Sayari, CO hydrogenation on Ru-promoted Co/MCM-41 catalysts, *J. Catal.* 211 (2002) 530-539.

[20] J.P.K. Reynhardt, Y. Yang, A. Sayari, H. Alper, Rhodium complexed C2-PAMAM dendrimers supported on large pore Davisil silica as catalysts for the hydroformylation of olefins, *Adv. Synth. Catal.* 347 (2005) 1379-1388.

[21] D.D. Das, A. Sayari, Applications of pore-expanded mesoporous silica 6. Novel synthesis of monodispersed supported palladium nanoparticles and their catalytic activity for Suzuki reaction, *J. Catal.* 246 (2007) 60-65.

[22] D. Das, A. Sayari, Amine grafted pore-expanded MCM-41 as base catalysts, *Stud. Surf. Sci. Catal.* 170 (2007) 1197-1204.

[23] Y. Belmabkhout, R. Serna-Guerrero, A. Sayari, Adsorption of CO_2 from dry gases on MCM-41 silica at ambient temperature and high pressure. 1: Pure CO_2 adsorption, *Chem. Eng. Sci.* 64 (2009) 3721-3728.

[24] R. Serna-Guerrero, E. Da'na, A. Sayari, New insights into the interactions of CO_2 with amine-functionalized silica, *Ind. Eng. Chem. Res.* 47 (2008) 9406-9412.

[25] P.J.E. Harlick, A. Sayari, Applications of pore-expanded mesoporous silicas. 3. Triamine silane grafting for enhanced CO_2 adsorption, *Ind. Eng. Chem. Res.* 45 (2006) 3248-3255.

[26] M. Bhagiyalakshmi, L.J. Yun, R. Anuradha, H.T. Jang, Synthesis of chloropropylamine grafted mesoporous MCM-41, MCM-48 and SBA-15 from rice husk ash: Their application to CO_2 chemisorption, *J. Porous Mater.* 17 (2010) 475-484.

[27] A. Zukal, J. Mayerová, J. Čejka, Alkali metal cation doped Al-SBA-15 for carbon dioxide adsorption, *Phys. Chem. Chem. Phys.* 12 (2010) 5240-5247.

[28] Y. Zhao, Q. Gao, T. Tang, Y. Xu, D. Wu, Effective NH2-grafting on mesoporous SBA-15 surface for adsorption of heavy metal ions, *Mater. Lett.* 65 (2011) 1045-1047.

[29] M.C. Bruzzoniti, A. Prelle, C. Sarzanini, B. Onida, S. Fiorilli, E. Garrone, Retention of heavy metal ions on SBA-15 mesoporous silica functionalized with carboxylic groups, *J. Sep. Sci.* 30 (2007) 2414-2420.

[30] L. Zhang, C. Yu, W. Zhao, Z. Hua, H. Chen, L. Li, J. Shi, Preparation of multi-amine-grafted mesoporous silicas and their application to heavy metal ions adsorption, *Non-Cryst. Solids* 353 (2007) 4055-4061.

[31] A. Walcarius, L. Mercier, Mesoporous organosilica adsorbents: Nanoengineered materials for removal of organic and inorganic pollutants, *J. Mater. Chem.* 20 (2010) 4478-4511

[32] M. Anbia, M. Lashgari, Synthesis of amino-modified ordered mesoporous silica as a new nano sorbent for the removal of chlorophenols from aqueous media, *Chem. Eng. J.* 150 (2009) 555-560.

[33] N. Baccile, F. Babonneau, Organo-modified mesoporous silicas for organic pollutant removal in water: Solid-state NMR study of the organic/silica interactions, *Microporous Mesoporous Mater.* 110 (2008) 534-542.

[34] Y.X. Zhao, M.Y. Ding, D.P. Chen, Adsorption properties of mesoporous silicas for organic pollutants in water, *Anal. Chim. Acta* 542 (2005) 193-198.

[35] R. Serna-Guerrero, A. Sayari, Applications of pore-expanded mesoporous silica. 7. Adsorption of volatile organic compounds, *Environ. Sci. Technol.*41 (2007) 4761-4766.

[36] Y. Liu, Z. Liu, Y. Wang, J. Dai, J. Gao, J. Xie, Y. Yan, A surface ion-imprinted mesoporous sorbent for separation and determination of Pb(II) ion by flame atomic absorption spectrometry, *Microchim. Acta* 172 (2011) 309-317.

[37] T. H. Weng, M. Y. Wey, H. H. Tseng, Enhanced O_2/N_2 separation performance of poly(phenylene oxide)/SBA-15/carbon molecule sieve multilayer mixed matrix membrane using SBA-15 zeolite particles, *ICCCE 2010 - 2010 International Conference on Chemistry and Chemical Engineering, Proceedings* (2010) 245-248.

[38] Y. Zhao, Y. Xu, D. Wu, W. Wei, Y. Sun, A.S.N. Al-Arifi, T. Aouak, Z.A. Al-Othman, Hydrophobic mesoporous silica applied in GC separation of hexene isomers, *J. Sol-Gel Sci. Technol.* 56 (2010) 93-98.

[39] P. Kumar, V.V. Guliants, Periodic mesoporous organic-inorganic hybrid materials: Applications in membrane separations and adsorption, *Microporous Mesoporous Mater.* 132 (2010) 1-14.

[40] C. Li, B. Di, W. Q. Hao, F. Feng, F. Yan, M. X. Su, Preparation and chromatographic application of novel periodic mesoporous organosilicas, *J. China Pharm. Univ.* 41 (2010) 151-155.

[41] T. L. Chew, A.L. Ahmad, S. Bhatia, Ordered mesoporous silica (OMS) as an adsorbent and membrane for separation of carbon dioxide (CO_2), *Adv. Colloid Interface Sci.* 153 (2010) 43-57.

[42] E.I. Basaldella, M.S. Legnoverde, Functionalized silica matrices for controlled delivery of cephalexin, *J. Sol-Gel Sci. Technol.* 56 (2010) 191-196.

[43] J.L. Vivero-Escoto, I.I. Slowing, V.S.Y. Lin, B.G. Trewyn, Mesoporous silica nanoparticles for intracellular controlled drug delivery, *Small Mol.* 6 (2010) 1952-1967.

[44] Y. Zhao, J.L. Vivero-Escoto, I.I. Slowing, B.G. Trewyn, V.S.Y. Lin, Capped mesoporous silica nanoparticles as stimuli-responsive controlled release systems for intracellular drug/gene delivery, *Expert Opin. Drug Delivery* 7 (2010) 1013-1029.

[45] Z. Zhou, X. Kong, W. Sheng, S. Zhu, Preparation of mesoporous composite PAA-PNIPA/APS-SBA-15 and its application in drug delivery, *Jiangsu Daxue Xuebao (Ziran Kexue Ban)/Journal of Jiangsu University (Natural Science Edition)* 31 (2010) 544-548.

[46] F. Qu, H. Lin, X. Wu, X. Li, S. Qiu, G. Zhu, Bio-templated synthesis of highly ordered macro-mesoporous silica material for sustained drug delivery, *Solid State Sci.* 12 (2010) 851-856.

[47] F. Sezões, M.M.L. Ribeiro Carrott, P.A.M. Mourão, P.A. Russo, P.J.M. Carrott, Ordered mesoporous silica materials for protein adsorption, *Mater. Sci. Forum* 637 (2010) 54-59.

[48] S. Wang, G. Men, Y. Wang, L. Zhao, Q. Hou, S. Jiang, , A Zn^{2+} optical sensor and logic actuator using Schiff base functionalized mesoporous material, *IEEE Sens. J.* 11 (2011) 137-141.

[49] J. Wang, S. Chu, F. Kong, L. Luo, Y., Wang, Z. Zou, Designing a smart fluorescence chemosensor within the tailored channel of mesoporous material for sensitively monitoring toxic heavy metal ions Pb(II), *Sens. Actuators, B* 150 (2010) 25-35.

[50] A. Walcarius, M. Etienne, S. Sayen, B. Lebeau, Grafted silicas in electroanalysis: Amorphous versus ordered mesoporous materials, *Electroanalysis* 15 (2003) 414-421.

[51] T. Yanagisawa, T. Shimizu, K. Kuroda, C. Kato, The preparation of alkyltrimethylammonium-kanemite complexes and their conversion to microporous materials, *Bull. Chem. Soc. Jpn.* 63 (1990) 988-992.

[52] J. S. Beck, J. C. Vartuli, W. J. Roth, M. E. Leonowicz, C. T. Kresge, K. D. Schmitt, C. T.W. Chu, D. H. Olson, E. W. Sheppard, S. B. McCullen, J. B. Higgins, J. L. Schlenker, A New Family of Mesoporous Molecular Sieves Prepared with Liquid Crystal Templates, *J. Am. Chem. Soc.*114 *(*1992) 10834-10843.

[53] C. T. Kresge, M.E. Leonowicz, W.J. Roth, J.C. Vartuli, J.S. Beck, Ordered mesoporous molecular sieves synthesized by a liquid crystal template mechanism, *Nature* 359 (1992) 710-712.

[54] P.T. Tanev, T.J. Pinnavaia, A neutral templating route to Mesoporous molecular sieves, *Science* 267 (1995) 865-867.

[55] D. Zhao, J. Feng, Q. Huo, N. Melosh, G. H. Fredrickson, B. F. Chmelka, G. D. Stucky, Triblock Copolymer Syntheses of Mesoporous Silica with Periodic 50 to 300 Angstrom Pores, *Science* 279 (1998) 548-552.

[56] D. Zhao, Q. Huo, J. Feng, B.F. Chmelka, G.D. Stucky, Nonionic triblock and star diblock copolymer and oligomeric sufactant syntheses of highly ordered, hydrothermally stable, mesoporous silica structures, *J. Am. Chem. Soc.* 120 (1998) 6024-6036.

[57] J. Liu, X. Feng, G.E. Fryxell, L.Q. Wang, A.Y. Kim, M. Gong, Hybrid mesoporous materials with functionalized monolayers, *Adv. Mater.*10 (1998) 161-165.

[58] L. Mercier, T.J. Pinnavaia, Heavy metal ion adsorbents formed by the grafting of a thiol functionality to mesoporous silica molecular sieves: Factors affecting Hg(II) uptake, *Environ. Sci. Technol.* 32 (1998) 2749-2754.

[59] J. Aguado, J.M. Arsuaga, A. Arencibia, Influence of synthesis conditions on mercury adsorption capacity of propylthiol functionalized SBA-15 obtained by co-condensation, *Microporous Mesoporous Mater.*109 (2008) 513-524.

[60] J. Aguado, J.M. Arsuaga, A. Arencibia, Adsorption of aqueous mercury (II) on propylthiol-functionalized mesoporous silica obtained by cocondensation, *Ind. Eng. Chem. Res.* 44 (2005) 3665-3671.

[61] D. Pérez-Quintanilla, I. Del Hierro, M. Fajardo, I. Sierra, Preparation of 2-mercaptobenzothiazole-derivatized mesoporous silica and removal of Hg(II) from aqueous solution, *J. Environ. Monit.* 8 (2006) 214-222.

[62] E. Da'na, A. Sayari, Adsorption of copper on amine-functionalized SBA-15 prepared by co-condensation: Equilibrium properties, *Chem. Eng. J.* 166 (2011) 445-453.

[63] E. Da'na, N. D. Silva, A. Sayari, Adsorption of copper on amine-functionalized SBA-15 prepared by co-condensation: Kinetics properties, *Chem. Eng. J.* 166 (2011) 454-459.

[64] Da'na, E., Sayari, A., Optimization of copper removal efficiency by adsorption on on amine-modified SBA-15: Experimental design methodology, *Chem. Eng. J. 167 (2010)91-98.*

[65] X. Wang, J.C.C. Chan, Y.H. Tseng, S. Cheng, Synthesis, characterization and catalytic activity of ordered SBA-15 materials containing high loading of diamine functional groups, *Microporous Mesoporous Mater.* 95 (2006) 57-65.

[66] A. Katiyar, S. Yadav, P.G. Smirniotis, N.G. Pinto, Synthesis of ordered large pore SBA-15 spherical particles for adsorption of biomolecules, *J. Chromatogr. A* 1122 (2006) 13-20.

[67] V. Zeleňák, M. Badaničová, D. Halamová, J. Čejka, A. Zukal, N. Murafa, G. Goerigk, Amine-modified ordered mesoporous silica: Effect of pore size on carbon dioxide capture, *Chem. Eng. J.* 144 (2008) 336-342.

[68] F. Zhang, Y. Yan, H. Yang, Y. Meng, C. Yu, B. Tu, D. Zhao, Understanding effect of wall structure on the hydrothermal stability of mesostructured silica SBA-15, *J. Phys. Chem. B* 109 (2005) 8723-8732.

[69] P. Rayo, M.S. Rana, J. Ramírez, J. Ancheyta, A. Aguilar-Elguézabal, Effect of the preparation method on the structural stability and hydrodesulfurization activity of NiMo/SBA-15 catalysts , *Catalysis Today* 130 (2008) 283-291.

[70] L.C. Lin, M. Thirumavalavan, Y.T. Wang, J.F. Lee, Effect of preparation conditions on the adsorption of heavy metal ions from aqueous solution by mesoporous silica materials prepared using organic template (HDTMAB), *J. Chem. Eng. Data* 55 (2010) 3667-3673.

[71] J. Jung, J.A. Kim, J.K. Suh, J.M. Lee, S.K. Ryu, Microscopic and macroscopic approaches of Cu(II) removal by FSM-16, *Water Res.* 4 (2001) 937-942.

[72] A. M. Liu, K. Hidajat, S. Kawi, D. Y. Zhao, A new class of hybrid mesoporous materials with functionalized organic monolayers for selective adsorption of heavy metal ions, *Chem. Commun.* 13 (2000) 1145–1146.

[73] H. Lee, J. Yi, Removal of copper ions using functionalized mesoporous silica in aqueous solution, *Sep. Sci. Technol.* 36 (2001) 2433-2448.

[74] M. Mureseanu, A. Reiss, I. Stefanescu, E. David, V. Parvulescu, G. Renard, V. Hulea, Modified SBA-15 mesoporous silica for heavy metal ions remediation, *Chemosphere* 73 (2008) 1499-1504.

[75] S. Goubert-Renaudin, M. Etienne, S. Brandès, M. Meyer, F. Denat, B. Lebeau, A. Walcarius, Factors affecting copper(II) binding to multiarmed cyclam-grafted mesoporous silica in aqueous solution, *Langmuir* 25 (2009) 9804-9813.

[76] J. Aguado, J.M. Arsuaga, A. Arencibia, M. Lindo, V. Gasco'n, Aqueous heavy metals removal by adsorption on amine-functionalized mesoporous silica, *J. Hazard. Mater.* 163 (2009) 213-221.

[77] Z.A. Alothman, A.W. Apblett, Metal ion adsorption using polyamine-functionalized mesoporous materials prepared from bromopropyl-functionalized mesoporous silica, *J. Hazard. Mater.* 182 (2010) 581-590.

[78] Z. Alothman, A.W. Apblett, Synthesis of mesoporous silica grafted with 3-glycidoxypropyltrimethoxy-silane, *Mater. Lett.* 63 (2009) 2331-2334.

[79] Z. Alothman, A.W. Apblett, Preparation of mesoporous silica with grafted chelating agents for uptake of metal ions, *Chem. Eng. J.* 155 (2009) 916-924.

[80] K.F. Lam, K.L. Yeung, G. McKay, A rational approach in the design of selective mesoporous adsorbents, *Langmuir* 22 (2006) 9632-9641.

[81] K.F. Lam, K.L. Yeung, G. Mckay, Selective mesoporous adsorbents for $Cr_2O_7^{2-}$ and Cu^{2+} separation, *Microporous Mesoporous Mater.* 100 (2007) 191-201.

[82] K.F. Lam, X. Chen, G. McKay, K.L. Yeung, Anion effect on Cu^{2+} adsorption on NH_2-MCM-41, *Ind. Eng. Chem. Res.* 47 (2008) 9376-9383.

[83] Y. Kim, B. Lee, J. Yi, Preparation of functionalized mesostructured silica containing magnetite (MSM) for the removal of copper ions in aqueous solutions and its magnetic separation, *Sep. Sci. Technol.* 38 (2003) 2533-2548.

[84] Y. Shiraishi, G. Nishimura, T. Hirai, I. Komasawa, Separation of transition metals using inorganic adsorbents modified with chelating ligands, *Ind. Eng. Chem. Res.* 41 (2002) 5065-5070.

[85] V. Manu, H.M. Mody, H.C. Bajaj, R.V. Jasra, Adsorption of Cu^{2+} on amino functionalized silica gel with different loading, *Ind. Eng. Chem. Res.* 48 (2009) 8954-8960.

[86] A. Walcarius, M. Etienne, B. Lebeau, Rate of access to the binding sites in organically modified silicates. 2. Ordered mesoporous silicas grafted with amine or thiol groups, *Chem. Mater.* 15 (2003) 2161-2173.

[87] L. Mercier, T.J. Pinnavaia, Access in mesoporous materials: Advantages of a uniform pore structure in the design of a heavy metal ion adsorbent for environmental remediation , *Adv. Mater.* 9 (1997) 500-503.

[88] T. Yokoi, H. Yoshitake, T. Tatsumi, Synthesis of amino-functionalized MCM-41 *via* direct co-condensation and post-synthesis grafting methods using mono-, di- and tri-amino-organoalkoxysilanes, *J. Mater. Chem.* 14 (2004) 951-957.

[89] A. Walcarius, M. Etienne, J. Bessière, Rate of access to the binding sites in organically modified silicates. 1. amorphous silica gels grafted with amine or thiol groups, *Chem. Mater. 14* (2002) 2757–2766.

[90] W. Yantasee, Y. Lin, G.E. Fryxell, B.J. Busche, J.C. Birnbaum, Removal of heavy metals from aqueous solution using novel nanoengineered sorbents: Self-assembled carbamoylphosphonic acids on mesoporous silica, *Sep. Sci. Technol.* 38 (2003) 3809-3825.

[91] Y. Jiang, Q. Gao, H. Yu, Y. Chen, F. Deng, Intensively competitive adsorption for heavy metal ions by PAMAM-SBA-15 and EDTA-PAMAM-SBA-15 inorganic–organic hybrid materials, *Microporous Mesoporous Mater.*, 103(2007) 316-324.

[92] M. Ghoul, M. Bacquet, M. Morcellet, Uptake of heavy metals from synthetic aqueous solutions using modified PEI - silica gels, *Water Res.* 37 (2003) 729-734.

[93] M. Etienne, S. Goubert-Renaudin, Y. Rousselin, C. Marichal, F. Denat, B. Lebeau, A. Walcarius, Multiarm cyclam-grafted mesoporous silica: a strategy to improve the chemical stability of silica materials functionalized with amine ligands, *Langmuir* 25 (2009) 3137-3145.

[94] K. Dimos, P. Stathi, M.A. Karakassides, Y. Deligiannakis, Synthesis and characterization of hybrid MCM-41 materials for heavy metal adsorption, *Microporous Mesoporous Mater.* 126 (2009) 65-71.

[95] X. Chen, K.F. Lam, Q. Zhang, B. Pan, M. Arruebo, K.L. Yeung, Synthesis of highly selective magnetic mesoporous adsorbent, *J. Phys. Chem. BC* 113 (2009) 9804-9813.

[96] W. Chouyyok, Y. Shin, J. Davidson, W.D. Samuels, N.H. Lafemina, R.D. Rutledge, G.E. Fryxell, W. Yantasee, Selective removal of copper(II) from natural waters by nanoporous sorbents functionalized with chelating diamines, *Environ. Sci. Technol.* 44 (2010) 6390-6395.

[97] R. Ballesteros, D. Pérez-Quintanilla, M. Fajardo, I. Del Hierro, I. Sierra, Adsorption of heavy metals by pirymidine-derivated mesoporous hybrid material, *J. Porous Mater.* 17 (2010) 417-424.

[98] M.R. Ganjali, L. Hajiagha Babaei, A. Badiei, G. M. Ziarani, A. Tarlani, Novel method for the fast preconcentration and monitoring of a ppt level of lead and copper with a modified hexagonal mesoporous silica compound and inductively coupled plasma atomic emission spectrometry, *Anal. Sci.* 20 (2004) 725-729.

[99] Y.F. Lin, H.W. Chen, P.S. Chien, C.S. Chiou, C.C. Liu, Application of bifunctional magnetic adsorbent to adsorb metal cations and anionic dyes in aqueous solution, *J. Hazard. Mater.* 185 (2011) 1124-1130.

[100] X. Xue, F. Li, Removal of Cu(II) from aqueous solution by adsorption onto functionalized SBA-16 mesoporous silica, *Microporous Mesoporous Mater.* 116 (2008) 116-122.

[101] M. Algarra, M.V. Jiménez, E. Rodríguez-Castellón, A. Jiménez-López, J. Jiménez-Jiménez, , Heavy metals removal from electroplating wastewater by aminopropyl-Si MCM-41, *Chemosphere* 59 (2005) 779-786.

[102] E.Y. Jeong, M.B. Ansari, Y.H. Mo, S.E. Park, Removal of Cu(II) from water by tetrakis(4-carboxyphenyl)porphyrin-functionalized mesoporous silica , *J. Hazard. Mater.* 185 (2011) 1311-1317.

[103] V. Manu, H. M. Mody, H.C. Bajaj, Effect of thermal treatment of silica gels on their amino functionalization and subsequent adsorption properties for Cu^{2+} from aqueous solution of copper sulfate, *Ind. Eng. Chem. Res.* 49 (2010) 8184-8191.

[104] R. M. Izatt, K. Pawlak, J.S. Bradshaw, R.L. Bruening, Thermodynamic and kinetic data for macrocycle interaction with cations, anions, and neutral molecules, *Chem. Rev. 95* (1997) 2529–2586.

[105] A. Sayari, S. Hamoudi, Y. Yang, Applications of pore-expanded mesoporous silica. 1. Removal of heavy metal cations and organic pollutants from wastewater, *Chem. Mater.* 17 (2005) 212-216.

[106] A. Benhamou, M. Baudu, Z. Derriche, J.P. Basly, Aqueous heavy metals removal on amine-functionalized Si-MCM-41 and Si-MCM-48, *J. Hazard. Mater.* 171 (2009) 1001-1008.

[107] M.H. Lim, A. Stein, Comparative studies of grafting and direct syntheses of inorganic−organic hybrid mesoporous materials, *Chem. Mater.* 11 (1999) 3285–3295.

[108] A. Vinu, K.Z. Hossain, K. Ariga, Recent advances in functionalization of mesoporous silica, *J. Nanosci. Nanotechnol.* 5 (2005) 347-371.

[109] A.S.M. Chong, X.S. Zhao, A.T. Kustedjo, S.Z. Qiao, Functionalization of large-pore mesoporous silicas with organosilanes by direct synthesis, *Microporous Mesoporous Mater.* 72 (2004) 33-42.

[110] A. Walcarius, C. Delacôte, Rate of access to the binding sites in organically modified silicates. 3. Effect of structure and density of functional groups in mesoporous solids obtained by the co-condensation route, *Chem. Mater.* 15 (2003) 4181-4192.

[111] M.A. Markowitz, J. Klaehn, R.A. Hendel, S.B. Qadriq, S.L. Golledge, D.G. Castner, B.P. Gaber, Direct synthesis of metal-chelating mesoporous silica: Effects of added organosilanes on silicate formation and adsorption properties, *J. Phys. Chem. B* 104 (2000) 10820-10826.

[112] M.C. Burleigh, M.A. Markowitz, M.S. Spector, B.P. Gaber, Amine-functionalized periodic mesoporous organosilicas, *Chem. Mater.* 13 (2001) 4760–4766.

[113] R.K. Dey, F.J.V.E. Oliveira, C. Airoldi, Mesoporous silica functionalized with diethylenetriamine moieties for metal removal and thermodynamics of cation-basic center interactions, *Colloids Surf., A* 324 (2008) 41-46.

[114] H. Yang, R. Xu, X. Xue, F. Li, G. Li, Hybrid surfactant-templated mesoporous silica formed in ethanol and its application for heavy metal removal, *J. Hazard. Mater.* 152 (2008) 690-698.

[115] L. Bois, A. Bonhommé, A. Ribes, B. Pais, G. Raffin, F. Tessier, Functionalized silica for heavy metal ions adsorption, *Colloids Surf., A* 221 (2003) 221-230.

[116] F. Fakhfakh, L. Baraket, J.M. Fraile, J.A. Mayoral, A. Ghorbel, Synthesis of diamine functionalized mesoporous organosilicas with large pores, *J. Sol-Gel Sci. Technol.* 52 (2009) 388-397.

[117] J.A.A. Sales, A.G.S. Prado, C. Airoldi, Interaction of divalent copper with two diaminealkyl hexagonal mesoporous silicas evaluated by adsorption and thermochemical data, *Surf. Sci.* 590 (2005) 51-62.

[118] A.S. Chong, X.S. Zhao, Functionalization of SBA-15 with APTES and characterization of functionalized materials, *J. Phys. Chem. B* 107 (2003) 12650–12657.

[119] D.R. Lide, W.M.M. Haynes, Handbook of Chemistry and Physics, 90th ed., (2010) 8–43.

[120] J.Y. Tseng, C.Y. Chang, C.F. Chang, Y.H. Chen, C.C. Chang, D.R. Ji , C.Y. Chiu, P.C. Chiang, Kinetics and equilibrium of desorption removal of copper from magnetic polymer adsorbent, *J. Hazard. Mater.* 171 (2009) 370–377.

[121] E. W. Wambu, G. K. Muthakia, P. M. Shiundu, K. J. Thiongo, Kinetics of copper desorption from regenerated spent bleaching earth, *Am-Euras. J. Sci. Res.* 4(2009) 317-323.

Chapter 3

Stability of amine-modified SBA-15 prepared by co-condensation in applications involving water

Abstract.

Different mesoporous materials, namely mesocellular siliceous foams (MCFs), pore-expanded MCM-41 (PE-MCM-41), pure and amine-functionalized SBA-15 (APTS-SBA-15), were prepared and subjected to different water treatments including water at room temperature and boiling water for different periods. In many instances, the apparent lack of stability was associated with the drying process, rather than water treatment. Acetone washing before drying helped in maintaining the structural properties of the materials. Moreover, it was shown that increasing pore sizes of the mesoporous materials increased its stability. The influence of the synthesis conditions of APTS-SBA-15 on its structural stability of upon treatment with water, acidic, basic or EDTA solution was systematically investigated. N_2 adsorption results indicated that the sample prepared by co-condensation and aging at 100 ºC was not stable and lost its ordering of the mesoporous structure after any aqueous treatment. Methods reported in the literature to improve the stability of pure SBA-15 such as aging at 130 ºC, addition of KCl or $(NH_4)_2SO_4$ were applied. The three methods resulted in materials that maintained its mesoporous structure under different aqueous treatment.

3.1 Introduction

Unmodified [1] as well as surface-modified [2] periodic mesoporous silicas (PMSs) have been the topic of much attention due to their wide variety of potential applications. The importance of PMSs stems from their open pore structure which allows better accessibility and mass transfer compared to the bottleneck pores of amorphous materials, which hindered molecular diffusion and accessibility to internal functional groups. Thus, loss of mesoporosity may lead to lower accessibility of functional groups and slower chemical and physical processes. Therefore, analysis of the structural consequences of exposure to harsh conditions becomes an important issue.

Many practical applications of PMSs are severely inhibited by this poor stability in aqueous solutions compared with those of zeolites [3]. For example, titanium-containing MCM-41 is a very active catalyst for partial oxidation of many organic compounds with aqueous solutions of hydrogen peroxide. However, the structure of TiMCM-41 was reported to collapse and the titanium was leached

out of the silicate frameworks under liquid-phase hydroxylation of phenol with 35% aqueous H_2O_2 in acetone at 333 K [4]. However, aluminum-containing MCM-41 was reported to be very stable in aqueous solutions during ion exchange for catalyst preparation [5]. Zhao et al. [3] studied the structural stability of MCM-41 silica upon hydration/dehydration and found that the pore structure of MCM-41 collapsed upon rehydration at room temperature due to the hydrolysis of the bare Si−O−Si bonds in the presence of water vapor. Furthermore, some MCM-41 silicas collapsed upon lengthy storage in ambient air.

The hydrothermal stability of unmodified PMSs has been extensively investigated using the effect of boiling water over time [6-8]. Several factors have been shown to improve such stability including increasing the pore walls thickness and the degree of silica condensation within the pore walls [7]. For example, SBA-15 silica was found to be much more hydrothermally stable than MCM-41, because of its 4 time thicker pore walls. In addition, several synthesis conditions were found to contribute toward higher hydrothermal stability. This includes the addition of salts such as NaCl [9], fluoride [10, 11] as well as sulfate anions [8], high aging temperature [12-16], and organic protection via increased surface hydrophopicity to minimize contact with water [17, 18]. Wang et al. [9] showed that with the aid of NaCl, the mesostructure ordering of the functionalized SBA-15 could be greatly enhanced. Chen et al. [11] reported greatly improved hydrothermal stability of the mesoporous silica synthesized in the presence of fluoride ions. Galarneau et al. [12] showed that SBA-15 silica prepared at 100 ºC exhibits lower stability in the presence of water compared to the same material synthesized at 130 ºC.

In this chapter, we looked at the structural stability of mesoporous silica focusing on the effect of the drying process. Different mesoporous samples were exposed to water under different conditions, then dried. By comparing the degree of structural collapse after different treatments, the effect of drying process was investigated. Furthermore, we studied the effect of aging temperature, addition of KCl and $(NH_4)_2SO_4$ on the stability of amine-modified SBA-15 prepared by co-condensation in aqueous solutions at room temperature.

3.2 Drying theory

Drying of solid materials involves several stages as shown in Scheme 3.1. In the first stage, the constant rate period (CRP), the liquid flows towards the surface. A point is reached when there is insufficient water to cover the surface without developing concave meniscus with a liquid tension (P) related to the radius of curvature (r) given by [20]:

$$P = - 2\gamma_{LV} / r \qquad (3.1)$$

where γ_{LV} is the surface tension (Nm^{-1}) of the liquid inside the pores. For liquid in cylindrical pores of radius a, the radius of meniscus (r) is given by [20]:

$$r = -a/\cos(\theta) \tag{3.2}$$

while for ordinary porous materials with no cylindrical pores, r can be defined in terms of pore volume (V_p) and specific surface area (S_p) as [20]:

$$a = 2V_p/S_p \tag{3.3}$$

where θ is the solid-liquid contact angle. This tension is balanced by compressive stresses on the solid phase that tend to suck the network under the liquid surface.

As drying proceeds, the solid network becomes increasingly stiff as a result of forming new bonds and decreasing porosity, and the tension in the liquid rises correspondingly. Once the radius of the meniscus becomes equal to the pore radius, the liquid exerts the maximum tension marking the critical point, which represents the end of CRP. Beyond this point, the liquid tension cannot overcome further solid stiffing. Hence, the meniscus recedes into the pores leaving air-filled pores near the external surface (Scheme 3.1c) during what is called falling rate period.

During the CRP, the tension in the liquid does two things: it compresses the network and induces flow from the interior. For the meniscus to remain at the surface of the network, the rate of evaporation (V_E) must equal the flux of liquid (J) to the surface, which is given by Darcy's law [20, 21]:

$$J = \frac{D}{\eta_L}\nabla P = V_E \tag{3.4}$$

Where, η_L is the liquid viscosity and D is the permeability of the network, which is related to mesoporous structure by [20]:

$$D \alpha (1-\rho) a^2 \tag{3.5}$$

As show by Eq. 3.4, the lower the permeability, the greater the pressure gradient must be to support a given evaporation rate. Thus, according to Eq. 3.5, one way of avoiding network fracture is to increase permeability by producing materials with larger mesopores. In addition to increasing permeability, larger pores generally lower capillary pressure. Another factor to prevent fracture is to reduce capillary forces by replacing water in the pores with more volatile liquid ($\gamma_{LV} < \gamma_{LVwater}$) such as acetone. According to Eq. 3.1, this will reduce the compressive forces exerted on the network as evaporation emptied the pores.

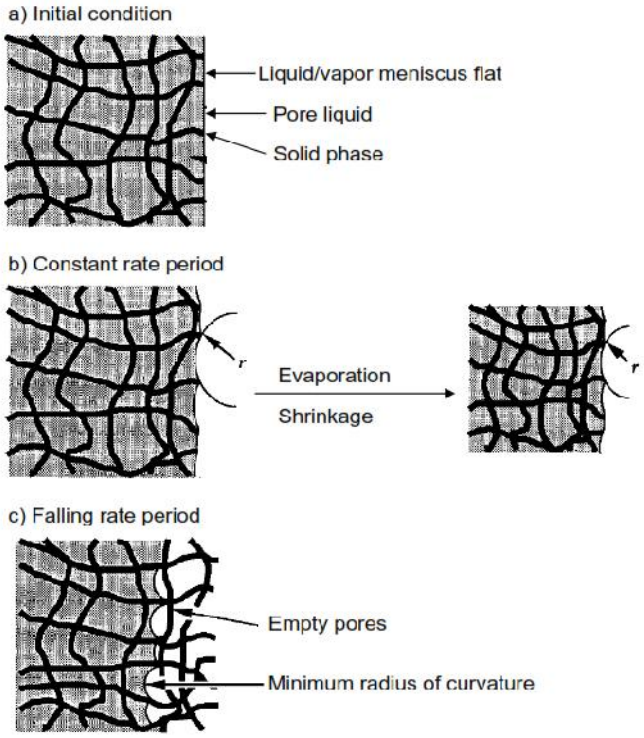

Scheme 3-1. Illustration of drying process. Initially the pores are all filled with liquid and the meniscus is flat (a). Tension in the liquid is low and the radius of the meniscus (r) is large (b). At the critical point, r becomes equal to the pore radius, then CRP ends and the liquid recedes into the gel (c) [20].

3.3 Materials and methods

3.3.1 Materials Synthesis

● Mesocellular siliceous foam (MCF) have been synthesized according to Schmidt-Winkel et al. [22]. In a typical preparation, 2.0 g of poly(ethylene oxide)-*block*-poly(propylene oxide)-*block*-poly(ethylene oxide) triblock copolymer (P123) was dissolved in 75 mL of 1.6 M aqueous HCl at room temperature. Then, 23 mg of NH_4F if desired and 2.0 g of 1,3,5-trimethylbenzene (TMB) were added. After 45 min at 40 °C, 4.4 g of tetraethoxysilane was added. After 20 h at 40 °C, the cloudy mixture was aged at 100 °C for 24 h. The filtered precipitate was dried in air then calcined in flowing N_2 under a thermal ramp of 1 °C/min to 550 °C and then held at 550 °C in flowing air for 5 h. The two samples prepared in the presence and in the absence of NH_4F, will be referred as MCF-F and MCF, respectively.

● Pure SBA-15 was prepared according to Zhao et al. [19] using the following procedure: 4.0 g of P123 was dissolved in 30 mL of water and 120 mL of a 2 M HCl solution at 40 °C. Then, 8.5 g of tetraethylorthosilicate (TEOS) was added and the mixture stirred for 20 h. After aging at 100 °C for 24

h, the white solid was collected by filtration, dried in air at room temperature for 1 day then calcined as described above.

● Amine-modified SBA-15 samples were prepared as before except that after adding TEOS, it was prehydrolized for 2h before adding 1.08 g of 3-aminopropyltrimethoxy-silane (APTS) which corresponds to a APTS/TEOS molar ratio of 0.15, and then extracted in ethanol instead of calcination. This sample will be denoted as APTS-SBA-15. Two samples of APTS-SBA-15 were prepared at different aging temperatures of 100 and 130 °C referred to as APTS-SBA-15-100 and APTS-SBA-15-130. Furthermore, a sample denoted as APTS-SBA-15-KCl was prepared exactly as APTS-SBA-15-100 except that 8 g of KCl was added. As for the effect of inorganic anions, APTS-SBA-15-SO_4^{2-} was prepared in the presence of ammonium sulfate according to Du et al. [8]. Typically, 1.0 g of P123 was dissolved in 30 mL of 1.2 M HCl solution, followed by addition of 2.08 g of TEOS. The mixture was stirred at 45 °C for 2 hr before adding 0.25 g APTS corresponding to APTS/TEOS molar ratio of 0.15. The mixture was stirred for 20 h, and then the pH was adjusted to 6 – 7 by adding ammonium hydroxide. After addition of 1.14 g (0.02 mol) of $(NH_4)_2SO_4$ and stirring for another 30 min, the mixture was transferred into an autoclave and heated under static condition at 100 °C for 24 h then collected and extracted as described before.

● MCM-41 silica was synthesized at 60 °C for 40 h as described by Sayari and Yang [23] using Cab-O-Sil M5 fumed silica as the silica source, cetyltrimethylammonium bromide (CTAB) as the surfactant template, and a 25% solution of tetramethylammonium hydroxide in water (TMAOH) for pH adjustment. The as-synthesized sample was calcined as described earlier.

● Pore-expanded MCM-41 (PE-MCM-41) silica was synthesized via a two-step procedure described earlier [23, 24]. The first step consisted of preparing an MCM-41 mesophase at a temperature of 100 °C for 40 h as described by Sayari and Yang [23]. The pore expansion process was carried out by post-synthesis hydrothermal treatment of non-calcined MCM-41 in an emulsion of *N*,*N*-dimethyldecylamine (DMDA) at 120 °C for 72 h as reported by Sayari et al. [24]. Calcination of the final product resulted in PE-MCM-41.

3.3.2 Adsorbent stability tests

● The stability in water was tested by stirring 100 mg of each sample in 100 mL of water for different time intervals (i.e., 5 min, 5 h, and 1 week) at ambient temperature, then separated and dried under vacuum at 100 °C for 3 h.

● The stability in boiling water was tested by adding 100 mg of each sample in 100 mL of boiling water with reflux for different time intervals (i.e., 5 h and 1 week), then separated and dried as before.

● To study the effect of moisture removal during drying on the textural properties of the materials, samples obtained by different water treatments described earlier were washed with 10 mL acetone for 30 min, in order to replace the water in the pores with acetone, then dried.

● To study the effects of different aqueous environments, stability tests were carried out using the APTS-SBA-15 prepared under different conditions by stirring 100 mg of each sample in 100 mL of distilled water, 0.1 M HCl, 0.1 M EDTA, or 0.1 M HCl followed by 0.1 M $NaHCO_3$ solution for 1 h. In all cases, the resulting product was recovered by filtration, washed with deionized water, dried in a vacuum oven at 100 °C for 4 h before characterization by N_2 adsorption and thermal gravimetric analysis (TGA). Samples will be referred to as -W, –EDTA, -A, and –AB for water, EDTA, acid and acid-base treated samples.

3.3.3 Characterization

The structural properties of all samples before and after different treatments were determined by nitrogen adsorption at 77 K using a Micromeritics ASAP 2020 volumetric apparatus. Prior to analysis, the samples were degassed under vacuum at 100 °C for 3 h. The surface area was determined by the BET method, whereas the pore size distribution was calculated using the Kruk−Jaroniec−Sayari (KJS) approach [25]. The pore volume was calculated as the volume of liquid nitrogen adsorbed at P/P_0 = 0.995. The amine loading was determined via thermal decomposition using a thermogravimetric analyzer (Q500 TGA, TA Instruments) based on the method developed by Harlick and Sayari (2006) [26].

3.4 Results

3.4.1 Effect of drying process

Fig. 3.1 - 5 show the N_2 adsorption isotherms of various samples treated in water and boiling water for different periods, followed by vacuum drying at 100 °C. After 5 min stirring in water at ambient temperature, APTS-SBA-15 (Fig. 3.1) lost 90% of its surface area and 86% of its pore volume (Table 3.1), together with the broadening in pore size distribution (Fig. 3.1 insert). Under the same treatment followed by acetone washing, the increase in the original surface area from 190 to 239 m^2g^{-1}, pore volume from 0.29 to 0.37 cm^3g^{-1} (Table 3.1) and the well-defined pore size distribution (Fig. 3.1 insert), clearly indicates a higher stability of APTS-SBA-15 washed with acetone. Furthermore, washing with acetone removed the residual template inside the pores as indicated by the higher surface area and pore volume, leading to better accessibility of the functional groups inside the pores. However, as shown in Table 3.1 and Fig. 3.2, pure SBA-15 preserved most of its surface area after the treatment in water for 5 min and in boiling water for 5h. Similarly, Fig. 3.3 shows a complete collapse

in the structure of PE-MCM-41 with a drastic decrease in surface area (from 1053 to about 700 m^2g^{-1}; Table 3.1) after any water treatment and for any period, together with the broadening in pore size distribution (Fig.3.3 insert). The difference between PE-MCM-41 and SBA-15 lies in the pore walls thickness mainly (1 nm vs. 4 nm).

Treatment of PE-MCM-41 in water at ambient temperature followed by acetone washing preserved the structural properties of the material as shown in Fig. 3.3. Table 3.1 shows that 100% of the surface area and the pore volume were preserved after treating PE-MCM-41 in water for 5 h followed by acetone washing. However, treating the PE-MCM-41 in boiling water for 5 h followed by acetone washing resulted in a slight decrease in surface area from 1053 to 929 m^2g^{-1} (Table 3.1) with minor variation of the pore volume from 2.31 to 2.20 cm^3g^{-1} (Table 3.1), while the pore size distribution remained relatively narrow (Fig. 3.3 insert), again showing higher stability by washing with acetone. Furthermore, treatment of PE-MCM-41 in boiling water for a week followed by acetone washing resulted in a drastic decrease in surface area from 1053 to 415 m^2g^{-1} and the pore volume from 2.31 to 1.94 cm^3g^{-1} (Sample 14, Table 3.1) with a narrow pore size distribution (Fig. 3.3 insert). Fig. 3.3 shows a shift in the condensation step from P/P_0 of 0.75 to about 0.95 as a result of increasing pore size due to thermal treatment for long time.

Results discussed so far provide evidence that replacing water in the pores with acetone before drying resulted in higher stability of APTS-SBA-15 as well as PE-MCM-41, which is related to the lower surface tension of acetone (22.72 Nm^{-1} at 25°C) compared to water (71.99 Nm^{-1} at 25°C) [27]. As discussed earlier in the drying theory, keeping the pore size constant, the liquid tension (P) created during the drying stage with water inside the pores is expected according to Eq. 3.1 to be 3.2 times higher than that obtained with acetone. Thus, the higher compressive stress on the solid phase led to the collapse of the structure.

Interestingly, MCF-F exhibited much higher stability. For example, the surface area of MCF-F decreased from 598 m^2g^{-1} to only 560, 524 and 352 m^2g^{-1} after treatment in water at ambient temperature for 5 min, or in boiling water for 5 h and 1 week, respectively. The treated MCF-F samples still exhibit type IV isotherms as shown in Fig. 3.4, indicating the presence of uniform mesopores that become somewhat larger during the treatment. As shown in Fig. 3.4 insert, after the three different treatments, the pore size distribution did not undergo significant changes.

One may relate the high stability of MCF-F to one of the well-known improving stability factors, i.e., addition of NH_4F in this case, as reported in the literature [10, 11]. To check this hypothesis, a similar sample denoted as MCF was prepared without addition of NH_4F. Fig. 3.5 as well as Table 3.1 (Samples 21-24) show that this material is equally stable. However, compared to APTS-

SBA-15 and PE-MCM-41, MCF-F and MCF samples have a significantly larger pore size (18.4 and 21.9 nm, respectively), which is expected to prevent the collapse of the pore structure by decreasing the liquid tension (P) created during the drying stage as discussed earlier (Section 3.2). According to Eq. 3.1, with water inside the pores, the liquid tension (P) is expected to be 2 times lower when the pore size is doubled. Thus, the compressive stress acting on the solid phase is also 2 times lower, leading to the retention of the pore structure. Furthermore, according to Eq. 3.4, the compressive stress could be decreased by increasing the permeability which is directly related to the pore size by Eq. 3.5.

To eliminate the effect of heat during drying process, PE-MCM-41 was treated with water for 5 min, then dried and degassed at ambient conditions for four days before being analyzed by N_2 adsorption. Fig. 3.3 shows that PE-MCM-41 completely collapsed with a drastic decrease in surface area (from 1053 to about 655 m^2g^{-1}; see Table 3.1) together with the broadening in pore size distribution (Fig. 3.4 insert) after this treatment, indicating that structural collapse was not associated with the drying temperature.

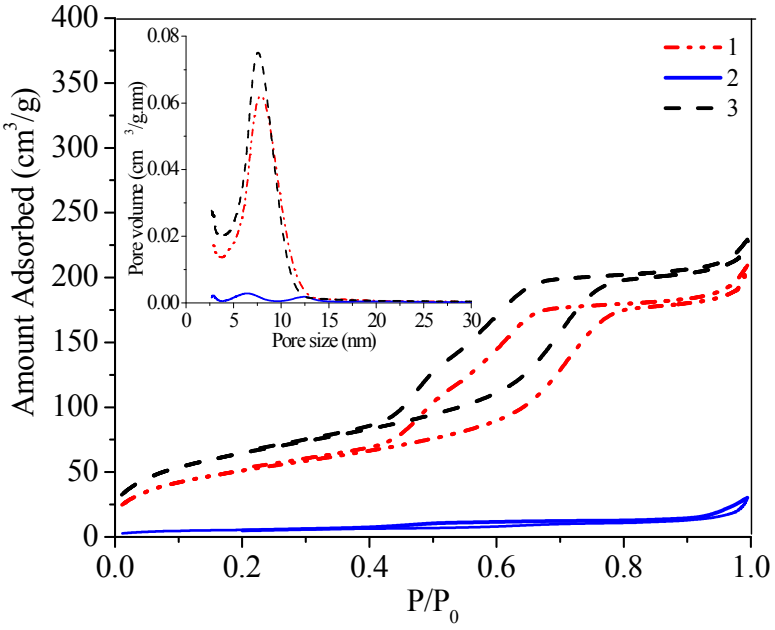

Figure 3-1. Stability tests for APTS-SBA-15. Sample numbers as in Table 3.1.

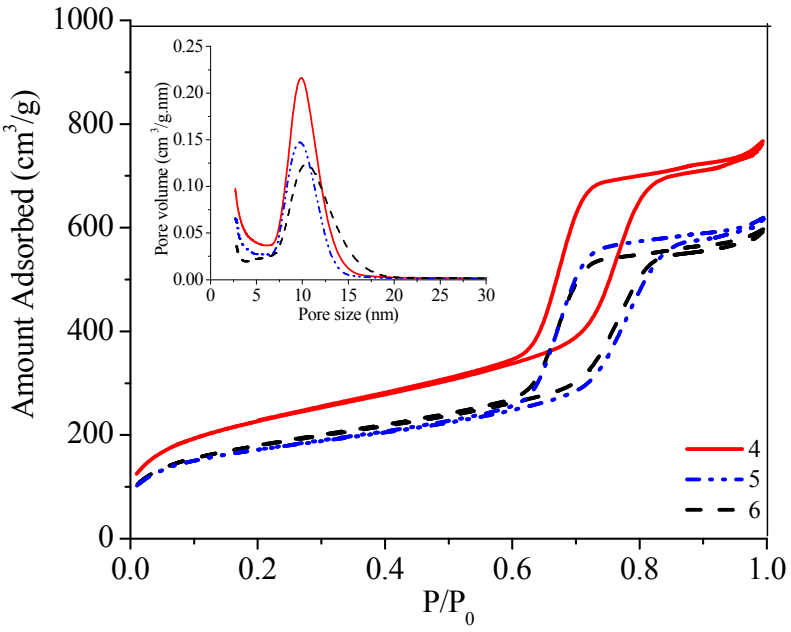

Figure 3-2. Stability tests for SBA-15. Sample numbers as in Table 3.1.

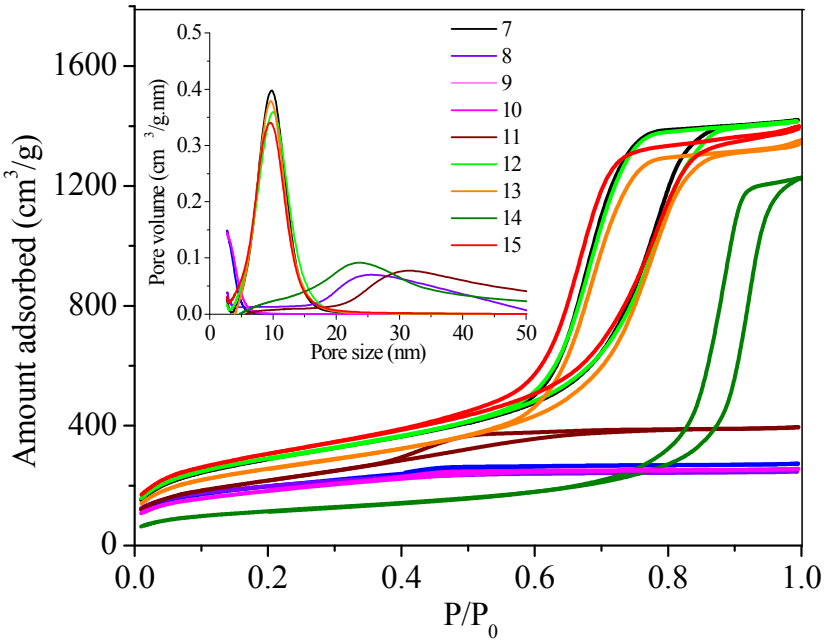

Figure 3-3. Stability tests for PE-MCM-41. Sample numbers as in Table 3.1.

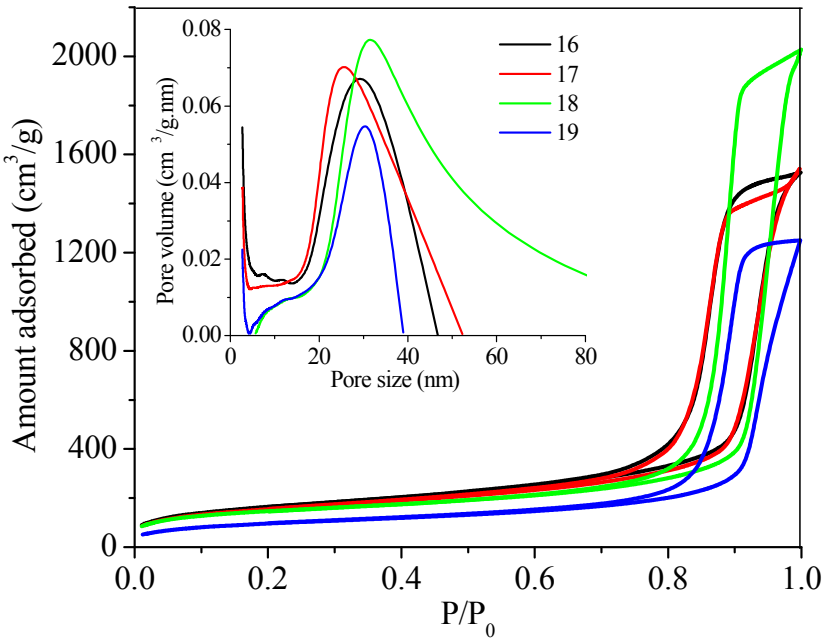

Figure 3-4. Stability tests for MCF-F. Sample numbers as in Table 3.1.

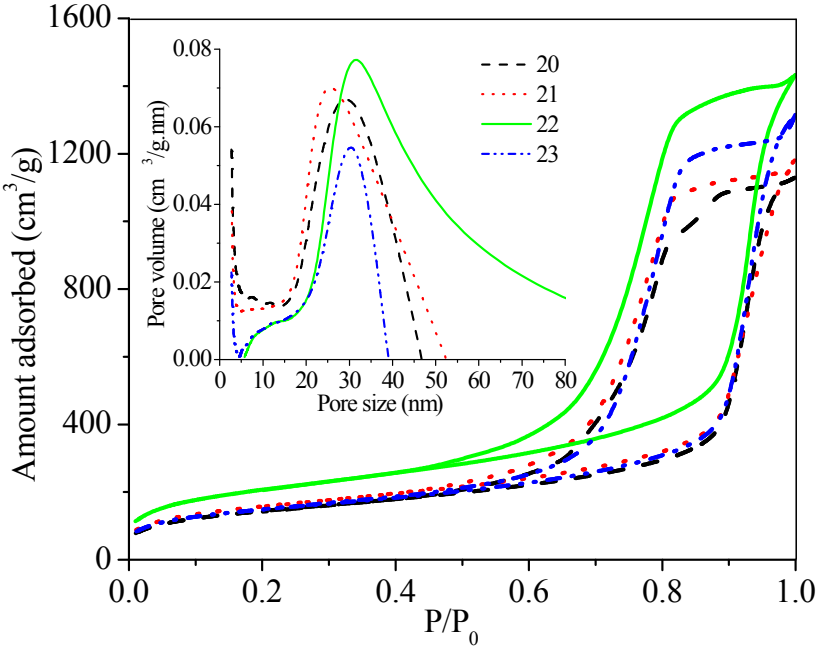

Figure 3-5. Stability tests for MCF. Sample numbers as in Table 3.1.

Table 3-1. Characterization results obtained from nitrogen adsorption data for different stability tests.

#	Sample	Treatment	Pore size (nm)	Pore volume (cm^3g^{-1})	Surface Area (m^2g^{-1})
1	APTS-SBA-15	none	7.8	0.29	190
2	APTS-SBA-15	Stirred in water for 5 min	-	0.04	20
3	APTS-SBA-15	Stirred in water for 5 min, then acetone	7.2	0.37	239
4	SBA-15	none	8.2	1.15	822
5	SBA-15	Stirred in water for 5 min	8.4	0.88	656
6	SBA-15	Boiled in water for 5 h	9.3	0.92	611
7	PE-MCM-41	none	9.3	2.31	1053
8	PE-MCM-41	Stirred in water for 5 min	-	0.19	700
9	PE-MCM-41	Stirred in water for 5 min dried and degassed at ambient temperature	-	0.27	655
10	PE-MCM-41	Stirred in water for 5 h	-	0.27	705
11	PE-MCM-41	Boiled in water for 5 h	-	0.45	787
12	PE-MCM-41	Stirred in water for 5 h then acetone.	9.4	2.29	1055
13	PE-MCM-41	Boiled in water for 5 h then acetone.	9.4	2.20	929
14	PE-MCM-41	Boiled in water for 1 week then acetone.	21.4	1.94	415
15	PE-MCM-41	Stirred in water for 1 week then acetone.	9.0	2.23	1106
16	MCF-F	none	21.9	2.36	598
17	MCF-F	Stirred in water for 5 min	23.5	2.39	560
18	MCF-F	Boiled in water for 5 h	35.3	3.12	524
19	MCF-F	Boiled in water for 1 week	28.4	1.95	352
20	MCF	none	18.4	1.74	523
21	MCF	Stirred in water for 5 min	18.1	1.81	571
22	MCF	Stirred in water for 5 h	17.0	2.19	750
23	MCF	Boiled in water for 5 h	20.8	2.03	535

3.4.2 Effect of synthesis conditions on APTS-SBA-15 stability

APTS-SBA-15 was found to be a good candidate for adsorption of heavy metals in aqueous solutions [28-31]. Hence, it is important to investigate the stability of this material under different harsh adsorption-regeneration conditions. The structural properties of the APTS-SBA-15 prepared by co-condensation under different synthesis conditions are presented in Fig. 3.6 - 9 and Table 3.2. N_2 adsorption–desorption isotherms for all samples before any treatment correspond to type IV isotherms according to the IUPAC classifications. The isotherms show hysteresis loops at $P/P_0 = 0.6–0.9$, characteristic of capillary condensation an evaporation in uniform pores. Table 3.2 shows that the surface area of the samples depends on the pore diameter and organic content. As expected, samples with larger pore diameters and higher organic content have lower surface area.

The changes in the structural properties of all the samples after being subjected to stability tests followed by nitrogen adsorption and TGA analysis are presented in Fig. 3.6 - 9 and Table 3.2. For APTS-SBA-15-100, treatment in water at room temperature caused a strong structural degradation as shown in Fig. 3.6, with extensive broadening of pore size distributions. The decreasing surface area and pore volume confirmed the deterioration of the textural structure of APTS-SBA-15-100 when placed in aqueous media. The surface area of 486 m^2g^{-1} for the as-synthesized sample (APTS-SBA-15-

100) decreased to 310, 27, and 85 m^2g^{-1} for APTS-SBA-15-100-EDTA, APTS-SBA-15-100-A and APTS-SBA-15-100-AB, respectively. The pore volume also droped greatly for APTS-SBA-15-100-A and APTS-SBA-15-100-AB. It appears then that the structural integrity of the APTS-SBA-15-100 was not maintained under any of the three treatments.

Galarneau et al. [12] related the poor stability of SBA-15 aged at 100 °C to the presence of micropores, which promotes silica solubilization even at room temperature. They showed that high aging temperature is a promoter to silanol groups condensation to $\equiv Si-O-Si \equiv$ siloxane bridges leading to higher polymerization and lower micropores content [6]. Cheng et al. [32] showed that higher synthesis temperature leads to an increased fraction of $Si(OSi)_4$ compared to $Si(OSi)_3OH$ i.e. to more highly condensed silicate walls. Thus, it is expected that higher silica condensation in APTS-SBA-15-130 minimizes major restructuration of the material in aqueous solutions as shown in Fig. 3.7. N_2 adsorption measurements showed that the pore diameter of the sample prepared at 130°C increased from 8.0 nm to 9.2 nm, since at higher temperature the effective volumes of the surfactant increase leading to increases of pore diameter and volumes after template removal [33]. It is clear that APTS-SBA-15-130 was very stable under different water treatments at room temperatures. After EDTA treatment, the surface area and pore volume increased as a result of decreasing organic content in the sample from 1.97 to1.64 $mmolg^{-1}$. After acidic treatment, the sample exhibited type IV nitrogen adsorption isotherm (Fig. 3.7), implying the good retention of the uniform mesostructure. Treating APTS-SBA-15-130-A with basic solution resulted in an increase in surface area from 551 to 870 m^2g^{-1} and in mesopore volume from 0.84 to 1.13 cm^3g^{-1} (Table 3.2) compared to APTS-SBA-15-130-A and an increase in surface area from 650 to 870 m^2g^{-1} and in mesopore volume from 0.64 to 1.13 cm^3g^{-1} compared to APTS-SBA-15-130. This is mainly because of decrease of organic content in the sample from 1.97 for APTS-SBA-15-130 to 1.64 $mmolg^{-1}$ for APTS-SBA-15-130-A and 1.47 $mmolg^{-1}$ for APTS-SBA-15-130-AB. These results confirmed that, compared with APTS-SBA-15-100, the sample aged at 130 °C has a better stability.

Addition of various inorganic salts such as $(NH_4)_2SO_4$ or KCl in the synthesis, led to higher degree of silica condensation thus, better stability. Addition of KCl or SO_4^{2-} might influence the hydrolysis and condensation kinetics of the silica precursors. Moreover, they might increase the stability of the micelle structure and facilitate the formation of well-ordered mesoporous silica [9]. For APTS-SBA-15-KCl, the strongest effect on the material structure occurred after EDTA treatment as shown in Fig. 3.8, but the material still maintained its mesoporosity. After EDTA treatment, the surface area and pore volume increased as a result of decreasing organic content in the sample from 4.04 to 1.81 $mmolg^{-1}$, which is related to removing residual template from the silica structure. After

acidic treatment, Fig. 3.8 shows that the sample was able to maintain a uniform mesostructure. Treating APTS-SBA-15-KCl with basic solution resulted in an increase in surface area from 509 to 673 m^2g^{-1} and in mesopore volume from 0.59 to 0.75 cm^3g^{-1} as a result of decreasing the organic content from 2.24 to1.68 $mmolg^{-1}$. For APTS-SBA-15-SO_4^{2-}, the material shows very good retention of the structural properties as shown in Fig. 3.9. After any of the treatments used, the surface area and pore volume increased as a result of decreasing organic content in the sample from 4.36 for APTS-SBA-15-SO_4^{2-} to 2.05, 3.81 and 3.41 $mmolg^{-1}$ after EDTA, acidic, and basic treatment, respectively. This decrease in organic was accompanied by increased surface area and pore volume for the three samples as shown in Table 3.2.

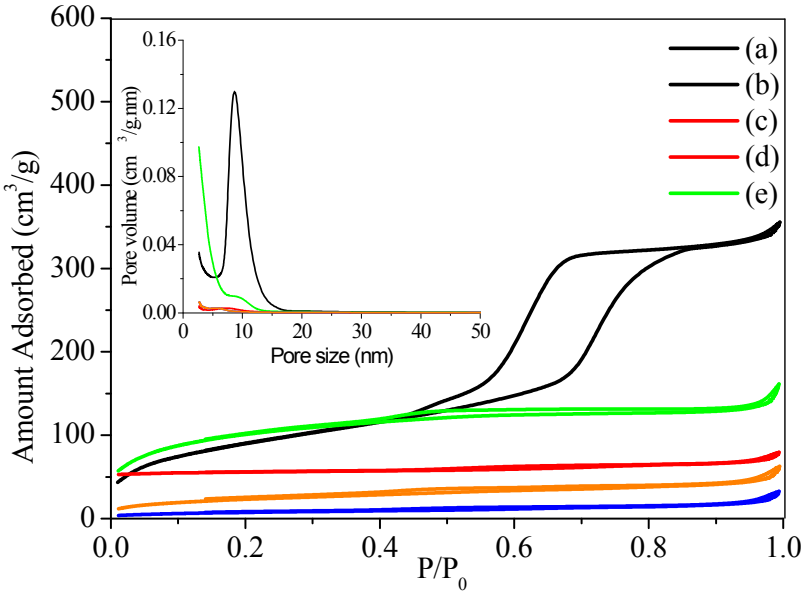

Figure 3-6. Nitrogen adsorption-desorption isotherms and pore size distribution for APTS-SBA-15-100 (a), APTS-SBA-15-100-W (b), APTS-SBA-15-100-EDTA (c), APTS-SBA-15-100-A (d), and APTS-SBA-15-100-AB (e).

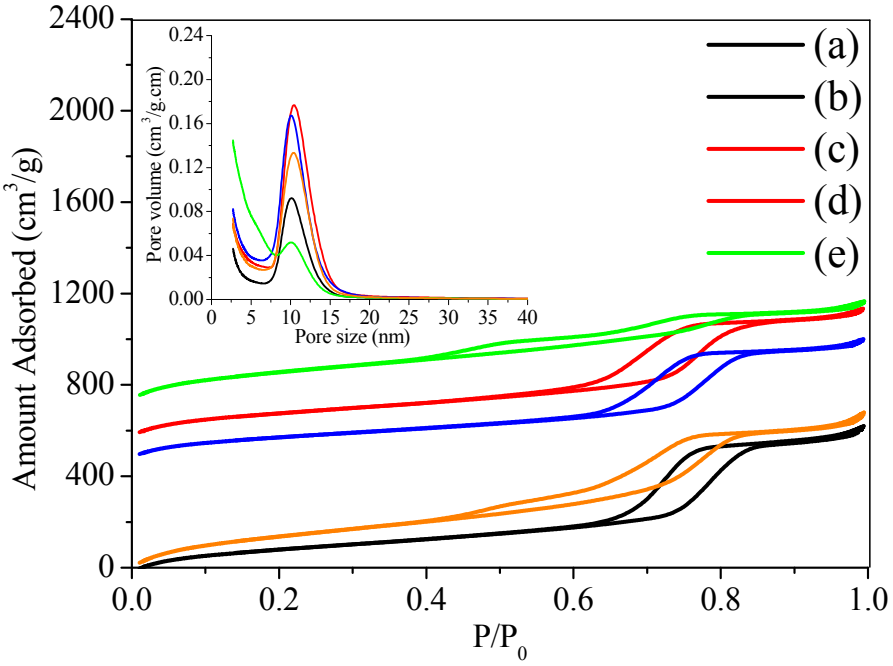

Figure 3-7. Nitrogen adsorption -desorption isotherms and pore size distribution for APTS-SBA-15-130 (a), APTS-SBA-15-130-W (b), APTS-SBA-15-130-EDTA (c), APTS-SBA-15-130-A (d), and APTS-SBA-15-130-AB (e).

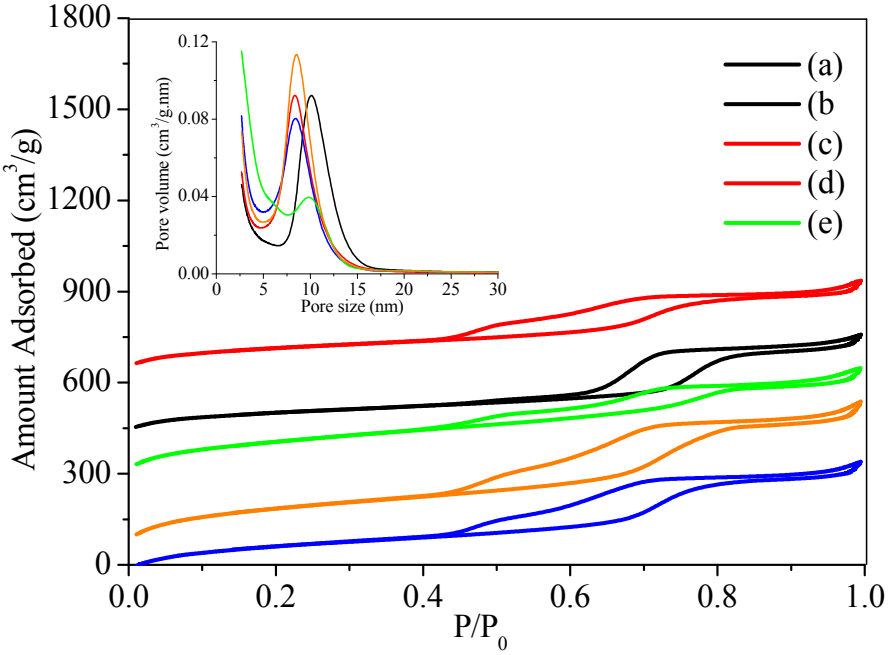

Figure 3-8. Nitrogen adsorption-desorption and pore size distribution isotherms for APTS-SBA-15-KCl (a), APTS-SBA-15-KCl-W (b), APTS-SBA-15-KCl-EDTA (c), APTS-SBA-15-KCl-A (d), and APTS-SBA-15-KCl-AB (e).

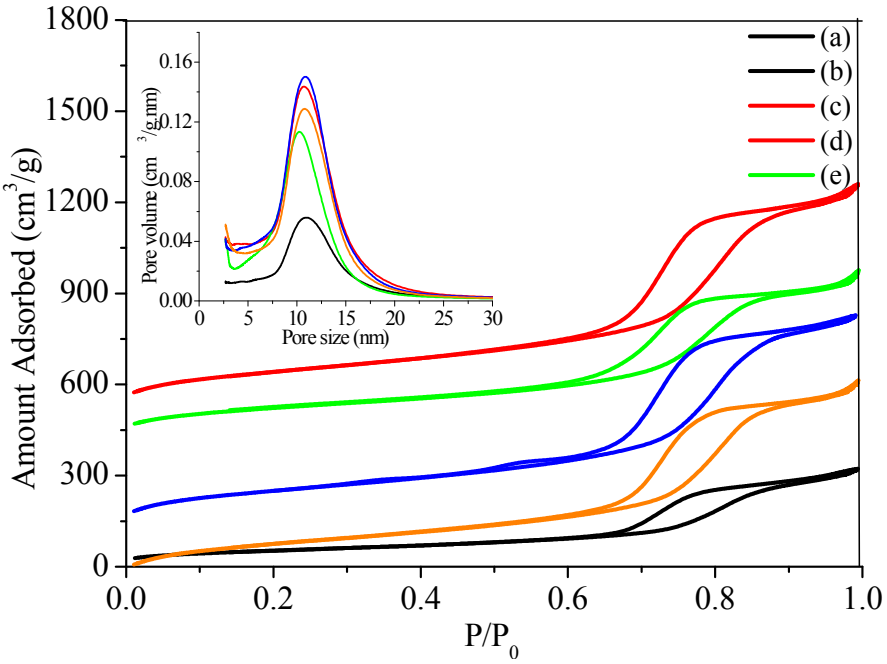

Figure 3-9. Nitrogen adsorption-desorption isotherms and pore size distribution for APTS-SBA-15-SO_4^{2-} (a), APTS-SBA-15-SO_4^{2-}-W (b), APTS-SBA-15-SO_4^{2-}-EDTA (c), APTS-SBA-15-SO_4^{2-}-A (d), and APTS-SBA-15-SO_4^{2-}-AB (e).

Table 3-2. Results of nitrogen adsorption and TGA analysis of S-100, S-130, S-KCl, and S-SO_4^{2-} after being subjected to different stability tests.

Sample	Surface area (m^2/g)	Pore size (nm)	Pore volume (cm^3/g)	Organic content (mmol/g)
APTS-SBA-15-100	486	8.0	0.52	2.97
APTS-SBA-15-100-EDTA	310	-	0.29	2.27
APTS-SBA-15-100-A	27	-	0.03	2.40
APTS-SBA-15-100-AB	85	-	0.07	1.92
APTS-SBA-15-130	650	9.2	0.54	1.97
APTS-SBA-15-130-EDTA	753	6.1	0.75	1.64
APTS-SBA-15-130-A	551	8.6	0.84	1.64
APTS-SBA-15-130-AB	870	7.5	1.13	1.47
APTS-SBA-15-KCl	350	9.0	0.50	4.04
APTS-SBA-15- KCl-EDTA	570	6.6	0.55	1.81
APTS-SBA-15- KCl-A	509	7.7	0.59	2.24
APTS-SBA-15- KCl-AB	673	7.6	0.75	1.68
APTS-SBA-15- SO_4^{2-}	196	11.0	0.47	4.36
APTS-SBA-15- SO_4^{2-}-EDTA	326	10.0	0.78	2.05
APTS-SBA-15- SO_4^{2-}-A	483	9.76	1.1	3.81
APTS-SBA-15- SO_4^{2-}-AB	469	9.9	0.96	3.14

3.5 Conclusions

Ordered mesoporous silicas, designated as SAB-15, APTS-SBA-15, PE-MCM-41, MCF-F and MCF, were synthesized and subjected to different water treatments before being dried. It was proved that structural properties of mesoporous silicates are mainly preserved or destroyed during the drying process and not during the treatment itself. In addition, the pore size of the material and the nature of liquid inside the pores during drying are factors that can influence the structural stability. Furthermore, the structural stability of amine-modified SBA-15 prepared by co-condensation under a variety of adsorption-regeneration conditions was assessed. It was shown that harsh adsorption-regeneration conditions lead to strong degradation of the APTS-SBA-15 material prepared by conventional method and aged at temperature close to 100 °C. Enhanced stability could be achieved by aging at 130 °C instead of 100 °C, addition of KCl or $(NH_4)_2SO_4$ producing materials with dramatically increased stability under all stability tests.

References

[1] M. Hartmann, Ordered mesoporous materials for bioadsorption and biocatalysis, *Chem. Mater.* 17 (2005) 4577-4593.

[2] A. Sayari, S. Hamoudi, Periodic mesoporous silica-based organic-inorganic nano-composite materials, *Chem. Mater.* 13 (2001) 3151-3168.

[3] X.S. Zhao, F. Audsley, G.Q. Lu, Irreversible change of pore structure of MCM-41 upon hydration at room temperature, *J. Phys. Chem. B* 102 (1998) 4143-4146.

[4] C.H. Rhee, J.S. Lee, Thermal and chemical stability of titanium-substituted MCM-41**,** *Catal. Lett.* 40 (1996) 261-264.

[5] R. Ryoo, C.H. Ko, J.M. Kim, R. Howe, Preparation of nanosize Pt clusters using ion exchange of $[Pt(NH_3)_4]^{2+}$ inside mesoporous channels of MCM-41, *Catal. Lett.* 37 (1996) 29-33. [6] F. Zhang, Y. Yan, H. Yang, Y. Meng, C. Yu, B. Tu, D. Zhao, Understanding the effect of wall structure on the hydrothermal stability of mesostructured silica SBA-15, *J. Phys. Chem. B* 109 (2005) 8723-8732.

[7] K. Cassiers, T. Linssen, M. Mathieu, M. Benjelloun, K. Schrijnemakers, P. Van Der Voort, P. Cool, E.F. Vansant, A detailed study of thermal, hydrothermal, and mechanical stabilities of a wide range of surfactant assembled mesoporous silicas, *Chem. Mater.* 14 (2002) 2317-2324.

[8] Y. Du, X. Lan, S. Liu, Y. Ji, Y. Zhang, W. Zhang, F.S. Xiao, The search of promoters for silica condensation and rational synthesis of hydrothermally stable and well ordered mesoporous silica

materials with high degree of silica condensation at conventional temperature, *Microporous Mesoporous Mater.* 112 (2008) 225-234.

[9] X. Wang, Y.H. Tseng, J.C.C. Chan, S. Cheng, Direct synthesis of highly ordered large-pore functionalized mesoporous SBA-15 silica with methylaminopropyl groups and its catalytic reactivity in flavanone synthesis, *Microporous Mesoporous Mater.* 85 (2005) 241-251.

[10] T. Jiang, H. Tao, J. Ren, X. Liu, Y. Wang, G. Lu, Fluoride ions assistant synthesis of extremely hydrothermal stable Al-SBA-15 with controllable Al content**,** *Microporous Mesoporous Mater.* 142 (2011) 341-346.

[11] G. Chen, L. Wang, J. Lei, J. Zhang, F- assistant synthesis of ultra-hydrothermally stable mesoporous silica by using nonionic organosilicon surfactant as templates**,** *Microporous Mesoporous Mater.* 124 (2009) 204-209.

[12] A. Galarneau, M. Nader, F. Guenneau, F. Di Renzo, A. Gedeon, Understanding the stability in water of mesoporous SBA-15 and MCM-41, *J. Phys. Chem. C* 111 (2007) 8268-8277.

[13] Z. Luan, C.F. Cheng, W. Zhou, J. Klinowski, Mesopore molecular sieve MCM-41 containing framework aluminum, *J. Phys. Chem.* 99 (1995) 1018-1024.

[14] M. Kruk, M. Jaroniec, A. Sayari, A unified interpretation of high-temperature pore size expansion processes in MCM-41 mesoporous silicas, *J. Phys. Chem. B* 103 (1999) 4590-4598.

[15] A. Corma, Q. Kan, M.T. Navarro, J. Pérez-Pariente, F. Rey, Synthesis of MCM-41 with different pore diameters without addition of auxiliary organics, *Chem. Mater.* 9 (1997) 2123-2126.

[16] D. Li, Y.Han, J. Song, L. Zhao, X. Xu, Y. Di, F.S. Xiao, High-temperature synthesis of stable ordered mesoporous silica materials by using fluorocarbon–hydrocarbon surfactant mixtures, *Chem. Eur. J.* 10 (2004) 5911–5922.

[17] T. Tatsumi, K.A. Koyano, Y. Tanaka, S. Nakata, Stabilization of M41S materials by trimethylsilylation**,** *Stud. Surf. Sci. Catal.* 117 (1998) 143-150.

[18] K.A. Koyano, T. Tatsumi, Y. Tanaka, S. Nakata, Stabilization of mesoporous molecular sieves by trimethylsilylation**,** *J. Phys. Chem. B* 101 (1997) 9436-9440.

[19] D. Zhao, Q. Huo, J. Feng, B.F. Chmelka, G.D. Stucky, Nonionic triblock and star diblock copolymer and oligomeric sufactant syntheses of highly ordered, hydrothermally stable, mesoporous silica structures, *J. Am. Chem. Soc.* 120 (1998) 6024-6036.

[20] C. J. Brinker, G. W. Scherer, Sol-gel science: The physics and chemistry of sol-gel processing, Academic Press, Inc., San Diego, 1990.

[21] R. B. Bird, W. E. Stewart, E. N. Lightfoot, Transport Phenomena, 2nd edition, John Wiley & Sons, Inc. New york, 2002.

[22] P. Schmidt-Winkel, D. Zhao, P. Yang, B. F. Chmelka, G. D. Stucky, Mesocellular siliceous foams with uniformly sized cells and windows, *J. Am. Chem. Soc.* 121 (1999) 254-255.

[23] A. Sayari, Y. Yang, Highly ordered MCM-41 silica prepared in the presence of decyltrimethylammonium bromide, *J. Phys. Chem. B* 104 (2000) 4835-4839.

[24] A. Sayari, Y. Yang, M. Kruk, M. Jaroniec, Expanding the pore size of MCM-41 silicas: use of amines as expanders in direct synthesis and postsynthesis procedures, *J. Phys. Chem. B* 103 (1999) 3651-3658.

[25] M. Kruk, M. Jaroniec, A. Sayari, Application of large pore MCM-41 molecular sieves to improve pore size analysis using nitrogen adsorption measurements, *Langmuir* 13 (1997) 6267-6273.

[26] P. Harlick, A. Sayari, Applications of pore-expanded mesoporous silica. 3. Triamine silane grafting for enhanced CO_2 adsorption, *Ind. Eng. Chem. Res.* 45 (2006) 3248-3255.

[27] http://www.hbcpnetbase.com/: Online HandBook of Chemistry & Physics, 91st Edition, 2010-2011, page 6-128

[28] E. Da'na, A. Sayari, Adsorption of copper on amine-functionalized SBA-15 prepared by co-condensation: Equilibrium properties, *Chem. Eng. J.* 166 (2011) 445-453.

[29] E. Da'na, N. D. Silva, A. Sayari, Adsorption of copper on amine-functionalized SBA-15 prepared by co-condensation: Kinetics properties, *Chem. Eng. J.* 166 (2011) 454-459.

[30] E. Da'na, A. Sayari, Optimization of copper removal efficiency by adsorption on amine-modified SBA-15: Experimental design methodology, *Chem. Eng. J.* 167 (2011) 91-98.

[31] E. Da'na, A. Sayari, Effect of regeneration conditions on the cyclic performance of amine-modified SBA-15 for removal of copper from aqueous solutions: Composite surface design methodology, *Desalination* 277 (2011) 54-60.

[32] C.F. Cheng, W. Zhou, D.H. Park, J. Klinowski, M. Hargreaves, Controlling the channel diameter of the mesoporous molecular sieve MCM-41, *J. Chem. Soc.* 93 (1997) 359-363.

[33] Y. Wang, B. Zibrowius, C.M. Yang, B. Spliethoff, F. Schüth, Synthesis and characterization of large-pore vinyl-functionalized mesoporous silica SBA-15, *Chem. Commun.* (2004) 46-47.

Chapter 4

Adsorption of copper on amine-functionalized SBA-15 prepared by co-condensation: Equilibrium properties

Chem. Eng. J. 166 (2011) 445-453

Abstract.

SBA-15 functionalized with 3-aminopropyltrimethoxy-silane was synthesized by co-condensation and used as adsorbent for Cu^{2+} ions in aqueous solution. The adsorption capacity increased dramatically with increasing temperature, initial copper concentration and pH (up to ca. 6.5). Under suitable conditions, the material exhibited high adsorption capacity even at very low copper concentration. Qualitative estimates of the thermodynamic parameters showed that the overall adsorption process is spontaneous ($\Delta G° < 0$) and endothermic ($\Delta H° > 0$). The adsorption isotherms of Cu^{2+} on propylamine-functionalized SBA-15 silica were best fitted by the Sips and Redlich–Peterson models. Regeneration of the adsorbent was investigated by treatment of the copper-loaded material with aqueous solution of 0.1 M HCl then 0.1 M $NaHCO_3$ or by 0.1 M EDTA solution. The adsorption uptake after ten cycles was 90% and 60% of the fresh material adsorption capacity for regeneration with EDTA and acid/base treatment, respectively.

4.1 Introduction

Because of the widespread presence of copper in industrial applications, e.g. electrical, electro-plating, metal finishing and paint industries, residual metal is often found in wastewater. Owing to the toxicity of copper, the World Health Organization (WHO) recommended the maximum acceptable concentration of this element in drinking water to be 2.0 mgL^{-1} [1]. Metal separation via adsorption is a very promising technique because of its simplicity and reversibility. Therefore, extensive research effort has been directed towards the development of new adsorbents for the removal of heavy metals from wastewater.

Periodic mesoporous materials exhibit many attractive characteristics such as large BET surface area, high porosity, controllable and narrowly distributed pore sizes, and often an ordered pore arrangement [2]. Thus, the development of functionalized mesoporous adsorbents for heavy metal ions using incorporated ligands with appropriate functional groups has generated considerable interest [3]. SBA-15 is among the most popular mesoporous silicas because of its large, adjustable pores (5–30 nm), which allow easier accessibility of target species to the inner surface of the material, leading to fast kinetics of chemical or physical processes, and also because of its thick pore walls, around 4 nm, which provide enhanced mechanical stability.

Two different routes were reported in the literature for the synthesis of amine-functionalized materials, namely co-condensation of the desired aminosilane with the silica precursor such as tetraethylorthosilicate (TEOS) [4-8], and post-synthesis grafting of the desired aminosilane onto the silica surface [9-16]. Compared to post-synthesis procedures, the direct co-condensation pathway often offers a better control of the resultant materials in terms of higher and more uniform surface coverage of the organic functionalities without the possible blockage of the mesopores [17-19]. In addition, co-condensation is preferred because of its simplicity and lower consumption of organic precursor. However, despite the advantages of SBA-15 as support and for co-condensation as a preparation route, amine-modified SBA-15 prepared by this method was found to have poor copper adsorption performance [20]. Since such material is synthesized in strong acidic medium, this leads to the protonation of amine, thus to the lack of adsorption capacity [21]. It was also reported that some of the amine groups might be H-bonded to neighboring surface hydroxyl groups, further diminishing their availability for adsorption [22].

To achieve the best performance for a copper ions adsorbent, a set of conditions must be met including the following (i) the occurrence of an open pore structure and accessible adsorption sites, e.g. large pore diameter; (ii) the adsorbent must be structurally stable under adsorption and regeneration conditions, e.g. treatment with acidic or basic solutions should not cause any structural damage; (iii) good contact between the copper ions and the adsorption sites, e.g. enhance the mobility of the ions within the pores and reduce the repulsion between the positive copper ions and the adsorbent surface by supplying enough energy to overcome these forces or by working under suitable pH conditions to avoid a positively charged adsorbent surface. The performance of an adsorbent is related to (i) its characteristics (e.g. density and distribution of adsorption sites, structural properties), (ii) the properties of the adsorbate (e.g. concentration, size, charge, structure), and (iii) the solution conditions (e.g. pH, temperature, ionic strength). Thus, the objectives of this chapter were (i) to determine the thermodynamic and the equilibrium properties of copper adsorption on amine-functionalized SBA-15

prepared by co-condensation, (ii) to investigate the effect of the experimental parameters such as temperature, concentration and pH on the adsorptive properties, and (iii) to compare the regeneration and recycling of adsorbent using acid/base treatment or EDTA complexation.

4.2 Materials and methods

4.2.1 Chemicals

Tetraethylorthosilicate (TEOS) used as the silica source for SBA-15 was supplied by Aldrich. Triblock poly(ethylene oxide)-*b*-poly(propylene oxide)-*b*-poly(ethylene oxide) copolymer Pluronic P123 (MW = 5800) purchased from Aldrich was used as structure directing agent. The functionalization agent, obtained from Sigma–Aldrich was 3-aminopropyltrimethoxy-silane, herein referred to as APTS. Ultra high purity grade nitrogen and certified gas mixtures of 5% CO_2 balance N_2 were supplied by BOC Canada. All reagents and gases were used without further purification.

4.2.2 Adsorbent synthesis

SBA-15 was prepared according to Zhao et al. [23] with addition of KCl, for enhanced stability and ordering. The procedure was as follows: 4.0 g of P123 and 8 g KCl were dissolved in 30 mL of water and 120 mL of a 2 M HCl solution at 40 °C. Then, 8.5 g (40.8 mmol) of TEOS was added and prehydrolyzed for 2 h before adding 1.08 g (6.0 mmol) of APTS which corresponds to APTS/TEOS molar ratio of 0.15. The mixture was stirred at the same temperature for 20 h, then heated at 100 °C for 24 h in static conditions. The white solid product was collected by filtration, dried in air at room temperature for 1 day, and then extracted with ethanol (140 mLg^{-1}) at the same temperature for 24 h to remove the organic template. The material was then filtered and dried under vacuum. It will be denoted as APTS-SBA-15. To ensure complete removal of template, 1 g of the ethanol-extracted material was stirred in 50 mL of aqueous 0.1 M HCl for 1 h, filtered and dried, then neutralized in 50 mL of 0.1 M $NaHCO_3$ for 1 h and finally filtered and dried under vacuum at 100 °C for 3 h. The final material will be referred to as APTS-SBA-15-AB.

4.2.3 Characterization

4.2.3.1 Nitrogen adsorption–desorption isotherms

The structural properties of the samples before and after acid/base treatment were determined by nitrogen adsorption at 77 K using a Micromeritics ASAP 2020 volumetric apparatus. Prior to each analysis, the samples were degassed under vacuum at 60 °C for 3 – 5 h. The surface area was determined by the BET method, whereas the pore size distribution was calculated using the Kruk–

Jaroniec–Sayari (KJS) approach [24]. The pore volume was calculated as the amount of liquid nitrogen adsorbed at $P/P_0 = 0.995$.

4.2.3.2 Thermal gravimetric analysis (TGA)

The amine content was determined using a thermogravimetric analyzer (Q500 TGA, TA Instruments) according to the method developed by Harlick and Sayari [25]. In the same experiment, CO_2 was used as a probe molecule to determine the accessibility of the amine functional groups within the pore channels. Briefly, the sample was first treated in a flow of ultra high purity (UHP) N_2 at 200 °C for a period of 2 h to remove preadsorbed moisture and any methanol stemming from the hydrolysis of unreacted methoxy groups. Then, it was equilibrated at 25 °C in a flow of 5% CO_2 in N_2 for 2 h. The weight gain corresponded to the CO_2 adsorption capacity. Subsequently, the organic layer was decomposed by heating at 10 °C/min to 800 °C under flowing N_2, then at 10 °C/min to 1000 °C in flowing air. The material was kept under isothermal conditions for 15 min. The amount of APTS was calculated from the weight loss, taking into consideration the CO_2 desorption, which occurs typically below 150 °C.

4.2.3.3 Elemental (CHN) analysis

The amine loading was also determined by elemental analysis on representative samples using a TF Flash 1112 analyzer (Thermo Finnigan). Weighed samples placed into capsules were flash-combusted at about 1800 °C and the gases were carried by helium through a reduction/oxidation column to yield N_2, CO_2 and H_2O. The gases were separated and quantified as they pass through a gas chromatograph column. The amine loading was calculated from the nitrogen content.

4.2.3.4 Scanning electron microscopy (SEM)

SEM was performed using a high resolution, JSM-7500F field emission scanning electron microscope from JEOL.

4.2.3.5 NMR measurements

^{13}C CP MAS NMR spectra were collected at room temperature on a Bruker ASX200 instrument in a magnetic field of 4.7 T (the resonance frequencies were 50.3 and 39.7 MHz, respectively).

4.2.3.6 Zero point charge (pH_{ZPC}) and potentiometric acid/base titrations

The surface charge properties of the APTS-SBA-15-AB were evaluated by batch equilibration technique [26]: a 100 mg sample of APTS-SBA-15-AB was introduced into a 100 mL of 0.1 M NaCl solution. The initial pH value (pH_i) of the NaCl solution was adjusted from ca. 3.0 to 11.0 by addition of 0.1 M HNO_3 or 0.1 M NaOH. The suspension was allowed to equilibrate at 20 °C for 24 h by stirring, then filtered and the pH value (pH_e) was measured again.

The surface charge properties of the APTS-SBA-15-AB were investigated by potentiometric acid/base titrations [27]: a 50 mg sample was suspended in a titration cell containing 50 mL of distilled water. The suspension was allowed to equilibrate for 24 h under continuous stirring, and then purged with N_2 for 30 min. It was subsequently divided into two portions, one each for the alkalimetric and the acidimetric titrations, using 0.1 M NaOH and 0.1 M HNO_3, respectively. In all titrations, the pH was measured with an Orion 5 stars instrument 20 min after each addition of acid or base to ensure that pH equilibrium was attained.

4.2.4 Preparation of copper solutions

Copper solutions were prepared by dissolving copper acetate mono-hydrate Cu $(CH_3COO)_2{\cdot}H_2O$ in distilled water to obtain solutions of different concentrations. The pH of the solutions was adjusted by addition of 0.1 M HNO_3 or 0.1 M NaOH.

4.2.5 Equilibrium adsorption measurements and modeling

To measure the equilibrium distribution of copper ions between the adsorbent and the liquid phase, an accurately weighed amount (100 mg) of adsorbent was continuously stirred in 100 mL of copper solutions with different initial concentrations from 5 to 320 ppm. The solution temperature was monitored using a temperature-controlled water bath. Agitation was maintained at 300 rpm for 4 h, which was verified to be sufficient to reach equilibrium. After filtration of the adsorbent, the concentration of copper in the solution was determined by inductivity coupled plasma (ICP) using a ICP-OES Varian Vista-Pro CCD spectrometer. The amount of metal adsorbed at equilibrium, q_e (mgg^{-1}), was thus calculated by:

$$q_e = \frac{(C_i - C_e)V}{W} \tag{4.1}$$

where C_i, C_e, V, and W are the initial and equilibrium concentrations (mgL^{-1}), volume of solution (L), and weight of adsorbent (g), respectively.

The isotherm models of Langmuir, Freundlich, Sips, and Redlich–Peterson were used to describe the equilibrium adsorption isotherms. The equations of the model isotherms are given below.

4.2.5.1 Langmuir isotherm

$$q_e = \frac{q_m K_L C_e}{1 + K_L C_e} \tag{4.2}$$

where q_m is the quantity of Cu^{2+} adsorbed at saturation or monolayer capacity (mgg^{-1}) and K_L is the Langmuir constant (Lg^{-1}).

4.2.5.2 Freundlich isotherm

$$q_e = K_F C_e^{\,1/n} \tag{4.3}$$

where K_F is the Freundlich constant and n is the Freundlich exponent (dimensionless).

4.2.5.3 Sips isotherm

$$q_e = \frac{q_m K_S C_e^{\,1/n}}{1 + K_S C_e^{\,1/n}} \tag{4.4}$$

where q_m is the quantity of Cu^{2+} adsorbed at saturation or monolayer capacity (mgg^{-1}) and K_S $(mgL^{-1})^{-1/n}$ is the Sips constant.

4.2.5.4 Redlich–Peterson isotherm

$$q_e = \frac{K_{RP} C_e}{1 + a_{RP} C_e^{\,\beta}} \tag{4.5}$$

where K_{RP} (Lg^{-1}) and a_{RP} $(mgL^{-1})^{-\beta}$ are the Redlich–Peterson constants and β is the Redlich–Peterson exponent (dimensionless).

The Langmuir, Freundlich, Sips, and Redlich–Peterson isotherms were used to fit the experimental data employing the linear fitting. In addition, the models were evaluated using the relative error function, which represents the summation of the squared differences of Cu^{2+} ions uptake

by the adsorbent predicted by the models and the actual quantity adsorbed, q_e, measured experimentally.

The linear region of the isotherms (see Section 4.3.5) was used to calculate the equilibrium constant (K_c) at 293, 313 and 333 K from the slope of q_e vs. C_e. Qualitative estimation of the thermodynamic properties of the adsorption process such as enthalpy change ($\Delta H°$), entropy change ($\Delta S°$) and Gibbs free energy change ($\Delta G°$) was carried out using the following equations [28]:

$$\Delta G° = -RT \ln K_c \tag{4.6}$$

$$\ln K_c = \frac{\Delta S°}{R} - \frac{\Delta H°}{RT} \tag{4.7}$$

where R is the ideal gas constant (8.314 $JK^{-1}mol^{-1}$), and T is the temperature in Kelvin. $\Delta H°$ and $\Delta S°$ were obtained from the slope and intercept of Van't Hoff plot of ln K_c vs. $1/T$.

4.2.6 Effect of pH

The solution pH may affect the surface charge of the adsorbents through protonation of the functional groups [21], protonation of the free surface hydroxyl groups [27], as well as the degree of ionization and hydrolysis of the species present in solution. To investigate the effect of pH, a set of experiments were performed at 293 K and several pH values between 4.0 and 6.7.

4.2.7 Regeneration of the adsorbent

The regeneration of the adsorbent was performed by two methods: (1) stirring the copper-loaded material in an aqueous solution of 0.1 M HCl for 1 h then neutralizing by stirring for 1 h in 0.1 M $NaHCO_3$ aqueous solution. The material was washed with distilled water and dried under vacuum at 373 K for 2 h; (2) treating the copper-loaded material with an aqueous 0.1 M sodium ethylene-diaminetetraacetic acid (EDTA) solution by stirring at 333 K for 1 h, followed by washing with distilled water and drying under vacuum at 373 K for 2 h. In both methods, the solid was used for ten successive adsorption–regeneration cycles.

4.3 Results and discussion

4.3.1 Material characterization

The nitrogen adsorption–desorption isotherms of APTS-SBA-15 and APTS-SBA-15-AB are presented in Fig. 4.1. Both samples exhibited Type IV isotherms implying that the mesostructure is highly stable

under acid/base treatment. The main structural characteristics determined experimentally are listed in Table 4.1. The APTS-SBA-15 exhibited pores averaging 7.9 nm in diameter, and a pore volume and surface area of 0.5 cm^3g^{-1} and 350 m^2g^{-1}, respectively. After the first acid/base treatment, although the mean pore size was almost the same (7.6 nm), the adsorbent exhibited significantly larger surface area (673 m^2g^{-1}) and pore volume (0.75 cm^3g^{-1}). This increase in surface area and pore volume is most likely associated with the removal of residual P123 block copolymer inside the pores as corroborated by the TGA results (Table 4.1). Furthermore, ^{13}C MAS NMR data provided direct evidence for the occurrence of P123 in ethanol-extracted APTS-SBA-15. Fig. 4.2A shows that this sample exhibits NMR signals at 18.0, 71.0, 74.0 and 75.9 ppm attributable to P123; whereas the sample that underwent acid/base treatment (Fig. 4.2B) showed only the three signals at 9.1, 21.4 and 43.2 associated with the surface-bound propylamine.

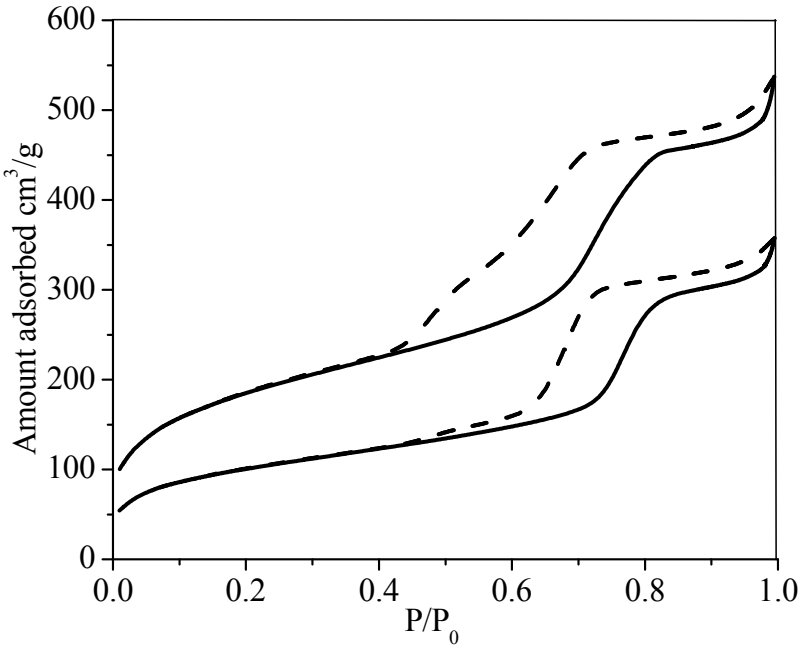

Figure 4-1. Nitrogen adsorption (solid line)-desorption (dashed line) isotherms for APTS-SBA-15-AB (upper) and APTS-SBA-15 (lower).

Table 4-1. Structural properties of APTS-SBA-15 and APTS-SBA-15-AB.

Sample	APTS-SBA-15	APTS-SBA-15-AB
Surface area (m^2g^{-1})	350	673
Pore size (nm)	7.9	7.6
Pore volume (cm^3g^{-1})	0.50	0.75
TGA amine content ($mmolg^{-1}$)	4.4	1.75
CHN amine content ($mmolg^{-1}$)	1.2	1.77
CO_2 adsorbed ($mmolg^{-1}$)	0.14	0.44
Cu^{2+} adsorbed ($mmolg^{-1}$)	0.05	0.21

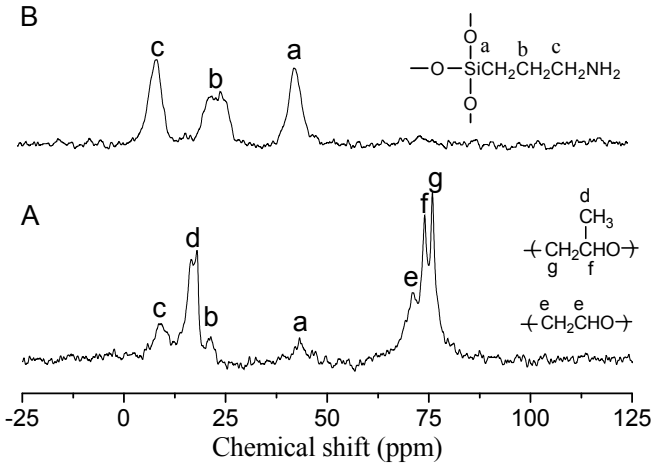

Figure 4-2. ^{13}C CP MAS NMR spectra of APTS-SBA-15 after ethanol-extracted (A), and after acid/base treatment (B).

Table 4.1 shows the amine content obtained by CHN elemental analysis and by TGA, CO_2 adsorption capacity obtained by TGA and copper adsorption capacity determined by ICP. The large difference in amine content obtained by the two methods for the ethanol-extracted APTS-SBA-15 sample indicates that the TGA-based value is overestimated. Indeed, the weight loss obtained by TGA of the ethanol-extracted sample did not correspond to only the decomposition of propylamine chains, but also to residual P123 polymer. Upon acid/base treatment, both amine content measurements were comparable, and the CO_2 and Cu^{2+} adsorption capacities increased significantly (Table 4.1). This is consistent with the complete removal of residual P123 by the acid treatment accompanied by amine protonation (Eq. (4.8)), and to the regeneration of the amine groups by sodium bicarbonate according

to Eq. (4.9). Furthermore, CHN elemental analysis showed that the amine content increased after acid/base treatment, this is mainly because it was calculated on the basis of the overall material, including the residual P123, if any. The CO_2/N ratio was calculated from the CO_2 adsorption capacity obtained by TGA and compared with the stoichiometric value of 0.5, corresponding to the formation of carbamate [29]. The percentage of amine groups available for adsorption increased from 24% to 52% after acid/base treatment of the sample. The enhanced CO_2 and Cu^{2+} adsorption capacity is associated with the increased accessibility of the amine groups. These results are consistent with the conclusions obtained from the nitrogen adsorption data discussed earlier. Aguado et al. [20] observed no copper adsorption using APTS-SBA-15 as prepared by co-condensation in spite of their significant nitrogen content and good structural and textural properties. This was most likely associated with the fact that the amine groups protonate under the acidic conditions of the material synthesis [21].

$$-NH_2 + H^+ \rightarrow -NH_3^+ \tag{4.8}$$

$$-NH_3^+ + HCO_3^- \rightarrow -NH_2 + "H_2CO_3" \tag{4.9}$$

Typical SEM images with different magnifications for APTS-SBA-15-AB are shown in Fig. 4.3. Fig. 4.3(a) reveals that the morphology of APTS-SBA-15-AB consists of rod-shaped particles aggregated into bundles approximately 20 μm in length and 1 μm in diameter. Higher magnification (Fig. 4.3(b)) shows that the particles are multifaceted and the pore channels run parallel to the particle main axis. Fig. 4.3(c) shows that APTS-SBA-15-AB exhibits a highly ordered hexagonal pore system, confirming the high stability of APTS-SBA-15 under acid/base treatment.

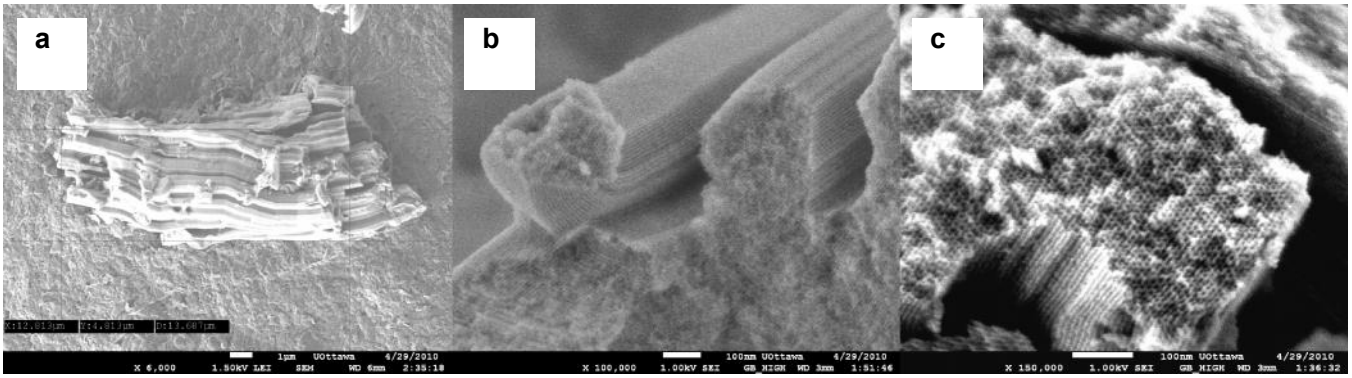

Figure 4-3 . SEM images of APTS-SBA-15-AB with different magnifications; bar of 1 μm for (a), and 100 nm for (b) and (c).

Since the surface charge of APTS-SBA-15-AB is a result of the protonation or deprotonation of surface hydroxyl as well as amine groups, one of the expected consequences of the pH_{ZPC}, which is

the pH value of the solution corresponding to a net surface charge of zero (Scheme 4.1-1), is the dependence of adsorption of copper on the solution pH. Fig. 4.4 shows the equilibrium pH_e vs. the initial pH_i obtained by the batch equilibration technique for a solid to solution ratio of 1 g/L. It is evident that APTS-SBA-15-AB acts as a buffer in a wide range of pH from ca. 4 to 10. This means that for all values of pH_i in this range, the pH_e is the same and equal to pH_{ZPC}, which was found to be 8.62. This value is very high and implies that in aqueous solution, as the pH decreases below 8.62, the $\equiv SiOH_2^+$ species will dominate and the APTS-SBA-15-AB surface will bear a progressively increasing positive charge (Scheme 4.1-2). The direct implication of the high pH_{ZPC} value is that the material is not an effective copper adsorbent in a wide range of pH as it bears positive charge at $pH < 8.62$ considering that for copper adsorption the pH value must be kept below 6.5 to avoid precipitation of copper hydroxide (*vide infra*).

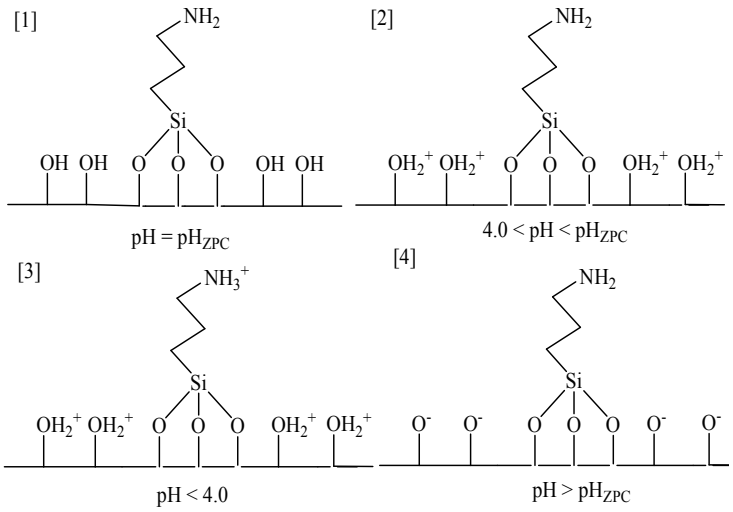

Scheme 4-1. Proposed surface of APTS-SBA-15-AB under different pH conditions.

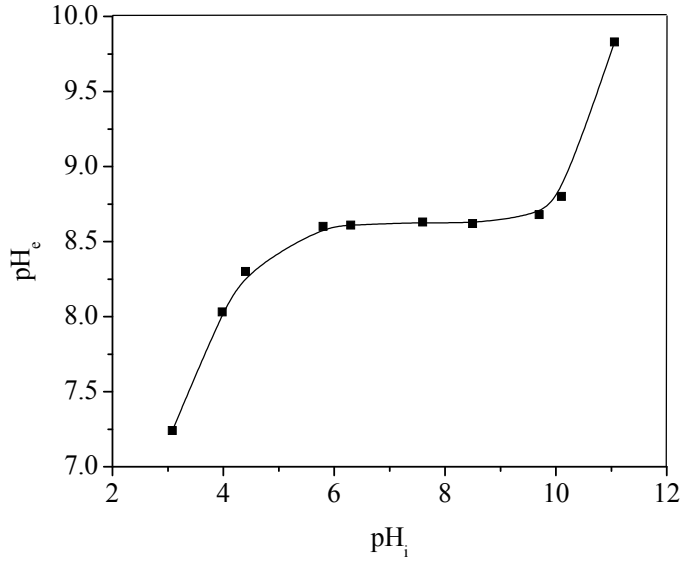

Figure 4-4. pH_e as a function of pH_i for solid to solution ratio of 1 g/L, time of equilibration 24 h and background electrolyte 0.1 M NaCl.

Fig. 4.5 shows the acid/base potentiometric titration data with adsorbent in the solution, and the theoretical pH values calculated for a solution without the adsorbent. The horizontal axis represents the amount of acid or base added to the solutions used for the acidimetric and alkalimetric titrations, respectively. The pH_{ZPC} can be obtained from the graph at the point of zero acid or base addition to the solution containing the adsorbent, which is very close to the value obtained by batch equilibrium method (8.33 vs. 8.62). In the pH region of 4 – 8, any acid addition is accompanied by a significant decrease in the pH value. However, the values obtained in the presence of adsorbent are higher than the ones calculated without adsorbent, which is mainly due to the consumption of protons for the protonation of $\equiv$SiOH sites to $\equiv SiOH_2^+$ in the region below pH_{ZPC} according to Eq. (4.10) (Scheme 4.1-2). In the pH region 3 – 4, the pH decreases too slowly as increasing amounts of acid are added, but always higher than the theoretical values indicating that the protons are readily consumed by the surface via amine protonation (Scheme 4.1-3) as the propylamine has a pK_b of 3.46 [30]. After addition of 0.2 mL of the acidic solution, the measured pH (3.3) was very close to the calculated value (3.1), indicating that most of the amine groups are protonated. At pH > 8.33, addition of base is accompanied by limited increase in the pH and the pH in this range is lower than the theoretical values due to the consumption of OH^- by the deprotonation of $\equiv$SiOH to $\equiv SiO^-$ according to Eq. (4.11) (Scheme 4.1-4). Although at pH > 8.33, the surface of the amine-modified SBA-15 is dominated by negatively charged $\equiv SiO^-$ species, this pH region is not suitable for copper adsorption, due to the precipitation of copper hydroxide.

$$\equiv SiOH + H^+ + \leftrightarrow \equiv SiOH_2^+ \quad (4.10)$$

$$\equiv SiOH \leftrightarrow \equiv SiO^- + H^+ \quad (4.11)$$

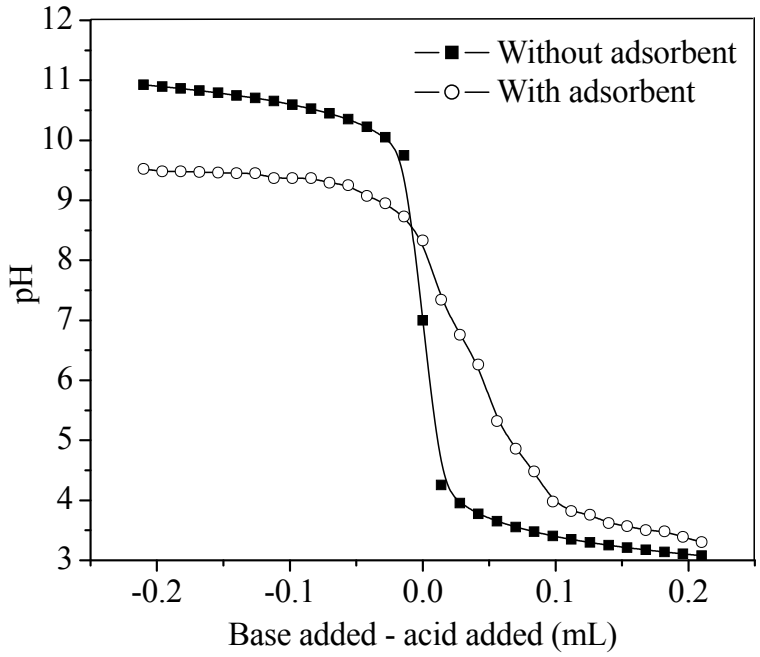

Figure 4-5. Potentiometric acid/base titration.

4.3.2 Effect of temperature and initial concentration of metal ions

Solutions of different initial Cu^{2+} concentrations were used to investigate the effect of concentration on the removal of Cu^{2+}. The adsorption yield was calculated using Eq. (4.12):

$$\text{Removal Efficiency } (R\%) = \left[\frac{C_i - C_e}{C_i}\right] \times 100 \quad (4.12)$$

As seen in Fig. 4.6, the removal efficiency (R%) decreases by increasing the initial Cu^{2+} concentration due to saturation of binding sites, which are the limiting factor, while the Cu/N atomic ratio increased as shown in Fig. 4.7. Kudryavtsev et al. [31] showed that at the beginning of the copper adsorption process on aminopropyl-modified silica, the ions tie with two ligands to form $[Cu(RNH_2)_2]^{2+}$complexes as shown in Scheme 4.2-1. Then, at higher Cu^{2+} concentration, some of the $[Cu(RNH_2)_2]^{2+}$ complexes convert into $[Cu(RNH_2)]^{2+}$ (Scheme 4.2-2), leading to higher adsorption capacity and higher Cu/N ratio (Fig. 4.7). At low concentrations, all Cu^{2+} ions present in solution could interact with two binding sites, leading to higher adsorption yield, and lower Cu/N ratio. Experiments

using very dilute solutions, i.e. 5 ppm, copper was removed completely, confirming the high sensitivity of the adsorbent to such cations, which is a crucial parameter to design a copper separation process based on adsorption.

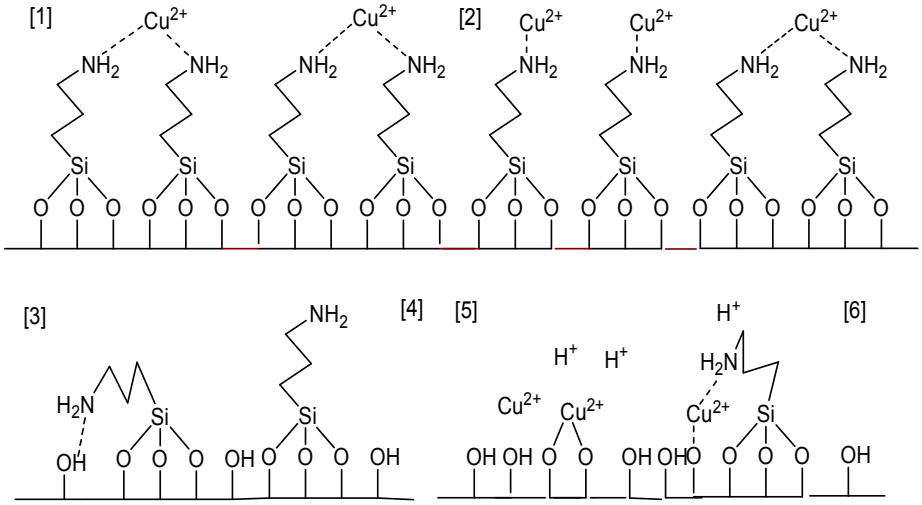

Scheme 4-2. Proposed mechanisms for copper adsorption on APTS-SBA-15-AB.

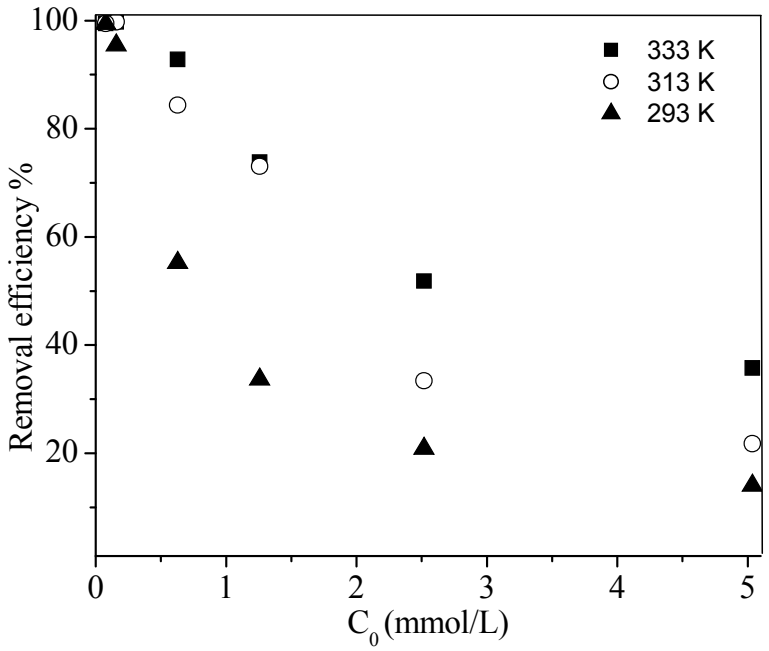

Figure 4-6. Effect of temperature and initial concentration on *R*%.

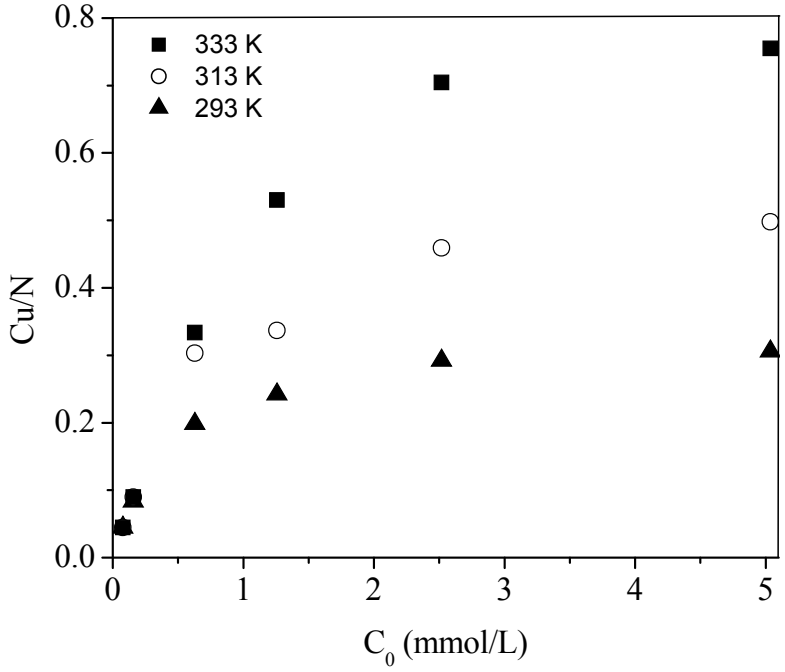

Figure 4-7. Effect of temperature and initial concentration on the Cu/N ratio.

It is clear from Fig 4.6 and Fig. 4.7 that temperature has a pronounced effect on the adsorption capacity of the adsorbent and that the effect of temperature increases as the initial copper concentration increases. The enhancement of copper uptake with increasing temperature may be attributed to the larger number of surface sites available for adsorption. As mentioned earlier, some of the amine groups might be hydrogen-bonded to the silica surface hydroxyl groups as shown in Scheme 4.2-3, diminishing their availability for adsorption [22]. Increasing temperature provides enough energy to break these bonds and release the amine groups (Scheme 4.2-4), leading to higher adsorption capacity [32]. Another possible reason is the ion-exchange reaction of Cu^{2+} with the surface hydroxyl groups via Si–O–Cu–O–Si bridging species as shown in Scheme 4.2-5. This was confirmed qualitatively by stirring unmodified SBA-15 silica in copper solutions at 293 and 333 K. A change in the material color into blue was observed at 333 K and the pH decreased from 6.12 to 5.09 as a result of ion-exchange between H^+ and Cu^{2+}, while the pH change at 293 K was from 6.12 to 5.88 with no change in the material color, indicating that less copper adsorption, if any was achieved. It is also possible that copper might react with one amine group and ion-exchange with an adjacent hydroxyl group as shown in Scheme 4.2-6. In addition, an increase in temperature provides energy to overcome repulsion forces between copper cations and the positively charged surface (Scheme 4.1-2), leading to higher rate of collisions between copper ions and the adsorption sites, hence, enhanced adsorption capacity.

4.3.3 Thermodynamic properties

Qualitative estimates of $\Delta H°$ and $\Delta S°$ can be obtained from the slope and intercept of Van't Hoff plot $\ln K_c$ vs. $1/T$ as shown in Fig. 4.8. The positive value of $\Delta H°$ (47.7 $kJmol^{-1}$) as shown in Table 4.2 indicates the endothermic nature of the overall adsorption process. This is consistent with the increase in the adsorption of Cu^{2+} with temperature. Endothermic adsorption of copper ions has been reported to occur on chemically modified chitosan [28], natural bentonite [33], and bentonite–polyacrylamide composites [34], while negative enthalpies have been obtained using 3-glycidoxypropyltrimethyl siloxane and propane-1,3-diamine immobilized on silica gel [35] and modified chrysotile fibers [36]. The formation of amine–copper complex being an exothermic reaction [37], it is inferred that the observed endothermic behavior is not related only to the Cu^{2+} complexation event. Since the adsorbent is highly porous and the adsorption sites are mostly located inside the pores, the endothermic behavior observed is likely to be associated with a number of endothermic processes such as diffusion resistance. In addition, the adsorption process was carried out at a pH of 6–6.5 under which the adsorbent surface is bearing a positive charge (Scheme 4.1-2) leading to additional energy consumption to overcome repulsive forces between the positively charged surface and the cations. Furthermore, energy is required to release the amine groups that might be hydrogen-bonded to free surface hydroxyl groups as shown in Scheme 4.2-3. All these processes are associated with positive enthalpies, the sum of which is larger than the negative enthalpy of formation of the amine–copper complex, leading to an overall positive enthalpy.

The spontaneity of the system is expressed by the negative Gibbs free energy. Furthermore, the values of $\Delta G°$ increased with increasing temperature, indicating that the adsorption of Cu^{2+} on this adsorbent is more favorable at higher temperature. The positive entropic value is consistent with the fact that the adsorption is favorable. In fact, the positive entropic value is counterbalanced by an unfavorable endothermic enthalpy value. The positive value, which is normally associated with the displacement of the solvent initially bonded either in the cation coordination sphere or through hydrogen bonds to the amine groups [8] and [35]. During the adsorption process, water molecules are displaced to the medium, to cause a degree of disorder to the system and, consequently, an increase in entropy [8] and [35]. Positive entropy was also reported for copper removal from aqueous solutions over thiourea immobilized onto silica [35], native and modified chrysotile fibers [37], and mesoporous silica functionalized with diethylenetriamine [8].

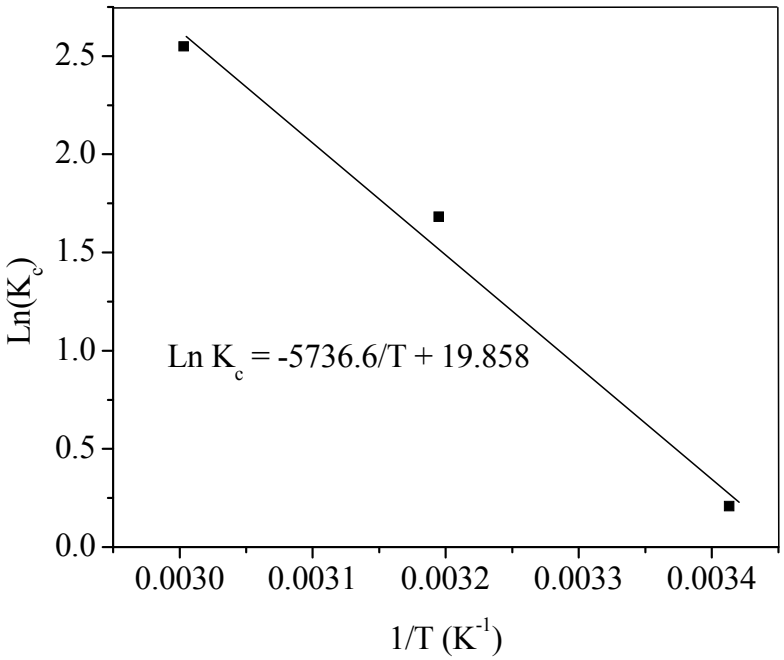

Figure 4-8. Van't Hoff plot for copper adsorption on APTS-SBA-15-AB.

Table 4-2. Thermodynamic properties of copper adsorption on APTS-SBA-15-AB.

Temperature (K)	K_c (Lg^{-1})	$\Delta G°$ ($kJmol^{-1}$)	$\Delta H°$ ($kJmol^{-1}$)	$\Delta S°$ ($kJmol^{-1}$)
293	1.23	−0.51	47.69	0.16
313	5.38	−4.38		
333	12.81	−7.06		

4.3.4 Effect of initial pH on the adsorption of Cu^{2+}

The effect of the solution pH on the adsorption performance is shown in Fig. 4.9. The Cu^{2+} adsorption capacity increased gradually as the solution pH increased from 4 to 6, followed by a sharp increase at pH up to 6.5. At pH 4, the Cu/N ratio was zero and only 0.013 at a pH of 4.5. Alkylamines generally have a pK_b value around 4 [30]. This means that, at such a pH, the amine groups are mostly in the protonated form (reaction (4.8), Scheme 4.1-3), with no Cu^{2+} complexation ability. Furthermore, as the pH is lowered, the surface becomes more positive, where reaction (4.10) takes place [27], leading to decreased interaction between copper and the binding sites due to stronger repulsive forces which inhibit the approach of positively charged copper cations to the adsorbent surface (Scheme 4.1-2 and -3). Moreover, as the pH of the solution increases from 4 to 6.5, not only amine protonation according to Eq. (4.8) (Scheme 4.1) decreases, but also columbic repulsion between the surface and copper cations decreases as a result of decreasing the extent of reaction (4.10) [27]. Consequently, the extent of formation of coordination complex between Cu^{2+} ions and the amine groups increases, leading to

higher adsorption capacity and Cu/N ratio. It is also possible that OH^- indirectly react with the weakly acidic silanol groups and breaks the hydrogen bond with the aminopropyl groups (Scheme 4.2-3), liberating it for adsorption. Fig. 4.9 shows that under otherwise the same conditions, the maximum Cu^{2+} adsorption capacity (0.6 $mmolg^{-1}$) was achieved at a pH of 6.5 with a Cu/N molar ratio of 0.34. When the pH increased to 6.7, precipitation of the metal hydroxide took place, accompanied by a sudden decrease in pH. It is thus inferred that the optimum pH for the removal of Cu^{2+} from aqueous solution at 293 K is 6.5. At this pH and initial concentration, neither precipitation of the metal hydroxide nor protonation of the amine groups occurs. It is worth mentioning that this optimum pH is only valid for a set of experimental conditions, i.e. temperature and concentration since precipitation depends on these parameters.

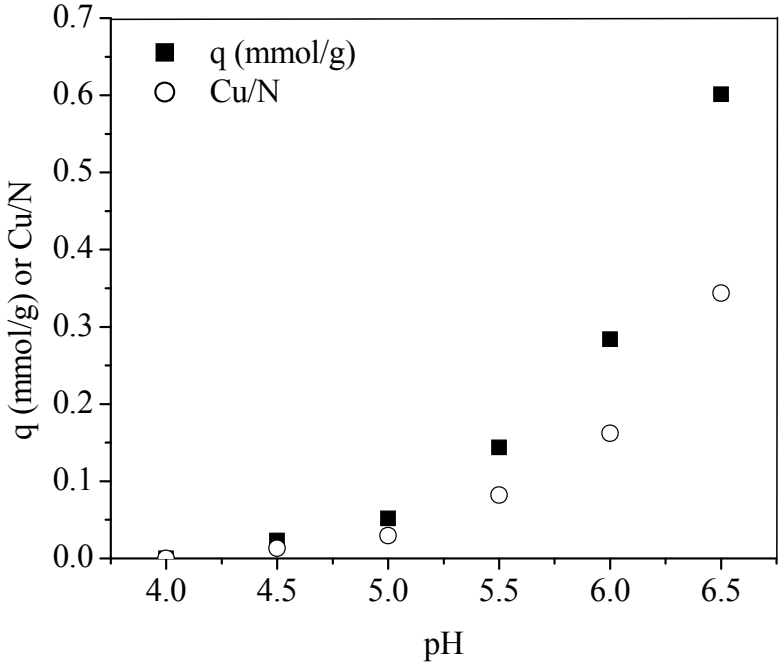

Figure 4-9. Effect of initial pH on the adsorption of Cu^{2+} on APTS-SBA-15-AB at 293K (C = 100 ppm).

4.3.5 Adsorption isotherms

The adsorption isotherms of Cu^{2+} at three different temperatures 293, 313, and 333 K are shown in Fig. 4.10 – 4.12. Two-parameter models (Langmuir and Freundlich) and three-parameters models (Sips and Redlich–Peterson) isotherms were used to describe the equilibrium between Cu^{2+} and APTS-SBA-15-AB. The obtained parameters for all the models used are listed in Table 4.3. All the isotherms (Fig. 4.10 – 4.12) show a sharp initial slope indicating high efficiency of the material at low concentration.

Furthermore, the adsorption isotherms and the calculated K_F and q_m values (Table 4.3) clearly show that the adsorption capacity increased with increasing temperature from 293 to 333 K, consistent with an overall endothermic process.

The isotherms constants and corresponding correlation coefficients at the three different temperatures are presented in Table 4.3. The three-parameter models yielded R^2 values of about 0.99, higher than the two-parameter models (R^2 values of about 0.95–0.98) demonstrating that Sips and Redlich–Peterson models more adequately fitted the data for Cu^{2+} adsorption as shown in Fig. 4.10 – 4.12. Table 4.3 shows that the for Sips model both q_s and K_s increased linearly with increasing temperature, while n decreased linearly. For Redlich–Peterson model, both K_{RP} and a_{RP} decreased exponentially with temperature while B increased linearly. The values of n in Freundlich isotherm are in the range 3.98–5.14, which indicates favorable adsorption process [33].

The maximum adsorption capacity of APTS-SBA-15-AB at 293, 313, and 333 K was found to be 0.54, 0.87 and 1.32 $mmolg^{-1}$, respectively, corresponding to Cu/N molar ratios of 0.31, 0.50 and 0.76. These results suggest that at 293 K, not all the amine groups were effectively used for adsorption, whereas at 333 K, the Cu/N mole ratio exceeded 0.5, which can be explained based on the effect of temperature and initial concentration as discussed earlier. Manu et al. [32] found the Cu/N mole ratio to be around 0.5 and 1 for two amine-modified silica gel samples with different loadings. They concluded that the surface density of amine groups determines the Cu/N ratio at saturation of Cu^{2+}. For comparison, the results obtained by Aguado et al. [20], at 298 K using three different samples of APTS-modified SBA-15 prepared by grafting were 0.39, 0.35, and 0.25 $mmolg^{-1}$ with Cu/N mole ratio of 0.14, 0.11, and 0.13, respectively.

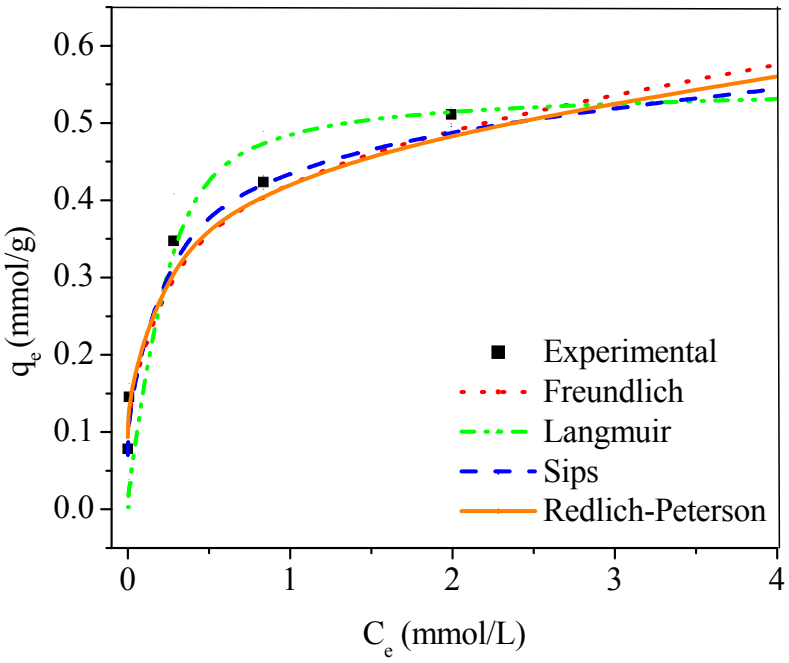

Figure 4-10. Adsorption isotherms for copper on APTS-SBA-15-AB at 293 K (pH = 6, C = 100 ppm).

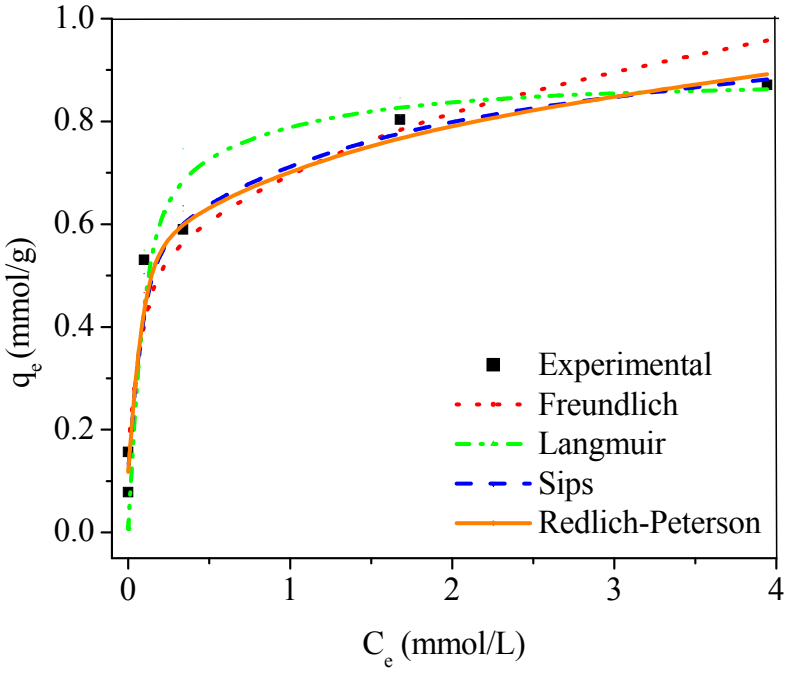

Figure 4-11. Adsorption isotherms for copper on APTS-SBA-15-AB at 313 K (pH = 6, C = 100 ppm).

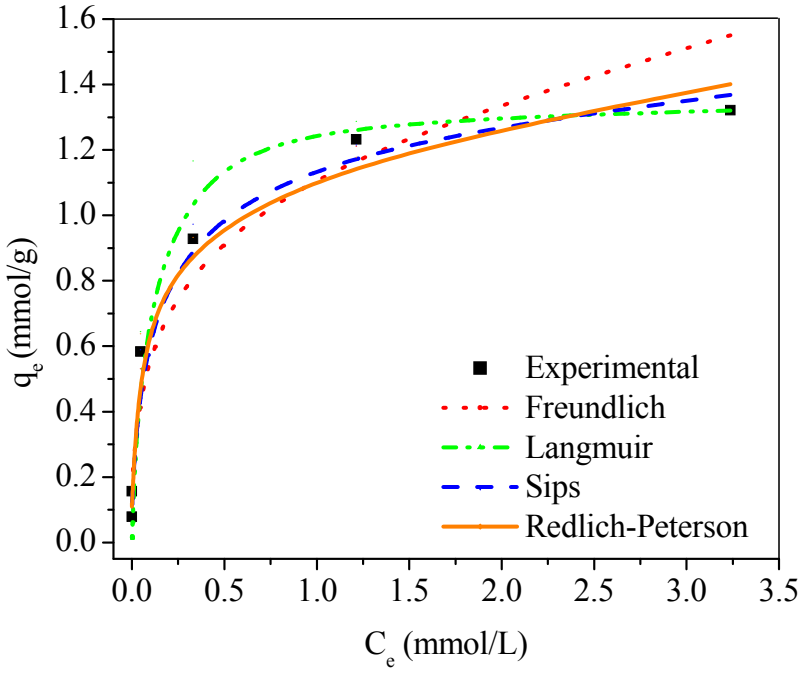

Figure 4-12. Adsorption isotherms for copper on APTS-SBA-15-AB 333 K (pH = 6, C = 100 ppm).

4.3.6 Regeneration of the adsorbent

In addition to excellent adsorption capacity, it is highly desirable that an adsorbent can be regenerated and reused repeatedly, for improved process economics. Fig. 4.13 shows that recycling using EDTA regeneration was more efficient than acid/base treatment. The adsorption capacity after ten cycles was 90% in comparison to the fresh material, while for acid/base treatment, the adsorption capacity after ten cycles was only 60% of the initial capacity. However, for both regeneration methods, the actual loss of amine after ten cycles was less than 10%, indicating that in the case of acid/base regeneration, not all the amine groups were recovered possibly due to incomplete release of copper after acidic treatment. This is consistent with the light blue color of regenerated samples.

Table 4-3. Model parameters for adsorption of copper on APTS-SBA-15-AB.

Isotherm model	293 K	313 K	333 K
Langmuir			
qm (mmolg^{-1})	0.54	0.88	1.34
K_L (Lg^{-1})	10.62	17.10	20.34
R^2	0.959	0.958	0.969
Function error, F_{error}	0.025	0.054	0.089
Freundlich			
K_F	0.43	0.73	1.15
N	4.70	5.14	3.98
R^2	0.983	0.970	0.964
Function error, F_{error}	0.003	0.019	0.067
Sips			
qs (mmolg^{-1})	0.93	1.24	1.74
K_s	0.91	1.53	2.01
N	3.16	2.87	2.22
R^2	0.997	0.989	0.990
Function error, F_{error}	0.001	0.006	0.007
Redlich–Peterson			
K_{RP} (Lg^{-1})	8613	932	781
a_{RP}	17613	1162	600
B	0.759	0.741	0.731
R^2	0.987	0.991	0.996
Function error, F_{error}	0.002	0.005	0.016

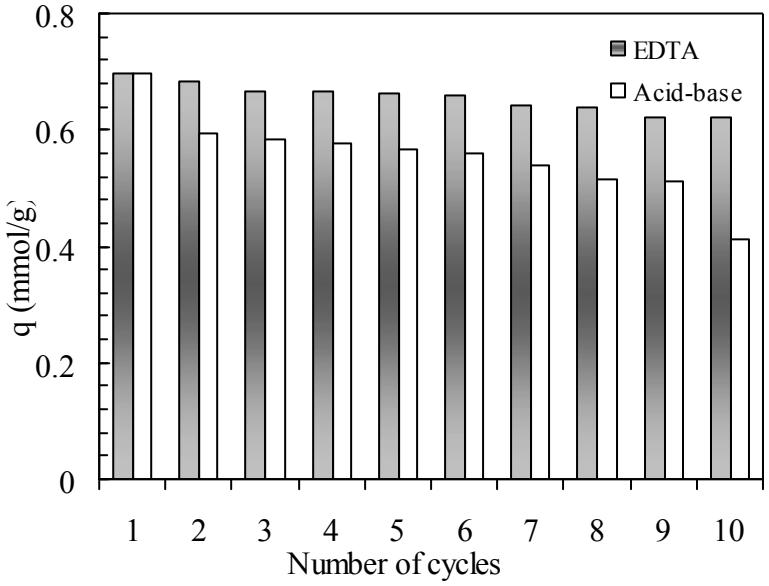

Figure 4-13. Adsorption capacity of regenerated adsorbent for 10 cycles.

4.4 Conclusions

Adsorption of Cu^{2+} on amine-functionalized SBA-15 prepared by co-condensation followed by treatment in acidic then basic solutions was studied under different conditions. The adsorbent showed very high sensitivity and efficiency for removing copper from very dilute solutions, which is a crucial requirement for practical applications. Increasing the temperature, the copper initial concentration and pH resulted in higher adsorption capacity. The calculated thermodynamic properties indicated the occurrence of a spontaneous and endothermic process. The adsorption data correlated well with the Sips model and Redlich–Peterson model. Regeneration of the adsorbent was evaluated by treatment of the copper-loaded materials with 0.1 M aqueous solutions of HCl then $NaHCO_3$ or by EDTA at 333 K. The adsorption capacity after ten cycles was 90% and 60% in comparison to the fresh material for regeneration with EDTA and acid/base, respectively.

References

[1] World Health Organization, Guidelines for drinking-water quality: Recommendations - Addendum, third edition - Volume 1 (2008).

[2] J.S. Beck, J.C. Vartuli, W.J. Roth, M.E. Leonowicz, C.T. Kresge, K.D. Schmitt, C.T-W. Chu, D.H. Olson, E.W. Sheppard, S.B. McCullen, J.B. Higgins, J.L. Schlenker, A new family of mesoporous molecular sieves prepared with liquid crystal templates, *J. Am. Chem. Soc. 114 (*1992) 10834-10843.

[3] A. Sayari, S. Hamoudi, Periodic mesoporous silica-based organic-inorganic nanocomposite materials, *Chem. Mater.* 13 (2001) 3151-3168.

[4] L. Bois, A. Bonhommé, A. Ribes, B. Pais, G. Raffin, F. Tessier, Functionalized silica for heavy metal ions adsorption, *Colloids Surf. A: Physicochem. Eng. Aspects* 221 (2003) 221-230.

[5] K. Inumaru, Y. Inoue, S. Kakii, T. Nakano, S. Yamanaka, Molecular selective adsorption of dilute alkylphenols and alkylanilines from water by alkyl-grafted MCM-41: tunability of the cooperative organic-inorganic function in the nanostructure, *Phys. Chem. Chem. Phys.* 6 (2004) 3133-3139.

[6] J. Aguado, J.M. Arsuaga, A. Arencibia, Adsorption of aqueous mercury (II) on propylthiol-functionalized mesoporous silica obtained by cocondensation, *Ind. Eng. Chem. Res.* 44 (2005) 3665-3671.

[7] J. Aguado, J.M. Arsuaga, A. Arencibia, Influence of synthesis conditions on mercury adsorption capacity of propylthiol functionalized SBA-15 obtained by co-condensation , *Microporous Mesoporous Mater.* 109 (2008) 513-524.

[8] R.K. Dey, F.J.V.E. Oliveira, C. Airoldi, Mesoporous silica functionalized with diethylenetriamine moieties for metal removal and thermodynamics of cation-basic center interactions, *Colloids Surf. A: Physicochem. Eng. Aspects* 324 (2008) 41-46.

[9] O. Olkhovyk, V. Antochshuk, M. Jaroniec, Benzoythiourea-modified MCM-48 mesoporous silica for mercury (II) adsorption from aqueous solutions, *Colloids Surf. A: Physicochem. Eng. Aspects* 236 (2004) 69-72.

[10] Y. Shiraishi, G. Nishimura, T. Hirai, I. Komasawa, Separation of transition metals using inorganic adsorbents modified with chelating ligands, *Ind. Eng. Chem. Res.* 41 (2002) 5065-5070.

[11] V. Antochshuk, M. Jaroniec, 1-Allyl-3-propylthiorea modified mesoporous silica for mercury removal, *Chem. Commun.* (2002) 258-259.

[12] A.M. Liu, K. Hidajat, S. Kawi, D.Y. Zhao, A new class of hybrid mesoporous materials with functionalized organic monolayers for selective adsorption of heavy metal ions, *Chem. Commun.* (2000) 1145-1146.

[13] L. Zhang, C. Yu, W. Zhao, Z. Hua, H. Chen, L. Li, J. Shi, Preparation of multi-amine-grafted mesoporous silicas and their application to heavy metal ions adsorption, *J. Non-Cryst. Solids* 353 (2007) 4055-4061.

[14] X. Feng, G. Fryxell, L.Q. Wang, A.Y. Kim, J. Liu, K.M. Kemner, Functionalized monolayers on ordered mesoporous supports, *Science* 276 (1997) 923-926.

[15] J. Liu, X. Feng, G. Fryxell, L-Q. Wang, A. Kim, M. Gong, Hybrid mesoporous materials with functionalized monolayers, *Adv. Mater.* 10 (1998) 161-165.

[16] H. Lee, J. Yi, Removal of copper ions using functionalized mesoporous silica in aqueous solution, *Sep. Sci. Technol.* 36 (2001) 2433-2448.

[17] T. Yokoi, H. Yoshitake, T. Tatsumi, Synthesis of amino-functionalized MCM-41 via direct co-condensation and post-synthesis grafting methods using mono-, di-, and tri-amino- organalkoxysilane, *J. Mater. Chem.* 14 (2004) 951-957.

[18] M. Jaroniec, K. Kruk, C. Jaroniec, A. Sayari, A., Modification of surface and structural properties of ordered mesoporous silicates, *Adsorption* 5 (1999) 39-45.

[19] X. Wang, J.C. Chan, Y.H. Tseng, S. Cheng, Synthesis, characterization and catalytic activity of ordered SBA-15 materials containing high loading of diamine functional groups, *Microporous Mesoporous Mater.* 95 (2006) 57-65.

[20] J. Aguado, J.M. Arsuaga, A. Arencibia, M. Lindo, V. Gascón, Aqueous heavy metals removal by adsorption on amine-functionalized mesoporous silica, *J. Hazard. Mater.* 163 (2009) 213-221.

[21] A.S. Chong, X.S. Zhao, Functionalization of SBA-15 with APTES and characterization of functionalized materials, *J. Phys. Chem. B* 107 (2003) 12650-12657.

[22] K.F. Lam, X. Chen, G. McKay, K.L. Yeung, Anion effect on Cu^{2+} adsorption on NH_2-MCM-41, *Ind. Eng. Chem. Res.* 47 (2008) 9376-9383.

[23] D. Zhao, Q. Huo, J. Feng, B.F. Chmelka, G.D. Stucky, Nonionic triblock and star diblock copolymer and oligomeric surfactant syntheses of highly ordered, hydrothermally stable, mesoporous silica structures, *J. Am. Chem. Soc.* 120 (1998) 6024-6036.

[24] M. Kruk, M. Jaroniec, A. Sayari, Application of large pore MCM-41 molecular sieves to improve pore size analysis using nitrogen adsorption measurements, *Langmuir* 13 (1997) 6267-6273.

[25] P. Harlick, A. Sayari, Applications of pore-expanded mesoporous silica. 3. Triamine silane grafting for enhanced CO_2 adsorption, *Ind. Eng. Chem. Res.* 45 (2006) 3248-3255.

[26] I.D. Smičiklas, S.K. Milonjić, P. Pfendt, S. Raičević, The point of zero charge and sorption of cadmium (II) and strontium (II) ions on synthetic hydroxyapatite, *Sep. Purif. Technol.* 18 (2000) 185-194.

[27] K. Dimos, P. Stathi, M.A. Karakassides, Y. Deligiannakis, Synthesis and characterization of hybrid MCM-41 materials for heavy metal adsorption, *Microporous Mesoporous Mater.* 126 (2009) 65-71.

[28] B. Kannamba, K.L. Reddy, B.V. AppaRao, Removal of Cu(II) from aqueous solutions using chemically modified chitosan, *J. Hazard. Mater.* 175 (2010) 939-948.

[29] R. Serna-Guerrero, E. Da'na, A. Sayari, New insights into the interactions of CO_2 with amine-functionalized silica, *Ind. Eng. Chem. Res.* 47 (2008) 9406-9412.

[30] D. R. Lide, W. M. M. Haynes, Handbook of Chemistry and Physics, 90th ed. (2010) 8-43

[31] G.V. Kudryavtsev, D.V. Miltchenko, V.V. Yagov, A.A. Lopatkin, Ion sorption on modified silica surface, *J. Colloid Interface Sci.* 140 (1990) 114-122.

[32] V. Manu, H.M. Mody, H.C. Bajaj, R.V. Jasra, Adsorption of Cu^{2+} on amino functionalized silica gel with different loading, *Ind. Eng. Chem. Res.*, *48* (2009) 8954–8960.

[33] N. Karapinar, R. Donat, Adsorption behaviour of Cu^{2+} and Cd^{2+} onto natural bentonite, *Desalination* 249 (2009) 123-129.

[34] G. Zhao, H. Zhang, Q. Fan, X. Ren, J. Li, Y. Chen, X. Wang, Sorption of copper(II) onto super-adsorbent of bentonite-polyacrylamide composites, *J. Hazard. Mater.* 173 (2010) 661-668.

[35] F.J.V.E. Oliveira, E.C. da Silva Filho, M.A.. Melo, C. Airoldi, Modified coupling agents based on thiourea, immobilized onto silica. Thermodynamics of copper adsorption, *Surf. Sci.* 603 (2009) 2200-2206.

[36] J.A.A. Sales, C. Airoldi, Calorimetric investigation of metal ion adsorption on 3-glycidoxypropyltrimethylsiloxane + propane-1,3-diamine immobilized on silica gel, *Thermochimica Acta* 427 (2005) 77-83.

[37] M.G. Fonseca, C. Airoldi, Thermodynamics data of interaction of copper nitrate with native and modified chrysotile fibers in aqueous solution, *J. Colloid Interface Sci.* 240 (2001) 229-236.

Chapter 5

Adsorption of copper on amine-functionalized SBA-15 prepared by co-condensation: Kinetics properties

Chem. Eng. J. 166 (2011) 454-459

Abstract.

Amino-functionalized SBA-15 prepared by co-condensation was tested for the removal of copper ions from aqueous solutions under different temperatures, pH, initial concentrations and agitation speeds. The obtained results indicated that the amino-functionalized SBA-15 was very efficient and equilibrium was achieved in less than 30 min at room temperature. The kinetic data was analyzed using four models, namely the first-order, the pseudo first- and second-order and the intraparticle diffusion model. Within the conditions used, the pseudo second-order kinetic model provided the best fit to the experimental data. Applying the intraparticle model showed that the adsorption involved three different stages.

5.1 Introduction

Similar to other heavy metals, copper enters the ecosystem through many processes including mining and refining, agricultural operations and industrial effluents, such as tanning processes, timber production, and electroplating industries. The release of large quantities of copper into the natural environment represents a serious threat to human health and other living species as well as ecological systems [1]. Therefore, efficient removal of copper from wastewater by appropriate treatments has long been a crucial issue. Adsorption is an attractive option because it is a simple, cost effective, and reversible process.

With the increasing demand for economical large-scale water treatment facilities, the development of efficient adsorbents for the removal of heavy metals that exhibit fast kinetics at high flow rates would be of great significance. A wide range of conventional porous solids, such as clay, fly ash, activated carbon and silica materials have attracted attention because of their relatively low-cost [2]. However, such materials have non uniform pore structures and often low adsorption capacities with slow adsorption kinetics [3]. Thus, the ideal adsorbent should have a stable and accessible pore

structure with uniform pore size distribution as well as high surface area. Periodic mesoporous SBA-15 silica has many attractive characteristics such as large surface area, high porosity, controllable and narrowly distributed pore sizes, and an ordered pore arrangement. In addition, SBA-15 has some of the largest mesopores (5–30 nm), which allow unhindered accessibility of the internal surface of the material, leading to fast kinetics of chemical or physical processes. Furthermore, its thick pore walls of around 4 nm, provide enhanced mechanical stability. Recently, many authors anchored functional groups on the surface of SBA-15 using post-synthesis procedures [4-7] or co-condensation [7-11], some of which were reported to be very efficient for the adsorption of heavy metals from water [6, 9-11].

The kinetics of adsorption, which dictates the residence time of the adsorption, is one of the most important tools to assess the adsorption efficiency. Therefore, it is important to be able to predict the rate of copper adsorption as a key step to design appropriate treatment units. In addition, investigating the copper adsorption kinetics is significant as it provides valuable insights into the reaction pathways. Walcarius and Delacôte investigated the effect of structural and surface properties of organically modified silicates on the kinetics of mercury adsorption [12]. Furthermore, Aguado et al. studied the effect of initial copper concentration on the adsorption kinetics of amine-functionalized SBA-15 prepared by grafting [7]. However, the effects of other factors such as temperature, pH, and agitation speed on the kinetics of metal removal by surface-functionalized SBA-15 has not been addressed. Hence, the goal of this chapter was to carry out an in-depth study on the effect of adsorption process parameters such as temperature, copper concentration, stirring speed, and pH on the performance of the amine-modified SBA-15 obtained by co-condensation. Furthermore, this chapter dealt with the development of general predictive models to describe the relationship between the initial concentration and the adsorption temperature with the rate of copper removal.

5.2 Materials and methods

5.2.1 Adsorbent synthesis and characterization

Details of adsorbent synthesis and characterization can be found in an earlier contribution [11]. Briefly, 4.0 g of P123 and 8 g KCl were dissolved in 30 mL of water and 120 mL of a 2 M HCl solution at 40 °C. Then, 8.5 g of tetraethylorthosilicate was added and prehydrolyzed for 2 h before adding 1.08 g of 3-aminopropyltrimethoxy-silane (APTS). The mixture was stirred for 20 h, then heated at 100 °C for 24 h in static conditions. The material was collected by filtration, dried in air at room temperature and then extracted with ethanol. The material was further treated in aqueous 0.1 M HCl for 1 h and

neutralized in 0.1 M $NaHCO_3$, then filtered and dried under vacuum at 100 °C for 3 h. The material will be referred to as APTS-SBA-15-AB.

5.2.2 Adsorption kinetics

Batch kinetic tests were performed in a 1 L glass reactor stirred at a specified rate (100 or 300 rpm) using a magnetic stirrer. The reactor was immersed in a water bath maintained at a constant temperature of 293, 313 or 333 K. The reaction mixture consisted of a total 1 L volume of 20, 100, or 200 ppm copper solution containing 1.0 g of adsorbent and the pH was adjusted at 5.5, 6.0, or 6.5. The reactor was coupled with an ICP-OES Varian Vista-Pro CCD spectrometer instrument for real-time measurement of copper concentration at intervals of 20 s for 2 h. The adsorption rate, defined as the change of copper concentration with time, was analyzed using the following models:

5.2.2.1 First-order model

For the first order kinetic, the adsorption of copper from liquid phase to solid phase may be expressed as:

$$A \underset{k_2}{\overset{k_1}{\rightleftharpoons}} B \tag{5.1}$$

where A is copper in solution, B is the adsorbed copper, k_1 and k_2 are the adsorption and desorption rate constants (h^{-1}). If C_0 is the initial concentration of copper (mgL^{-1}) and X the amount transferred from liquid phase to solid phase (mgL^{-1}) at any time t, then the rate can be expressed as:

$$\frac{dX}{dt} = k_1(C_0 - X) - k_2X \tag{5.2}$$

If X_e represents the concentration of copper adsorbed at equilibrium (mgL^{-1}), then,

$$-ln\left(1 - \frac{X}{Xe}\right) = \left(k_1 + k_2\right)t \tag{5.3}$$

Further, the overall rate constant k (h^{-1}) is given by:

$$k = \left(k_1 + k_2\right) \tag{5.4}$$

Using the kinetic equation, the overall rate constant (k) can be calculated by plotting $\ln\left(1-\frac{X}{X_e}\right)$ versus t.

5.2.2.2 Pseudo first-order model

The pseudo first-order kinetic model is based on the assumption that the adsorption rate is proportional to the number of free sites. The rate constant of adsorption can be determined using the following rate expression:

$$\frac{dq}{dt} = k_{p1}(q_e - q_t) \tag{5.5}$$

where q_t and q_e are the amounts of copper adsorbed (mgg^{-1}) at time t and at equilibrium, respectively. Integration and rearrangement of Eq. (5.5) gives:

$$ln(q_e - q_t) = lnq_e - k_{p1}t \tag{5.6}$$

k_{p1} is the pseudo first-order rate constant for adsorption (h^{-1}) and can be calculated from the slope of the linear plot of $\ln(q_e - q_t)$ versus t.

5.2.2.3 Pseudo second-order model

Pseudo second-order model is based on the assumption that the adsorption rate is linearly related to the square of the number of unoccupied sites, and thus the kinetic rate law can be written as follows:

$$\frac{dq}{dt} = k_{p2}(q_e - q_t)^2 \tag{5.7}$$

The differential equation is usually integrated and transformed in its linear form.

$$\frac{t}{q_t} = \frac{1}{k_{p2}q_e^2} + \frac{1}{q_e}t \tag{5.8}$$

where k_{p2} is the pseudo second-order rate constant for adsorption (g/mmol.min) and can be determined by plotting t/q_t versus t.

5.2.2.4 Intraparticle diffusion model

The adsorbate transport from the solution phase to the surface of the adsorbent particles occurs in several steps. The overall adsorption process may be influenced by one or more steps, e.g. film or external diffusion, pore diffusion, and adsorption on the pore surface. A process is diffusion-controlled

when its rate depends upon the rate at which diffusion takes place. The possibility of intraparticle diffusion will be explored using the intraparticle diffusion model:

$$q_t = k_{id}t^{1/2} \tag{5.9}$$

where k_{id} is the rate constant for intraparticle diffusion ($mgg^{-1}h^{-0.5}$). If the plot of qt versus $t^{0.5}$ gives a straight line, then the adsorption process is controlled by intraparticle diffusion only. However, if the data exhibit multi-linear plots, then two or more steps influence the adsorption process [13, 14].

5.3 Results and discussion

5.3.1 Effect of initial concentration

The copper uptake versus time at 333 K was measured for three different initial concentrations of Cu^{2+} ions, namely 20, 100 and 200 ppm. The curves in Fig. 5.1 show that initially, the amount of copper ions adsorbed increases significantly with time, then slows down gradually until the equilibrium is reached. This is mainly because initially most of the external and easy accessible sites were available and the copper concentration gradient was high. As the time passes the extent of copper adsorption decreases significantly because the number of vacant sites as well as the concentration gradient decrease. Fig. 5.1 shows the effect of initial concentration on adsorption kinetics, and Table 5.1 summarizes the calculated parameters for each initial copper concentration. Regression coefficients (R^2) obtained from the linear fits indicate good correlation for the three concentrations with the pseudo second-order model, indicating that this mechanism is predominant within this concentration range, i.e. that copper ion occupied two adsorption sites in agreement with literature data for similar adsorbents, including amine-functionalized SBA-15 prepared by grafting [7], amine-functionalized MCM-41 and MCM-48 [15], mesoporous aluminas [3], silica gel [16], and NaX zeolite [13]. Table 5.1 shows also that the pseudo second-order constants decreased from 6.20 to 0.47 and 0.29 $gmmol^{-1}min^{-1}$ when the initial copper concentration increased from 20 to 100 and 200 mgL^{-1}, respectively. A similar behavior was reported for amine-functionalized SBA-15 prepared by grafting [7], amino-modified silica gel [16], NaX zeolite [13] and rubber leaf powder [14]. Fig. 5.1 shows that, the maximum adsorption capacity was reached in about 6, 15, and 25 min for initial concentrations of 20, 100, and 200 ppm respectively, indicating very high accessibility of the amine sites to Cu^{2+} adsorption. At the beginning, copper adsorption occurred on the external and most accessible sites. Thus, the initial reaction rate is expected to be high even at low initial concentration since only external diffusion resistance is predominant, while longer reaction time should be required for copper ions to reach less accessible sites. Fig. 5.1 shows that 6 min was enough to achieve 100% removal of the copper from 20 ppm

solution indicating very high efficiency of the adsorbent at low concentration which is a crucial requirement for achieving a viable adsorbent.

Table 5-1. Effect of experimental conditions on Cu^{2+} adsorption kinetics.

T (K)	pH	C_0 (ppm)	Agitation (rpm)	q_e [a] (mmol/g)	q_{exp} [b] (mmol/g)	k_{p2} [c] (g/mmol.min)	R^2	k_{id} [d] (mmol/g.min$^{0.5}$)
293	6.0	100	300	0.180	0.182	11.793	0.995	0.036
313	6.0	100	300	0.415	0.438	1.957	0.996	0.048
333	6.0	100	300	0.676	0.688	0.471	0.998	0.076
333	5.5	100	300	0.632	0.656	2.111	0.995	0.080
293	6.5	100	300	0.566	0.584	0.359	0.994	0.052
333	6.0	200	300	1.077	1.118	0.293	0.996	0.151
333	6.0	20	300	0.314	0.311	6.195	0.999	0.063
333	6.0	100	100	0.672	0.680	0.445	0.994	0.073

a: Adsorption capcity obtained from the pseudo second-order model, b: Adsorption capacity obtained from the experimental data, c: pseudo second-order rate constant, d: Intraparticle diffusion constant obtained from applying the intraparticle diffusion model.

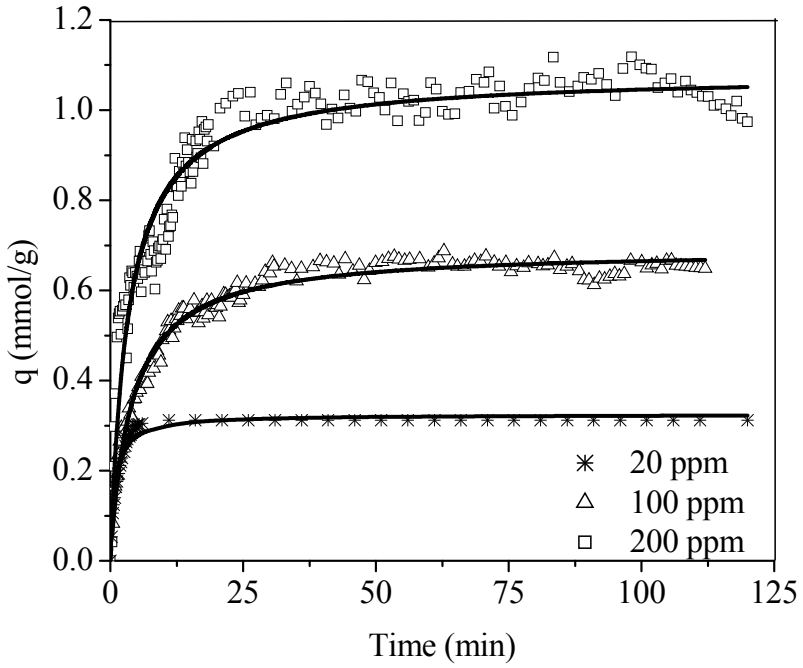

Figure 5-1. Kinetics of copper adsorption on APTS-SBA-15-AB at different initial concentrations (Solid lines: model, symbols: experimental data) (T = 293 K, pH = 6).

5.3.2 *Effect of temperature*

The effect of solution temperature was investigated at 293, 313 and 333 K for fixed initial concentration of 100 ppm. Fig. 5.2 shows that the amount of copper ions adsorbed at equilibrium increases at increasing temperature indicating an overall endothermic process, in agreement with the thermodynamic data reported earlier [11]. Model fitting indicates that the pseudo second-order model provides good correlations for data at all three temperatures. The model constant decreased from 11.79 to 1.96 and 0.47 $gmmol^{-1}min^{-1}$ when temperature increased from 293 to 313 and 333 K, respectively. The decrease in the pseudo first-order and second-order rate constants at increasing temperature is due to the fact that such factors are actually fitting parameters for modeling purposes without being real rate constants. Similar behavior was reported by other workers [17, 18].

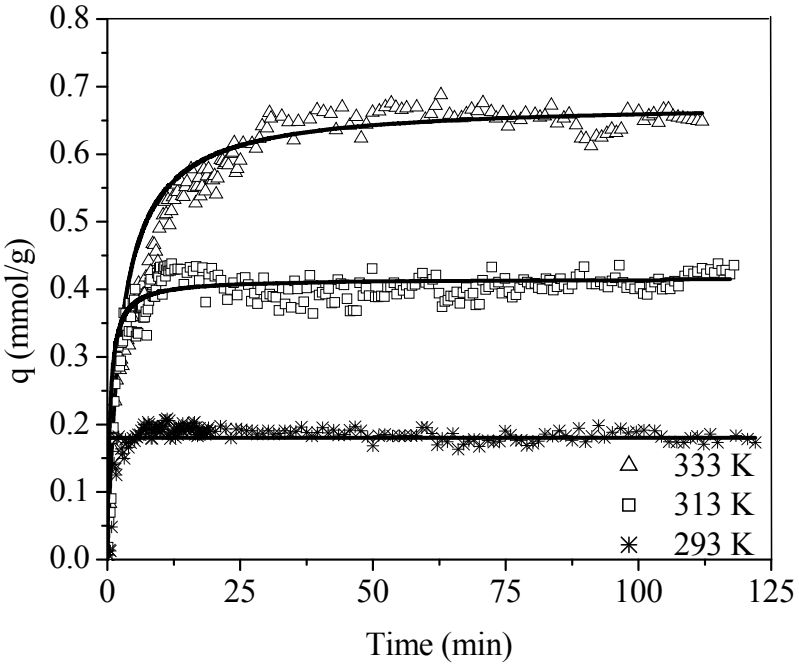

Figure 5-2. Kinetics of copper adsorption on APTS-SBA-15-AB at different temperatures (Solid lines: model, symbols: experimental data) (C = 100 ppm, pH = 6).

5.3.3 *Effect of the agitation speed*

The agitation speed is an important parameter in any transfer phenomena, since it can promote a certain turbulence which insures a good contact between the phases, a fact which improves the mass transfer. In order to assess the effect of the agitation speed, two different speeds chosen as shown in Fig. 5.3, where it can be noted that the retention of copper did not change progressively with the agitation speed vs. time, and equilibrium was reached almost in the same time. Therefore it can be

concluded that under the current conditions, the agitation speed has no effect on the kinetic performance. This is mainly because for this adsorbent, most of the surface area and therefore the adsorption sites are located within the pores and not on the external surface. Thus, the process is expected to be more dependent on the intraparticle diffusion than the external diffusion. Models fitting shows that at both agitation speeds the kinetics data fit well with the pseudo second-order model with constants of 0.44 and 0.47 $gmmol^{-1}min^{-1}$ for 100 and 300 rpm.

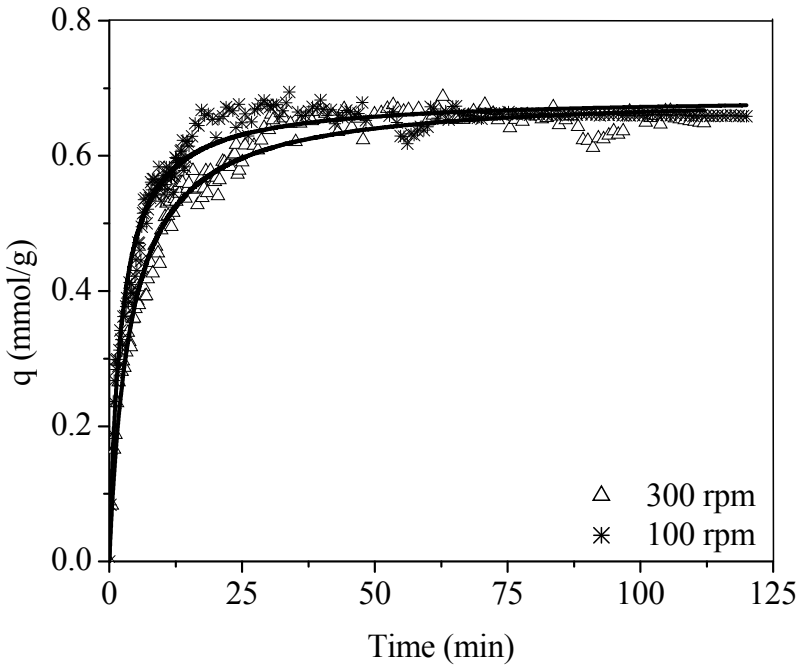

Figure 5-3. Kinetics of copper adsorption on APTS-SBA-15-AB at different agitation speeds (Solid lines: model, symbols: experimental data) (T = 333 K, pH = 6, C = 100 ppm).

5.3.4 Effect of pH

Fig. 5.4 shows that changing the pH of the solution from 5.5 to 6.0 at 333 K resulted in negligible effect on the equilibrium capacity, while the pseudo second-order constant decreased from 2.11 to 0.47 g $mmol^{-1}min^{-1}$. However, increasing the pH from 6.0 to 6.5 at 293 led to more dramatic changes (Fig. 5.5). Fig. 5.5 shows that the adsorption of copper at pH 6.5 was significantly enhanced in comparison to pH = 6 due to the pH effect discussed earlier [11]. Furthermore, at pH 6.5, a period of 40 min was required to reach the equilibrium adsorption capacity (0.58 $mmolg^{-1}$), while only two min was required to reach equilibrium (0.18 mmol/g) at pH of 6.0. The value of pseudo second-order constant decreased from 11.79 to 0.36 $gmmol^{-1}min^{-1}$ when the pH increased from 6.0 to 6.5. A decrease in pseudo second-order constant with increasing the pH was also reported by Öncel [19].

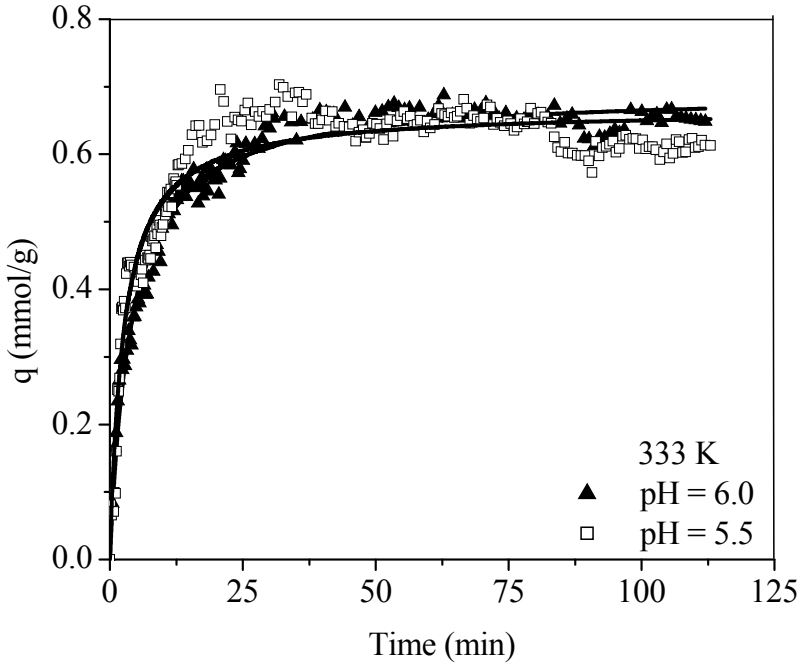

Figure 5-4. Kinetics of copper adsorption on APTS-SBA-15-AB at 333 K and different pH (Solid lines: model, symbols: experimental data) (T = 333 K, C = 100 ppm).

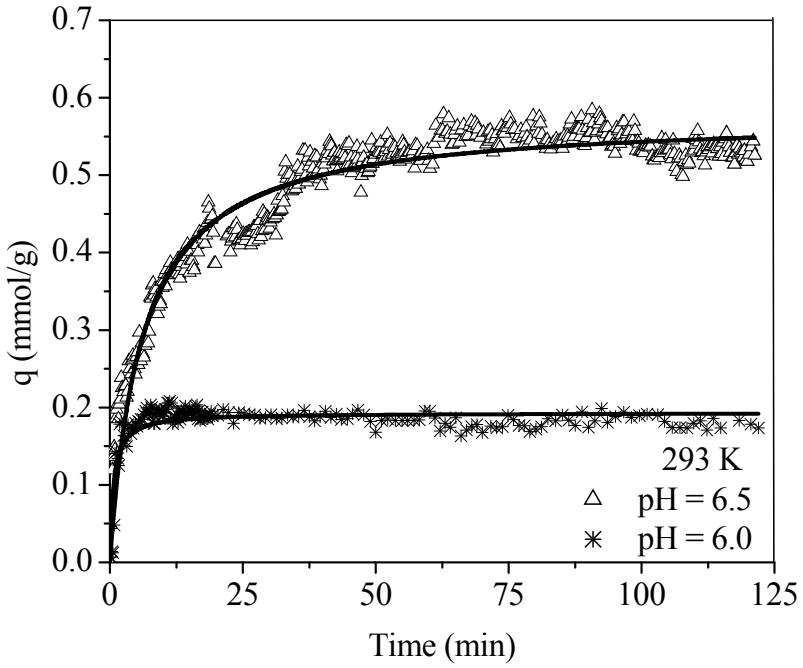

Figure 5-5. Kinetics of copper adsorption on APTS-SBA-15-AB at 293 K and different pH (Solid lines: model, symbols: experimental data) (T = 293 K, C = 100 ppm).

5.3.5 Intraparticle diffusion

Applying the intraparticle model to the experimental data by plotting q (mmol/g) vs. $t^{0.5}$, Fig. 5.6 is an illustrative example, shows three distinct stages, as indicated by the solid lines, regarding the rate of change in copper adsorbed: a rapid initial increase, followed by a more gradual increase for about 30 min, followed by a much slower uptake of Cu^{2+}. The initial fast rate is due to the availability of free sites on the external surface and easily accessible sites, in addition to the initial high copper concentration gradient. The rate of adsorption in this stage depends mainly on the external diffusion, thus, as shown in Fig. 5.6 the higher the concentration, the larger the slope of the solid lines in this region. As time passed, the extent of copper sorption decreased significantly because of the saturation of the external and easily accessible sites as well as the decreasing concentration gradient. Adsorption on sites within the pores takes place. In this stage, copper ions migrate from the bulk of solution to the external surface of the adsorbent followed by diffusion within the pores, which makes the rate slower than in the initial stage. It is obvious that intraparticle diffusion is not the sole rate determining step as the second portion of plots of q versus $t^{0.5}$ did not have zero intercept [14]. The values of k_{id} determined from the slopes of the second stages of the plots are shown in Table 5.1. Increasing the initial concentration from 20 to 100, then 200 ppm resulted in increasing values of k_{id} from 0.063 to 0.076 and 0.151 mmol/g.min$^{0.5}$, respectively as a result of increasing concentration gradient, which is the driving force for diffusion. The same effect was noticed for temperature, the k_{id} increased from 0.036 to 0.048 and 0.076 mmol/g.min$^{0.5}$ when the temperature increased from 293 to 313 and 333 K, respectively. At 333 K, the effect of pH on k_{id} was negligible. This is mainly because at this temperature enough energy is supplied to the copper cations to overcome the effect of pH. Moreover, increasing pH from 6 to 6.5 at 293 K led to increasing k_{id} from 0.036 to 0.052 mmol/g.min$^{0.5}$ as a result of decreasing the repulsion force between the cations and the surface. The agitation speed had no effect on the kinetics as shown previously with k_{id} of 0.076 and 0.073 mmol/g.min$^{0.5}$ at 300 and 100 rpm, respectively. Fig. 5.6 shows that the second part of the fitted curve for initial concentration of 20 ppm was minimal compared to 100 ppm and 200 ppm indicating the suppressed intraparticle diffusion within the pores. This is mainly because very low concentration of copper may result in Cu^{2+} uptakes below the saturation level of all available amine sites, with Cu^{2+} becoming the limiting reactant leading to adsorption mostly on external sites. It is worth mentioning that the third section of the plots has no kinetic meaning since the material is already saturated. The almost horizontal line corresponds to the equilibrium adsorption capacity, and its intersection with the line of the second section correspond to the time required to achieve equilibrium.

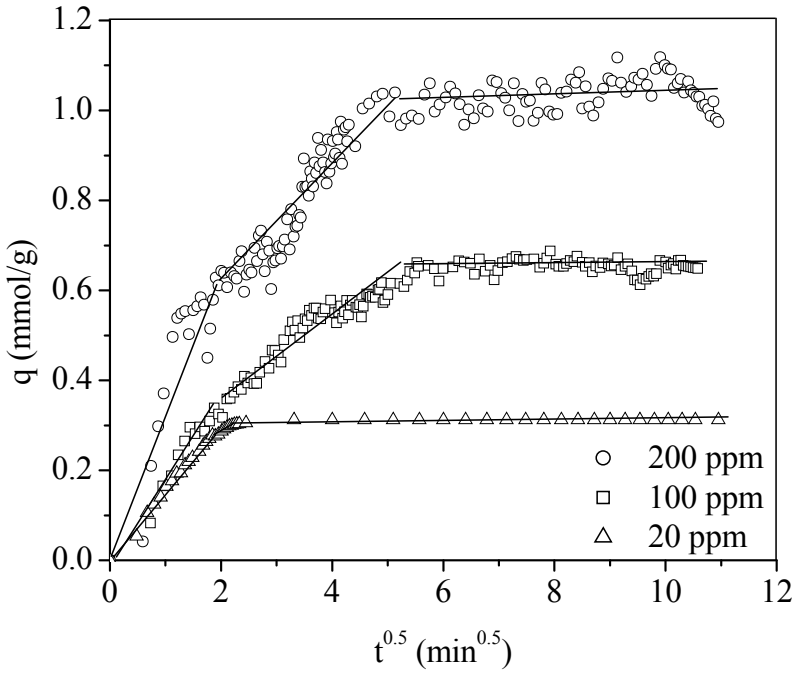

Figure 5-6. Intraparticle diffusion plots of copper adsorption onto APTS-SBA-15-AB at different initial concentrations.

5.3.6 Predicting the adsorption kinetics

Fig. 5.7 shows that within the range of initial concentration and temperature used, the equilibrium capacity increased linearly with an increase in C_0 and T according to the following relationships:

$$q_e = 0.0042\ C_0 + 0.2375 \tag{5.10}$$

$$q_e = 0.0124\ T - 3.4552 \tag{5.11}$$

The rate constant, and the temperature or the initial concentration are related by Eqs. (5.12) and (5.13) as shown in Fig. 5.8.

$$k_{p2} = 2 \times 10^{11} e^{-0.0805T} \tag{5.12}$$

$$k_{p2} = 349.47 C_0^{-1.3743} \tag{5.13}$$

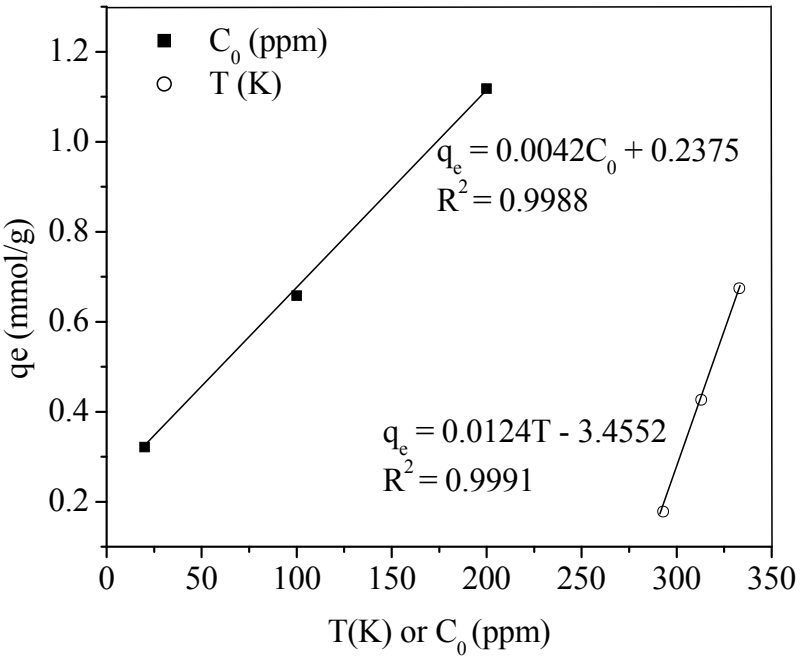

Figure 5-7. Equilibrium capacity vs. initial concentration and temperature.

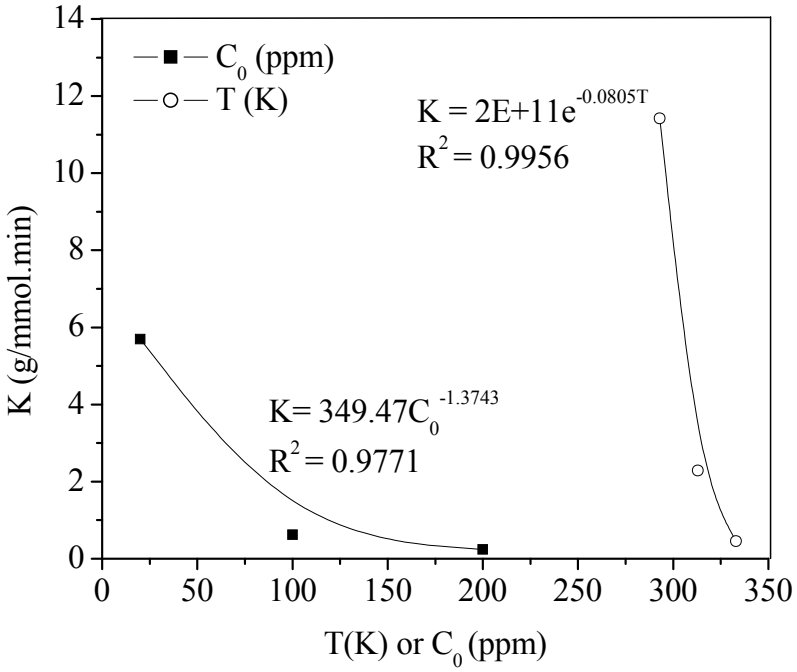

Figure 5-8. Pseudo second-order rate vs. initial concentration and temperature.

These relationships between q_e (mmol/g), T (K) and C_0 (ppm) as well as k_{p2} (g/mmol.min), T (K) and C_0 (ppm) were used in the pseudo second-order kinetic model to develop a general predictive model describing the adsorption kinetics of copper ions on APTS-SBA-15-AB at any initial concentration or any initial temperature and at any time of contact. This approach is valid within the range of validity of Eqs. (5.10), (5.11), (5.12) and (5.13). From the equations above, the relationships between q, C_0, and T can be represented as:

$$q(T) = \frac{2\times 10^{11} e^{-0.0805T}\left(0.0124\,T - 3.4552\right)^2 t}{1 + 2\times 10^{11} e^{-0.0805T}\left(0.0124\,T - 3.4552\right) t} \tag{5.14}$$

$$q(C_0) = \frac{349.47\; C_0^{-1.3743}\left(0.0042\,C_0 + 0.2375\right)^2 t}{1 + 349.47\; C_0^{-1.3743}\left(0.0042\,C_0 + 0.2375\right) t} \tag{5.15}$$

These general kinetic models were tested with three different initial concentrations and temperatures as shown in Fig. 5.9 and Fig. 5.10. The experimental data show an excellent agreement with the data predicted by the general models for the three concentrations and temperatures.

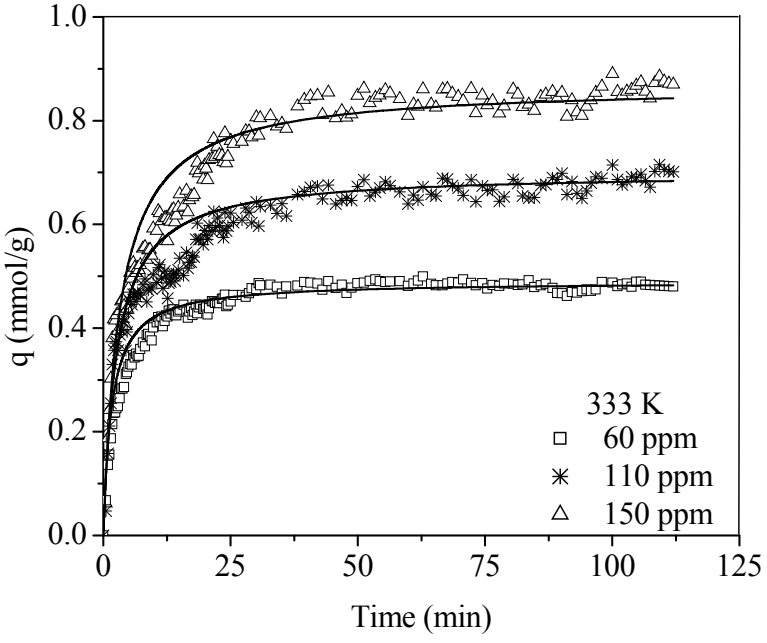

Figure 5-9. Validity of the generalized predictive model for different initial copper concentrations (Solid lines: model, symbols: experimental data).

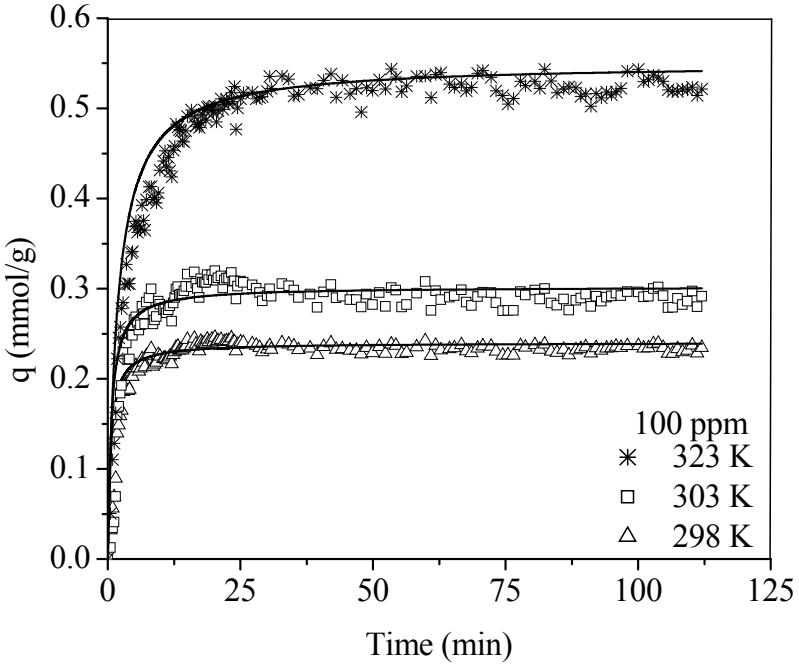

Figure 5-10. Validity of the generalized predictive model for different temperatures (Solid lines: model, symbols: experimental data).

5.4 Conclusions

Amino-functionalized SBA-15 prepared by co-condensation was used for the removal of copper ions from aqueous solutions. The adsorption capacity and rate were found to be dependent on temperature, pH and initial concentration, while the impact of agitation speed was negligible. The adsorption capacity was favored by increasing initial concentration or temperature. The pH had a beneficial effect at 293 K, but hardly any at 333 K. The pseudo second-order kinetic model provided an excellent fit to the kinetic data. The rate constant decreased with temperature, initial concentration and pH. The intraparticle model showed that the adsorption takes place in three different stages: rapid adsorption controlled by external diffusion, slower adsorption controlled by intraparticle diffusion, and final equilibrium stage. Two general models to predict the kinetic as a function of temperature and initial concentration were developed and found to be in excellent agreement with the experimental results.

References

[1] World Health Organization, Guidelines for drinking-water quality: recommendations – Addendum, third edition, vol. 1, 2008.

[2] S. Babel and T.A. Kurniawan, Low-cost adsorbents for heavy metals uptake from contaminated water: a review, *J. Hazard. Mater.* 97 (2003) 219–243.

[3] S. Rengaraj, Y. Kim, C.K. Joo and J. Yi, Removal of copper from aqueous solution by aminated and protonated mesoporous aluminas: kinetics and equilibrium, *J. Colloid Interface Sci.* 273 (2004), 14–21.

[4] M. Liu, K. Hidajat, S. Kawi and D.Y. Zhao, A new class of hybrid mesoporous materials with functionalized organic monolayers for selective adsorption of heavy metal ions, *Chem. Commun.* (2000) 1145–1146.

[5] L. Zhang, C. Yu, W. Zhao, Z. Hua, Hi Chen, L. Li and J. Shi, Preparation of multi-amine-grafted mesoporous silicas and their application to heavy metal ions adsorption, *J. Non-Cryst. Solids* 353 (2007) 4055–4061.

[6] y. Jiang, Q. Gao, H. Yu, Y. Chen and F. Deng, Intensively competitive adsorption for heavy metal ions by PAMAM-SBA-15 and EDTA-PAMAM-SBA-15 inorganic-organic hybrid materials, *Microporous Mesoporous Mater.* 103 (2007) 316–324.

[7] J. Aguado, J.M. Arsuaga, A. Arencibia, M. Lindo and V. Gasco'n, Aqueous heavy metals removal by adsorption on amine-functionalized mesoporous silica, *J. Hazard. Mater.* 163 (2009) 213–221.

[8] J. Aguado, J.M. Arsuaga and A. Arencibia, Influence of synthesis conditions on mercury adsorption capacity of propylthiol functionalized SBA-15 obtained by co-condensation, *Microporous Mesoporous Mater.* 109 (2008) 513–524.

[9] J. Aguado, J.M. Arsuaga and A. Arencibia, Adsorption of aqueous mercury (II) on propylthiol-functionalized mesoporous silica obtained by cocondensation, *Ind. Eng. Chem. Res.* 44 (2005) 3665–3671.

[10] M.C. Bruzzoniti, A. Prelle, C. Sarzanini, B. Onida, S. Fiorilli and E. Garrone, Retention of heavy metal ions on SBA-15 mesoporous silica functionalised with carboxylic groups, *J. Sep. Sci.* 30 (2007), 2414–2420.

[11] E. Da'na and A. Sayari, Adsorption of copper on amine-functionalized SBA-15 prepared by co-condensation: Equilibrium properties, Chem. Eng. J. 166 (2011) 445-453.

[12] A. Walcarius and C. Delacôte, Rate of access to the binding sites in organically modified silicates. 3. Effect of structure and density of functional groups in mesoporous solids obtained by the co-condensation route, *Chem. Mater.* 15 (2003) 4181–4192.

[13] S. Svilovic, D. Rusic and R. Stipisic, Modeling batch kinetics of copper ions sorption using synthetic zeolite NaX, *J. Hazard. Mater.* 170 (2009) 941–947.

[14] W.S. Wan Ngah and M.A.K.M. Hanafiah, Adsorption of copper on rubber (Hevea brasiliensis) leaf powder: kinetic, equilibrium and thermodynamic studies, *Biochem. Eng. J.* 39 (2008) 521–530.

[15] A. Benhamou, M. Baudo, Z. Derriche and J.P. Basly, Aqueous heavy metals removal on amine-functionalized Si-MCM-41 and Si-MCM-48, *J. Hazard. Mater.* 171 (2009) 1001–1008.

[16] V. Manu, M. Haresh, C.B. Hari and V.J. Raksh, Adsorption of Cu^{2+} on amino functionalized silica gel with different loading, *Ind. Eng. Chem. Res.* 48 (2009) 8954–8960.

[17] M. Mohammad, S. Maitra, N. Ahmad, A. Bustam, T.K. Sen and B.K. Dutta, Metal ions removal from aqueous solution using physic seed hull, *J. Hazard. Mater.* 179 (2010) 363–372.

[18] M.H. Kalavathy and L.R. Miranda, Comparison of copper adsorption from aqueous solution using modified and unmodified Hevea brasiliensis saw dust, *Desalination* 255 (2010) 165–174.

[19] M.S. Öncel, Adsorption of copper (II) from aqueous solution by Beidellite, *Environ. Geol.* 55 (2007) 1767–1775.

Chapter 6

Optimization of copper removal efficiency by adsorption on amine-modified SBA-15: Experimental design methodology

Chem. Eng. J. 167 (2011) 91-98

Abstract.

A 2^4 factorial design experiments were used to screen the factors affecting the copper removal efficiency using aminopropyl-functionalized SBA-15 silica. The obtained linear model was statistically tested using analysis of variance (ANOVA), Student's *t*-test, residuals test, and test of curvature. All the tests showed that all the parameters main effects were significant within a 95% confidence level. The test of curvature implied the presence of quadratic effect in the response. Therefore, surface composite design was used to develop a more reliable model. The statistical tests used proved the adequacy of the obtained second order model. Optimization of the factors levels was carried out by minimizing the amount of adsorbent used, minimizing the adsorption temperature, and maximizing the removal efficiency. The recommended optimum conditions are: copper concentration of 20 mg/L, adsorbent/solution ratio of 1.57 g/L, pH of 6.5, and T = 294 K with the % copper removal of 95%.

6.1 Introduction

Industrial activity generates large quantities of aqueous effluents that contain high levels of harmful species. Copper is a hazardous metal due to its non-biodegradability and accumulation in the environment such as the food chain. It may thus pose a serious effect not only to human beings [1], but also to plants, animals and aquatic life [2]. As a result, the World Health Organization (WHO) set the maximum concentration of Cu in drinking water at 2 mg/L [3]. Therefore, industrial effluents containing high levels of copper need to be treated before being released into the environment.

To remove copper from wastewater, a low cost, robust technology with minimum manpower, and limited energy consumption is required. Adsorption has been demonstrated to be a suitable candidate if applied under appropriate conditions [4] and [5]. A wide range of low-cost porous solids,

such as clays, fly ash, activated carbon and silica materials have been used [6]. However, such materials have non uniform pore structures and often poor performance. Periodic mesoporous materials exhibit many attractive characteristics such as large specific surface area, high porosity, controllable and narrowly distributed pore sizes, and often ordered pore arrangements. Thus, the development of functionalized mesoporous adsorbents for heavy metal ions using incorporated ligands with appropriate functional groups has generated considerable interest [7]. SBA-15 is among the most attractive mesoporous silicas because of its large, adjustable pores (5–30 nm) and thick pore walls, around 4 nm. Furthermore, functionalization of mesoporous materials via co-condensation was reported to yield higher and more uniform surface coverage of the organic functionalities without the possible blockage of the mesopores [8-10]. However, amine-modified SBA-15 prepared by this method was found to have poor copper adsorption performance [11]. In earlier contributions, we showed that upon proper pretreatment, this material became a highly efficient copper adsorbent with high sensitivity and fast kinetics [12, 13].

Many studies concerning adsorption uptake of copper have indicated that temperature, pH, initial copper concentration, adsorbent dosage and other experimental parameters influence the removal efficiency [12-14]. However, optimization of these variables has been relatively little studied [15-18]. Optimization of copper uptake by changing one variable (i.e. dosage, pH, concentration, temperature) while maintaining all others at a specified level, is time consuming and expensive. In addition, this method is not able to determine the magnitude of interactions between the process variables. Thus, reliable conclusions regarding optimum working conditions cannot be drawn.

Statistical experimental design methodology can be utilized to optimize the adsorption of copper, improve copper uptake, and reduce process variability, with less development time, number of experiments and overall cost. In addition, statistical design is very useful to determine the magnitude of interactions, which can be used with the estimated major effects to predict an optimum combination of the factors by the developed model [19]. Recently, there have been a number of investigations using experimental design methods to model copper adsorption processes [15, 17, 18, 20]; however, to the best of our knowledge, this approach has never been applied to adsorption of metals using functionalized mesoporous materials. Hence, the aim of the present chapter was to explore the effects of copper concentration, adsorbent/solution ratio, solution pH, and solution temperature on the removal efficiency of copper from aqueous solution using SBA-15 functionalized with 3-aminopropyl-trimethoxy-silane, and to optimize the process conditions using the statistical experimental design methodology. The overall approach used throughout this work including the numerous equations, has been described in a number of publications [19, 22, 23]. The first step was to approximate the removal

efficiency in terms of experimental variables by employing low-order polynomial within two levels of the independent variables using 2^k factorial design of experiments, where k is the number of variables to be considered. If the factorial design generates a nonlinear response behavior upon changing the factor levels, response surface methods are often employed next. This statistical design was used in the current study to determine the quantitative relationship between the response and the levels of the experimental factors. Subsequently, optimization of those levels was carried out.

6.2 Materials and methods

6.2.1 Material synthesis and characterization

The adsorbent used was propylamine-functionalized SBA-15 mesoporous silica prepared by co-condensation. More details regarding the synthesis and characterization of the adsorbent may be found elsewhere [12, 13].

6.2.2 Adsorption experiments

Adsorption of copper was performed using batch procedures in 200 mL glass beaker magnetically stirred at a specified rate (300 rpm). The reactor was immersed in a water bath at a constant temperature within the range 293–333 K. The reaction mixture consisted of a total 100 mL volume of 20–200 mg/L copper solution containing 1–2 g/L of adsorbent, and the pH was adjusted with 0.1 M NaOH or 0.1 M HNO_3 within 4.5–6.5 using an Orion 5 stars instrument, according to the adsorption experimental design levels shown in Table 6.1 and Table 6.2. The suspensions were agitated for 120 min, sufficient time to reach equilibrium. Then, the solution was filtered and the residual copper in solution was analyzed by inductivity coupled plasma (ICP) using a ICP-OES Varian Vista-Pro CCD spectrometer.

Table 6-1. Independent variables and their levels used for 2^4 factorial design.

Variables	Symbol	Range and levels		
		$^{-}$**1**	**0**	$^{+}$**1**
Copper concentration (mg/L)	C	20	60	100
Temperature (K)	T	293	303	313
Solution pH	pH	5.5	6.0	6.5
Adsorbent dosage (g/L)	m	1	1.5	2

Table 6-2. Independent variables and their levels used for surface composite design.

Variables	Symbol	Range and levels				
		$^{-}2$	$^{-}1$	0	$^{+}1$	$^{+}2$
Copper concentration (mg/L)	C	20	40	60	80	100
Temperature (K)	T	293	298	303	308	313
Solution pH	pH	4.5	5.0	5.5	6.0	6.5
Adsorbent dosage (g/L)	m	1	1.2	1.4	1.6	1.8

6.3 Results and discussion

6.3.1 Full factorial model

Copper concentration (C), temperature (T), solution pH and dosage of adsorbent (m) were chosen as the independent variables with their levels and ranges shown in Table 6.1. Results for Cu^{2+} uptake are shown in Table A1 in Appendix A, with the removal efficiency (R%) defined as:

$$R\% = \frac{C_0 - C_e}{C_0} \times 100 \tag{6.1}$$

where C_0 and C_e are the initial and equilibrium concentrations of copper, respectively.

The results were analyzed using the software Minitab, release 15.1, and the main effects and interactions between factors were determined. The main effect of a factor is the change in the removal efficiency associated with a change in the level of the factor. The effects, regression coefficients, and the associated standard errors are shown in Table 6.3. The codified mathematical model employed for the 2^4 factorial design is:

$$R\% = A_0 + \sum_{i=1}^{4} A_i X_i + \sum_{i<j}^{4} \sum_{j=1}^{4} A_{ij} X_i X_j + \sum_{k<i}^{4} + \sum_{i<j}^{4} \sum_{j=1}^{4} A_{ijk} X_i X_j X_k + \varepsilon \tag{6.2}$$

where X_i, X_j, and X_k are the codified values of adsorbent mass, solution pH, initial concentration, and temperature, and ε is the residual error. These codified values were calculated as follows:

$$X_i = \frac{\left(X_{operating\ value}\right) - \frac{1}{2}\left(X_{1+} + X_{1-}\right)}{\frac{1}{2}\left(X_{1+} - X_{1-}\right)} \tag{6.3}$$

A_0 represents the global mean and calculated as follows:

$$A_0 = \frac{\sum response\ of\ factorial\ runs}{number\ of\ factorial\ runs} \tag{6.4}$$

A_{is} are the main effects. They were calculated from the difference between the average high and low factor level responses:

$$Ai = \frac{\sum\left(Response\ at\ X_{1+}\right) - \sum\left(Response\ at\ X_{1-}\right)}{\left(Half\ the\ number\ of\ factorial\ runs\right)} \tag{6.5}$$

A_{ijs} and A_{ijks} are the interaction effects. They were calculated by the same procedure as the main effects. Substituting the coefficients in Eq. (6.2) by their values from Table 6.3, the following relationship was obtained:

$$R\% = 69.32 + 8.37\ m + 6.53\ pH - 6.79\ C + 11.21\ T - 0.73\ mpH - 5.54\ mC - 2.82\ mT + 0.64\ pHC - 1.15\ pHT - 6.91\ CT + 1.46\ mpHC - 0.04\ mpHT + 4.90\ mCT + 1.87\ pHCT + 0.14\ mpHCT \tag{6.6}$$

Since duplicate runs were performed for each individual measurement, standard errors (SE) in the effect values can be calculated by Eq. (6.7) [17]:

$$SE = \left(\frac{\sum\left(d_i\right)^2}{16N}\right)^{0.5} \tag{6.7}$$

where d_i is the difference between each duplicate value and N is the number of duplicated experiments.

The main effects (m, pH, C, T) represent deviations of the average removal efficiency between high and low levels for each one of them as shown in Fig. A1 in Appendix A. Upon changing m, pH, and T values from low to high level, the removal efficiency increased by 16.7%, 13.1%, and 22.4%, respectively. Thus, their effects are considered to be positive. In contrast, the C effect is negative, since a decrease in removal efficiency by 13.6% occurred, when variation from low to high level of C took place.

The interaction effect plots shown in Fig. A2 (Appendix A) provide the mean response of two factors at all possible combinations of their settings. If the lines are not parallel, it is an indication of interaction between the two factors [19]. The interaction plots show that the maximum interaction effect was between T and C with an effect value of 13.83 (Table 6.3). This shows also that the R% was higher at solution temperature of 313 K and concentration of 20 ppm. The R% changed very little at solution concentration of 100 ppm irrespective of the temperature (from 58.2% to 66.8%), while significant change was achieved by increasing T from 293 to 313 K with the solution concentration at 20 ppm (from 58.2% to 94.2%). Interaction effect between m and C showed that the R% was higher at

solution concentration of 20 ppm and adsorbent dosage of 2 mg/mL. The R% changed slightly at low dosage level irrespective of the concentration (63.2–58.7%), while at higher dosage level, the removal efficiency decreased from 89.0% to 66.4% by increasing C from 20 to 100 ppm. Similar observations regarding the effects of these parameters were reported elsewhere for biosorbents [16, 17].

Table 6-3. Statistical parameters for 2^4 design.

Term	Effect	Coefficient	P	DF	SE	SS	MS	F
A_0		69.32	0000		4.08			
m	16.74	8.37	0000	1	4.08	2241	2241	135
pH	13.06	6.53	0000	1	4.08	1365	1365	82
C	-13.58	-6.79	0000	1	4.08	1475	1475	89
T	22.42	11.21	0000	1	4.08	4021	4021	241
mpH	-1.45	-0.73	0.329	1	4.08	17	17	1
mC	-9.08	-4.54	0000	1	4.08	660	660	40
mT	-5.63	-2.82	0.001	1	4.08	254	254	15
pHC	1.27	0.64	0.391	1	4.08	13	13	0.8
pHT	-2.30	-1.15	0.130	1	4.08	42	42	2.5
CT	-13.83	-6.91	0.000	1	4.08	1529	1529	92
mpHC	2.92	1.46	0.060	1	4.08	68	68	4
mpHT	-0.08	-0.04	0.958	1	4.08	0.05	0.05	0
mCT	9.80	4.90	0.000	1	4.08	768	768	46
CTpH	3.75	1.87	0.022	1	4.08	112	112	6.7
mpHCT	0.26	0.14	0.851	1	4.08	0.61	0.61	0.04
Error				16		266.45	16.65	
Total				31		12832		
Lack of fit				6		141	23.5	1.41

6.3.1.1 Analysis of variance (ANOVA)

Determination of the significant main and interaction effects of factors affecting the removal efficiency was followed by performing an analysis of variance (ANOVA). Since all runs were carried out in duplicate, an estimation of error or residue was used to determine the statistically significant factors for removal efficiency of copper ions based on ANOVA. In Table 6.3 the sum of squares (SS) used to estimate the F-ratios (F), which are defined as the ratio of the respective mean square effect (MS_{effect}) and the mean square error (MS_{error}) according to the following equations [19, 22]:

$$\mathrm{SS} = \frac{\left(\sum X_i \times R_i\%\right)^2}{0.5 \times \text{Factorial runs}} \tag{6.8}$$

$$SS_{error} = \sum Variance \tag{6.9}$$

$$MS = \frac{SS}{DF} \tag{6.10}$$

$$F = \frac{MS_{effect}}{MS_{error}} \tag{6.11}$$

Since F value for 95% confidence interval, 1 degree of freedom (DF) and 16 factorial runs (F0.05,1.16) is 4.49 [19], all effects with F higher than 4.49 are statistically significant. Furthermore, since the factors were studied at two levels, each ANOVA main effect and interactions effects have one DF. The smallest level of significance (P) shows that all the main effects and their interaction effects are statistically significant when $P < 0.05$, except the interaction factors containing pH, which means pH has no interaction with the other factors. The only pH interaction effect with significance is CTpH.

6.3.1.2 Student's t-test

Student's t-test was employed in order to determine whether calculated effects were significantly different from zero. For a 95% confidence level and 16 degrees of freedom, the t-value is equal to 2.12 [19]. Fig. 6.1 shows this evaluation as Pareto chart. The vertical line indicates minimum statistically significant effect magnitude for a 95% confidence level. Values shown in the horizontal columns are Student's t-test values for each effect.

Based on F-test and Student's t-test, some effects were eliminated since they did not have any statistical significance, leading to the following model:

$$R\% = 69.32 + 8.37\ m + 6.53\ pH - 6.79\ C + 11.21\ T - 5.54\ mC - 2.82\ mT - 6.91\ CT + 4.90\ mCT + 1.87\ pHCT \tag{6.12}$$

Based on Eq. (6.12), the model was recalculated, eliminating the interaction effects mpH, pHC, pHT, mpHC, mpHT, and mpHCT. The lack of fit resulted from elimination of these factors has F = 1.41 (Table 6.3). Since this value is less than tabulated $F_{0.05,\ 1.16} = 4.49$, this factor is considered to have no statistical significance. The cumulative probability graph in Fig. 6.2 is consistent with the above analysis for significant results. Significant effects are represented by square symbols located away from the center line, while the circle symbols representing the insignificant effects tend to follow a normal distribution since they represent experimental errors.

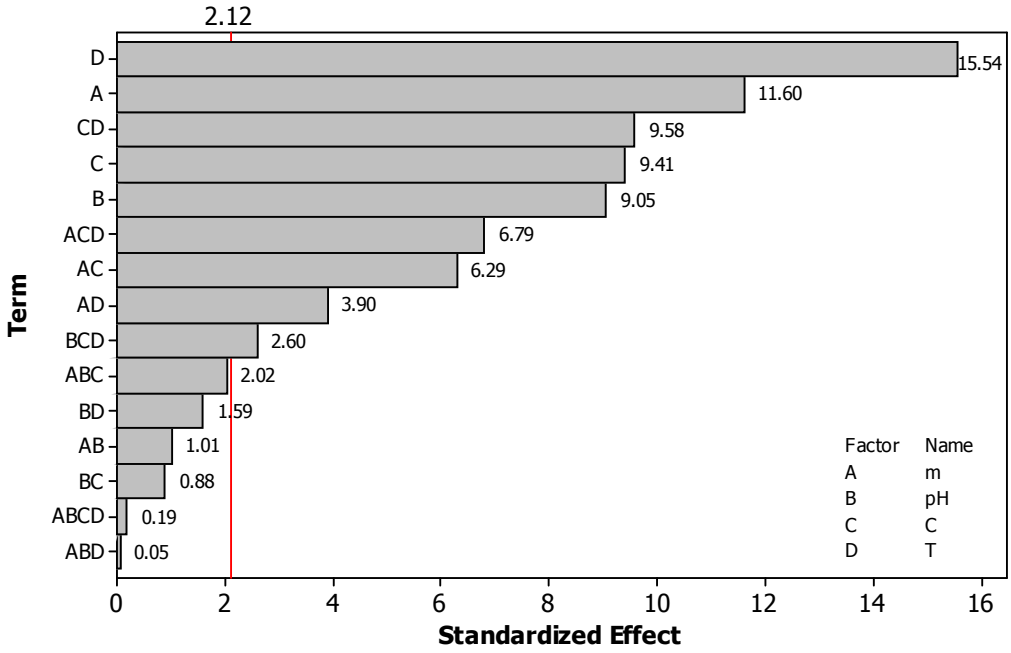

Figure 6-1. Pareto chart of effects on removal efficiency.

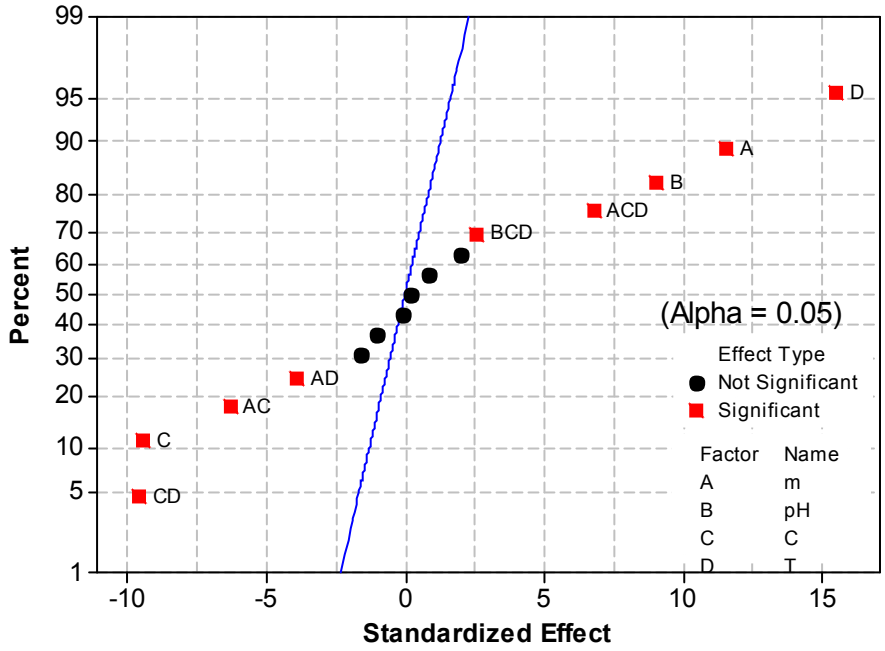

Figure 6-2. Cumulative probability plot of the full factorial model.

6.3.1.3 Residuals and model adequacy

It is important to mention that the model given in Eq. (6.12) is based on many assumptions including constant and independence of the variance on time or run order, which required complete randomization of the experimental runs as shown in Table A1 in Appendix A. Thus, residual plots must be tested to ensure the model adequacy and that this assumption of regression has been met. The residuals are the differences between the observed and fitted values of R%. Fig. A3 (Appendix A) presents the normal probability plot of residuals for copper removal efficiency. It is clear that, experimental points are reasonably aligned suggesting a normal distribution. Furthermore, if the model is correct and the assumptions are satisfied, the residuals should be structureless; they should not be related to any other variable including the predicted response. This is checked by simply plotting the residuals versus fitted values. This plot should not reveal any pattern as shown in Fig. A3. In addition, the assumption of constant variance, i.e. independent on time or run order, is tested by plotting the residuals versus run order, as shown in Fig. A3. There is no reason to suspect any violation of the independent or constant variance assumptions. The histogram distribution of residual removal efficiencies for Cu^{2+} indicated that the data point corresponding to m = $^{-}$1, T = $^{-}$1, C = $^{-}$1, and pH = 1 is considered an outlier since it has standardized residual value larger than 2. After elimination of this outlier, the main effects and interactions were recalculated and shown in Table A2 in Appendix A. It was found that the values of effects did not change significantly. However, the standard error decreased from 4.08 to 3.86, revealing that the discarded data point was in fact an outlier. Table A2 shows the analysis of variance of reduced model fit without outliers, all the factors and interactions effects significantly affect the removal efficiency after modification of the model. Table A2 shows the regression coefficients for the determination of Cu^{2+} uptake models in three versions: full, reduced, and without outliers, with a maximum regression coefficient of 0.9792 obtained for the reduced model without outliers.

6.3.1.4 Test for curvature

A main concern in the use of two-level factorial designs is the assumption of linearity in the factor effects. In fact, if the interaction terms are added to a main effect, then the obtained model is expected to represent some curvature in the response function [19]. This curvature results from the interaction terms. In some situations, the curvature in response function will not be adequately modeled by Eq. (6.2), since curvature in the response is due to quadratic effect. Replication of the central point of the factorial design provides protection against this kind of curvature. To do so, the central point was repeated 6 times, two at the beginning of experiment, two at the middle, and two at the end to ensure

stability of the test. The obtained R% were: 28.1, 34.7, 32.7, 28.1, 30.9 and 30.0%, which will be used to calculate the single degree of freedom sum of square for pure quadratic curvature by Eq. (6.13) [19]:

$$SS_{\text{pure quadratic}} = \frac{n_F n_C (y_{Fave} - y_{Cave})^2}{n_F + n_C} \quad (6.13)$$

where n_F, n_C, y_{Fave}, and y_{Cave} are the number of factorial points, number of central points, average of factorial experiments and average of central experiments, respectively. Thus,

$$SS_{\text{pure quadratic}} = \frac{16 \times 6(69.317 - 30.743)^2}{16 + 6} = 6493$$

And the corresponding F value using data in Table 6.4 and Eq. (6.11) is:

$$F_{pure\ quadratic} = \frac{MS_{pure\ quadratic}}{MS_{error}} = \frac{6493}{16.65} = 390 >> 4.49$$

This high value of $F_{\text{pure quadratic}}$ implies the significance of curvature, therefore using surface composite design is important to generate a more reliable model.

6.3.2 Surface composite design (SCD)

As obtained from the factorial design results, all the main effects (C, T, pH, and m) were found to be important. Thus, all of them were used as independent variables with their levels and ranges listed in Table 6.2. Table A3 (Appendix A) shows the actual values of the independent variables at which the experiments were conducted to estimate the removal efficiency. Experimental results obtained from the SCD model were described using Eq. (6.14):

$$R\% = A_0 + \sum_{i=1}^{4} A_i X_i + \sum_{i=1}^{4} A_{ii} X_i^2 + \sum_{i<j}^{4} \sum_{j=1}^{4} A_{ij} X_i X_j + \varepsilon \quad (6.14)$$

where A_0 is the value for the fixed response at the central point of the experiment; A_i, A_{ii}, and A_{ij} are the linear, quadratic and interaction coefficients, respectively. The results of experiments are shown in Table A3 (Appendix A) and the R% was found to range from 1.6 to 76.9% in response to the variation in the experimental conditions. Substituting the coefficients A_i in Eq. (6.14) by their values from Table 6.4 we obtain:

$$R\% = 26.88 + 4.37m + 8.52pH - 13.04C + 3.92T - 2.42mm + 0.20pHpH + 5.4CC - 0.28TT - 0.63mpH - 2.77mC + 0.25mT - 0.13pHC - 0.70pHT + 0.72CT \quad (6.15)$$

6.3.2.1 Analysis of variance (ANOVA)

The ANOVA and response surfaces were performed using the Design-Expert software (version 8.0.2.0) and the results are presented in Table 6.4. It is shown that copper concentration has the greatest effect on the R% with the highest F-value of 277, which is mainly because the ¯1 level is now 40 mg/L, not 20 mg/L as in the case of factorial design presented earlier. The model F-value of 41 implies the significance of the model.

Since an inadequate model could generate misleading conclusions, model testing is important for data analysis procedure. Not all the effects of parameters were significant. Only values of P less than 0.05 indicate that the corresponding model terms are significant. In this case, m, pH, C, T, mC, m^2, C^2 were significant model terms, whereas the others were insignificant. The significance of m^2, C^2 indicates the non linearity of these effects, which is confirmed by the main effects plot shown in Fig. A4 (Appendix A).

Furthermore, the negative quadratic term for m indicates curvature characteristic of a region containing maximum R%, while the positive quadratic term for C indicates curvature characteristic of a region containing minimum R%. The negative interaction effect between m and C indicates that increasing the levels of both factors is not an efficient way to achieve maximum removal efficiency. The lack of fit F-value of 1.49 implies that the lack of fit is not significant relative to the pure error. In order to improve the effect of significant parameters, the insignificant parameters were eliminated and the final equation in terms of coded factors is shown in Eq. (6.16). The R^2 value for Eq. (6.16) was found to be 0.973, indicating a good agreement between the experimental and the predicted R% [23]. These results indicate that the response surface model constructed in this study for predicting copper removal efficiency is fairly reasonable.

$$R\% = 26.88 + 4.37m + 8.52pH - 13.04C + 3.92T - 2.42mm + 5.4CC - 2.77mC \quad (6.16)$$

6.3.2.2 Residuals and model adequacy

To judge if the selected model provides adequate approximation of the real system or not, the statistical plots provided by the Design Expert 8.0.2.0 software, such as normal probability plots of the studentized residuals, as well as the predicted versus actual value plots were applied. Fig. 6.3 shows the normal probability plots of the studentized residuals for copper removal efficiency. It is clear from the figure that the residuals follow a normal distribution, in which the points follow a straight line. Fig. 6.4 indicates that the predicted values of copper removal efficiency obtained from the model and the actual experimental data were in good agreement, providing evidence for the validity of the regression model.

Table 6-4. Estimated regression coefficients and ANOVA for response surface quadratic model.

Term	Effect	Coeff.	P	SE	DF	SS	MS	F
A_0		26.88	<0.0001	1.41	14	7900	564	41
m	8.74	4.37	<0.0001	0.76	1	458	458	31
pH	17.04	8.52	<0.0001	0.76	1	1742	1742	118
C	-26.08	-13.04	<0.0001	0.76	1	4083	4083	277
T	7.84	3.92	0.002	0.76	1	368	368	25
mm	-4.84	-2.42	0.0031	0.76	1	833	833	60
CC	10.80	5.40	<0.0001	0.70	1	787	787	53
TT	-0.56	-0.28	0.6901	0.70	1	2	2	0.0
pHpH	0.40	0.20	0.7829	0.70	1	1	1	0.0
pHT	-1.40	-0.70	0.4621	0.93	1	8	8	0.0
CT	1.44	0.72	0.4495	0.93	1	8	8	1
mpH	-1.26	-0.63	0.5061	0.93	1	6	6	0
mC	-5.54	-2.77	0.0089	0.93	1	123	123	9
mT	0.50	0.25	0.7881	0.93	1	1	1	0
pHC	-0.26	-0.13	0.895	0.93	1	0	0	0
Residuals					16	222	14	
Lack of fit			0.3246		10	158	16	1.49
Error					6	64	11	
Total					29	8112	280	

*The main factors affecting the adsorption process, m, pH, C, and T are indicated in Italic.

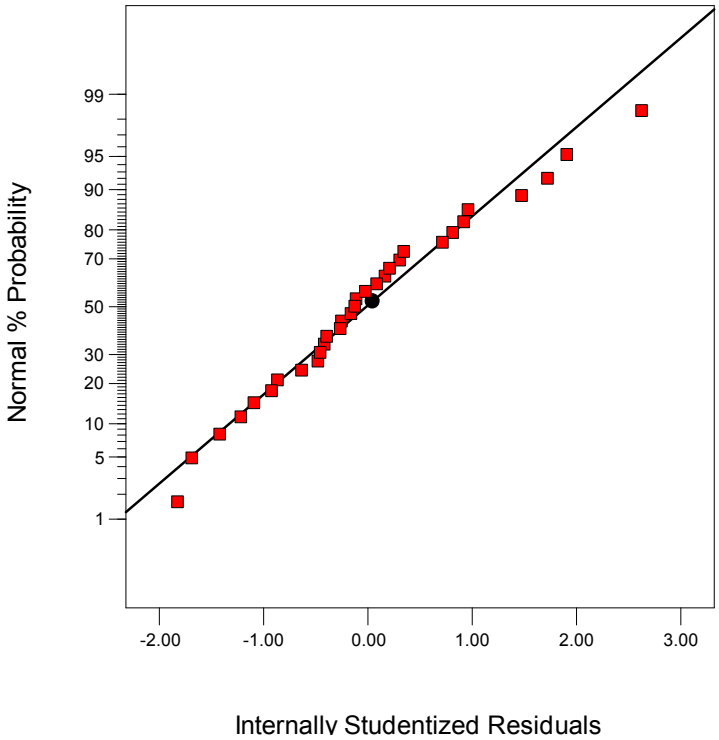

Figure 6-3. Normal % probability versus internally studentized residuals.

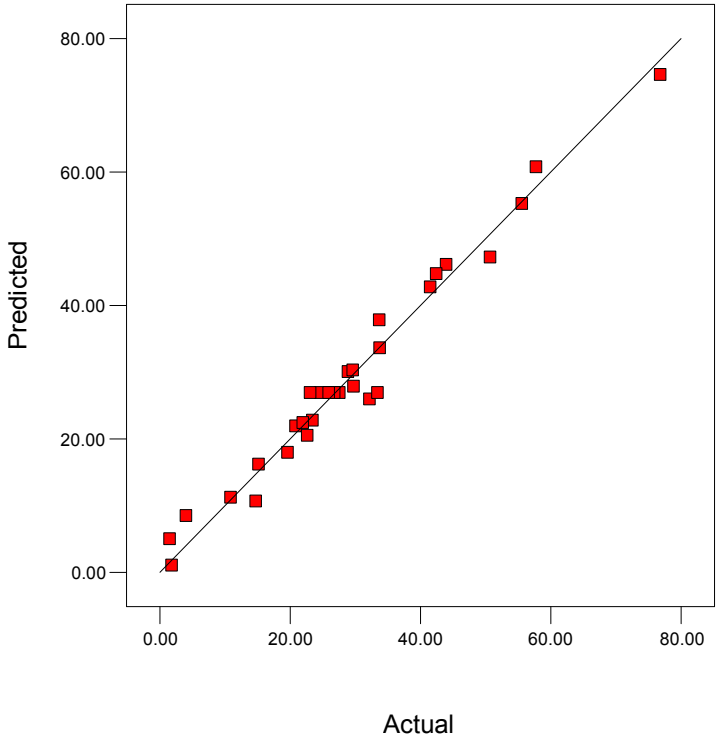

Figure 6-4. Comparison of model predictions with the experimental data.

6.3.2.3 Copper removal efficiency

The 3D surface response plots of the quadratic model were prepared by the Minitab software (release 15.1) and utilized to investigate the interactive relationships between independent variables and removal efficiency. As shown in Fig. 6.5, in each plot, two variables were kept constant at levels of preferred R% (313 K, 1.8 g/L, 6.5, and 20 ppm for T, m, pH, and C, respectively) while the other two were varied within the experimental ranges. Fig. 6.5e shows R% as a function of T and pH, while m and C were kept constant, it is clear that increasing pH to 6.5 results in about 96% removal efficiency even if the temperature was at 293. This is mainly because under this pH value, the positive surface charge decreased and all the amine groups are expected to be neutral and available for adsorption as shown in Scheme 6.1 [12]. In addition, since the concentration was maintained at 20 ppm, there was enough free and easily accessible amine groups to remove most of the copper according to Scheme 6.2a, without additional heat for enhanced diffusion of copper ions within the pores, release of hydrogen-bonded amine groups (Scheme 6.2b), or enhanced surface ion-exchange (Scheme 6.2c) [12]. Freitas et al. [16] reported similar observations, but with stronger dependence on temperature at high pH level, which is possibly due to the higher concentration (50 ppm) and lower pH (4.5) they used. Moreover, increasing T to 313 K while pH is at 4.5 resulted in only 76% removal since under such low pH, some of the amine groups are protonated as shown in Scheme 6.1c [12, 21], thus unavailable for adsorption in addition to higher density of positive charge resulting in increased diffusion resistance. The later could be overcome by increasing T whereas the effect of protonated amine cannot be decreased by increasing T. Combining T at 313 K with 6.5 for pH resulted in 100% removal efficiency. Combining C with the other parameters (Figs. 6.5b, d, and f) confirm the previously discussed significance of concentration. It is clear from these plots that under the experimental conditions used, higher removal efficiency could be achieved by decreasing the concentration level. This is mainly due to saturation of adsorption sites at high concentration as reported by Sahan et al. [21]. Fig. 6.5d shows that changing the C level from 100 to 20 ppm at pH level of 4.5 and 6.5 resulted in R% increase from 10 to 77% and from 32 to 100%, respectively, while R% increased by only 23 and 22 units upon changing pH levels from 4.5 to 6.5 at C levels of 20 and 100 ppm, respectively, confirming that application of this material for low copper concentrations (around 20 ppm) is more efficient than pH control. Frietas et al. [16] reported similar effect for C compared to pH in the presence of cophyllum nodosum biosorbent. Using another biosorbent, namely trametes versicolor fungi, Sahan et al. [21] reported optimum concentration at around 60 ppm. Similarly, Fig. 6.5f shows that almost 100% copper removal could be achieved by maintaining C at 20 ppm regardless of T, since at this low concentration, the amount of easily accessible amine groups (Scheme 6.2a) is enough to remove all the copper. Thus,

as mentioned earlier there is no need for additional heat. A maximum of only 33% removal was possible by increasing T to 313 K for concentration at 100 ppm, because at this high concentration, the amount of copper exceeds the maximum capacity of the material. Fig. 6.5c shows that the effect of m is more important than the effect of T. This is simply because by increasing m, the number of available adsorption sites increases. Thus, higher adsorption capacity is achieved without the need for copper cations to diffuse to the internal adsorption sites nor the need to release hydrogen-bonded amine groups (Scheme 6.2b) or for surface ion-exchange (Scheme 6.2c). Furthermore, Fig. 6.5a shows that combination of 1.8 g/L for m with 6.5 for pH is required to achieve 100% removal efficiency due to the increased number of adsorption sites, all present as active NH_2 groups. Decreasing any level resulted in lower removal efficiency as a result of either decreasing the number of adsorption sites or the number of unprotonated amine groups with the worst removal efficiency when both of them are at the low level.

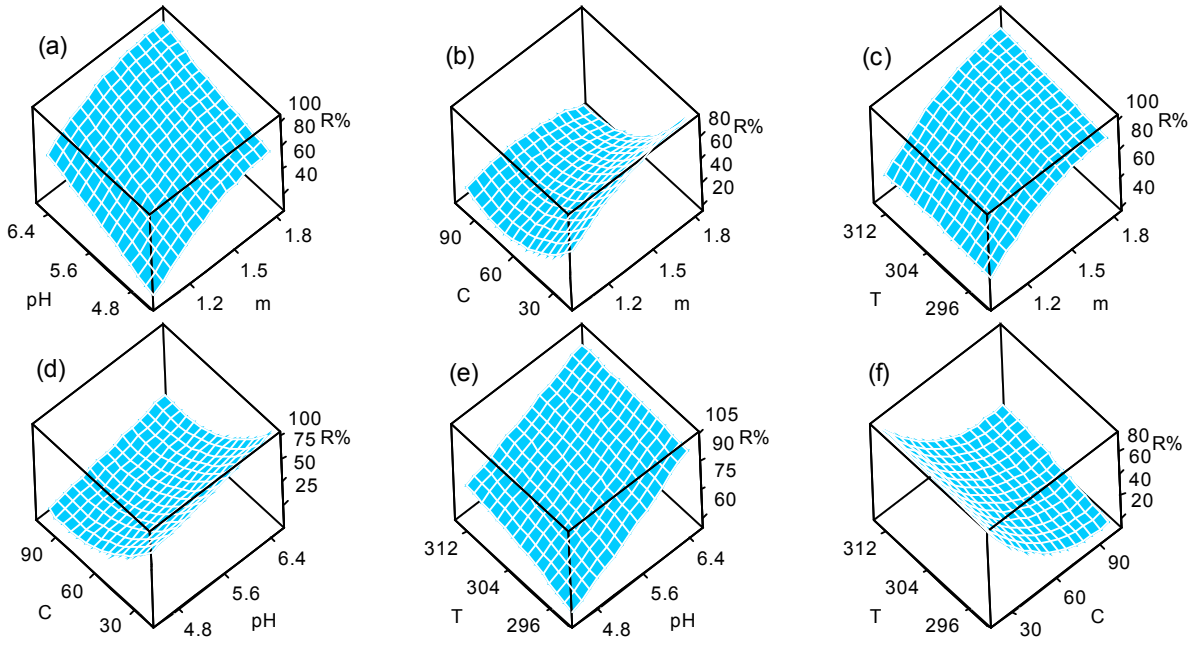

Figure 6-5. 3D surface response plots of the quadratic model.

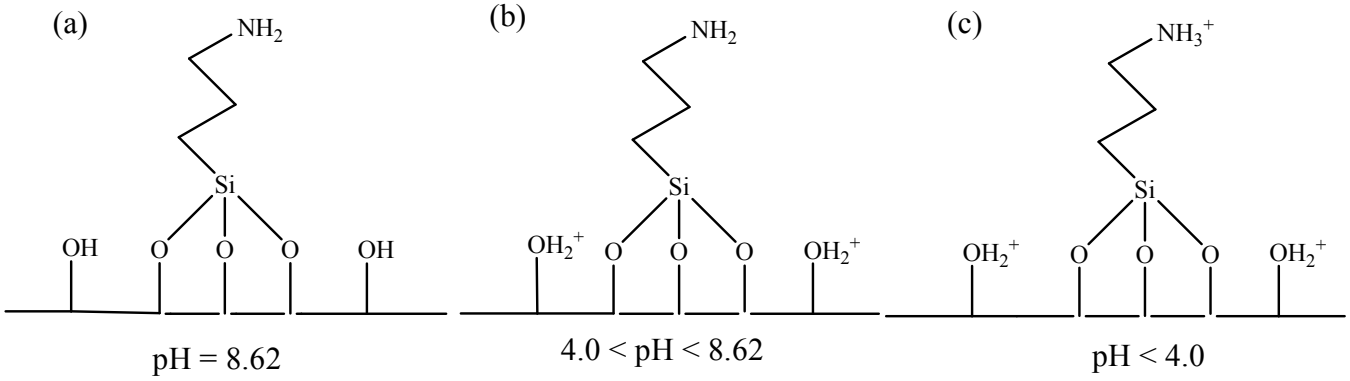

Scheme 6-1. Proposed surface of APTS-SBA-15-AB under different pH conditions.

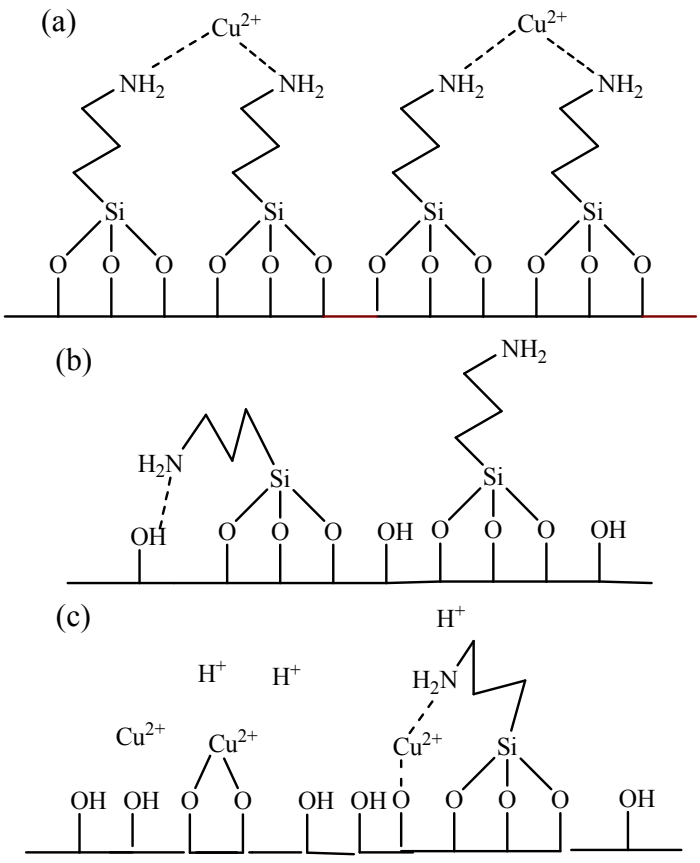

Scheme 6-2. Proposed mechanisms for copper adsorption on APTS-SBA-15-AB.

6.3.2.4 Optimization of operational conditions

To maximize the removal efficiency with the lowest possible m and T, the optimum adsorption conditions were identified using the Design-Expert (version 8.0.2) software. According to the software optimization steps, the desired goal for adsorbent dosage and temperature were chosen as "minimize" since both adsorbent and heating are costly, so it is desirable to keep them as low as possible, while for concentration and pH were chosen as "within the range" and as "maximize" for the removal efficiency (R%) to achieve highest performance. The program begins at a random starting point from 10,000 different combinations and proceeds up to maximum removal efficiency by the goal seeking. Accordingly, the optimum working conditions and respective percent removal efficiencies were established, and the best 18 results can be found in Table A4 (Appendix A). All the 18 combinations of the factors resulted in effluent concentration that meets the World Health Organization limitations of 2 mg Cu/L [3]. However, economically, it is preferred to work at the lowest possible temperature and amount of adsorbent. It is clear in Table A4 (Appendix A) that for all combinations, almost the same amount of adsorbent was required, about 1.55 g/L, while the temperature varied from 293.66 K to 305.88 K. Therefore it is recommended to work with combination no. 12 with 94.72% removal of copper and effluent concentration of 1.06 mg/L under optimized operational conditions of: m = 1.57 g/L; pH = 6.5; C = 20 mg/L, and T = 293.66 K.

6.4 Conclusions

Optimization of the conditions of copper adsorption from aqueous solution using SBA-15 functionalized with 3-aminopropyl-trimethoxy-silane synthesized by co-condensation, to maximize the removal efficiency was achieved using the statistical experimental design methodology. The linear model obtained by 2^4 factorial design showed that all the studied parameters were significant. However, it failed to count for curvature in the system due to higher order interactions effect. The proposed quadratic model obtained by SCD agrees well with the experimental data, with correlation coefficients (R^2) of 0.973. The copper concentration was found to have the most significant effect on the removal efficiency, while other parameters showed less effect. Using Design-Expert software, the optimum conditions were identified to be copper concentration of 20 mg/L, adsorbent/solution ratio of 1.57 g/L, pH of 6.5, and T = 293.66 K with the copper removal efficiency of 95%.

Supplementary Data

Supplementary data for this chapter can be found in Appendix A.

References

[1] M. Komárek, E. Čadková, V. Chrastný, F. Bordas and J.-C. Bollinger, Contamination of vineyard soils with fungicides: a review of environmental and toxicological aspects, *Environ. Int.* 36 (2010) 138–151.

[2] W. de Vries, S. Lofts, E. Tipping, M. Meili, J.E. Groenenberg and G. Schütze, Impact of soil properties on critical concentrations of cadmium, lead, copper, zinc, and mercury in soil and soil solution in view of ecotoxicological effects, *Rev. Environ. Contam. Toxicol.* 191 (2007) 47–89.

[3] World Health Organization, Guidelines for Drinking-Water Quality: Recommendations, third ed., vol. 1, Geneva, 2008.

[4] D. Swami and D. Buddhi, Removal of contaminants from industrial wastewater through various non-conventional technologies: a review, *Int. J. Environ. Pollut.* 27 (2006) 324–346.

[5] W.S. Wan Ngah and M.A.K.M. Hanafiah, Removal of heavy metal ions from wastewater by chemically modified plant wastes as adsorbents: a review, *Bioresour. Technol.* 99 (2008), pp. 3935–3948.

[6] S. Babel and T.A. Kurniawan, Low-cost adsorbents for heavy metals uptake from contaminated water: a review, *J. Hazard. Mater.* 97 (2003) 219-243.

[7] A. Sayari and S. Hamoudi, Periodic mesoporous silica-based organic-inorganic nanocomposite materials, *Chem. Mater.* 13 (2001) 3151–3168.

[8] T. Yokoi, H. Yoshitake and T. Tatsumi, Synthesis of amino-functionalized MCM-41 via direct co-condensation and post-synthesis grafting methods using mono-, di-, and tri-amino-organalkoxysilane, *J. Mater. Chem.* 14 (2004) 951–957.

[9] M. Jaroniec, K. Kurk, C. Jaroniec and A. Sayari, Modification of surface and structural properties of ordered mesoporous silicates, *Adsorption* 5 (1999) 39–45.

[10] X. Wang, J.C. Chan, Y.H. Tseng and S. Cheng, Synthesis, characterization and catalytic activity of ordered SBA-15 materials containing high loading of diamine functional groups, *Microporous Mesoporous Mater.* 95 (2006) 57–65.

[11] J Aguado, J.M. Arsuaga, A. Arencibia, M. Lindo and V. Gascón, Aqueous heavy metals removal by adsorption on amine-functionalized mesoporous silica, *J. Hazard. Mater.* 163 (2009) 213–221.

[12] E. Da'na, A. Sayari, Adsorption of copper on amine-functionalized SBA-15 prepared by co-condensation: equilibrium properties, *Chem. Eng. J.* 166 (2011) 445-453.

[13] E. Da'na, N.D. Silva, A. Sayari, Adsorption of copper on amine-functionalized SBA-15 prepared by co-condensation: kinetic properties, *Chem. Eng. J.* 166 (2011) 454-459.

[14] M.H. Kalavathy and L.R. Miranda, Comparison of copper adsorption from aqueous solution using modified and unmodified Hevea brasiliensis saw dust, *Desalination* 255 (2010) 165–174.

[15] D. Özçimen and A. Ersoy-Meriçboyu, Removal of copper from aqueous solutions by adsorption onto chestnut shell and grapeseed activated carbons, *J. Hazard. Mater.* 168 (2009) 1118–1125.

[16] O. Freitas, C. Delerue-Matos and R. Boaventura, Optimization of Cu(II) biosorption onto Ascophyllum nodosum by factorial design methodology, *J. Hazard. Mater.* 167 (2009) 449–454.

[17] A.R. Cestari, E.F.S. Vieira, I.A. de Oliveira and R.E. Bruns, The removal of Cu(II) and Co(II) from aqueous solutions using cross-linked chitosan: evaluation by the factorial design methodology, *J. Hazard. Mater.* 143 (2007) 8–16.

[18] B. Preetha and T. Viruthagiri, Application of response surface methodology for the biosorption of copper using Rhizopus arrhizus, *J. Hazard. Mater.* 143 (2007) 506–510.

[19] D.C. Montgomery, Design and Analysis of Experiments (seventh ed.), John Wiley and Sons, New York (2008).

[20] E.C. Lima, B. Royer, J.C.P. Vaghetti, J.L. Brasil, N.M. Simon, A.A. dos Santos Jr., F.A. Pavan and E.A.D. Silva, Adsorption of Cu(II) on Araucaria angustifolia wastes: determination of the optimal conditions by statistic design of experiments, *J. Hazard. Mater.* 140 (2007) 211–220.

[21] T. Şahan, H. Ceylan, N. Şahiner and N. Aktaş, Optimization of removal conditions of copper ions from aqueous solutions by Trametes versicolor, *Bioresour. Technol.* 101 (2001) 4520–4526.

[22] R.H. Lochner and J.E. Matar, Designing for Quality: An Introduction to the Best of Taguchi and Western Methods of Statistical Experimental Design, ASQS Quality Press, White Plains (1999).

[23] T.P. Rayan, Modern Experimental Design, John Wiley and Sons, Hoboken (2007).

Chapter 7

Effect of regeneration conditions on the cyclic performance of amine-modified SBA-15 for removal of copper from aqueous solutions: Composite surface design methodology

Desalination 277 (2011) 54-60

Abstract.

The effect of regeneration conditions (solution type, concentration, volume, and temperature) on propylamine-functionalized mesoporous silica was investigated after three adsorption–desorption cycles, under different batchwise regeneration conditions. Three criteria were used to determine the effect of regeneration conditions, namely: adsorption capacity, structural stability and amine loading and accessibility. Using a composite surface design methodology, the effect of these regeneration conditions on the performance of the adsorbent was investigated. It was found that all the studied parameters have a statistically significant influence on the working adsorption capacity with the order: concentration > solution type > temperature > solution volume. With respect to structural properties and amine content, none of the factors was found to be significant. Regeneration using EDTA was found to be more efficient than acid treatment.

7.1 Introduction

The removal of copper ions from aqueous solutions for pollution control is an important industrial challenge. The main sources of this metal in wastewater include electrical, electro-plating, metal finishing and paint industries [1] as well as mine drainage [2]. As many other metals, beyond a certain concentration in water, copper can be harmful [3]. The toxic effect of copper ranges from gastrointestinal distress to liver or kidney damage depending on its concentration and the length of exposure [1]. As a result, its presence in wastewater streams has driven environmental protection

organizations to set up strict regulations to protect water sources for human consumption. As an example, the World Health Organization has limited the amount of copper in drinking water to 2 mgL^{-1} [4]. Therefore, there is a need for highly selective and efficient technologies to remove it from wastewater.

Several techniques are available for removing copper from aqueous solutions including ion exchange [5], biological treatment [6], precipitation [7], conventional coagulation [1], and ultra-filtration [8]. One major issue about some of these techniques is the large volume of sludge produced which may also have potential risks of copper leaching. Therefore, techniques for removing copper and other metal ions that are simple, robust, and environment friendly such as adsorption are needed [9-11].

In a recent review about the current processes for the removal of heavy metal from waste water, Fu and Wang [12] concluded that adsorption is one of the most frequently used methods. In this context, there has been a growing interest in developing adsorption materials with large specific surface area such as mesoporous MCM-41, HMS, and SBA-15 silicas functionalized by several groups, such as $-NH_2$ and -SH, capable of interacting efficiently with metallic cations [13]. Anchoring functional groups on the internal surface of mesoporous silica may be achieved via post-synthesis procedures [14-22] or co-condensation [23-27]. Surface-modified SBA-15 materials prepared by grafting [28, 29], or co-condensation [14, 25, 30, 31] were found to be extremely efficient for the removal of heavy metals from water. In previous contributions, we synthesized SBA-15 functionalized with 3-aminopropyltrimethoxy-silane by co-condensation and used it as adsorbent for Cu^{2+} ions in aqueous solution under different equilibrium [32] and kinetic conditions [33]. Under suitable conditions, the material was found to be very efficient with high adsorption capacity and fast kinetics [32, 33]. Furthermore, we carried out an optimization of the adsorption parameters to maximize the removal efficiency and recommended optimum conditions to achieve at least 95% copper removal efficiency [34]. The maximum adsorption capacity of functionalized SBA-15 at 293, 313, and 333 K was found to be 0.54, 0.87 and 1.32 $mmolg^{-1}$, respectively, corresponding to Cu/N molar ratios of 0.31, 0.50 and 0.76. For comparison, the results obtained by Aguado et al. [35] at 298 K using three different samples of amine-modified SBA-15 prepared by grafting were 0.39, 0.35, and 0.25 $mmolg^{-1}$ with Cu/N mole ratio of 0.14, 0.11, and 0.13, respectively.

All adsorption data reported earlier were obtained via the use of fresh material. However, to be economically feasible, the adsorbent has to be recycled. It is thus essential to ensure that the adsorbent has an adequate mechanical stability and steady metal uptake in a series of adsorption–desorption cycles. Besides reutilization of the adsorbents, desorption studies provide useful insights into the nature

and reversibility of the adsorption process. Furthermore, desorption is important as a metal pre-concentration step to undertake further treatments such as precipitation.

Despite the extensive work on adsorption of heavy metals on functionalized mesoporous materials, limited attention has been paid to the recycling of the metal-loaded materials. Some researchers reported recycling of metal-loaded adsorbents by washing with acidic solutions [17, 19, 27, 32, 36] or via treatment with a complexing agent such as ethylenediamine-tetraacetic-acid (EDTA) [30, 32, 37], to elute the metal cations. After metal desorption with acids, amine-containing adsorbents are regenerated typically in the presence of $NaHCO_3$ solution to neutralize the positively charged ammonium groups into free amine [27, 32, 38]. However, all of these works were performed under limited conditions and focused only on the change in the adsorption capacity without considering the factors that may affect the adsorbent cyclic performance. The kinetics of copper desorption was also investigated by Tseng et al. [37] and Wambu et al. [39].

Many factors are expected to affect the adsorbent during the regeneration process including the type of solution used (i.e. acidic treatment or complexing agent), concentration of solution, volume of solution, and temperature of regeneration. Thus, the objective of this chapter was to study the behavior of amine-functionalized SBA-15 as copper adsorbent over three cycles as a function of regeneration conditions using the composite surface design methodology described by Montgomery [40]. Keeping in mind that this is the first attempt to study the regeneration of a copper-loaded adsorbent by this method, it is worth mentioning that the purpose of this statistical study was to shed light on the effect of desorption conditions rather than developing a mathematical model for predicting adsorption capacity after a certain number of cycles.

7.2 Materials and methods

7.2.1 Adsorbent synthesis and characterization

Details of adsorbent synthesis and characterization may be found elsewhere [32]. Briefly, 4 g of P123 and 8 g KCl were dissolved in 30 mL of water and 120 mL of a 2 M HCl solution at 40 °C. Then, 8.5 g of tetraethylorthosilicate was added and prehydrolyzed for 2 h before adding 1.08 g of 3-aminopropyltrimethoxy-silane (APTS). The mixture was stirred for 20 h then heated at 100 °C for 24 h in static conditions. The material was collected by filtration, dried in air at room temperature and then extracted with ethanol. The material was further treated in aqueous 0.1 M HCl for 1 h and neutralized in 0.1 M $NaHCO_3$, then filtered and dried under vacuum at 100 °C for 3 h. The material will be referred to as APTS-SBA-15-AB.

The structural properties of the samples before and after regeneration were determined by nitrogen adsorption at 77 K using a Micromeritics ASAP 2020 volumetric apparatus. Prior to each analysis, the samples were degassed under vacuum at 60 °C for 3–5 h. The surface area was determined by the BET method, whereas the pore size distribution was calculated using the Kruk–Jaroniec–Sayari (KJS) approach [41]. The pore volume was calculated as the amount of liquid nitrogen adsorbed at $P/P_0 = 0.995$.

The amine content was determined using a thermogravimetric analyzer (Q500 TGA, TA Instruments) according to the method developed by Harlick and Sayari [42]. Briefly, the sample was first treated in a flow of ultra high purity (UHP) N_2 at 200 °C for a period of 2 h to remove pre-adsorbed moisture and any methanol stemming from the hydrolysis of unreacted methoxy groups. Subsequently, the organic layer was decomposed by heating at 10 °C/min to 800 °C under flowing N_2, then at 10 °C/min to 1000 °C in flowing air. The material was kept under isothermal conditions for 15 min. The amount of APTS was calculated from the weight loss beyond 200 °C.

7.2.2 Adsorption experiments

Adsorption of copper was performed batchwise in 500 mL glass beaker magnetically stirred at 300 rpm. The reactor was immersed in a water bath at a constant temperature of 333 K. The reaction mixture consisted of a total 300 mL volume of 100 mgL^{-1} copper solution and 1 gL^{-1} of adsorbent. The suspensions were agitated for 2 h, which was sufficient to reach equilibrium. Then, the solution was filtered and the residual copper in solution was analyzed by inductivity coupled plasma (ICP) using an ICP-OES Varian Vista-Pro CCD spectrometer.

7.2.3 Desorption experiments

The copper-loaded adsorbent (200 mg) was added to 7 to 23 mL solution of 0.02 to 0.12 M HCl or EDTA solution in a 50 mL glass beaker. The mixture was stirred at 300 rpm in a water bath at a constant temperature within the range 293–313 K. The conditions for copper removal were as indicated in the experimental design shown in Table 7.1.The suspensions were agitated for 1 h, then filtered, and the powder was dried under vacuum at 373 K for 3 h before being used for another adsorption–desorption cycle. For regeneration experiments carried out with HCl solution, the material was further stirred in 0.1 M $NaHCO_3$ solution for 1 h before filtration and drying.

Table 7-1. Independent variables and their levels used for surface composite design.

Variables	Symbol	Range and levels				
		$^{-}$**1.68**	$^{-}$**1**	**0**	$^{+}$**1**	$^{+}$**1.68**
Concentration (M)	C	0.02	0.04	0.07	0.10	0.12
Temperature (K)	T	293	298	303	308	313
Solution volume (mL)	V	7	10	15	20	23
Solution type	S	Acid (HCl)			EDTA	

7.3 Results and discussion

7.3.1 Composite surface design modeling

Solution concentration (C), temperature (T), solution type (S), and solution volume (V) were chosen as the independent variables with their levels and ranges shown in Table 7.1. The Cu^{2+} removal efficiency after the third adsorption-desorption cycles (R_3) was calculated as:

$$R_3 = \frac{q_3}{q_1} \times 100\% \tag{7.1}$$

where q_1 and q_3 are the adsorption capacity of fresh adsorbent and after the third cycle, respectively. The codified mathematical model employed for the surface composite design is:

$$R_3 = A_0 + \sum_{i=1}^{4} A_i X_i + \sum_{i<j}^{4} \sum_{j=1}^{4} A_{ij} X_i X_j + \sum_{k<i}^{4} + \sum_{i<j}^{4} \sum_{j=1}^{4} A_{ijk} X_i X_j X_k + \varepsilon \tag{7.2}$$

Detailed information about A_0, A_i, A_{ii}, and A_{ij} coefficients and their calculations may be found in an earlier contribution [34]. The experimental findings are shown in Table 7.2. The material efficiency R_3 was found to range from 23 to 113%, indicating a significant effect of the experimental conditions on the cyclic performance of the adsorbent. Substituting the coefficients Ai in Eq. (7.2) by their values from Table 7.3, we obtained the final equation in terms of coded values:

$$R_3 = 61.18 + 5.42\,A + 7.47\,B + 15.83\,C - 11.56\,D + 5.48\,AB - 4.34\,AC - 2.07\,AD + 0.8\,BC + 1.23\,BD - 0.14\,CD + 3.98\,AA + 4.38\,BB + 3.42\,CC \tag{7.3}$$

and in terms of actual factors for EDTA:

$$R_3 = 72.74 + 7.50\,V + 6.24\,T + 15.96\,C + 5.48\,VT - 4.33\,VC + 0.80\,TC + 3.98\,VV + 4.38TT + 3.42\,CC \tag{7.4}$$

and for HCl:

$$R_3 = 49.63 + 3.35\,V + 8.70\,T + 15.69\,C + 5.48\,VT - 4.33\,VC + 0.80\,TC + 3.98\,VV + 4.38\,TT + 3.42\,CC \quad (7.5)$$

7.3.1.1 Analysis of variance (ANOVA)

The ANOVA was performed using the Design-Expert software (version 8.0.2) and the results are presented in Table 7.3. It is shown that the solution concentration has the greatest effect on R_3 with the highest F-value of 89.0. Furthermore, not all the effects of parameters were significant; only values of significance level (P) less than 0.05 indicate that the corresponding model terms are significant. In this case, V, T, C, S, VT, V^2, T^2 and C^2 were significant model terms, whereas the others were insignificant. The significance of V^2 and T^2 indicates the non linearity of V and T. Furthermore, the positive quadratic terms for V, T, and C indicate curvature characteristic of a region containing minimum R_3. The negative effect of S indicates that within the range of conditions studied, the regeneration of APTS-SBA-15-AB with EDTA solution resulted in higher values of R_3.

7.3.1.2 Residuals and model adequacy

To judge whether the selected model provides adequate approximation of the real system or not, the statistical plots, such as normal probability plots of the Studentized residuals, as well as the predicted versus actual value plots were applied. Fig. 7.1 shows the normal probability plots of the Studentized residuals for R_3. It is clear from the figure that the residuals follow a normal distribution, as the data points follow a straight line. Fig. 7.2 indicates that the predicted values of copper removal efficiency obtained from the model and the actual experimental data were in good agreement, providing evidence for the validity of the regression model.

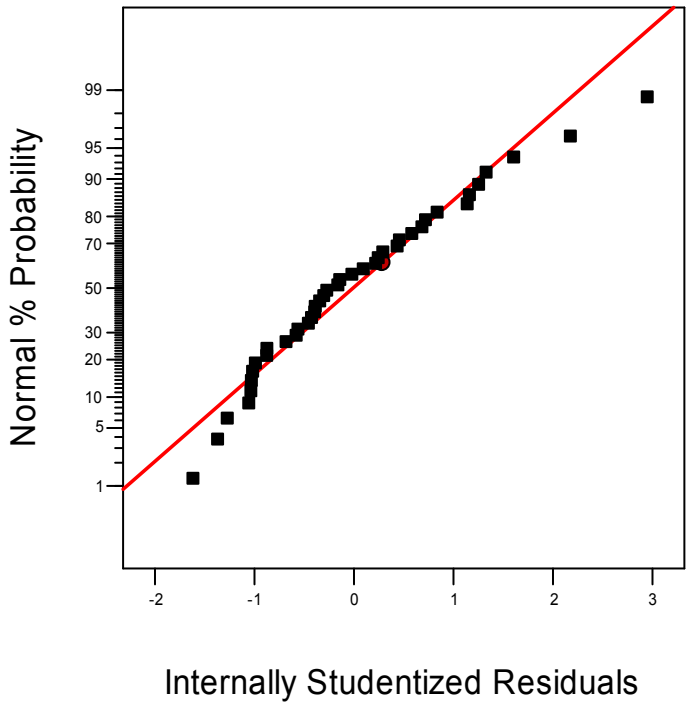

Figure 7-1. Normal % probability versus internally studentized residuals.

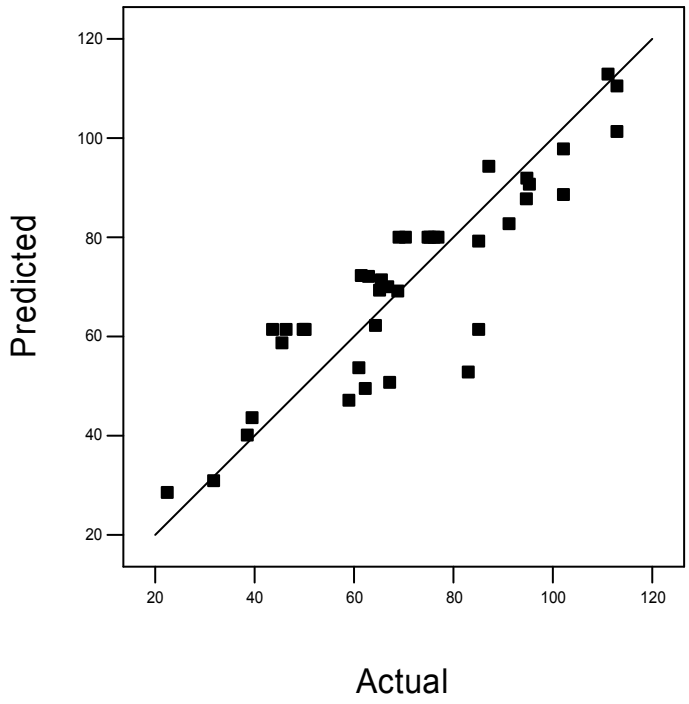

Figure 7-2. Comparison of model predictions of R_3 with the experimental data.

Table 7-2. Response values for different experimental conditions.

Standard order	Random order	V	T	C	S	R_3%	Cu/N
1	25	-1	-1	-1	EDTA	62	0.19
2	24	1	-1	-1	EDTA	66	0.21
3	23	-1	1	-1	EDTA	65	0.20
4	2	1	1	-1	EDTA	85	0.28
5	36	-1	-1	1	EDTA	95	0.34
6	39	1	-1	1	EDTA	102	0.36
7	40	-1	1	1	EDTA	97	0.35
8	37	1	1	1	EDTA	113	0.40
9	14	-1.68	0	0	EDTA	62	0.20
10	7	1.68	0	0	EDTA	95	0.29
11	5	0	-1.68	0	EDTA	65	0.22
12	1	0	1.68	0	EDTA	95	0.32
13	5	0	0	-1.68	EDTA	59	0.19
14	38	0	0	1.68	EDTA	111	0.40
15	25	0	0	0	EDTA	70	0.23
16	9	0	0	0	EDTA	77	0.22
17	10	0	0	0	EDTA	76	0.23
18	11	0	0	0	EDTA	75	0.24
19	20	0	0	0	EDTA	75	0.24
20	13	0	0	0	EDTA	69	0.21
21	32	-1	-1	-1	HCl	32	0.32
22	35	1	-1	-1	HCl	39	0.10
23	34	-1	1	-1	HCl	40	0.14
24	8	1	1	-1	HCl	83	0.12
25	15	-1	-1	1	HCl	67	0.24
26	21	1	-1	1	HCl	46	0.22
27	16	-1	1	1	HCl	91	0.15
28	12	1	1	1	HCl	95	0.30
29	22	-1.68	0	0	HCl	62	0.19
30	19	1.68	0	0	HCl	69	0.22
31	4	0	-1.68	0	HCl	67	0.21
32	17	0	1.68	0	HCl	63	0.20
33	26	0	0	-1.68	HCl	23	0.07
34	3	0	0	1.68	HCl	87	0.29
35	31	0	0	0	HCl	50	0.15
36	29	0	0	0	HCl	51	0.14
37	18	0	0	0	HCl	50	0.16
38	30	0	0	0	HCl	50	0.15
39	27	0	0	0	HCl	44	0.10
40	33	0	0	0	HCl	46	0.15

Table 7-3. Estimated regression coefficients and ANOVA for response surface quadratic model.

Source	F Value	p-value	Coefficient Estimate	Standard Error
A_0	16.6	< 0.0001	61.18	2.53
A-V	10.5	0.0033	5.42	1.68
B-T	19.8	0.0001	7.47	1.68
C-C	89.0	< 0.0001	15.83	1.68
D-S	69.5	< 0.0001	-11.56	1.39
AB	6.2	0.0191	5.48	2.19
AC	3.9	0.0586	-4.34	2.19
AD	1.5	0.2274	-2.07	1.68
BC	0.1	0.7183	0.80	2.19
BD	0.5	0.4713	1.23	1.68
CD	0.0	0.9359	-0.14	1.68
A^2	5.9	0.0220	3.98	1.63
B^2	7.2	0.0125	4.38	1.63
C^2	4.4	0.0460	3.42	1.63

7.3.2 Effect of regeneration conditions on adsorption performance

The 3D surface response plots of the quadratic model were generated by the Minitab software (release 15.1) and utilized to investigate the interactive relationships between independent variables and the removal efficiency after the third cycle. As shown in Fig. 7.3 and Fig 7.4, in each plot, one variable was kept constant at level 0, while the other two were varied within the experimental ranges. It is clear from these plots that under the conditions used in this study, sufficient concentration is the main requirement for efficient desorption of copper. In Fig. 7.3 and Fig 7.4, the 3D response surface plots were established for EDTA and HCl regeneration, respectively. Fig. 7.3b shows that 10 mL of 0.12 M EDTA was more efficient than using 20 mL of 0.04 M solution. This obviously associated with the larger number of moles of EDTA, which is important to ensure that the regeneration process could be used to concentrate copper from wastewater sources using as little water as possible. Moreover, regeneration in the presence of EDTA seems to be more efficient than HCl. For example, using 20 mL of 0.1 M EDTA solution resulted in 98% R_3, whereas Fig. 7.4b shows that desorption with 20 mL of 0.1 M HCl resulted in only 70% R_3. It is also clear that the effect of C is more significant when working at low level of V. An increase in R_3 of about 40 units was obtained by changing C from 0.04

to 0.1 M using 10 mL of solution while R_3 increased by only 22 units when working with 20 mL of solution. Comparing Fig. 7.3 with Fig. 7.4 shows that the HCl level used in this work provided only a limited driving force to elute the adsorbed copper.

Fig. 7.3 and Fig 7.4 show that regeneration at high temperature is advantageous as this provided additional driving force to facilitate diffusion within the pores and elute the copper ions. Fig. 7.3c shows that increasing the EDTA concentration from 0.04 to 0.1 M at T of 293 and 308 K resulted in R_3 increase from 59 to 89% and from 70 to 103%, respectively, while only 11 and 15 units increase in R_3 were obtained by increasing temperature from 293 to 308 K with C of 0.04 and 0.1 M, respectively. Fig. 7.3a shows that R_3 of 100% could be achieved by combining high level of both V and T, while a maximum of only 72% was possible when desorption was performed with 10 mL at 298 K. It is also clear that the benefit of increasing V or T level can only be achieved if the other is at high level also. As an example, it would be a waste of energy if one decided to improve regeneration using 10 mL of solution by increasing the temperature to 308 K. Similarly, Fig. 7.4a shows R_3 as a function of V and T using HCl regeneration solution. As seen, R_3 is considerably higher when the adsorbent is regenerated at high level of both V and T. Furthermore, at low level of V or T, the other regeneration conditions (T or V) did not seem to have a significant impact on R_3. When high level of V was used, an increase in R_3 from 47 to 75% was achieved by increasing T from 298 to 308 K. Similarly, at high level of T, increasing V from 10 to 20 mL resulted in 22 units increase in R_3. The maximum possible value of R_3 within the experimental range shown in Fig. 7.3 was 75% compared to 100% under similar conditions, but using EDTA instead of HCl.

It is clear in Fig. 7.4c that R_3 of 83% can be achieved when using 0.1 M HCl at 308 K and level 0 of V compared to 104% when HCl was replaced with EDTA (Fig. 7.3c). It is also clear that under such conditions, the effect of concentration was higher than that of temperature. R_3 increased by 20 and 16 units by increasing T from low to high level when working at high and low level of C, respectively. While an increase of 33 units can be achieved by changing the level of T when working under low and high level of C.

Fig. 7.3 and Fig 7.4 show clearly that under all regeneration conditions, EDTA was more efficient than HCl. Treatment of the copper-loaded material three times with a aqueous solution HCl with all factors maintained at level 1 resulted in a maximum R_3 of 90% vs. 113% for EDTA solution. This is most likely associated with the high stability of corresponding complex. The lower performance associated with acidic treatment may be due to one or more of the following possible reasons: (i) loss of amine groups with acid washing, (ii) protonation of functional groups after copper release, which might not be completely neutralized by $NaHCO_3$ treatment, (iii) strong interaction of some of the Cu^{2+}

ions with the amine groups, which cannot be released with HCl washing. Overall, EDTA treatment of this material showed excellent regeneration. In a previous work [32], we obtained 10% loss of adsorption capacity after ten cycles using EDTA compared to 60% loss using HCl. Tseng et al. [37] reported also that EDTA is an excellent regenerator to remove copper from a polymer adsorbent. Furthermore, EDTA regeneration requires less steps. However, it is more expensive than acid-base treatment. Thus, evaluation of the process economics is necessary to decide whether penalty in terms of adsorption capacity or extra EDTA cost is more favorable.

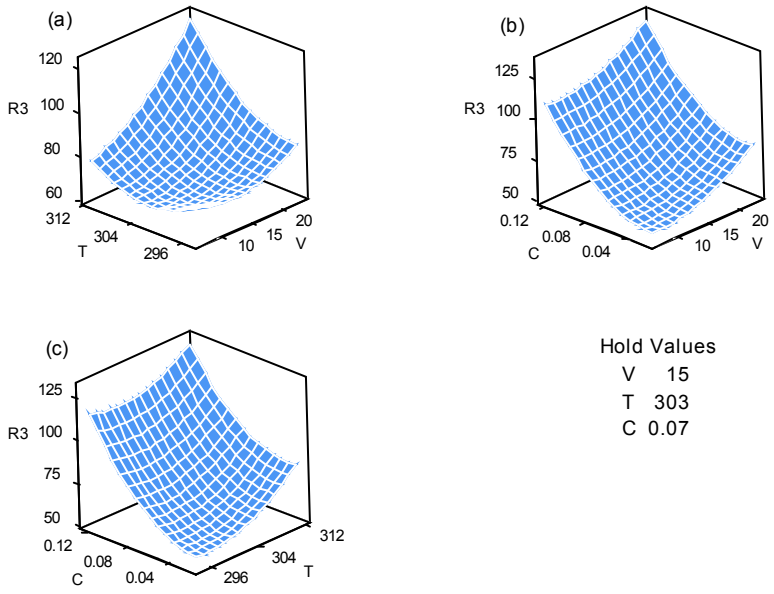

Figure 7-3. 3D surface response plots of the quadratic model for regeneration with EDTA solution.

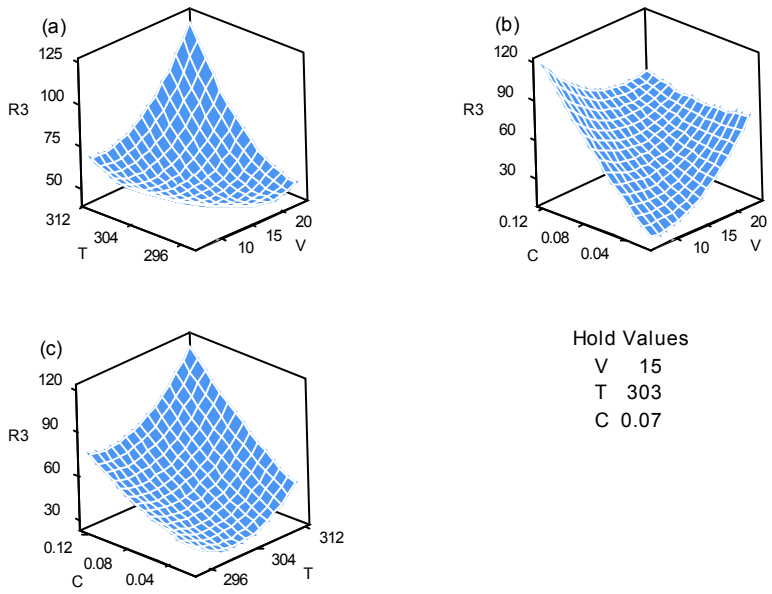

Figure 7-4. 3D surface response plots of the quadratic model for regeneration with HCl solution.

7.3.3 Effect of regeneration conditions on amine loading and accessibility

Fig. 7.5 shows the values of R_3 under the different regeneration conditions listed in Table 7.2 as a function of the residual amine content defined as the ratio of amine content after the third cycle to the amine content of the fresh adsorbent. It is clear that, within the regeneration conditions studied, the use of EDTA solution generally resulted in higher values of R_3 compared to HCl regeneration. Furthermore, it is clear from the figure that there is no relationship between R_3 and the residual amine content. Indeed, R_3 may fluctuate strongly at constant amine content. For example, at an amine content of 0.92, R_3 values of 23, 32, 59, and 67% were obtained. A possible explanation of this variation is that not all the copper has been removed upon regeneration, thus not all the amine groups have been freed. Indeed, it is possible that some conditions lead to incomplete regeneration of the adsorbent due to the absence of driving force capable of removing all the copper adsorbed. This is consistent with the light blue color of some of the regenerated samples, especially when HCl solution was used. Furthermore, some of the amine groups generated after the acidic treatment may not have been neutralized by the basic treatment leading to diminished R_3. Similarly, for a residual amine loading of 0.82, samples regenerated with EDTA have different R_3 values of 95, 97, 102, 111, and 113%, confirming that regeneration conditions other than the type of solution affect the availability and accessibility of amine groups by facilitating diffusion within the pores, enhancing EDTA-Cu complex formation, or supplying sufficient EDTA to combine with all available copper. Table 7.2 shows the Cu/N ratio as mol Cu adsorbed/mol amine. It is clear that, compared to fresh sample (Cu/N = 0.32), the Cu/N ratio

increased by about 15% for some samples regenerated with EDTA, while decreased in all samples regenerated with HCl confirming that EDTA is a better regeneration medium than HCl.

To further investigate the effect of regeneration conditions on the amine residual content, a statistical analysis was applied to shed light on the importance of each parameter. This analysis (results are not shown) indicated that, as far as amine residual content is concerned, none of the parameters can be considered significant. This is consistent with the data shown in Fig. 7.5, where it is evident that the quality or the state in which amine exists after regeneration is more important than the actual amount of amine.

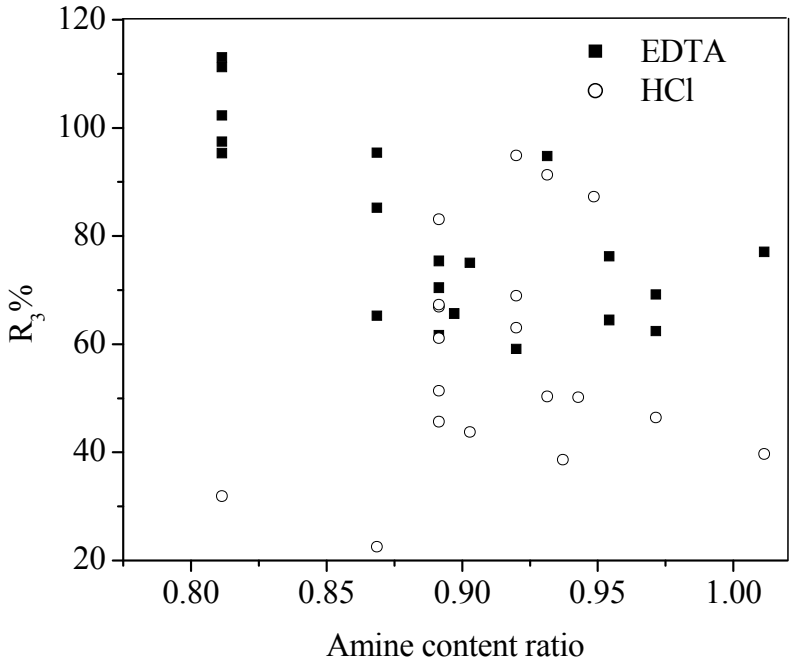

Figure 7-5. R_3 as a function of amine content (%) for all experimental conditions.

7.3.4 Effect of regeneration conditions on structural properties

The structural stability of APTS-SBA-15-AB samples was evaluated using N_2 adsorption measurements before and after three adsorption–regeneration cycles under the different conditions shown in Table 7.2. The N_2 adsorption–desorption isotherms and pore size distributions for some of the samples are shown in Fig. 7.6 and Fig. 7.7 for illustration. After being recycled three times, the materials exhibited higher capillary condensation steps at higher relative pressure, suggesting the occurrence of larger pores and pore volume as shown in Table 7.4. The results suggest that the recycling treatment may cause some changes in the structural properties of the materials. Nevertheless, all the N_2 adsorption–desorption isotherms were still of type IV but with less sharp capillary

condensation steps, indicative of some broadening of pore size distributions. Table 7.4 lists the BET surface area, pore volume, and pore size of APTS-SBA-15-AB before and after recycling. It is clear that the surface area of APTS-SBA-15-AB decreased upon recycling, but remained significantly high, and the pore size distribution remained relatively narrow (Fig. 7.7).

Table 7-4. Structural properties of APTS-SBA-15-AB before and after regeneration.

Samples in standard order	**Surface Area (m^2g^{-1})**	**Pore volume (cm^3g^{-1})**	**Pore size (nm)**
Fresh	673	0.75	7.6
2	508	1.07	10.0
10	332	0.71	8.5
13	489	1.13	9.2
16	468	0.96	8.1
19	500	1.09	8.7
21	378	1.01	10.7
23	389	0.89	9.2
32	461	1.07	9.3
33	428	1.06	9.9
38	450	1.05	9.3

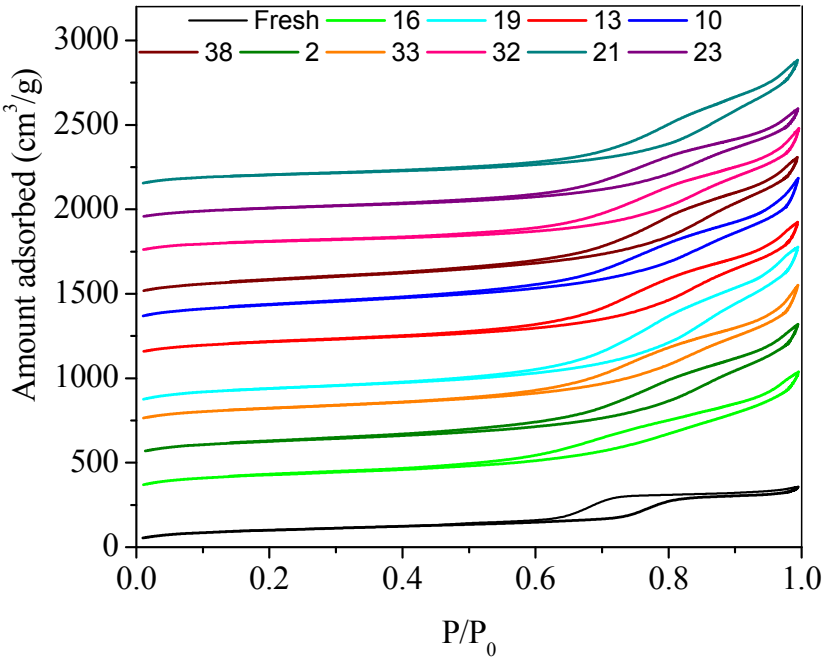

Figure 7-6. Nitrogen adsorption-desorption isotherms for APTS-SBA-15-AB before and after regeneration.

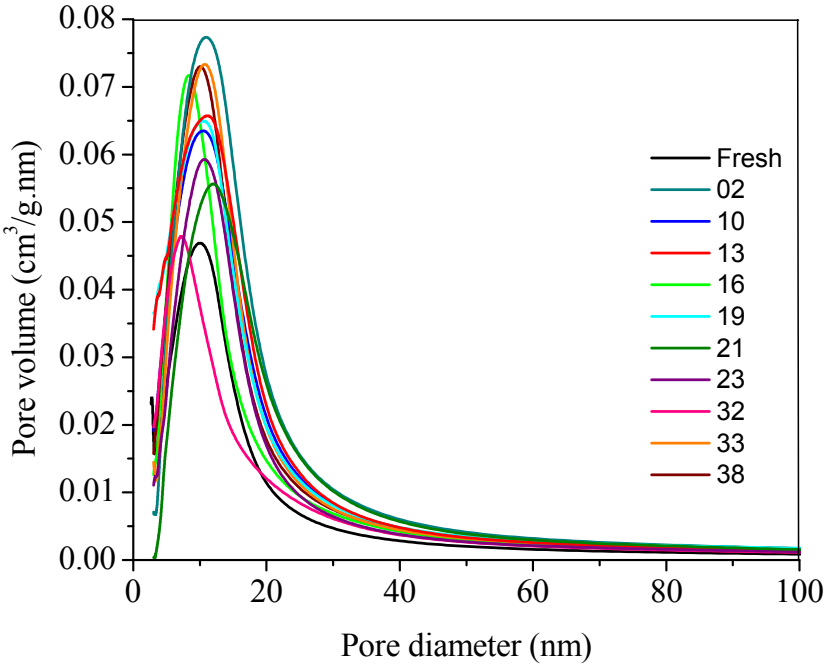

Figure 7-7. Pore size distributions for APTS-SBA-15-AB before and after regeneration.

7.4 Conclusions

The performance of APTS-SBA-15-AB for copper adsorption was investigated under different regeneration conditions including type of solution, concentration, volume, and temperature over three adsorption–desorption cycles. Statistical surface design analysis indicated that all the studied parameters have significant effect on the adsorption capacity, while none of them was significant for amine content or structural properties. APTS-SBA-15-AB was found to have good structural stability during adsorption–desorption cycles, using HCl or EDTA as desorbing agents. Despite an average 10% amine loss due to adsorbent reuse in successive cycles, the metal uptake increased by 13% in some of the samples regenerated with EDTA. Overall, EDTA treatment of this material showed excellent regeneration. However, in-depth economical evaluation is needed to make a reliable assessment regarding the most suitable desorption conditions.

References

[1] D.W. O'Connell, C., Birkinshaw and T.F. O'Dwyer, Heavy metal adsorbents prepared from the modification of cellulose: a review, *Bioresour. Technol.* 99 (2008) 6709–6724.

[2] X. Huang, M. Sillanpää, E.T. Gjessing, S. Peräniemi and R.D. Vogt, Environmental impact of mining activities on the surface water quality in Tibet: Gyama valley, *Sci. Total Environ.* 408 (2010), 4177–4184.

[3] H.P. Cheng, L.C. Su and C.Y. Chen, Thermodynamics and kinetics of adsorption of Cu(II) onto waste iron oxide, *J. Hazard. Mater.* 144 (2007) 406–411.

[4] World Health Organization (Third edition), Guidelines for drinking-water quality: Recommendations Volume 1 (2008) Geneva.

[5] O. Hamdaoui, Removal of copper(II) from aqueous phase by Purolite C100-MB cation exchange resin in fixed bed columns: Modeling, *J. Hazard. Mater.* 161 (2009) 737–746.

[6] H. Guo, S. Luo, L. Chen, X. Xiao, Q. Xi, W. Wei, G. Zeng and Y. He, Bioremediation of heavy metals by growing hyperaccumulaor endophytic bacterium Bacillus sp. L14, *Bioresour. Technol.* 101 (2010) 8599–8605.

[7] D. Feng, C. Aldrich and H. Tan, Treatment of acid mine water by use of the heavy metal precipitation and ion exchange, *Miner. Eng.* 13 (2000) 623–642.

[8] K. Trivunac and S. Stevanovic, Removal of heavy metals ions from water by complexation-assisted ultrafiltration, *Chemosphere* 64 (2006) 486–491.

[9] C. Xiong and C. Yao, Synthesis, characterization and application of triethylenetetramine modified polystyrene resin in removal of mercury, cadmium and lead from aqueous solutions, *Chem. Eng. J.* 155 (2009) 844–850.

[10] C.H. Xiong and C.P. Yao, Study on the adsorption of cadmium(II) from aqueous solution by D152 resin, *J. Hazard. Mater.* 166 (2009) 815–820.

[11] C. Xiong, C. Yao, L. Wang and J. Ke, Adsorption behavior of Cd(II) from aqueous solutions onto gel-type weak acid resin, *Hydrometallurgy* 98 (2009) 318–324.

[12] F. Fu and Q. Wang, Removal of heavy metal ions from wastewaters: A review, *J. Environ. Manage.* 92 (2011) 407–418.

[13] A. Sayari and S. Hamoudi, Periodic mesoporous silica-based organic–inorganic nanocomposite materials, *Chem. Mater.* 13 (2001) 3151–3168.

[14] O. Olkhovyk and M. Jaroniec, Ordered mesoporous silicas with 2,5-dimercapto-1,3,4-thiadiazole ligands: high capacity adsorbents for mercury ions, *Adsorption* 11 (2005) 205–214.

[15] O. Olkhovyk, V. Antochshuk and M. Jaroniec, Benzoythiourea-modified MCM-48 mesoporous silica for mercury (II) adsorption from aqueous solutions, *Colloids Surf., A* 236 (2004) 69–72.

[16] Y. Shiraishi, G. Nishimura, T. Hirai and I. Komasawa, Separation of transition metals using inorganic adsorbents modified with chelating ligands, *Ind. Eng. Chem. Res.* 41 (2002) 5065–5070.

[17] V. Antochshuk and M. Jaroniec, 1-Allyl-3-propylthiorea modified mesoporous silica for mercury removal, *Chem. Commun.* (2002) 258–259.

[18] A.M. Liu, K. Hidajat, S. Kawi and D.Y. Zhao, A new class of hybrid mesoporous materials with functionalized organic monolayers for selective adsorption of heavy metal ions, *Chem. Commun.* (2000) 1145–1146.

[19] L. Zhang, C. Yu, W. Zhao, Z. Hua, H. Chen, L. Li and J. Shi, Preparation of multi-amine-grafted mesoporous silicas and their application to heavy metal ions adsorption, *J. NonCryst. Solids* 353 (2007) 4055–4061.

[20] X. Feng, G.E. Fryxell, L.Q. Wang, A.Y. Kim, J. Liu and K.M. Kemner, Functionalized monolayers on ordered mesoporous supports, *Science* 276 (1997) 923–926.

[21] J. Liu, X. Feng, G.E. Fryxell, L.Q. Wang, A.Y. Kim and M. Gong, Hybrid mesoporous materials with functionalized monolayers, *Adv. Mater.* 10 (1998) 161–165.

[22] H. Lee and J. Yi, Removal of copper ions using functionalized mesoporous silica in aqueous solution, *Sep. Sci. Technol.* 36 (2001) 2433–2448.

[23] l. Bois, A. Bonhommé, A. Ribes, B. Pais, G. Raffin and F. Tessier, Functionalized silica for heavy metal ions adsorption, *Colloids Surf., A* 221 (2003) 221–230.

[24] K. Inumaru, Y. Inoue, S. Kakii, T. Nakano and S. Yamanaka, Molecular selective adsorption of dilute alkylanilines from water by alkyl-grafted MCM-41: tunability of the cooperative organic-inorganic function in the nanostructure, *Phys. Chem. Chem. Phys*. 6 (2004) 3133–3139.

[25] J. Aguado, J.M. Arsuaga and A. Arencibia, Adsorption of aqueous mercury (II) on propylthiol-functionalized mesoporous silica obtained by co-condensation, *Ind. Eng. Chem. Res*. 44 (2005) 3665–3671.

[26] R.K. Dey, F.J.V.E. Oliveira and C. Airoldi, Mesoporous silica functionalized with diethylenetriamine moieties for metal removal and thermodynamics of cation-basic center interactions, *Colloids Surf., A* 324 (2008) 41–46.

[27] X. Xue and F. Li, Removal of Cu(II) from aqueous solution by adsorption onto functionalized SBA-16 mesoporous silica, *Microporous Mesoporous Mater.* 116 (2008) 116–122.

[28] A. Shahbazi, H. Younesi, A. Badiei, Functionalized SBA-15 mesoporous silica by melamine-based dendrimer amines for adsorptive characteristics of Pb(II), Cu(II) and Cd(II) heavy metal ions in batch and fixed bed column, *Chem. Eng. J.* 168 (2011) 505–518.

[29] D. Pérez-Quintanilla, A. Sánchez, I. del Hierro, M. Fajardo and I. Sierra, Preconcentration of Zn(II) in water samples using a new hybrid SBA-15-based material, *J. Hazard. Mater.* 166 (2009) 1449–1458.

[30] Y. Jiang, Q. Gao, H. Yu, Y. Chen and F. Deng, Intensively competitive adsorption for heavy metal ions by PAMAM-SBA-15 and EDTA-PAMAM-SBA-15 inorganic-organic hybrid materials, *Microporous Mesoporous Mater.* 103 (2007) 316–324.

[31] M.C. Bruzzoniti, A. Prelle, C. Sarzanini, B. Onida, S. Fiorilli and E. Garrone, Retention of heavy metal ions on SBA-15 mesoporous silica functionalised with carboxylic groups, *J. Sep. Sci.*30 (2007), 2414–2420.

[32] E. Da'na and A. Sayari, Adsorption of copper on amine-functionalized SBA-15 prepared by co-condensation: equilibrium properties, *Chem. Eng. J.* 166 (2011) 445–453.

[33] E. Da'na, N.D. Silva and A. Sayari, Adsorption of copper on amine-functionalized SBA-15 prepared by co-condensation: kinetics properties, *Chem. Eng. J.* 166 (2010) 454–459.

[34] E. Da'na and A. Sayari, Optimization of copper removal efficiency by adsorption on amine-modified SBA-15: experimental design methodology, *Chem. Eng. J.* 167 (2011) 91–98.

[35] J. Aguado, J.M. Arsuaga, A. Arencibia, M. Lindo and V. Gascón, Aqueous heavy metals removal by adsorption on amine-functionalized mesoporous silica, *J. Hazard. Mater.* 163 (2009) 213–221.

[36] A. Sayari, S. Hamoudi and Y. Yang, Applications of pore-expanded mesoporous silica 1: removal of heavy metal cations and organic pollutants from wastewater, *Chem. Mater.* 17 (2005) 212–216.

[37] J.Y. Tseng, C.Y. Chang, C.F. Chang, Y.H. Chen, C.C. Chang, D.R. Ji, C.Y. Chiu and P.C. Chiang, Kinetics and equilibrium of desorption removal of copper from magnetic polymer adsorbent, *J. Hazard. Mater.* 171 (2009) 370–377.

[38] H. Yang, R. Xu, X. Xue, F. Li and G. Li, Hybrid surfactant-templated mesoporous silica formed in ethanol and its application for heavy metal removal, *J. Hazard. Mater.* 152 (2008) 690–698.

[39] E.W. Wambu, G.K. Muthakia, P.M. Shiundu and K.J. Thiongo, Kinetics of copper desorption from regenerated spent bleaching earth, *J. Sci. Res.* 4 (2009) 317–323.

[40] D.C. Montgomery, Design and Analysis of Experiments (Seventh edition), John Wiley and Sons, New York (2008).

[41] M. Kruk, M. Jaroniec and A. Sayari, Application of large pore MCM-41 molecular sieves to improve pore size analysis using nitrogen adsorption measurements, *Langmuir* 13 (1997) 6267–6273.

[42] P. Harlick and A. Sayari, Applications of pore-expanded mesoporous silica. 3. Triamine silane grafting for enhanced CO_2 adsorption, *Ind. Eng. Chem. Res.* 45 (2006) 3248–3255.

Chapter 8

Adsorption of heavy metals on amine-functionalized SBA-15 prepared by co-condensation: Applications to real water samples

Desalination (2011) Accepted manuscript

Abstract.

SBA-15 functionalized with 3-aminopropyltrimethoxy-silane was studied as potential absorbent for Cd^{2+}, Co^{2+}, Cu^{2+}, Zn^{2+}, Pb^{2+}, Ni^{2+}, Al^{3+} and Cr^{3+}. The adsorption capacity and selectivity of the material were investigated in single and multi-metal solutions. Using single-metal solutions, the adsorbent was found to have an affinity (molar basis) for metal ions in decreasing order of $Al^{3+} > Cu^{2+} > Ni^{2+} > Zn^{2+} > Co^{2+} > Cd^{2+} > Pb^{2+} > Cr^{3+}$. Using very dilute solutions, i.e., 10 ppm, more than 95% of cations were removed, except Co^{2+} and Cr^{3+}, indicating the high sensitivity of the current adsorbent. The affinity for coexisting metal cations decreased in the order of $Al^{3+} > Ni^{2+} > Cr^{3+} > Pb^{2+} > Zn^{2+} > Cd^{2+} > Co^{2+} > Cu^{2+}$. The adsorption capacities in multi-metal solutions were lower than in single-metal ones because of competition between metallic elements for the amine groups, with a preference for Al^{3+}. The amine-modified SBA-15 adsorbent exhibited an excellent selectivity against sodium, potassium, and calcium, indicating that the ionic strength does not affect the adsorption properties. Application of this material to remove copper in tap water, river water, and electroplating wastewater was shown to be successful.

8.1 Introduction

High levels of heavy metals in wastewater represent a serious threat to human health and ecological systems. Therefore, various methods for removing heavy metals from wastewater including chemical precipitation, ion-exchange, adsorption, membrane filtration, coagulation-flocculation, flotation and electrochemical processes have been extensively studied. Adsorption was shown to be one of the most promising techniques for this purpose. Hence, it has the potential to replace conventional methods, which are often ineffective or costly, particularly when the initial heavy metals concentrations are in the range of 10 – 100 ppm and the discharge concentrations are less than 2 ppm.

Adsorption of heavy metals by functionalized mesoporous materials is a relatively recent method. The earliest report on this topic dealt with the removal of mercury in wastewater using propylthiol-functionalized mesoporous silicas [1]. Since then, there have been a large number of literature reports dealing with adsorption of metallic species, primarily cations, in wastewater over mostly amine-modified mesoporous silicas [2]. SBA-15 is among the most prominent silica mesophases due to its large surface area (600 - 1000 m^2/g), narrow pore size distribution, and large and tunable pore diameter (5 - 30 nm), which allow easy access of target molecules to the inner surface of the material, leading to fast kinetics of chemical or physical processes. In addition, its thicker silica walls, around 4 nm compared to 1 nm for MCM-4, is believed to improve its hydrothermal and mechanical stability. All of these factors make SBA-15 an ideal support to anchor different functionalities such as -NH_2 [3], -SH [4], and -COOH [5] to develop novel materials for a variety of applications.

It is known that different parameters such as pH, temperature, adsorbent dosage, and initial metals concentration affect the adsorption process [6-8]. Furthermore, many other factors may also affect this process such as: (i) the presence of other metal ions; it has been reported that the adsorption of a given metal ion can be inhibited or promoted by another [9], (ii) metal ion charge to radius ratio (Z/r); the adsorption of metals was found to increase with the Z/r ratio [10, 11], (iii) metal−functional group complex stability constant; a study by Shiraishi [12] on silica gel modified with ethylene diamine tetraacetic acid (EDTA) showed that the removal efficiency of metals follows the order of stability constants for the metal−EDTA complexes obtained in aqueous solution, (iv) ion strength or existence of alkaline and alkaline-earth cations such as Na^+, K^+, and Ca^{2+}. Hence, the objective of this chapter was to screen the effect of these factors by investigating the ability of amine-functionalized SBA-15 prepared by co-condensation to adsorb Cr^{3+}, Al^{3+}, Co^{2+}, Pb^{2+}, Ni^{2+}, Zn^{2+}, Cu^{2+}, and Cd^{2+} from single-metal solutions with different concentrations. Furthermore, kinetic experiments were performed to study the simultaneous adsorption of all metal ions in a single solution, as well as the adsorption of copper ions in distilled/deionized water, tap water, river water and electroplating effluent.

8.2 Materials and methods

8.2.1 Adsorbent synthesis

Details of adsorbent synthesis and characterization can be found in an earlier contribution [6]. Briefly, 4.0 g of P123 and 8 g KCl were dissolved in 30 mL of water and 120 mL of a 2 M HCl solution at 40 ºC. Then, 8.5 g of tetraethylorthosilicate was added and prehydrolyzed for 2 h before adding 1.08 g of 3-aminopropyltrimethoxy-silane (APTS). The mixture was stirred for 20 h, then heated at 100 ºC for

24 h in static conditions. The material was collected by filtration, dried in air at room temperature and then extracted with ethanol. It was further treated in aqueous 0.1 M HCl for 1 h and neutralized in 0.1 M $NaHCO_3$, then filtered and dried under vacuum at 100 °C for 3 h. The material will be referred to as APTS-SBA-15-AB. As reported in our earlier contribution [6], the main structural characteristics of SBA-15 prepared with and without addition of APTS are listed in Table 8.1.

Table 8-1. Structural properties of APTS-SBA-15-AB [6].

Sample	**APTS-SBA-15-AB**	**SBA-15**
Surface area (m^2/g)	673	942
Pore size (nm)	7.6	7.9
Pore volume (cm^3/g)	0.75	1.21
Amine content (mmol/g)[a]	1.75	0.00
Amine content (mmol/g)[b]	1.77	0.00
Cu^{2+} adsorbed (mmol/g)	0.21	0.00

[a]: Amine content obtained from thermal gravemetric analysis, [b]: Amine content obtained from elemental analysis.

8.2.2 Preparation of metal solutions

Metal (Al^{3+}, Cr^{3+}, Co^{2+}, Pb^{2+}, Ni^{2+}, Zn^{2+}, Cu^{2+}, and Cd^{2+}) solutions were prepared by dissolving the corresponding nitrate in distilled/deionized water to obtain a concentration of 320 ppm, then diluted to obtain different concentrations ranging from 10 to 320 ppm, and the pH of all solutions was adjusted at 6.0. For competitive adsorption, a quantity of each metal nitrate corresponding to 0.2 $mmolL^{-1}$ was dissolved in distilled/deionized water, then the pH was adjusted at 6.0. The copper concentration in tap water, river water, and electroplating wastewater samples was almost zero, so it was adjusted to 20 ppm using copper nitrate. The pH of these solutions was not adjusted to study the effect of real conditions.

8.2.3 Adsorption from single-metal solutions

To study the effect of metal ions concentration, an accurately weighed amount (100 mg) of adsorbent was continuously stirred in 100 mL of metal solutions with different initial concentrations from 10 to 320 ppm. The solution temperature was maintained at 333 K using a temperature-controlled water bath. Agitation was maintained at 300 rpm for 2 h, which was verified to be sufficient to reach equilibrium. After filtration of the adsorbent, the metal concentration in the solution was determined by

inductivity coupled plasma (ICP) using a ICP-OES Varian Vista-Pro CCD spectrometer. The amount of metal adsorbed at equilibrium, qe (mgg^{-1}), was thus calculated by:

$$q_e = \frac{(C_0 - C_e)V}{W} \tag{8.1}$$

where C_0, C_e, V, and W are the initial and equilibrium concentrations (mgL^{-1}), volume of solution (L), and weight of adsorbent (g), respectively. The removal efficiency was calculated as:

$$R = \frac{(C_0 - C_e)}{C_0} \times 100 \tag{8.2}$$

8.2.4 Competitive adsorption

To evaluate the competitive adsorption of metal ions on APTS-SBA-15-AB, a similar experimental procedure as in section 8.2.3 was performed using an equimolar (0.2 $mmolL^{-1}$) solution of Al^{3+},Cr^{3+}, Co^{2+}, Pb^{2+}, Ni^{2+}, Zn^{2+}, Cu^{2+}, and Cd^{2+}.

8.2.5 Adsorption of copper from distilled, tap, river, and electroplating water

Batch kinetic tests were performed in a 1 L glass reactor stirred at 300 rpm using a magnetic stirrer. The reactor was immersed in a water bath maintained at a constant temperature of 333 K. The reaction mixture consisted of a total 1 L volume of 0.2 $mmolL^{-1}$ solution of Al^{3+}, Cr^{3+}, Co^{2+}, Pb^{2+}, Ni^{2+}, Zn^{2+}, Cu^{2+}, and Cd^{2+} containing 1.0 g of adsorbent. To determine the metal concentration as a function of time, samples were withdrawn after different time intervals (1, 2, 4, 6, 8, 10, 15, 20, 30, and 60 min) and analyzed by ICP. A similar procedure was used to investigate the adsorption of copper in different samples, namely distilled, tap and river water, as well as electroplating wastewater, after adjusting the initial copper concentration to 20 ppm.

8.3 Results and discussion

3.4.3 Single metals adsorption

Batch tests with Al^{3+},Cr^{3+}, Co^{2+}, Pb^{2+}, Ni^{2+}, Zn^{2+}, Cu^{2+}, and Cd^{2+} in single-metal solutions were used to estimate the adsorption capacity of the material. Two-parameter models (Langmuir and Freundlich) and three-parameter models (Sips and Redlich-Peterson) isotherms, whose equations can be found in an earlier contribution [6], were used to describe the equilibrium between metal ions and APTS-SBA-15-AB. The corresponding parameters are listed in Table 8.2. Contrary to other models, the Freundlich

model yielded R^2 values higher than 0.90 for all metal ions demonstrating the adequacy of this model to be used for comparison purpose.

The equilibrium adsorption uptake for heavy metals onto APTS-SBA-15-AB at different initial concentrations is shown in Fig. 8.1. As observed, increasing the initial metal ions concentration increased significantly the equilibrium adsorption uptake of the adsorbent since adsorption onto APTS-SBA-15-AB is a diffusion based process as was shown in an earlier contribution [7]. Thus, at higher initial concentration, the mass transfer driving force is larger, and hence, this results in enhanced adsorption of metal ions. Fig. 8.2 shows the removal efficiency for all metal ions as a function of the initial metal concentration. It is clear that in all cases, except for Co and Cr, > 95% of cations were removed from very dilute solutions, i.e., 10 ppm, indicating the high sensitivity of the current adsorbent to such cations. Full adsorption isotherms were obtained for all metals as shown in Fig. 8.3. All the isotherms, except for Cr^{3+}, showed a sharp initial slope indicating that the material acts as a highly efficient adsorbent at low metal concentration. Furthermore, the values of $1/n_F$ were less than 1 for all metals, indicative of high adsorption strength.

For cationic metal ions, there is a direct relationship between the charge to radius ratio (*Z*/*r*) and adsorption capacity in case of a pure cation-exchange mechanism [10, 11]. Thus, according to the *Z*/r ratio of the cations Cd^{2+} (2.11), Cu^{2+} (2.74), Ni^{2+} (2.90) and Zn^{2+} (2.70), Co^{2+} (2.70), Pb^{2+} (1.70), Cr^{3+} (4.88), and Al^{3+} (5.70) [10, 11], the selectivity sequence is expected to be $Ni^{2+} > Cu^{2+} > Co^{2+} = Zn^{2+} > Cd^{2+} > Pb^{2+}$ for divalent ions, which would be in good agreement with the Irving-Williams series order of metal complexes stability [13]. As for trivalent cations, the order is expected to be $Al^{3+} > Cr^{3+}$. However, depending on the K_F values shown in Table 8.2, the observed adsorption sequence for this adsorbent, i.e. $Cu^{2+} > Ni^{2+} > Co^{2+} = Zn^{2+} > Cd^{2+} > Pb^{2+}$, did not show a greater selectivity for Ni^{2+} over Cu^{2+}. Several studies were conducted using various types of adsorbents for simultaneous adsorption of heavy metals [14-18]. Table 8.3 presents a comparison of the adsorption selectivity obtained from single and multi-metals solutions. It is seen that the adsorption selectivity was not identical for all the adsorbents, revealing that depending on the experimental conditions and adsorbent properties, data may deviate significantly from the predicted behavior based on the *Z*/*r* ratio or the Irving-Williams series.

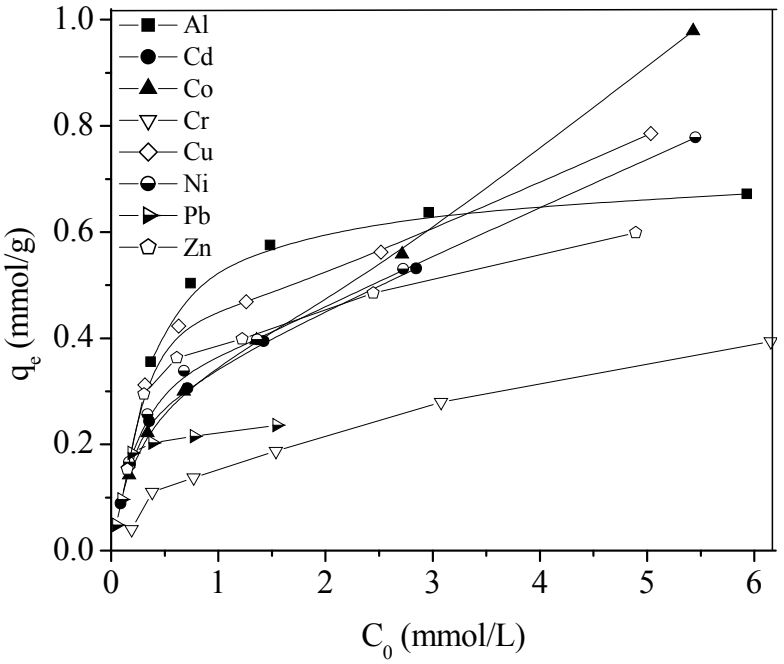

Figure 8-1. Amount adsorbed ($mmolg^{-1}$) as a function of initial metal concentration for Al^{3+}, Cr^{3+}, Co^{2+}, Pb^{2+}, Ni^{2+}, Zn^{2+}, Cu^{2+}, and Cd^{2+} in single metal solutions (T = 333, pH = 6).

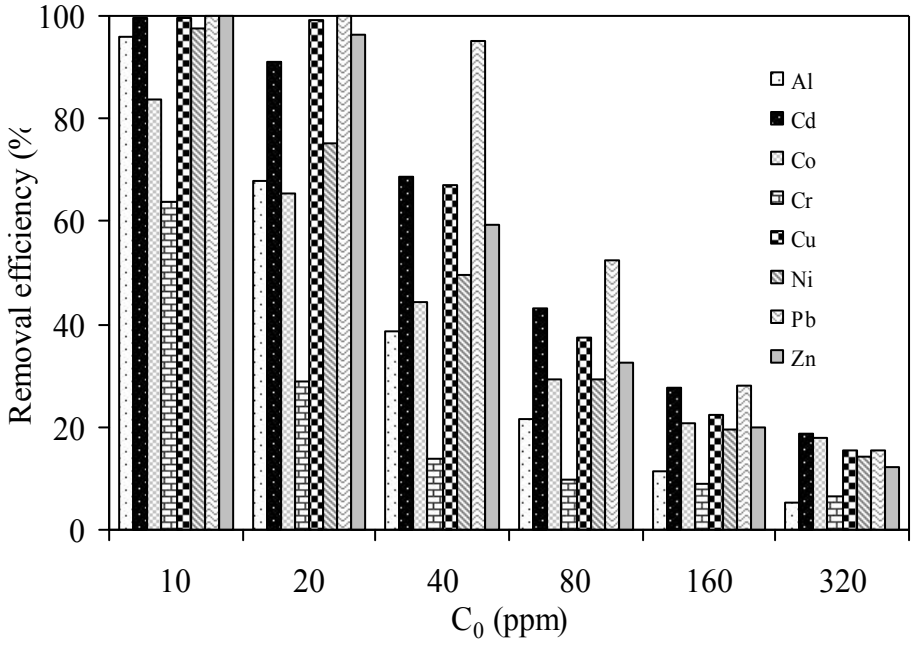

Figure 8-2. Removal efficiency (%) as a function of initial metal concentration for Al^{3+}, Cr^{3+}, Co^{2+}, Pb^{2+}, Ni^{2+}, Zn^{2+}, Cu^{2+}, and Cd^{2+} in single metal solutions (T = 333 K, pH = 6)

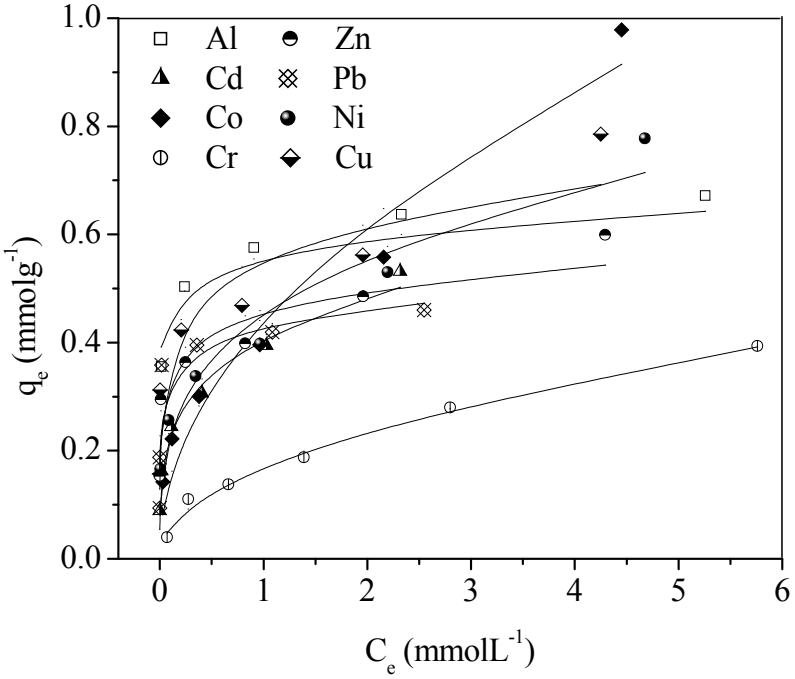

Figure 8-3. Freundlich isotherm fitting for Al^{3+}, Cr^{3+}, Co^{2+}, Pb^{2+}, Ni^{2+}, Zn^{2+}, Cu^{2+}, and Cd^{2+} in single metal solutions (T = 333, pH = 6).

Table 8-2. Isotherms fitting parameters for Al^{3+},Cr^{3+}, Co^{2+}, Pb^{2+}, Ni^{2+}, Zn^{2+}, Cu^{2+}, and Cd^{2+} in single metal solutions (T = 333, pH = 6).

Metal ions	**Cu^{2+}**	**Cr^{3+}**	**Co^{2+}**	**Zn^{2+}**	**Cd^{2+}**	**Ni^{2+}**	**Pb^{2+}**	**Al^{3+}**
				Freundlich				
K_F	0.559	0.170	0.449	0.459	0.412	0.464	0.236	0.560
$1/n_F$	0.147	0.476	0.476	0.115	0.236	0.280	0.097	0.084
R^2	0.934	0.993	0.958	0.938	0.978	0.941	0.904	0.973
				Langmuir				
q_m	0.686	0.334	0.429	0.469	0.472	0.720	0.210	0.626
K_L	6	1	10	138	10	2	18203	78
R^2	0.782	0.964	0.951	0.722	0.872	0.826	0.929	0.795
				Sips				
q_s	0.686	0.334	0.429	0.469	0.472	0.720	0.409	0.613
K_s	2.52	1.19	3.08	3.08	3.02	1.64	86.00	9.05
$1/n_s$	2.41	1.05	2.39	12.44	3.22	1.46	108.72	9.25
R^2	0.983	0.964	0.951	0.722	0.870	0.826	0.923	0.793
				Redlich-Peterson				
K_{RP}	392	781	780	778	5	2	3827	49
a_{RP}	600	600	600	600	600	600	601	600
B	1.21	7.44	4.04	2.98	0.016	0.004	30.30	0.13
R^2	0.657	0.633	0.732	0.564	0.870	0.826	0.929	0.795

Table 8-3. Metals selectivity results obtained by other authors.

Adsorbent	**Functional group**	**mixed**	**Single**	**Ref.**
Silica gel	EDTA	$Cu^{2+} > Ni^{2+} > Zn^{2+} > Co^{2+}$	$Cu^{2+} > Ni^{2+} > Zn^{2+} > Co^{2+}$	[12]
SBA-15	*N*-propylsalicylaldimine	$Cu^{2+} > Ni^{2+} > Co^{2+} > Zn^{2+}$	$Cu^{2+} > Zn^{2+} > Ni^{2+} > Co^{2+}$	[14]
MCM-41	*N*,*N*-dimethyldecylamine		$Cu^{2+} > Co^{2+} > Ni^{2+}$	[15]
MCM-41	carbamoylphosphonic acids	$Pb^{2+} > Cu^{2+} > Cd^{2+} > Zn^{2+} > Co^{2+} > Ni^{2+}$		[16]
Mesoporous silica	[amino-ethylamino]propyl		$Cu^{2+} > Co^{2+} > Ni^{2+}$	[17]
Mesoporous silica	(2-aminoethylamino)-ethylamino]propyl		$Cu^{2+} > Co^{2+} > Ni^{2+}$	[17]
Mesoporous silica	3-aminopropyl-triethoxysilane		$Pb^{2+} > Cu^{2+} > Zn^{2+}$	[18]

3.4.4 Multi-metal adsorption

The selectivity of adsorbent toward different metal ions from multi-metal solutions is generally determined by equilibrating a unit mass of the adsorbent with a volume of solution containing equimolar metal ions concentration. It is important to have equal initial molar concentration for all metal ions in the solution to obtain unbiased thermodynamically controlled selectivity toward metal ions of different atomic weights. Fig. 8.4 summarizes the extent of adsorption of metal ions on APTS-SBA-15-AB at the same initial concentration of each metal ion (C_0) of 0.2 $mmolL^{-1}$ for all metal ions. Maximum removal efficiencies of 97.5%, 11.5%, 9.7%, 9.1%, 7.2 %, 6.9%, 6.0% and 5.9% were obtained for Al^{3+}, Ni^{2+}, Cr^{3+}, Pb^{2+}, Zn^{2+}, Cd^{2+}, Co^{2+},and Cu^{2+}, respectively. These results suggest the following order of adsorption affinity: $Al^{3+} > Ni^{2+} > Cr^{3+} > Pb^{2+} > Zn^{2+} > Cd^{2+} > Co^{2+} > Cu^{2+}$. As shown, competition for the adsorption sites is likely to occur and in this situation, the adsorption preference is for Al^{3+}. Higher affinity for Al^{3+} over other metallic cations was also observed in single solute adsorption, while the order of affinity towards other metal cations was different than that in single-metal solutions. Table 8.4 shows that the copper removal efficiency obtained from single-metal solutions were higher, > 92%, than in multi-metals solutions, 6%, because of competition between metallic elements for adsorption by amine groups. To eliminate the effect of Al^{3+} ions, a similar experiment was performed using a solution containing all metal ions except Al^{3+}. The obtained removal efficiencies listed in Table 8.4 show that in this case, the adsorption preference is for Cr^{3+}. The higher affinity for Cr^{3+} over other metallic cations is related to the higher Z/r ratio of 4.88. The affinity order obtained in the absence of Al^{3+} was as follows: $Cr^{3+} > Cu^{2+} > Zn^{2+} > Pb^{2+} > Co^{2+} > Cd^{2+} > Ni^{2+}$.

3.4.5 Applications to real water samples

To investigate the selectivity of APTS-SBA-15-AB for the removal of Cu^{2+} in the presence of Na^{+}, K^{+}, and Ca^{2+}, tap water and river water are interesting samples to be studied and compared with distilled water, because these minerals are abundant in these water sources. The results obtained for copper removal from the three samples are presented in Fig. 8.5 – 8.7 and Table 8.4. Clearly, it is seen that sodium, potassium, and calcium cations do not affect the copper removal, therefore it can be concluded that this process is independent of the ionic strength, and the complexation is the main factor responsible for copper retention. Thus, metals belonging to alkaline and alkaline-earth groups, which do not form complexes with amine groups do not interfere with the adsorption process. It is also clear that the performance of APTS-SBA-15-AB for the removal of Cu^{2+} from river (Fig. 8.7) and tap (Fig. 8.6) water was faster than in distilled water (Fig. 8.5), which is maybe related to the pH effect

discussed earlier [6-8]. The pH of the three samples were found to be 6.35, 9.35, and 10.30 for distilled, river, and tap water, respectively, whereas the point of zero charge of this adsorbent was earlier found to be around 8.62 [6]. Thus, for tap water and river water solutions, the adsorbent is expected to have a negatively charged surface, which in turn increases the rate at which copper cations reach the adsorption sites, due to increased attraction forces with the surface.

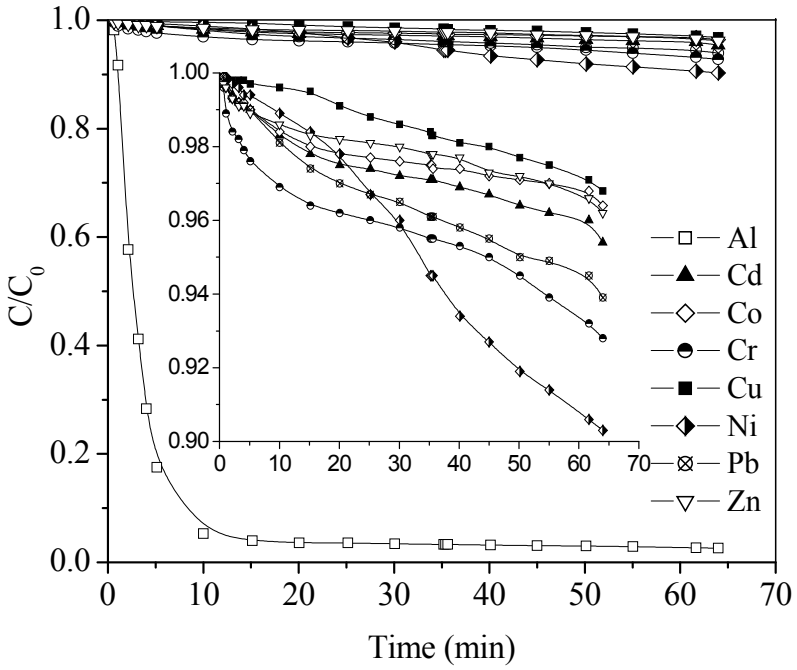

Figure 8-4. Concentration profile as a function of time for Al^{3+}, Ni^{2+}, Cr^{3+}, Pb^{2+}, Zn^{2+}, Cd^{2+}, Co^{2+}, and Cu^{2+} in a single solution. Insert: Close-up for the C/C_0 range 0.9 - 1.

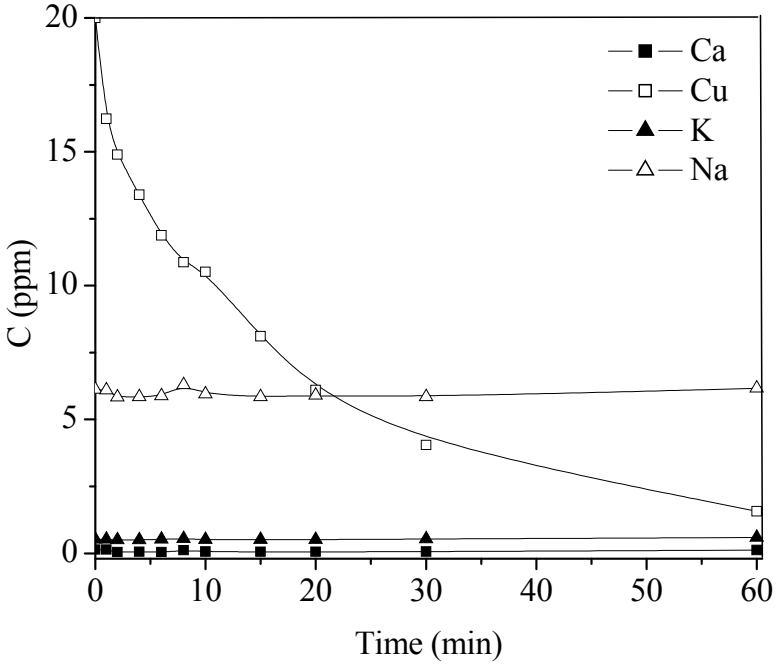

Figure 8-5. Concentration profile as a function of time for Ca^{2+}, K^{+}, Na^{+}, and Cu^{2+} in distilled water.

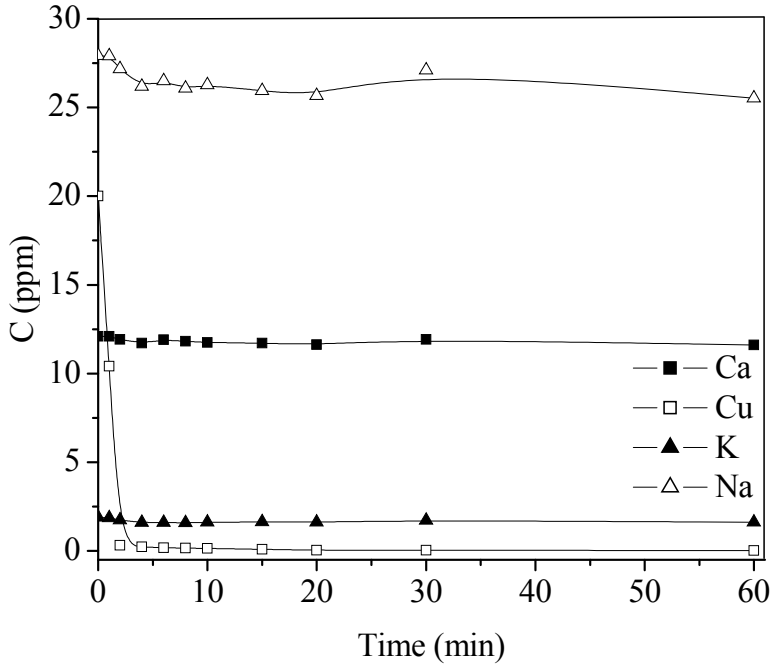

Figure 8-6. Concentration profile as a function of time for Ca^{2+}, K^{+}, Na^{+}, and Cu^{2+} in tap water.

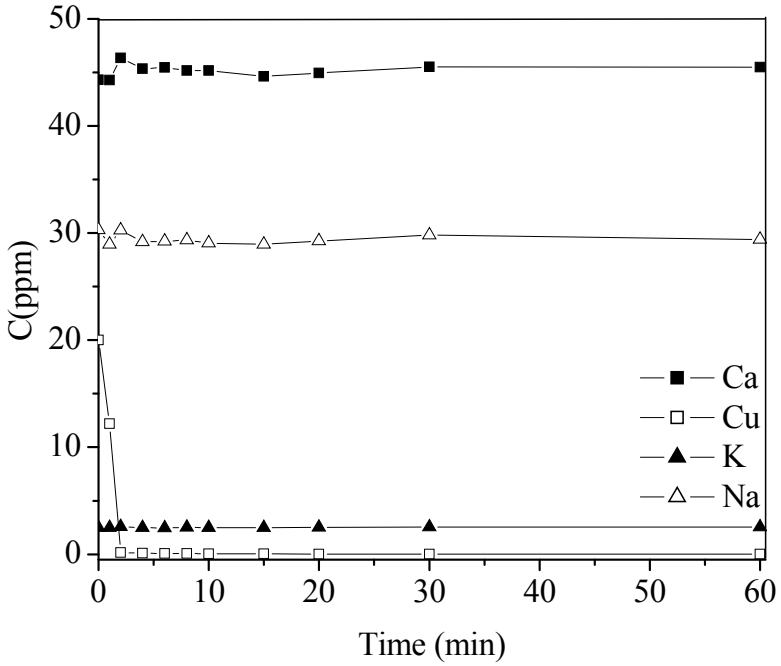

Figure 8-7. Concentration profile as a function of time for Ca^{2+}, K^{+}, Na^{+}, and Cu^{2+} in river water.

In accordance with the results obtained previously, the procedure was applied to a real electroplating wastewater sample with composition shown in Table 8.4. Fig. 8.8 and Table 8.4 show that for a adsorbent/wastewater ratio of 1 gL^{-1}, the amounts of adsorbed Hg^{2+} ions on APTS-SBA-15-AB was almost zero despite the fact that, the Hg^{2+} concentration was much larger than the other metals. This indicated that the APTS-SBA-15-AB had a much stronger affinity for Zn^{2+} and Cu^{2+} ions than Hg^{2+} ions. It is known that softer metal ions are prone to forming stable complexes with ligands carrying softer donor atoms, and vice versa. Sulfur has been regarded as a softer donor atom compared with nitrogen, and therefore it is expected that thiolated adsorbents exhibit higher complexation affinity for the softer metal ion Hg^{2+}, while the other relatively harder metal ions (Cu^{2+}, Zn^{2+}) to show higher binding ability with the amine-modified adsorbents. Similar observations were reported by Liu et al. [4] using thiol- and amino-grafted SBA-15 silicas. They reported that the thiolated SBA-15 adsorbent exhibited a higher complexation affinity for Hg^{2+}, while the other metal ions (Cu^{2+}, Zn^{2+}, Cr^{3+} and Ni^{2+}) showed exceptional binding ability with the aminated sample. It is also clear from Fig. 8.8 and Table 8.4 that Na^{+}, K^{+}, and Ca^{2+} retention was zero, which confirms that these ions have no effect. However, when other heavy metals are present in the solution, Zn^{2+} in this case, a drastic decrease in the copper removal efficiency is denoted with 24.7% compared to 100% for tap water and river water and 92% for distilled water sample. It is also clear that the removal efficiency order obtained for the electroplating

sample was different from the laboratory solution of equimolar metallic cations, because the relative concentrations of the cations were not equal, with very low content of Pb^{2+} and Ni^{2+}. This explains the higher removal efficiency obtained for Zn^{2+}, Pb^{2+}, and Ni^{2+} taking into consideration that this sample did not contain Al^{3+} and had very low Cr^{3+} content.

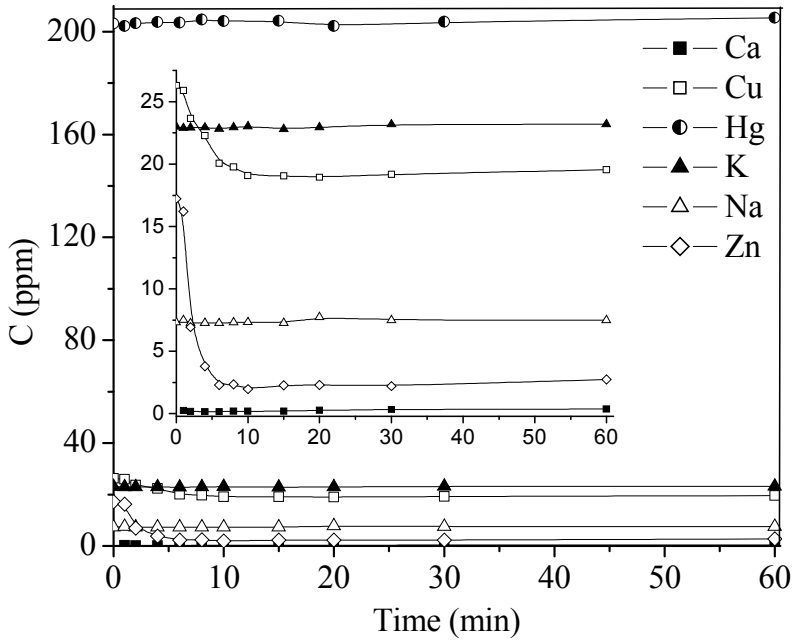

Figure 8-8. Concentration profile as a function of time for Ca^{2+}, K^{+}, Na^{+}, Zn^{2+}, Cu^{2+}, and Hg^{2+} in electroplating wastewater. Insert: Close-up for C in the range 0 - 30 ppm.

8.4 Conclusions

Based on the results obtained using SBA-15 functionalized with 3-aminopropyltrimethoxy-silane for adsorption of Cd^{2+}, Co^{2+}, Cu^{2+}, Cr^{3+}, Pb^{2+}, Ni^{2+}, Al^{3+} and Zn^{2+} , the following remarks can be made: (i) the adsorbent has an affinity (molar basis) for metal ions in single metal solutions following the order : $Al^{3+} > Cu^{2+} > Ni^{2+} > Zn^{2+} > Co^{2+} > Cd^{2+} > Pb^{2+} > Cr^{3+}$, and for mixed metals, the order is: $Al^{3+} > Ni^{2+} > Cr^{3+} > Pb^{2+} > Zn^{2+} > Cd^{2+} > Co^{2+} > Cu^{2+}$, (ii) the adsorbent showed very high sensitivity for all metal ions in dilute solutions (i.e. 10 ppm), (iii) the qe values corresponding to single-metal solutions were much larger than those obtained with the multi-metal ones, confirming the existence of competition between metallic elements for the amine groups, (iv) the ionic strength does not affect the adsorption process and the adsorbent was successfully used in removing copper ions from river water, tap water and electroplating wastewater.

Table 8-4. The initial concentrations (ppm) of metal ions in different solutions and removal efficiency obtained by APTS-SBA-15-AB.

Sample		Al	Ca	Co	Cr	Cd	Cu	Hg	K	Na	Zn	Ni	Pb
Distilled	C_0(ppm)	0.0	0.0	0.0	0.0	0.0	20.0	0.0	0.6	6.1	0.0	0.0	0.0
	R%	-	-	-	-	-	92.0	-	0.0	0.0	-	-	-
River	C_0(ppm)	0.0	45.8	0.0	0.0	0.0	0.03[a]	0.0	2.5	29.5	0.0	0.0	0.0
	R%	-	0.0	-	-	-	100	-	0.0	0.0	-	-	-
Tap	C_0(ppm)	0.0	12.1	0.0	0.0	0.0	0.20[a]	0.0	1.9	27.9	0.0	0.0	0.0
	R%	-	3.3	-	-	-	100	-	10.5	0.3	-	-	-
Electroplating	C_0(ppm)	0.0	0.3	0.0	0.5	0.0	25.9	202.0	23.0	7.5	17.5	1.9	0.6
	R%	-	0.0	-	0.0	-	24.7	0.0	0.0	0.0	84.3	57.9	83.3
Multi metal	C_0(ppm)	4.4	-	13.2	11.3	26.0	20.0	-	-	-	13.8	13.2	50.9
	R%	97.5	-	6.0	9.7	6.9	6.0	-	-	-	7.2	11.5	9.1
Multi metal[b]	R%	-	-	2.2	46.4	2.1	26.9	-	-	-	21.0	1.1	17.3

[a]: the concentration was adjusted to 20 ppm before running adsorption experiment, [b]: Without Al^{3+} ions.

References

[1] X. Feng, G. E. Fryxell, L.Q. Wang, A. Y. Kim, J. Liu, K. M. Kemner, Functionalized monolayers on ordered mesoporous supports, *Science* 276 (1997) 923-926.

[2] A. Sayari, S. Hamoudi, Periodic mesoporous silica-based organic-inorganic nano-composite materials, *Chem. Mater.* 13 (2001) 3151-3168.

[3] L. Zhang, C. Yu, W. Zhao, Z. Hua, H. Chen, L. Li, J. Shi, Preparation of multi-amine-grafted mesoporous silicas and their application to heavy metal ions adsorption, *Non-Cryst. Solids* 353 (2007) 4055-4061.

[4] A. M. Liu, K. Hidajat, S. Kawi, D. Y. Zhao, A new class of hybrid mesoporous materials with functionalized organic monolayers for selective adsorption of heavy metal ions, *Chem. Commun.* 13 (2000) 1145–1146.

[5] M.C. Bruzzoniti, A. Prelle, C. Sarzanini, B. Onida, S. Fiorilli, E. Garrone, Retention of heavy metal ions on SBA-15 mesoporous silica functionalized with carboxylic groups, *J. Sep. Sci.* 30 (2007) 2414-2420.

[6] E. Da'na, A. Sayari, Adsorption of copper on amine-functionalized SBA-15 prepared by co-condensation: Equilibrium properties, *Chem. Eng. J.* 166 (2011) 445-453.

[7] E. Da'na, N. D. Silva, A. Sayari, Adsorption of copper on amine-functionalized SBA-15 prepared by co-condensation: Kinetics properties, *Chem. Eng. J.* 166 (2011) 454-459.

[8] E. Da'na, A. Sayari, Optimization of copper removal efficiency by adsorption on amine-modified SBA-15: Experimental design methodology, *Chem. Eng. J.* 167 (2011) 91-98.

[9] A. Benhamou, M. Baudu, Z. Derriche, J.P. Basly, Aqueous heavy metals removal on amine-functionalized Si-MCM-41 and Si-MCM-48, *J. Hazard. Mater.* 171 (2009) 1001-1008.

[10] P. Wu, Y.S. Zhou, Simultaneous removal of coexistent heavy metals from simulated urban stormwater using four sorbents: A porous iron sorbent and its mixtures with zeolite and crystal gravel, *J. Hazard. Mater.*168 (2009) 674-680.

[11] A. Demirbas, E. Pehlivan, F. Gode, T. Altun, G. Arslan, Adsorption of Cu(II), Zn(II), Ni(II), Pb(II), and Cd(II) from aqueous solution on amberlite IR-120 synthetic resin, *J. Colloid Interface Sci.* 282 (2005) 20-25.

[12] Y. Shiraishi, G. Nishimura, T. Hirai, I. Komasawa, Separation of transition metals using inorganic adsorbents modified with chelating ligands, *Ind. Eng. Chem. Res.* 41 (2002) 5065-5070.

[13] H. Irving, R.J.P. Williams, Order of stability of metal complexes, *Nature* 162 (1948) 746-747.

[14] M. Mureseanu, A. Reiss, I. Stefanescu, E. David, V. Parvulescu, G. Renard, V. Hulea, Modified SBA-15 mesoporous silica for heavy metal ions remediation, *Chemosphere* 73 (2008) 1499-1504.

[15] A. Sayari, S. Hamoudi, Y. Yang, Applications of pore-expanded mesoporous silica. 1. Removal of heavy metal cations and organic pollutants from wastewater, *Chem. Mater.* 17 (2005) 212-216.

[16] W. Yantasee, Y. Lin, G.E. Fryxell, B.J. Busche, J.C. Birnbaum, Removal of heavy metals from aqueous solution using novel nanoengineered sorbents: Self-assembled carbamoylphosphonic acids on mesoporous silica, *Sep. Sci. Technol.* 38 (2003) 3809-3825.

[17] L. Bois, A. Bonhommé, A. Ribes, B. Pais, G. Raffin, F. Tessier, Removal of heavy metals from aqueous solution using novel nanoengineered sorbents: Self-assembled carbamoylphosphonic acids on mesoporous silica, *Colloids Surf., A* 221 (2003) 221-230.

[18] H. Yang, R. Xu, X. Xue, F. Li, G. Li, Hybrid surfactant-templated mesoporous silica formed in ethanol and its application for heavy metal removal, *J. Hazard. Mater.* 152 (2008) 690-698.

Chapter 9

Modeling adsorption of copper on amine-functionalized SBA-15: Predicting breakthrough curves

J. Environ. Eng. (Submitted manuscript)

Abstract.

Dynamic experiments on the adsorption of copper ions were carried out in a laboratory packed-bed of amine-modified SBA-15 pellets. Breakthrough curves were analyzed at different flow rates and after two adsorption-desorption cycles. A model based on mass balance was developed and tested for predicting the breakthrough curves under the different experimental conditions used. The developed model was found to be in good agreement with the experimental data. Bed regeneration was performed by circulating 0.2 M EDTA solution through the column for 30 min.

9.1 Introduction

Copper ions find their way to rivers and lakes through many industries, including painting, metal finishing, fertilizers, and electroplating. Copper is biologically essential to mammals as it maintains an effective glucose, lipid and protein metabolism [1]. However, if a certain limit is exceeded, copper will exert a toxic effect to living organisms, especially on enzymes whose activities depend on amine groups, since copper, like many other metals, has a high affinity for ligands containing nitrogen [1]. Therefore, World Health Organization (WHO) recommended an upper limit for copper in drinking water to be 2 mgL^{-1} [2].

Adsorption is a comparatively simple method for removing copper, with a great potential of becoming an alternative technology to conventional ones, overcoming the problems of insufficient efficiency and difficult waste handling derived from other methods such as precipitation. Among the various adsorbents, functionalized mesoporous silica-based materials have attracted much attention [3]. The main advantages of these adsorbents are their high surface area, controlled pore sizes and narrow pore-size distributions. Furthermore, it is possible to introduce a wide range of functional groups to the

surface to increase its efficiency to remove the target species [4]. Earlier, we have investigated the use of SBA-15 functionalized with 3-aminopropyltrimethoxy-silane synthesized by co-condensation as adsorbent for Cu^{2+} ions in aqueous solutions. Under suitable conditions, the material exhibited high adsorption capacity even at very low copper concentration [5]. Furthermore, kinetic studies under different conditions indicated that the material was very efficient and equilibrium was achieved in less than 30 min [6]. Optimization of the factors affecting the adsorption process was also performed and the recommended optimum conditions corresponding to 95% copper removal were as follows: copper concentration of 20 mgL^{-1}, adsorbent/solution ratio of 1.57 gL^{-1}, pH of 6.5, and T = 294 K [7]. These findings based on batch experiments are useful in providing information about the effectiveness of the metal-adsorbent system. However, the data obtained under batch conditions are generally not applicable to most treatment systems where the contact time is not sufficiently long for the attainment of equilibrium. In practical applications, adsorption of heavy metals is most effectively carried out in a packed-bed column, as it efficiently utilizes the adsorbent capacity, leading to improved quality effluent. There are several literature reports on the removal of copper by adsorption in packed-bed columns [8-11]. However, the applicability of mesoporous silica in packed-bed has been little explored [12, 13]. Hence, in the present investigation, the ability of amine-functionalized SBA-15 to remove copper in a packed up-flow column was evaluated. In addition, a model predicting the breakthrough curves has been developed and tested under different conditions.

9.2 Materials and Methods

9.2.1 Material synthesis

Details of adsorbent synthesis and characterization may be found in an earlier contribution [5]. Briefly, 4.0 g of P123 and 8 g KCl were dissolved in 30 mL of water and 120 mL of a 2 M HCl solution at 40 ºC. Then, 8.5 g of tetraethylorthosilicate was added and prehydrolyzed for 2 h before adding 1.08 g of 3-aminopropyltrimethoxy-silane (APTS). The mixture was stirred for 20 h then aged at 100 ºC for 24 h in static conditions. The material was collected by filtration, dried in air at room temperature and then extracted with ethanol. It was further treated in aqueous 0.1 M HCl for 1 h and neutralized in 0.1 M $NaHCO_3$, then filtered and dried under vacuum at 100 °C for 3 h. The material will be referred to as APTS-SBA-15-AB.

As fine powder produces large pressure drop in packed-bed columns, pellets were produced by compressing the powdered form of APTS-SBA-15-AB under a load of 450 $kgcm^{-2}$ using a hydraulic press. It was demonstrated that such a pressure did not affect significantly the structural properties of the adsorbent. The particles thus produced were crushed and sieved between openings of 0.85 and 0.425 mm (i.e., 20 and 40 mesh, respectively).

9.2.2 Experimental set-up

The adsorption system consisting of a 1 L glass flask was immersed in a water bath maintained at a constant temperature of 333 K and magnetically stirred at 300 rpm. The feed, a 40 mgL^{-1} copper solution, was pumped upward to the bottom of the packed-bed using a variable flow peristaltic mini-pump at a specified flow rate within the range of 1 – 4 $mLmin^{-1}$. The packed-bed consisted of a 14 cm long glass column with 5.9 mm internal diameter. The packing material consisted of APTS-SBA-15-AB pellets with sizes in the range of 0.425 to 0.850 mm. The column was kept at a constant temperature of 333 K using a water jacket. The characteristics of the adsorbent and the adsorption bed are listed in Table 9.1 .

Table 9-1. Characteristics of the adsorbent and column used.

Average pellet diameter (mm)	0.425-0.850
Void fraction in the pellet*	0.84
BET surface area (m^2g^{-1})	517
Column length (cm)	14
Column internal diameter (mm)	5.9
Void fraction in the column	0.38
Bulk density of the bed (kgm^{-3})	329

* Void fraction in the pellets was calculated by the method in reference [14].

9.2.3 Experimental procedure

Before each experiment, the adsorbent was activated under vacuum at 373 K for 3 h. Then, the column was packed with the pellets and heated in the water jacket until the temperature reached equilibrium at 333 K. The copper solution was prepared by dissolving copper acetate mono-hydrate ($Cu(CH_3COO)_2.H_2O$) in distilled water to obtain a concentration of 40 mgL^{-1} at pH = 6.0. The copper solution was heated to 333 K in a water bath, and once the column and the feed solution reached a steady state, the solution was pumped through the column. Samples were collected at the exit of the column at different time intervals and analyzed by a ICP-OES Varian Vista-Pro CCD spectrometer instrument. The concentration of copper in the outlet stream as a function of time was used to establish the breakthrough curves, and subsequently determine the column adsorption capacity for copper. Regeneration of the bed was performed by circulating 20 mL of 0.2 M EDTA solution at 333 K for 30 min.

9.2.4 Theoretical background

9.2.4.1 Adsorption capacity

The copper adsorption capacity for APTS-SBA-15-AB in the presence of a 40 mgL^{-1} copper solution was determined using the breakthrough curve and Eq. 9.1, where q_e, M and W represent the adsorption capacity for copper (mgg^{-1}), mass flow rate for copper (mgs^{-1}), and the mass of the adsorbent (g), respectively.

$$q_e = \frac{t \bullet M}{W} \tag{9.1}$$

Working time (t) corresponds to the area above the normalized breakthrough curve, as shown in Eq. 9.2, where C and C_0 represent the outlet and inlet concentrations for copper (mgL^{-1}), respectively.

$$t = \int_0^\infty \left(1 - \frac{C}{C_0}\right) dt \tag{9.2}$$

9.2.4.2 Material Balances

The adsorption process was modeled using only the material balance for the column. Assumptions made to simplify the calculations include: constant void fraction throughout the column, no radial change in concentration in the column, no channeling effects, perfectly spherical adsorbent particles, and physical characteristics of bulk flow are close to those for pure water since the copper solution used was very dilute. In addition, because of the low concentration of copper, the column operation was assumed to be isothermal. It should also be mentioned that the experiments were performed in a column located inside a temperature-controlled enclosure, which further support the approximation of isothermal conditions. This assumption simplifies the model since the mass balance can be described without the use of an energy balance.

The material balance for the column has been written taking into account the diffusion of species in the particles. The governing differential equation representing the material balance within the column is given by Eq 9.3.

$$\frac{\partial C_L}{\partial t} = E\frac{\partial^2 C_L}{\partial z^2} - u_L\frac{\partial C_L}{\partial z} - \frac{k_L.a}{\varepsilon_c}\left(C_L - C_L^*\right) \tag{9.3}$$

The boundary and initial conditions for Eq. 9.3 are:

$$C_L = 0 \qquad t = 0 \ \forall z$$
$$C_L^{input} = C_{L0} \qquad z = 0$$
$$\frac{dC_L}{dz} = 0 \qquad z = 0$$
$$\frac{dCL}{dz} = 0 \qquad z = L$$

Eq. 9.3 must be coupled with the equation that describes solute transport inside the particles:

$$D_e\left(\frac{\partial^2 C_p}{\partial r^2} + \frac{2}{r}\frac{\partial C_p}{\partial r}\right) - \frac{k_{ads}.a_p}{\varepsilon_p}\left(C_p - C_p^*\right) = \frac{\partial C_p}{\partial t} \tag{9.4}$$

The boundary and initial conditions for Eq. 9.4 are:

$$C_p = 0 \qquad t = 0 \ \forall r$$
$$\frac{dC_p}{dr} = 0 \qquad r = 0$$
$$-D_e\frac{dC_p}{dr} = k_L.a\left(C_L - C_p\right)_{r=rp} \qquad r = r_p$$

The column was divided into a number of cells (N) and equations (9.3) and (9.4) were solved by finite differences using proper discretization of the equations, then coded and solved using Compaq Visual FORTRAN 6.1.

9.2.4.3 Empirical Equations

The value of the external mass transfer coefficient (k_L) depends on the flow conditions in the column. It was determined by empirical correlations reported in the literature assuming that dilute copper solution has the same properties as water. In this study, k_L was determined by the following empirical correlation [15]:

$$Sh = \frac{k_L.D_p}{D_b} = 2.4\,\varepsilon_b^{0.66}\,\mathrm{Re}^{0.34}Sc^{0.33} \qquad 0.04 < \mathrm{Re} < 52 \tag{9.5}$$

where D_b is the bulk diffusivity of copper ions, while the Reynolds (Re) and Schmidt (Sc) numbers are defined by:

$$Sc = \frac{v}{D_b} \tag{9.6}$$

$$Re = \frac{u_s D_p}{v} \tag{9.7}$$

Bulk diffusivity D_b was considered to be the same as the effective diffusivity (D_e) assuming that the adsorbent exhibits non intersecting pores [15].

9.2.4.4 Copper effective diffusivity

The diffusivities of copper ions in APTS-SBA-15-AB pellets were calculated using Boyd's theory described elsewhere [16], which is expressed as:

$$F = 1 - \frac{6}{\pi^2} \sum_{n=1}^{\infty} \frac{1}{n^2} \bullet e^{-n^2 B_t} \tag{9.8}$$

where F is the fractional attainment of equilibrium at time t (min) and is obtained by the expression:

$$F = \frac{q_t}{q_e} \tag{9.9}$$

n is an integer that defines the infinite series solution and B_t is a mathematical function of F and can be approximated by:

$$for\ F\ values < 0.85,\ B_t = \left(\sqrt{\pi} - \sqrt{\pi - \frac{\pi^2 F}{3}} \right)^2 \tag{9.10}$$

$$for\ F\ values > 0.85,\ B_t = -0.4977 - ln(1 - F) \tag{9.11}$$

The slope denoted B of B_t against t, which is known as Boyd's plot, for the initial stages of metal adsorption can be used to calculate the diffusivity of metal ions in the sorbent particles according to Eq. 9.12:

$$B = \frac{\pi^2 D_e}{r_p^2} \tag{9.12}$$

where D_e ($cm^2 s^{-1}$) is the effective diffusion coefficient of the metal ions in the adsorbent phase and r_p (cm) is the radius of the adsorbent particle assuming a spherical shape.

9.2.4.5 Adsorption isotherms

The adsorption isotherms of Cu^{2+} were reported in an earlier contribution [5]. It was shown that the Sips model yielded R^2 values of about 0.99, demonstrating that it adequately fitted the data for Cu^{2+} adsorption with parameters shown in Table 9.2.

Table 9-2. Sips parameters for adsorption of copper on APTS-SBA-15-AB at 333 K.

q_S ($mmol g^{-1}$)	1.74
K_S	2.01
N_S	2.22
R^2	0.990

9.3 Results and discussion

9.3.1 Pellets characterization

Nitrogen adsorption–desorption isotherms and pore size distributions for APTS-SBA-15-AB powder and pellets are presented in Fig. 9.1. The structural properties deduced from nitrogen adsorption data are presented in Table 9.3. The shape of the nitrogen adsorption isotherms for APTS-SBA-15-AB powder and pellets correspond to type IV, which is associated with mesoporous materials with narrow pore size distributions. Fig. 9.1 also shows that after compression of APTS-SBA-15-AB powder into pellets, its pore volume increased, possibly because of the occurrence of intraparticle porosity as indicated by the significant increase in nitrogen adsorption at P/P_0 close to 1. Nonetheless, the surface area decreased by ca, 20%, while the pore size did not change, which may be related to the loss of SBA-15 microporosity during mechanical compression, as it is known that SBA-15 contain significant amount of micropores [17]. The loading of amine groups for APTS-SBA-15-AB powder was 1.75 $mmolg^{-1}$.

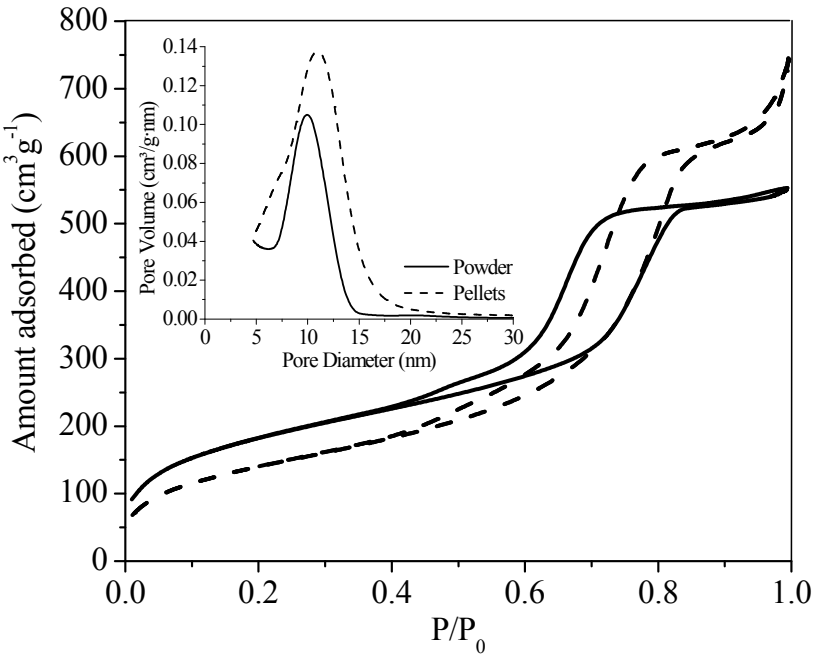

Figure 9-1. Nitrogen adsorption and desorption isotherms for APTS-SBA-15-AB powder (solid lines) and pellets (dashed lines) .

Table 9-3. Structural properties of mesoporous materials.

Material	Surface area (m^2g^{-1})	Pore volume (cm^3g^{-1})	Mean pore size (nm)
APTS-SBA-15-AB powder	635	0.84	10.2
APTS-SBA-15-AB pellets	517	1.2	10.2

9.3.2 Copper diffusivity (D_e)

Fig. 9.2 shows the Boyd's plots for copper adsorption by amine-modified SBA-15 pellets obtained by stirring the adsorbent in copper solution. All the data points were collected during the first 5 min, i.e., before reaching equilibrium. The diffusivity was obtained for three different initial copper concentrations. Table 9.4 shows that higher diffusivities corresponded to higher initial concentration.

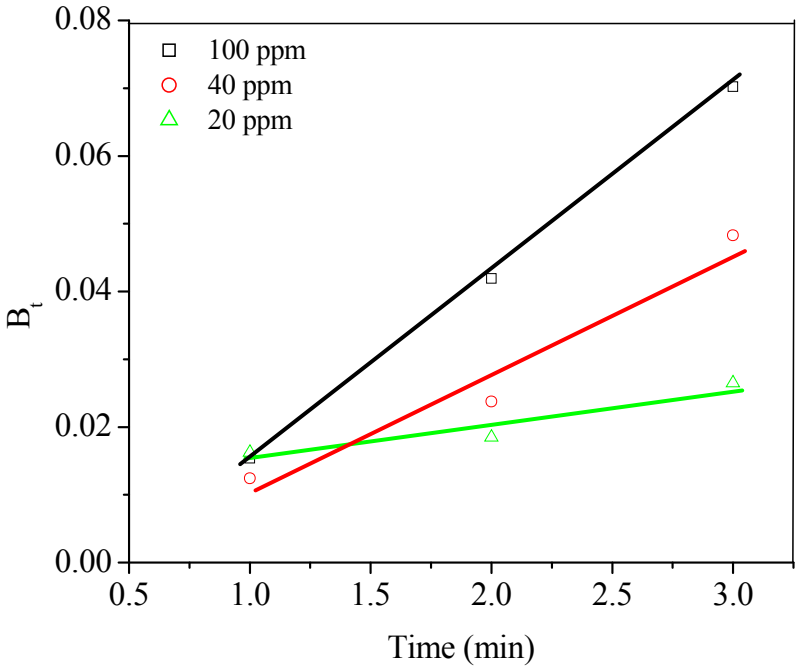

Figure 9-2. Boyd's plots for copper adsorption by amine-modified SBA-15 pellets.

Table 9-4. Values of copper diffusivities using different copper concentration solutions.

	20 mgL^{-1}	**40 mgL^{-1}**	**100 mgL^{-1}**
$\frac{\pi^2 D_e}{r_p^2}$	0.0051	0.0179	0.0274
$D_e \times 1015$ (cm^2/min)	0.30	1.05	1.60

9.3.3 Effect of flow rate

The performance of packed bed is described through the concept of breakthrough curves. Both, the time when the adsorbate is detected in the column effluent (breakthrough point) at a given inlet concentration, and the shape of the concentration – time profile or breakthrough curve, are very important characteristics for operation, dynamic response and process design of adsorption columns, because they directly affect the feasibility and economics of the process. Experimental determination of these parameters is very dependent on column design (column length, diameter and porosity) and operating conditions (feed concentration and flow rate).

In the first stage on adsorption studies in the continuous flow fixed column, the flow rate varied from 1 to 4 $mLmin^{-1}$, while the inlet Cu^{2+} concentration in the feed was held constant at 40 mgL^{-1}. The plots of normalized Cu^{2+} concentration versus time at different flow rates are given in Fig. 9.3. As indicated in Fig. 9.3, at the lowest flow rate of 1 $mLmin^{-1}$, relatively high uptake values were observed for Cu^{2+}. In general, sharper breakthrough curves were obtained at higher flow rates. As mentioned earlier, the World Health Organization (WHO) recommended guideline value for copper in drinking water is 2 mgL^{-1} [2]. This value was used as a breakpoint for this study. Thus, for feed concentration of 40 mgL^{-1}, the tb was defined as the time required to reach C/C_0 of 0.05. Table 9.5 shows that the breakpoint time decreased with increasing flow rate. This behavior can be explained by the fact that Cu^{2+} adsorption is affected by insufficient residence time of the solute in the column. This insufficient time decreases the ability of copper ions to reach amine groups located deep inside the porous structure. Even though shorter breakpoint times were observed at higher flow rates, the total metal removal percentage, an indicator of system performance, and the metal uptake were actually maximum at the highest flow rate.

As seen in Table 9.5, the predicted tb and qe were in all cases close to the experimental data. These results reflect the adequacy and usefulness of the proposed model. Some differences between the predicted breakthrough curves and the experimental data presented in Fig. 9.3 were observed when C/C_0 approached 1. Indeed, experimental results showed a faster than expected approach to saturation. This behavior occurred in all cases, indicating that it is most likely attributable to the occurrence of a systematical error. This error might be a result of the assumptions made to solve the fixed bed model, in addition to errors associated with the diffusivity calculations and the equilibrium model. Furthermore, no optimization was performed to fit the parameters of the model such as axial dispersion coefficient (E) and mass transfer coefficient (k_{ad}). To clarify the effect of these parameters on the performance of the model, Fig. 9.4 and Fig. 9.5 were developed using two different values of E and k_{ad}, respectively. It is apparent from these figures that the adequacy of the model depends strongly on these two parameters. Thus, it is expected that optimization of these parameters would result in better performance. Nonetheless, considering all the potential sources of errors, the level of accuracy observed is a strong indication that the proposed models provide an acceptable representation of copper adsorption in a fixed-bed column containing amine-functionalized mesoporous silica pellets.

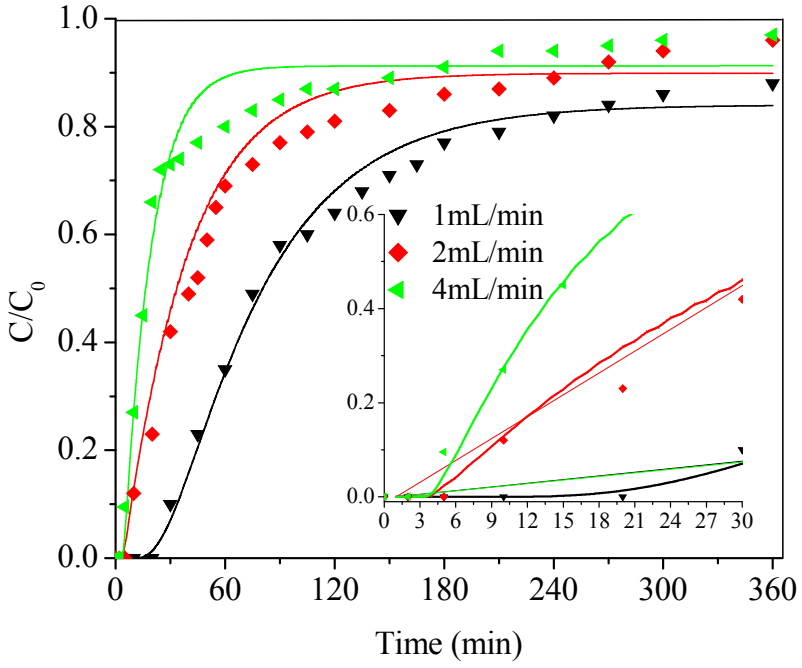

Figure 9-3. Breakthrough curves for different flow rates at constant feed concentration of 40 mg/L and bed height of 14 cm.

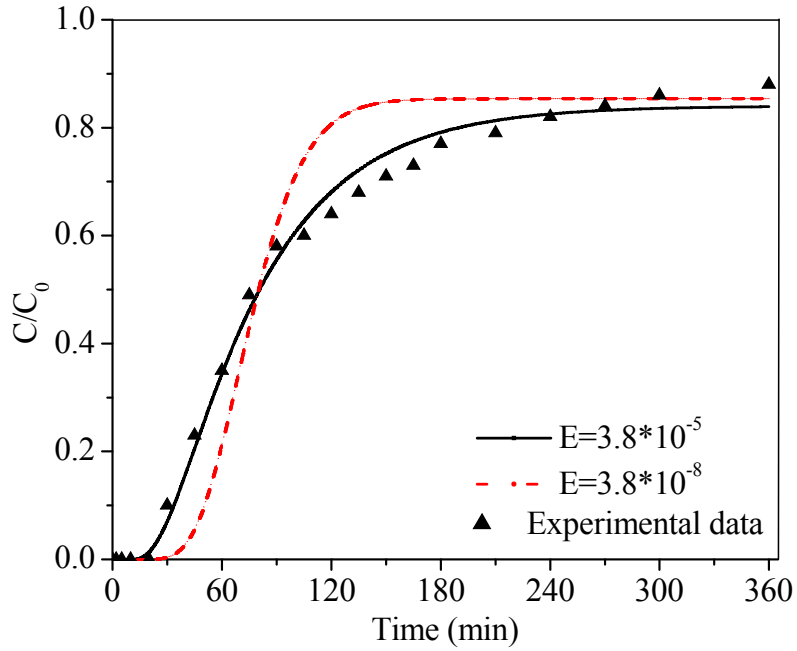

Figure 9-4. Effect of axial dispersion coefficient (E) on model fitting at flow rate of 1 mL/min for k_{ad} = 1.95.

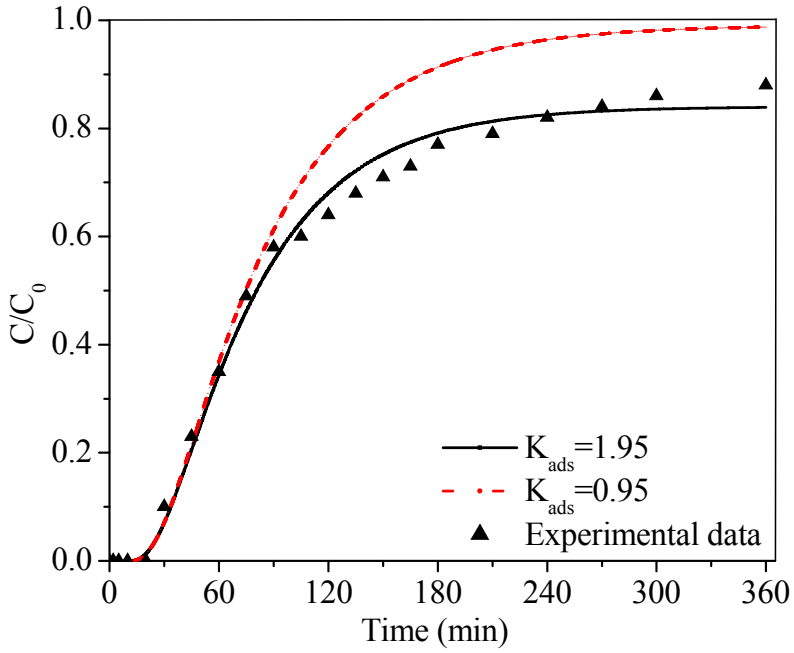

Figure 9-5. Effect of mass transfer coefficient (k_{ad}) on model fitting at flow rate of 1 mL/min for E = $3.8*10^{-5}$.

Table 9-5. Experimental and predicted values of t_b and q_b.

Q ($mLmin^{-1}$)	Experimental			Model		
	t (min)	t_b (min)	q_e (mgg^{-1})	t (min)	t_b (min)	q_e (mgg^{-1})
1	124.5	24.3	4.61	127.3	27.2	4.72
2	78.2	7.2	5.79	66.1	6.5	4.90
4	46.9	3.6	6.95	43.9	5.1	6.50

9.3.4 Column regeneration

One of the most important properties of adsorption systems is their steady performance during multiple adsorption-desorption cycles, which greatly reduces the process cost. In this study, in order to maintain the concentration of $Cu^{+2} \leq 2$ mgL^{-1} at the column outlet, the column needs to be regenerated at every tb time interval.

APTS–SBA-15 was reused for two adsorption-desorption cycles. Elution of copper from the adsorbent was achieved by using 0.2 M EDTA at a flow rate of 1 $mLmin^{-1}$. After desorption or column regeneration, the APTS–SBA-15 was used again in another adsorption experiment. The result obtained in Fig. 9.6 shows that after regeneration, almost the same breakthrough curve was obtained, while a decreased tb from 24.3 to 22.0 min was calculated, resulting in a loss of adsorption performance. Nonetheless, the decrease in adsorption capacity of the regenerated bed compared to the fresh one was

calculated to be only 0.03 mg/g, i.e., less than 1% of the total capacity of the fresh adsorbent. This behavior demonstrates the stability of the adsorption sites on the surface of APTS–SBA-15.

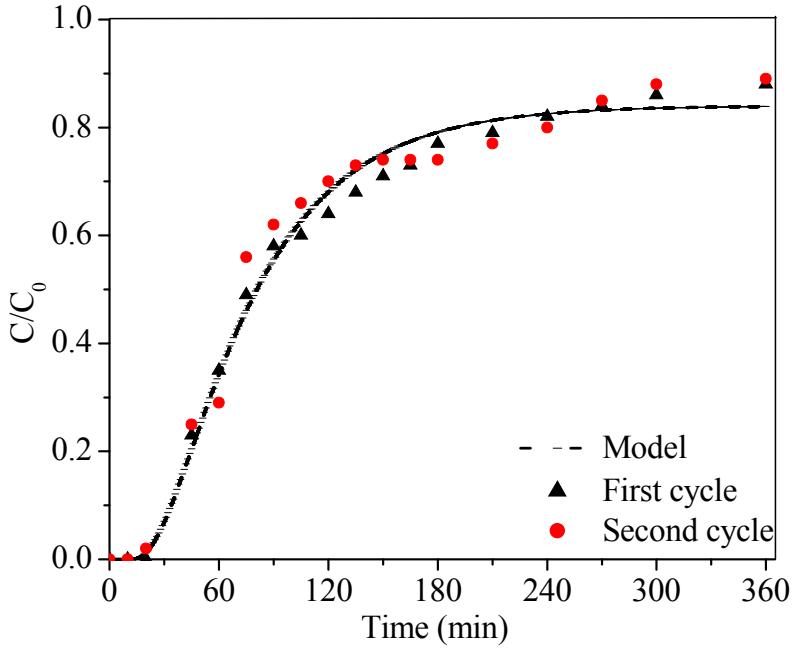

Figure 9-6. Breakthrough curves for two successive cycles at constant flow rate of 1 mL/min, feed concentration of 40 mgL^{-1} and bed height of 14 cm.

Table 9-6. Experimental and predicted values of t_b and q_e for the regenerated column.

Q ($mLmin^{-1}$)	**Fresh**			**Regenerated**		
	t (min)	t_b (min)	q_e (mgg^{-1})	t (min)	t_b (min)	q_e (mgg^{-1})
124.5	24.3	4.61	123.7	22.0	4.58	124.5

9.4 Conclusions

This study dealt with a dynamic analysis of copper adsorption on amine-functionalized mesoporous silica and an attempt at modeling the behavior of a fixed-bed column. By solving the mass balance equations of a fixed-bed adsorption column, tb was accurately predicted for different flow rates. Moreover, the shape of the breakthrough curve as predicted by the model was in good agreement with the experimental data. The results obtained from the analysis of the breakthrough curves at various

flow rates showed that with a decrease in the flow rate from 4 to 1 $mLmin^{-1}$, both the adsorption capacity and the breakthrough time decreased.

References

[1] S. Rengaraj, Y. Kim, C.K. Joo, J. Yi, Removal of copper from aqueous solution by aminated and protonated mesoporous aluminas: Kinetics and equilibrium, *J. Colloid Interf. Sci.* 273 (2004) 14-21.

[2] World Health Organization, Guidelines for drinking-water quality: Recommendations - Addendum, Third edition - Volume 1 (2008).

[3] H. Yoshitake, Highly-controlled synthesis of organic layers on mesoporous silica: Their structure and application to toxic ion adsorptions, *New J. Chem.* 29 (2005) 1107-1117.

[4] A. Sayari, S. Hamoudi, Periodic mesoporous silica-based organic-inorganic nanocomposite materials, *Chem. Mater.* 13 (2001) 3151-316.

[5] E. Da'na, A. Sayari, Adsorption of copper on amine-functionalized SBA-15 prepared by co-condensation: Equilibrium properties, *Chem. Eng. J.* 166 (2011) 445-453.

[6] E. Da'na, N. D. Silva, A. Sayari, Adsorption of copper on amine-functionalized SBA-15 prepared by co-condensation: Kinetics properties, *Chem. Eng. J.* 166 (2011) 454-459.

[7] E. Da'na, A. Sayari, Optimization of copper removal efficiency by adsorption on amine-modified SBA-15: Experimental design methodology, *Chem. Eng. J.* 167 (2011)91-98.

[8] P.O. Osifo, H.W.J.P. Neomagus, R.C. Everson, A. Webster, M.A. Gun, The adsorption of copper in a packed-bed of chitosan beads: Modeling, multiple adsorption and regeneration, *J. Hazard. Mater.* 167 (2009) 1242-1245.

[9] O. Hamdaoui, Removal of copper(II) from aqueous phase by Purolite C100-MB cation exchange resin in fixed bed columns: Modeling, *J. Hazard. Mater.* 161 (2009) 737-746.

[10] S.R. Shukla, V.G. Gaikar, R.S. Pai, U.S. Suryavanshi, Batch and column adsorption of Cu(II) on unmodified and oxidized coir, *Sep. Sci. Technol.* 44 (2009) 40-62.

[11] T. Banjonglaiad, E. Croiset, P. Silveston, P.L. Douglas, S. Douglas, W. Teppaitoon, S. Pongamphai, Dynamic measurement of copper (II) ion adsorption in activated carbon fixed bed columns, *Am. J. Environ. Sci.* 4 (2008) 412-419.

[12] A. Shahbazi, H. Younesi, A. Badiei, Functionalized SBA-15 mesoporous silica by melamine-based dendrimer amines for adsorptive characteristics of Pb(II), Cu(II) and Cd(II) heavy metal ions in batch and fixed bed column, *Chem. Eng. J.* 168 (2011) 505-518.

[13] M.C. Bruzzoniti, A. Prelle, C. Sarzanini, B. Onida, S. Fiorilli, E. Garrone, Retention of heavy metal ions on SBA-15 mesoporous silica functionalized with carboxylic groups, *J. Sep. Sci.* 30 (2007) 2414-2420.

[14] A.S. Pushnov, Calculation of average bed porosity, *Chem. Pet. Eng.* 42 (2006) 14-17.

[15] M. Dadwhal, M.M. Ostwal, P.K.T. Liu, M. Sahimi, T.T. Tsotsis, Adsorption of arsenic on conditioned layered double hydroxides: Column experiments and modeling, *Ind. Eng. Chem. Res.* 48 (2009) 2076-2084.

[16] R. Lagoa, J.R. Rodrigues, Kinetic analysis of metal uptake by dry and gel alginate particles, *Biochem. Eng. J.* 46 (2009) 320-326.

[17] C. M. Yang, H. A. Lin, B. Zibrowius, B. Spliethoff, F. Schüth, S. C. Liou, M. W. Chu, C. H. Chen, Selective surface functionalization and metal deposition in the micropores of mesoporous silica SBA-15, *Chem. Mater.* 19 (2007) 3205-3211.

Chapter 10

General discussion, conclusions and recommendations

Nowadays the world is becoming a too small place to be in isolation because of many technological advancements. Problems like water pollution and shortage are no longer the concern of individual nations. The entire global community is responsible for water, which was ranked by experts as second only to oxygen as essential for life. Therefore the responsibility for keeping it pollution-free must necessarily be shared by all of us. Consequently, during the last few decade governments all around the world expressed increased concerns about the rapid deterioration of the environment. Although several drastic measures have been taken during the last few years, the problem of water pollution continues to be a serious challenge to mankind and much effort is still required to develop new technologies to achieve the required environmental standards.

As a small contribution to solving this water problem, our research group explored the adsorption of heavy metals, including copper, to which this thesis was devoted. This is a particularly important topic in water pollution prevention and control, because adsorption is now considered one of the most effective, economic and selective method for water treatment and analysis purposes.

To achieve the best performance for an adsorbent, a set of requirements must be met including:(i) well-designed pore size and geometry with open pore structure to achieve fast kinetics, (ii) accessible adsorption sites and suitable surface properties to achieve high adsorption capacity, (iii) high selectivity, (iv) simple synthesis, (v) low cost, taking in consideration not only material synthesis cost, but also equipment cost, which depends on adsorbent performance, (vi) regeneration ability under mild conditions, and (vii) long term stability upon adsorption-desorption cycling.

Periodic mesoporous materials exhibit many attractive properties such as large surface area and controllable and narrowly distributed pore sizes. Thus, the development of functionalized mesoporous adsorbents for heavy metal ions using incorporated ligands with appropriate functional groups has generated considerable interest. SBA-15 is among the most popular mesoporous silicas because of its large, adjustable pores (5-30 nm), and also because of its thick pore walls, around 4 nm, which provide enhanced mechanical stability.

For the synthesis of amine-functionalized materials, co-condensation of the desired aminosilane with the silica precursor often offers a better control of the resultant materials in terms of higher and more uniform surface coverage of the organic functionalities compared to the post-synthesis grafting methodology. In addition, co-condensation is preferred because of its simplicity and lower consumption of organic precursor.

In this thesis, amine-functionalized SBA-15 prepared by co-condensation was proposed as heavy metal ions adsorbent. In preliminary studies, this adsorbent showed promising adsorption performances.

10.1 Summary of the main findings in this thesis

- **Direct evidence that the structural collapse observed in some mesoporous silica materials when being in contact with aqueous solutions is associated with the drying process and not the treatment itself.** Before this work, structural collapse of mesoporous silica materials was directly related to the interaction between the silica structure and the water. This work (Chapter3) provided clear evidence of the effect of drying process. It was observed that structural collapse can be avoided by minimizing compressive stress created during the drying process such as reducing the capillary forces by replacing water with a more volatile liquid.

- **Recipes for the preparation of stable amine-modified SBA-15 by co-condensations were achieved with successful results.** Methods reported in the literature for improving the stability of pure silica were used for the amine-modified SBA-15 such as aging at higher temperature and addition of inorganic salts.

- **A recipe for increasing the accessibility of the fuctional groups incorporated into the silica structure, and improve the performance of the adsorbent which was reported in the literature to have negligible metal adsorption capacity and poor accessibility of functional groups.** A procedure to completely remove the surfactant template from the pores and to improve the complexing ability of the amine groups with heavy metals was developed in Chapter 4.
- **Evidence of excellent selectivity of APTS-SBA-15-AB toward copper in the presence of common ions in water such as Ca^{2+}, Na^{2+}, and k^{+}.** One main requirement for a good adsorbent is its selectivity toward the adsorbate of interest. As presented in Chapter 8, it was demonstrated that the uptake of Ca^{2+}, Na^{2+}, and k^{+} was negligible. Furthermore, this behavior provides direct evidence that complexation was the only mechanism for removing copper and not physical adsorption. Thus, since these ions do not form complexes with amine they were not adsorbed.

- **Developing two predictive kinetics models for the description of copper uptake on APTS-SBA-15-AB at different initial concentrations and solution temperatures.** After running kinetics experiments under different initial concentrations and temperatures, it was found that there

were relations between equilibrium adsorption capacity and the pesudo second order rate constant with both temperature and concentrations. Based on these relations, two general predictive models were developed and found to be in excellent agreement with the experimental data.

- **Assessment of the influence of the regeneration conditions on the performance of APTS-SBA-15-AB material during adsorption and regeneration.** To be economically viable, the adsorbent has to be recycled as many times as possible. Thus, it was essential to ensure that the adsorbent has an adequate mechanical stability and steady metal uptake in a series of adsorption–regeneration cycles. Consequently, copper adsorption on APTS-SBA-15-AB was investigated for 3 cycles. APTS-SBA-15-AB was found to have good structural stability during adsorption–desorption cycles. Overall, EDTA treatment of this material showed excellent regeneration.

- **Evaluation of APTS-SBA-15-AB adsorbents using real water samples and for different heavy metal ions, addressing the current limitations of this adsorbent.** The material was shown to have very high sensitivity for many metal ions, using very dilute solutions, i.e., 10 ppm, more than 95% of cations were removed. The presence of Al^{3+} ions decrease the adsorption capacity of all metal ions in multi-metal solutions because of competition between metallic elements for the amine groups. Application of this material to remove copper in tap water, river water, and electroplating wastewater was shown to be successful.

- **Simulation of copper adsorption in a fixed bed column to predict breakthrough curves using the finite volume method.** As practical applications of heavy metal adsorption are most effectively carried out in packed-bed columns, it was necessary to study the ability of APTS-SBA-15-AB to remove copper in a fixed bed column. In addition, a model predicting the breakthrough curves has been developed and tested under different conditions and found to be in good agreement with the experimental data.

10.2 Publications

The work performed in this thesis resulted in the publication of 5 articles in peer-reviewed journals, whose manuscripts are included here as Chapters 4 – 8, and one submitted (Chapter 9). Other two manuscripts (Chapters 2 and 3) will be submitted soon for publication.

10.3 Recommendations and future work

Based on the findings of this Thesis, a series of recommendations were made to improve the performance of the material in future efforts in research and development:

- Scaling up the synthesis of APTS-SBA-15, which is a key step for commercial production. So far this material was prepared as ca, 4 g batches of APTS-SBA-15. A main challenge in scaling up this material production is the corrosive reaction conditions because of the use of HCl.
- Optimization of synthesis conditions required to provide the highest yield of silica and organic material used. This can be achieved by preparing samples with different amine/silica and template/silica ratios while monitoring the yield, characteristics, and the performance of each batch.
- As a part of the optimization procedure, it is interesting to study the effect of synthesis conditions on the morphology (shape and size) of the particles. The morphology of the particles can be used to model adsorption process based on the actual particle shape instead of assuming spherical particles as done in this thesis.
- Recovery and recycling of chemicals can further optimize the synthesis of APTS-SBA-15. In particular, propylaminesilane is of interest because it is the most expensive ingredient, and is used in excess. Furthermore, separation of ethanol used for extraction of the template can help in reusing both ethanol and template surfactant and further minimize the cost.
- One of the interesting variables to be explored in designing amine-modified SBA-15 adsorbent is the type of amine-bearing silanes. In this thesis we focused on using a monoamine, but it could be very useful to explore a triaminosilane, which may produce adsorbents with interesting properties.
- Efforts could be placed on further optimization of the conditions used to make pellets. This can be achieved by studying the effect of particle size and shape, pressure used to make the pellets, and also find other ways to make pellets instead of mechanical pressure such as the use of cross linkers.
- As it was found that the performance of the adsorbent improved at higher temperature, it could be useful to test the possibility of heat integration to utilize the waste heat in warming up the waste water before being treated with the adsorbent.
- EDTA treatment of APTS-SBA-15 showed excellent regeneration. However, it is more expensive than acid-base treatment. Thus, evaluation of the process economics is necessary to decide whether penalty in terms of adsorption capacity or extra EDTA cost is more favorable for the regeneration of the material.

Appendix A

Supplementary Data for Chapter 6

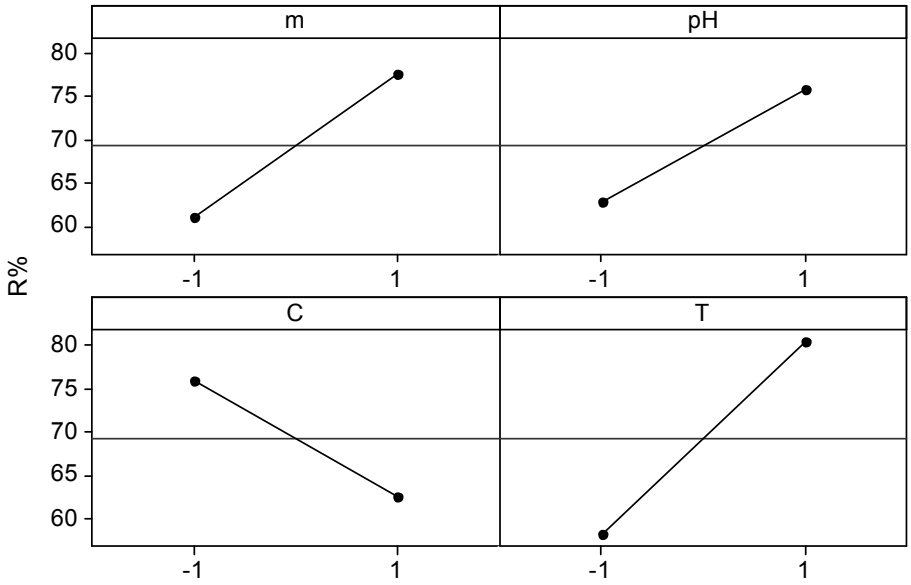

Figure A1. Main effects plot for factorial design

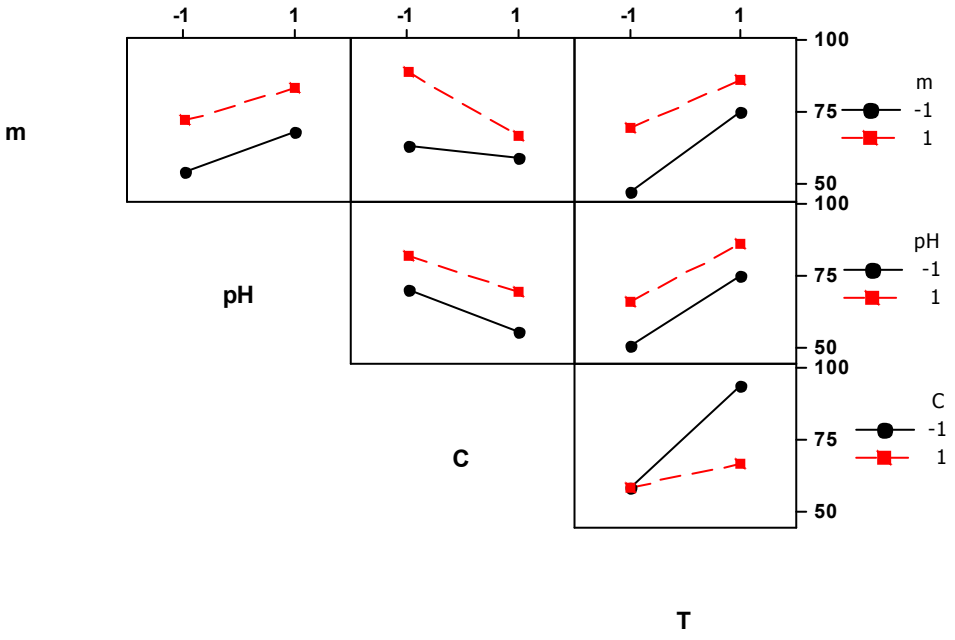

Figure A2. Interaction effects plot

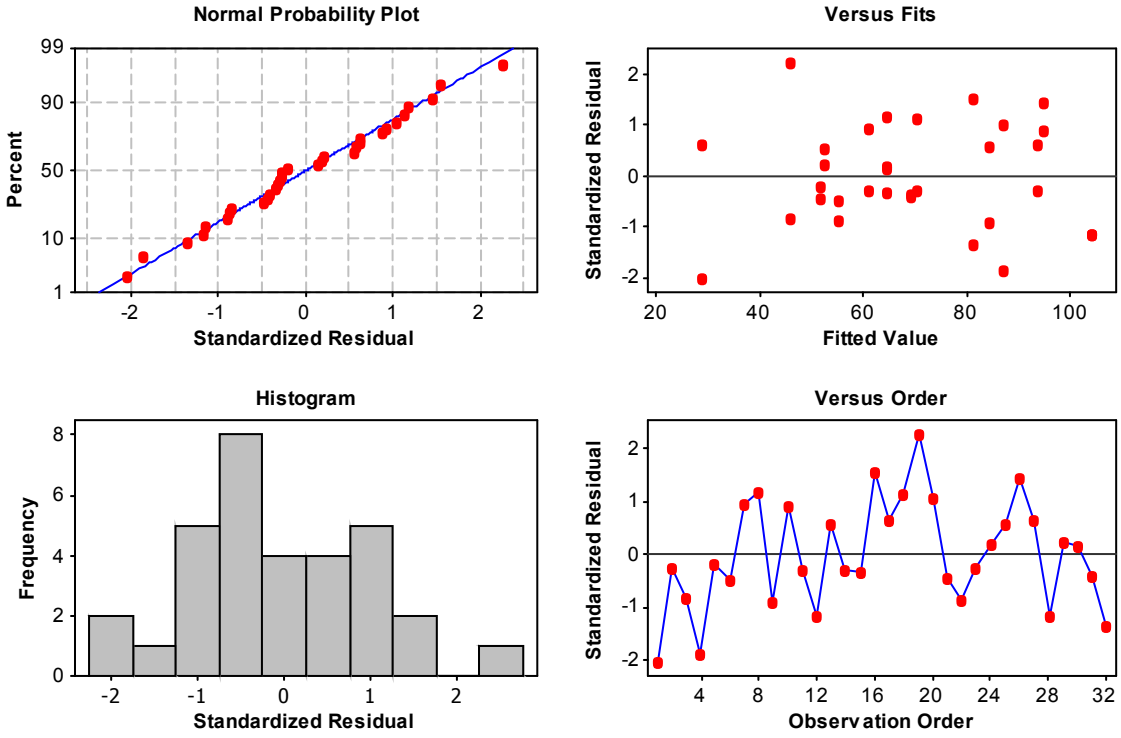

Figure A3. Residual tests for removal efficiency of Cu^{2+}.

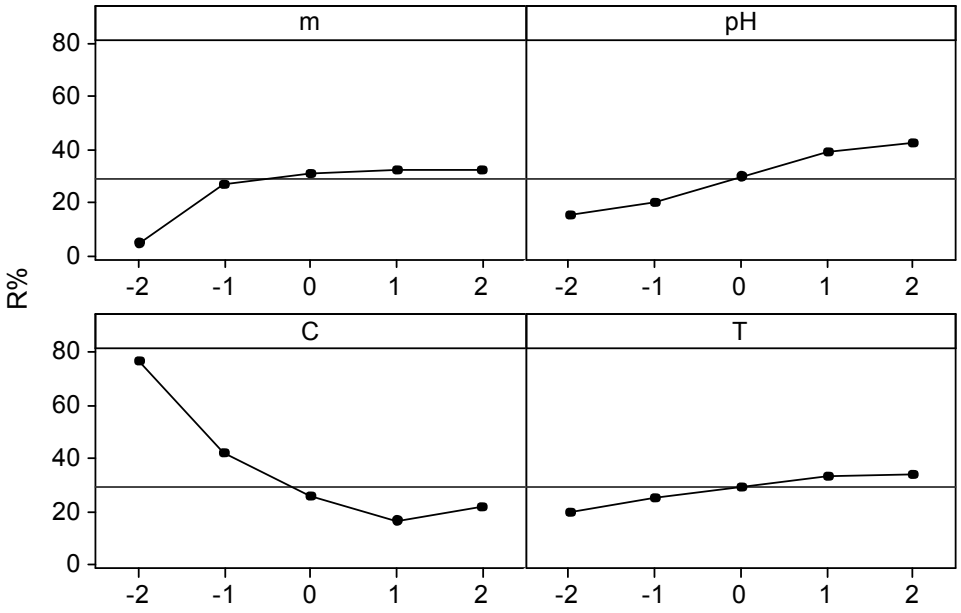

Figure A4. Main effects plot of SCD design.

Table A1. Experimental factorial design results for Cu^{2+} removal efficiency (R%).

Order		Factor				R1 %	R2 %	Rave. %
Standard	Random	T	C	pH	m			
1	15	-1	-1	-1	-1	21.66	31.2	26.43
2	4	-1	-1	-1	1	69.2	74.2	71.7
3	11	-1	-1	1	-1	42.74	53.83	48.29
4	16	-1	-1	1	1	80.32	90.7	85.51
5	2	-1	1	-1	-1	51.12	50.24	50.68
6	13	-1	1	-1	1	53.59	52.2	52.9
7	10	-1	1	1	-1	64.47	60.13	62.3
8	9	-1	1	1	1	68.8	65.31	67.06
9	7	1	-1	-1	-1	81.16	86.44	83.8
10	5	1	-1	-1	1	97.91	99.91	98.91
11	1	1	-1	1	-1	92.64	95.9	94.27
12	8	1	-1	1	1	99.92	99.93	99.93
13	3	1	1	-1	-1	54.46	53.25	53.85
14	12	1	1	-1	1	63.18	64.85	64.02
15	14	1	1	1	-1	68.08	67.86	67.97
16	6	1	1	1	1	86.61	76.32	81.46

Table A2. Analysis of variance of the reduced model without outliers.

Term	Effect	Coefficient	P	SE	DF	SS	MS	F
Average		68.95	0000	3.86				
m	17.47	8.74	0000	3.86	1	2241	2241	135
pH	12.33	6.16	0000	3.86	1	1365	1365	82
C	-12.84	-6.42	0000	3.86	1	1475	1475	89
T	23.15	11.6	0000	3.86	1	4021	4021	241
mC	-9.81	-4.91	0000	3.86	1	660	660	40
mT	-6.36	-3.18	0.001	3.86	1	254	254	15
CT	-14.56	-7.28	0.000	3.86	1	1529	1529	92
mCT	10.53	5.27	0.000	3.86	1	768	768	46
pHCT	3.01	1.51	0.043	3.86	1	112	112	6.7
Lack of fit			0.309		6	108	18	1.32
Error					15	205	13.7	
Total					30	12584		

	R^2
Full model	97.51
Reduced model	96.82
Reduced model without outliers	97.92

Table A3. Response values for different experimental conditions.

Standard order	Random order	m	pH	C	T	R%
1	16	-1	-1	-1	-1	23.5
2	12	1	-1	-1	-1	33.7
3	27	-1	1	-1	-1	41.6
4	13	1	1	-1	-1	55.6
5	31	-1	-1	1	-1	1.8
6	4	1	-1	1	-1	1.6
7	6	-1	1	1	-1	22.7
8	19	1	1	1	-1	20.9
9	13	-1	-1	-1	1	28.9
10	18	1	-1	-1	1	44.0
11	2	-1	1	-1	1	50.7
12	7	1	1	-1	1	57.8
13	5	-1	-1	1	1	10.9
14	11	1	-1	1	1	15.2
15	29	-1	1	1	1	29.8
16	17	1	1	1	1	29.7
17	20	-2	0	0	0	4.1
18	25	2	0	0	0	32.2
19	1	0	-2	0	0	14.8
20	24	0	2	0	0	42.5
21	8	0	0	-2	0	76.9
22	3	0	0	2	0	22.0
23	28	0	0	0	-2	19.6
24	21	0	0	0	2	33.8
25	9	0	0	0	0	33.5
26	30	0	0	0	0	24.7
27	22	0	0	0	0	26.5
28	15	0	0	0	0	27.6
29	10	0	0	0	0	26.8
30	26	0	0	0	0	23.1
31	23	0	0	0	0	26.0

Table A4. Optimization results for copper maximum removal efficiency, optimum 18 adsorption conditions out off 10,000 different combinations.

No.	m		pH		C		T		R%
	Coded	Actual (g/L)	Coded	Actual	coded	Actual (mg/L)	Coded	Actual (K)	
1	0.769	1.554	2	6.5	-2	20	-1.025	297.88	96.29
2	0.773	1.555	2	6.5	-2	20	-0.944	298.28	96.46
3	0.767	1.553	2	6.5	-2	20	-1.034	297.83	96.26
4	0.689	1.538	2	6.5	-2	20	-0.927	298.37	96.09
5	0.865	1.573	2	6.5	-2	20	-0.971	298.15	96.81
6	0.608	1.522	2	6.5	-2	20	-0.824	298.88	95.84
7	0.69	1.538	2	6.5	-2	20	-1.588	295.06	94.74
8	0.693	1.539	2	6.5	-2	20	-0.341	301.3	97.08
9	0.751	1.550	2	6.5	-2	20	-0.297	301.52	97.43
10	0.557	1.511	2	6.5	-2	20	-0.482	300.59	96.12
11	0.983	1.597	2	6.5	-1.993	20.14	-1.084	297.58	96.78
12	0.85	1.570	2	6.5	-1.998	20.04	-1.868	293.66	94.72
13	0.747	1.549	1.972	6.486	-2	20	-0.166	302.17	97.34
14	0.686	1.537	1.999	6.499	-2	20	0.103	303.52	97.62
15	0.911	1.582	1.983	6.492	-2	20	0.003	303.02	98.41
16	0.687	1.537	2	6.5	-2	20	0.263	304.32	97.81
17	0.788	1.558	2	6.5	-2	20	0.564	305.82	98.63
18	1.157	1.631	2	6.5	-2	20	0.44	305.2	99.98